Higher Order Mortar Finite Elements with Dual Lagrange Multiplier Spaces and Applications

Von der Fakultät Mathematik und Physik der Universität Stuttgart
zur Erlangung der Würde eines Doktors der Naturwissenschaften
(Dr. rer. nat.)
genehmigte Abhandlung

Vorgelegt von
Bishnu Prasad Lamichhane
geboren in Nepal

Hauptberichter:	Prof. Dr. B.I. Wohlmuth
Mitberichter:	Prof. Dr. B.D. Reddy
	Prof. Dr. R. Krause

Tag der mündlichen Prüfung: 10 April 2006

Institut für Angewandte Analysis und Numerische Simulation
Universität Stuttgart
2006

Acknowledgements

Presented in this work are the results of my research activities at the chair "Numerische Mathematik für Höchstleistungsrechner" of the Institute für Angewandte Analysis und Numerische Simulation, Universität Stuttgart.

I would like to express my deep gratitude to my supervisor Prof. Dr. Barbara I. Wohlmuth for initiating me in this interesting topic and for providing me invaluable guidance to complete this thesis. Especially, I am thankful to her for creating a free, open and challenging research environment at the institute. During these years at the institute I not only learn many things but also extremely increase my confidence in doing independent research in mathematics. I was naturally attracted to mathematics because of its artistic beauty. Overwhelmed with the beauty of mathematics, I am now heavily impressed with the applied aspects of mathematics.

My special thanks goes to Prof. Dr. B.D. Reddy from University of Cape Town, South Africa, for introducing me an interesting three-field principle of computational mechanics, the Hu-Washizu principle.

I am indebted to Prof. Dr. R. Stevenson for initiating a joint work in three-dimensional mortar finite elements. Theoretical discussion with him has turned out to be quite fruitful.

I would like to express my thanks to Prof. Dr. R. Krause, University of Bonn, Institute for Numerical Simulation, for his constant help in finding problems in our software.

I am also very grateful to Prof. Dr. R. Krause and Prof. Dr. B.D. Reddy for participating in the thesis commitee, and to Prof. Dr.-Ing. Dr. h.c. W. L. Wendland and Prof. Dr. A.-M. Sändig for participating in the oral defense.

I am thankful to my colleagues at the Institute of Applied Analysis and Numerical Simulation (IANS), Stephan Brunßen, Bernd Flemisch, Stefan Hüeber, Alexander Weiß, and most of all, Andreas Klimke for their help during my stay at the institute.

I cannot express my thankfulness to my parents through words. They have always loved and supported me with all their efforts. Especially, I would like to remember my father, whom I cannot see in the earth any more. I am grateful to my brother Thakur P. Lamichhane in Nepal for taking care of mother.

Finally, I express my 'wordless' gratefulness to my wife Uma for her love and support all these years and to my daughter Nanuji for her understanding.

When I remind myself of the truth that I am a part of the whole existence, and the whole is not 'whole' without me, the formality of thanking and showing gratefulness is completely assimilated in the whole and myself.

Stuttgart, April 2006 Bishnu P. Lamichhane

Contents

Abstract

The numerical approximation of partial differential equations coming from physical and engineering modeling is often a challenging task. Most often these partial differential equations are discretized with finite elements and can be solved by modern super-computers. Working with different discretization techniques in different subdomains or independent triangulations, the challenging task is to couple these different discretization schemes or non-matching triangulation without losing the optimality of the approach. Mortar methods yield optimal and flexible coupling techniques for different discretization schemes. Especially when combined with dual Lagrange multiplier spaces, the efficient realization of the weak matching condition is possible, and efficient multigrid methods can be adapted to the non-conforming situation.

In this thesis, we concentrate on higher order dual Lagrange multiplier spaces for mortar finite elements. These non-standard Lagrange multipliers show the same qualitative a priori estimates and quantitative numerical results as the standard ones and yield locally supported basis functions for the constrained space leading to an efficient numerical realization. Working with abstract assumptions on Lagrange multiplier spaces, we prove optimal a priori estimates for mortar finite elements allowing that the dimension of the Lagrange multiplier space can be smaller than the dimension of the trace space of the finite element space from the slave side (with zero boundary condition on the interface). Geometrically non-conforming decompositions and locally refined meshes are also covered.

In two dimensions, we show that a dual Lagrange multiplier space can be constructed for a finite element space of any order satisfying these abstract assumptions. In contrast to earlier approaches, these Lagrange multiplier basis functions have the same support as the nodal finite element basis functions. Using an interesting relation between biorthogonality and quadrature formulas, we prove that an optimal dual Lagrange multiplier space for a finite element space can be constructed if and only if the finite element space is based on Gauß-Lobatto nodes. The two-dimensional construction can easily be extended to the three-dimensional case for a finite element space with tensor product structure. If a finite element space does not have the tensor product structure, e.g., serendipity elements on hexahedra or conforming finite elements on simplices, the situation is more difficult. To deal with this problem, we generalize the idea of a dual Lagrange multiplier space by introducing a quasi-dual Lagrange multiplier space for quadratic serendipity elements. Furthermore, working with a more general assumption that the Lagrange multiplier space can have smaller dimension than the trace space of the finite element space at the slave side (with zero boundary condition on the interface), we introduce dual Lagrange multiplier spaces for quadratic tetrahedral and serendipity elements. Numerical results are presented to illustrate the performance of our approach.

We also study interface problems arising from heat conduction with a discontinuous flux and solution within the framework of mortar finite element methods. Taking into account non-homogeneous jumps of the solution and the flux across the interface, we give a saddle point formulation of the interface problems. Optimal a priori estimates are proved and numerical results are provided.

We have applied mortar finite elements to couple different physical models, material laws and discretization schemes. Furthermore, time-dependent heat transfer problems with sliding meshes are also considered.

Another particular interest for us is the locking phenomenon in linear and nonlinear elasticity. We analyze low order finite element methods based on the Hu-Washizu formulation in linear elasticity and prove the robust and optimal convergence of the finite element approximation of the displacement for the nearly incompressible case. A three-field mixed formulation for finite elasticity is also introduced and numerical results are presented. Mortar finite elements for coupling two different materials in elasticity, where one is a nearly incompressible material and the other one is a compressible material are analyzed for the linear elastic case, and numerical results are provided to verify the theoretical results.

I would like to finish my abstract by repeating three quotations by David Hilbert (1862-1943):

"How thoroughly it is ingrained in mathematical science that every real advance goes hand in hand with the invention of sharper tools and simpler methods which, at the same time, assist in understanding earlier theories and in casting aside some more complicated developments";

"The art of doing mathematics consists in finding that special case which contains all the germs of generality"; and

"The further a mathematical theory is developed, the more harmoniously and uniformly does its construction proceed, and unsuspected relations are disclosed between hitherto separated branches of the science".

Zusammenfassung

Die numerische Approximation partieller Differenzialgleichungen, die zur Beschreibung physikalischer und technischer Anwendungen dienen, ist oft eine herausfordernde Aufgabe. Meist werden die Gleichungen mit Hilfe von finiten Elementen diskretisiert und dann mit modernen Supercomputern gelöst. Besonders herausfordernd ist in diesem Zusammenhang das Arbeiten mit verschiedenen Diskretisierungtechniken auf verschiedenen Teilgebieten oder unabhängigen Triangulierungen, da diese verschiedenen Diskretisierungs-Schemata oder nicht zusammen passenden (non-matching) Triangulierungen gekoppelt werden müssen, ohne dabei die Optimalität der Approximation zu verlieren. Mortar-Methoden, die zur Klasse der nicht-konformen Gebietszerlegungsmethoden gehören, stellen einen attraktiven Ansatz zur numerischen Simulation im Bereich partieller Differenzialgleichungen dar. Insbesondere wenn Mortar-Methoden mit dualen Lagrange-Multiplikatorräumen kombiniert werden, ist eine effiziente Realisierung der schwachen Kopplungsbedingung möglich, und effiziente Mehrgitterverfahren können eingesetzt werden.

In dieser Arbeit stehen duale Lagrange-Multiplikatorräume höherer Ordnung für Mortar-Finite-Elemente im Mittelpunkt. Diese speziellen Lagrange-Multiplikatoren weisen die gleichen qualitativen und quantitativen numerischen Eigenschaften auf wie Standard-Lagrange-Multiplikatoren und liefern Basisfunktionen mit lokalem Träger für den die Kopplungsbedingung respektierenden Raum, was zu einer effizienten numerischen Unsetzung führt. Indem mit abstrakten Annahmen für die Lagrange-Multiplikatorräume gearbeitet wird, können a priori Abschätzungen für Mortar-Finite-Elemente gezeigt werden, die es erlauben, dass die Dimension des Lagrange-Multiplikatorraumes kleiner sein darf als die Dimension der Spur des finite Element-Raumes, der die Null-Randbedingung am Interface der Slave-Seite erfüllt. Geometrisch nicht-konforme Zerlegungen und lokal verfeinerte Gitter sind auch verwendbar.

Für zweidimensionale Mortar-Finite-Elemente wird gezeigt, dass ein dualer Lagrange-Multiplikatorraum für einen Finite-Element-Raum beliebiger Ordnung konstruiert werden kann, der diesen abstrakten Annahmen genügt. Im Gegensatz zu früheren Ansätzen haben diese Lagrange-Multiplikator-Basisfunktionen den gleichen Träger wie die nodalen Finiten-Element-Basisfunktionen. Indem eine interessante Beziehung zwischen der Biorthogonalität und Quadraturformeln verwendet wird, wird bewiesen, dass ein optimaler dualer Lagrange-Multiplikatorraum für einen Finite-Element-Raum nur dann konstruiert werden kann, wenn der Finite-Element-Raum auf Gauß-Lobatto-Knoten basiert. Das zweidimensionale Konstruktionsschema kann leicht auf den dreidimensionalen Fall erweitert werden, sofern ein Finite-Element-Raum mit Tensorprodukt-Struktur vorliegt. Wenn ein Finite-Element-Raum keine Tensorprodukt-Struktur aufweist, wie z.B. bei Serendipity-Elementen auf Hexaedernetz oder bei konforme simplizialen Elementen, ist die Lage schwieriger. Um dieses Problem zu behandeln, wird die Idee des dualen Lagrange-Multiplikatorraums verallgemeinert, indem ein quasi-dualer Lagrange-Multiplikatorraum für quadratische Serendipity-Elemente eingeführt wird. Ferner werden anhand der allgemeineren Annahme, dass der Lagrange-Multiplikatorraum eine kleinere Dimension als der Spur-Raum des Approximationsraums auf der Slave-Seite (mit Null-Randbedingung am Interface) haben kann, duale Lagrange-Multiplikatorräume für quadratische simpliziale- und Serendipity-Elemente eingeführt. Numerische Ergebnisse demonstrieren die Effizienz des Ansatzes.

Des Weiteren werden Interface-Probleme im Rahmen der Mortar-Finite-Element-Methoden behandelt, die aus der Wärmeleitung mit unstetigem Fluss herrühren. Unter Berücksichtigung von inhomogenen Sprüngen in der Lösung und im Fluss am Interface wird eine Sattelpunktformulierung des Interface-Problemes hergeleitet. Deren Optimalität wird bewiesen und durch numerische Ergebnisse untermauert. Zusätzlich werden Mortar-Finite-Elemente zur Kopplung verschiedener physikalischer Modelle, Materialgesetze und Diskretisierungs-Schemata angewandt.

Der letzte wichtige Punkt, der in dieser Arbeit beleuchtet wird, ist das sogenannte "Locking"-Phänomen in der linearen und nichtlinearen Elastizität. Analysiert werden Finite-Element-Methoden von niedrigster Ordnung, die auf der Hu-Washizu-Formulierung basieren. Es wird gezeigt, dass die numerische Approximation robust und optimal konvergiert. Eine Drei-Feld-gemischte Formulierung für nichtlineare (finite) Elastizität wird ebenfalls eingeführt und numerische Ergebnisse dazu präsentiert. Der Fall finiter Elemente zur Kopplung zweier verschiedener Materialien, wobei eines davon nahezu inkompressibel und das andere kompressibel ist, wird für den linear-elastischen Fall analysiert; numerische Ergebnisse bestätigen die theoretischen Aussagen.

CHAPTER 1

Introduction and a Priori Estimates

1.1. An overview

Domain decomposition techniques provide a powerful tool for the numerical approximation of partial differential equations. The computational domain is decomposed into overlapping or non-overlapping subdomains, and a complex global problem is subdivided into simpler local subproblems corresponding to these subdomains. Since these subproblems are coupled, the exchange of information among different subdomains is of crucial importance. The domain decomposition techniques can be used to optimally discretize the underlying physical problems, to develop efficient iterative solvers or to parallelize numerical algorithms. In the recent past years, many efficient iterative methods based on domain decomposition techniques have been developed, see [**126, 151**], and the references therein. For the mathematical foundation and the parallel multilevel approach of domain decomposition methods, we refer to [**131, 145**] and the references therein.

In this thesis, we focus on *mortar finite element methods*, which are non-conforming domain decomposition methods. Decomposing the global domain into overlapping or non-overlapping local subdomains in a geometrically conforming or non-conforming way, the central idea of the mortar technique is to replace the strong continuity condition of the solution across the interface by a weak one with the help of a Lagrange multiplier space. Keeping almost all flexibility of domain decomposition approach, mortar methods can be applied to couple different physical models, non-matching triangulations or independent discretization schemes. These non-conforming domain decomposition techniques provide a more flexible approach than standard conforming approaches. The non-conforming approach is of particular interest in many situations, for example, in problems with discontinuous diffusion coefficients and local anisotropies, contact problems, time-dependent problems or problems with sliding meshes. A complex global domain can be decomposed into several smaller subdomains of simple structure, and these subdomains can be meshed independently. To obtain a stable and optimal discretization scheme for the global problem, the information transfer among the subdomains has to be analyzed. Mortar methods are based on handling the information transfer among the subdomains by means of a Lagrange multiplier space so that if the Lagrange multiplier space satisfies some conditions, then the resulting discretization scheme is stable, optimal and efficient.

Mortar methods were originally introduced to couple spectral and finite element approximations, see [**32, 33, 34**]. An optimal a priori estimate for the mortar finite element methods has been established in [**33, 34, 26, 22, 44**]. The analysis of three-dimensional mortar finite elements is provided in [**26, 42, 99**], and a *hp* version is studied in [**140, 27**]. In [**99, 43, 68**], mortar finite elements in combination with locally quasi-uniform meshes have been considered, and optimal a priori estimates are proved. A mortar finite element

method for the Stokes problem is considered in [**23, 24**]. The stabilized mortar finite element approach with discontinuous Lagrange multipliers has been introduced in [**24**] in the context of the three-dimensional Stokes problem and further studied in [**87, 88**]. The advantage of this mortar technique is that the cumbersome boundary modification is avoided. However, the slave side of the interface should be enriched with some bubble functions in this approach to get the stability. A mortar finite element method for fourth order problems are considered in [**118**], and mortar finite elements are applied to contact problems in [**19, 25, 92, 95**].

Although the boundary value problem is elliptic, the mortar approach has the disadvantage that the arising linear system is, in general, of saddle point type, usually for which iterative methods are known to be less efficient than for symmetric positive definite systems. In the recent years, numerous iterative solvers have been developed for mortar finite elements. Most of these iterative solvers are based on the multigrid solver for a saddle point problem, see [**42, 82, 162, 44, 160**]. However, working with dual Lagrange multiplier spaces, the mass matrix on the slave side of the interface is diagonal, and hence the degrees of freedom associated to Lagrange multipliers can be locally eliminated leading to a sparse, positive definite formulation based on the unconstrained product space. The modification of the saddle point system arising from mortar finite elements is carried out in [**166**], and a multigrid method based on the new positive definite system is proposed, see also [**163**]. Another variant of the multigrid approach for the mortar finite element method with dual Lagrange multiplier spaces is proposed in [**165**] based on the constrained formulation. This multigrid approach is also applied to nonlinear contact problems [**167**]. For the analysis of mortar finite elements for overlapping domain decomposition, we refer to [**59, 1, 76**]

In this thesis, we focus on mortar finite elements with dual Lagrange multiplier spaces, see [**161, 163**]. In particular, we introduce dual Lagrange multiplier spaces for higher order finite elements. Over the recent past years, mortar finite elements with dual Lagrange multiplier spaces have become an active area of research, see, e.g., [**99, 68, 104, 107, 95, 118**]. These non-standard Lagrange multiplier spaces yield efficient discretization schemes and optimal a priori estimates. The a priori analysis of mortar finite elements is based on the stability of the mortar projection and the approximation property of the Lagrange multiplier space. Working with higher order finite element spaces, it is difficult to preserve the duality and the approximation property of the Lagrange multiplier space at the same time. In case of two-dimensional mortar finite elements, we introduce a theory confirming the existence of such an optimal dual Lagrange multiplier space for the finite element space of any order. If hexahedral meshes with finite element spaces of tensor product structure are used, the two-dimensional construction can easily be extended to the three-dimensional case through the tensor product construction. However, this construction cannot be followed anymore, if a finite element space without tensor product structure is used. To deal with these cases, we generalize the idea of a dual Lagrange multiplier space in two ways. First, we introduce a quasi-dual Lagrange multiplier space for quadratic serendipity elements. Secondly, we relax the condition that the trace space of the approximation space at the slave side with zero boundary condition on the interface and the Lagrange multiplier space should have the same dimension, with which the introduction of additional degrees of

freedom at the multiplier side only to satisfy this condition on the dimension is avoided. As a result, we can work with a subspace of the trace space for which it is easier to construct a dual Lagrange multiplier basis. We provide a new theoretical framework within this relaxed setting, which opens a new and simpler way to construct dual Lagrange multiplier bases for higher order finite element spaces. Different coupled problems are considered, and numerical results are provided to verify theoretical claims.

In the first chapter, we prove optimal a priori estimates for mortar finite elements without assuming that the trace of the finite element space with zero boundary condition on the interface from the slave side has the same dimension as the Lagrange multiplier space. Abstract assumptions are provided for a Lagrange multiplier space so that the resulting discretization scheme yields optimal a priori results. As in [**99, 68**], we allow locally refined finite element partitions and geometrically non-conforming subdivisions into subdomains. Furthermore, as in [**107, 68**], we do not require that the partitions match on the boundaries of the interfaces. For the case of having quasi-uniform meshes on each subdomain, we prove an error estimate, where the constant depending on the maximum of ratios of meshsizes at master and slave sides is replaced by the constant only depending on the logarithm of the maximum of ratios of these meshsizes. This shows that the possible disadvantageous effect of having at the slave side a finer mesh than at the master side is much milder than that is indicated by existing error estimates, e.g., in [**163**]. This part along with the last portion of the third chapter is a joint work with Prof. R. Stevenson and has appeared in [**103**].

The second chapter is concerned with the construction of locally supported basis functions which are biorthogonal to the nodal finite element space of order p. In contrast to earlier approaches, see [**124**], these Lagrange multiplier basis functions have the same support as the nodal finite element basis functions and reproduce the conforming finite element space of order $p-1$. Working with Gauß-Lobatto nodes, we find an interesting relation between biorthogonality and quadrature formulas. Several numerical examples are presented to verify our a priori estimates. Most of the theoretical and numerical results of this chapter can be found in [**104, 108**]

In the third chapter, we discuss the construction of dual Lagrange multiplier spaces for three-dimensional mortar finite elements. Restricting ourselves to the quadratic case, we consider finite element spaces based on hexahedral and tetrahedral meshes. In a first step, we consider dual Lagrange multiplier spaces whose dimension is the same as the trace of the finite element space with zero boundary condition on the interface from the slave side. Unfortunately, under this condition no dual Lagrange multiplier spaces can be constructed for quadratic simplicial and serendipity finite element spaces. We give non-existence results for dual Lagrange multiplier spaces for these cases. Then we consider a quasi-dual Lagrange multiplier space for the quadratic serendipity elements. In a next step, working with a Lagrange multiplier space having lower dimension than the trace space of the approximation space at the slave side with zero boundary condition on the interface, we construct dual Lagrange multiplier spaces for quadratic serendipity and simplicial finite element spaces. For all cases, we provide numerical results.

In Chapter 4, we analyze interface problems within the framework of mortar finite elements. We start with the saddle point formulation of interface problems and show that

the interface conditions enter in the right-hand side without affecting the stiffness matrix. We consider the non-homogeneous jump in the flux and the solution and prove a priori estimates. Using dual Lagrange multipliers, we can work with scaled sparse matrices, and static condensation gives rise to a symmetric and positive definite system on the unconstrained product space, on which the modified multigrid solver introduced in [**166**] can be applied. Some numerical results are presented to show the performance of our approach. This chapter is published in [**105**].

Chapter 5 is concerned with applications of mortar finite elements for some coupled problems. In particular, we consider the coupling of different material laws and physical models. In particular, we apply mortar finite elements to an elasto-acoustic coupling and transient heat transfer problems on sliding meshes.

For all our examples, we provide numerical results demonstrating the flexibility and efficiency of mortar techniques.

This thesis is also concentrated on applications of mortar finite elements to different coupled problems of engineering interest. Of particular interest for us is to couple two materials in elasticity, where one is a nearly incompressible material and the other one is a compressible material. In Chapter 6, we analyze low order finite element methods based on the Hu-Washizu formulation in linear elasticity, and prove a robust a priori estimate showing that the estimate is uniformly valid with respect to the Lamé parameter λ, which becomes very large for a nearly incompressible material. This analysis is performed with recourse to a modified Hu-Washizu formulation depending on a parameter, which is equivalent to the classical Hu-Washizu formulation in the continuous setting. This modified Hu-Washizu formulation has also been generalized to the geometrically nonlinear elasticity with Saint-Venant Kirchhoff law. We also propose a three-field formulation to get locking-free response in general hyperelasticity. However, the presented mathematical analysis is restricted to linear elasticity. The first part of this chapter is a joint work with Prof. B.D. Reddy and Dr. J.K. Djoko and has appeared in [**102, 73**], and the second part is a joint work with Dr. K.S. Chavan and is summarized in [**61**].

In Chapter 7, we consider the coupling of a compressible and a nearly incompressible material in linear elasticity. Working with a suitable discretization scheme to deal with a nearly incompressible material, we provide an error estimate uniform with respect to the Lamé parameter λ for the nearly incompressible material. Locking behavior anticipated by the theory is verified numerically in linear and nonlinear elasticity. Finally, we provide conclusion and outlook of the work.

1.2. Sobolev spaces

Sobolev spaces play a fundamental role in the theory and numerical solutions of partial differential equations. These spaces are made up of functions with 'generalized' or weak derivatives. Using the variational formulation of partial differential equations, the existence and uniqueness of the solution in an appropriate Sobolev space can be established by using some well known tools like the Lax-Milgram Lemma. In this section, we present some standard results on Sobolev spaces in a way that is relevant to this thesis. There are many excellent references to this topic, see, e.g., [**3, 114, 83**]. Suppose that $\Omega \subset \mathbb{R}^d,\ d \in \{1, 2, 3\}$ be a bounded domain with Lipschitz boundary. We restrict our attention to a real-valued

function u defined on Ω. For $1 \leq p < \infty$, the Lebesgue space $L^p(\Omega)$ is defined as

$$L^p(\Omega) := \{u| \int_\Omega |u(x)|^p \, dx < \infty\}$$

with a natural norm defined by $\|u\|_{L^p(\Omega)} := \left(\int_\Omega |u(x)|^p \, dx\right)^{1/p}$, and for $p = \infty$

$$L^\infty(\Omega) := \{u| \text{ ess sup}\{|u(x)|, x \in \Omega\} < \infty\}$$

with a norm $\|u\|_{L^\infty(\Omega)} := \text{ess sup}\{|u(x)|, x \in \Omega\}$.

The short-hand notation for the mixed partial derivative of a function can be written in terms of the so-called multi-index notation α, which is an d-tuple of non-negative integers α_i so that $\alpha := (\alpha_1, \cdots, \alpha_d)$. The length of α is given by $|\alpha| := \sum_{i=1}^d \alpha_i$, and for a function $\phi \in C^\infty(\Omega)$, $D^\alpha \phi$ will denote the usual point-wise mixed partial derivative $\left(\frac{\partial}{\partial x_1}\right)^{\alpha_1} \cdots \left(\frac{\partial}{\partial x_d}\right)^{\alpha_d} \phi$. Let k be a non-negative integer. Taking into account the definition of the set of locally integrable functions

$$L^1_{loc}(\Omega) := \{u| \, u \in L^1(K), \text{ compact } K \subset \Omega\},$$

and the norm $\|u\|_{W^{k,p}(\Omega)} := \left(\sum_{|\alpha| \leq k} \|D^\alpha_w u\|^p_{L^p(\Omega)}\right)^{1/p}$ for $1 \leq p < \infty$, and $\|u\|_{W^{k,\infty}(\Omega)} := \max_{|\alpha| \leq k} \|D^\alpha_w u\|_{L^\infty(\Omega)}$ for $p = \infty$, we can define Sobolev spaces $W^{k,p}(\Omega)$ as

$$W^{k,p}(\Omega) := \{u \in L^1_{loc}(\Omega)| \, \|u\|_{W^{k,p}(\Omega)} < \infty\},$$

where $D^\alpha_w \phi$ denotes the so-called weak mixed partial derivative of the function ϕ. The definition of the weak derivative is given in terms of the set of functions $\mathcal{D}(\Omega)$ with $\mathcal{D}(\Omega) := \{u \in C^\infty(\Omega) : \text{ supp } u \text{ is compact}\}$. A function $f \in L^1_{loc}(\Omega)$ has a weak derivative D^α_w if there exists a function $g \in L^1_{loc}(\Omega)$ such that

$$\int_\Omega g(x)\phi(x) \, dx = (-1)^{|\alpha|} \int_\Omega f(x) D^\alpha_w \phi(x) \, dx, \quad \phi \in \mathcal{D}(\Omega).$$

If such a g exists, we define $D^\alpha_w f := g$. From now on, we will merely use $D^\alpha \phi$ instead of $D^\alpha_w \phi$ to denote the weak derivative of ϕ. We state two results of particular interests, for proofs, see [**3, 114, 83, 136**].

THEOREM 1.1. *The Sobolev space $W^{k,p}(\Omega)$ is a Banach space.*

For the special case $p = 2$ the Sobolev space $W^{k,p}(\Omega)$ is denoted by $H^k(\Omega)$, and a natural inner product is induced by the norm in this case.

THEOREM 1.2. *The space $H^k(\Omega)$ is a Hilbert space.*

The space $W^{s,p}(\Omega)$ for an arbitrary real positive s is defined in terms of the real method of interpolation. For $s = k+t$, where k is a non-negative integer and $t \in (0,1)$, the intrinsic norm on $W^{s,p}(\Omega)$ is defined as

$$\|u\|^p_{W^{s,p}(\Omega)} := \|u\|^p_{W^{k,p}(\Omega)} + \sum_{|\alpha|=k} \int_\Omega \int_\Omega \frac{|D^\alpha u(x) - D^\alpha u(y)|^p}{|x-y|^{d+tp}} \, dxdy. \tag{1.2.1}$$

If X and Y be two separable Hilbert spaces with $X \subset Y$, and X is dense in Y, then for any $u \in Y$ and $t > 0$, we define

$$K(t,u)^2 := \inf_{v \in X} (t^2 \|u - v\|_Y^2 + \|v\|_X^2).$$

Suppose that $0 < \theta < 1$. Defining a norm

$$\|u\|_{[X,Y]_\theta} := \left(\int_0^\infty t^{-2\theta} K(t,u)^2 \, \frac{dt}{t} \right)^{1/2},$$

the interpolation space

$$[X,Y]_\theta := \left\{ u \in Y |\ \|u\|_{[X,Y]_\theta} < \infty \right\}$$

forms an interpolating space with the norm $\|\cdot\|_\theta$, see [**114**]. In particular, if Ω has a Lipschitz boundary and k is a non-negative integer

$$[H^k(\Omega), L^2(\Omega)]_\theta = H^{(1-\theta)k}(\Omega)$$

with equivalent norms. The space $H_0^s(\Omega)$ is a subspace of $H^s(\Omega)$ defined as the closure of $C_0^\infty(\Omega)$ in the norm of $H^s(\Omega)$. The trace theorem is of special interest for a variational formulation of partial differential equations. Before giving a standard trace theorem [**83**], we need a definition of $C^{k,1}$ boundary.

Definition 1.3. *Let Ω be an open subset of $\mathbb{R}^d$. We say that its boundary $\partial\Omega$ is continuous (respectively Lipschitz continuous, of class C^k, of class $C^{k,1}$ for some integer $k > 0$) if for every $x \in \partial\Omega$ there exists a neighborhood $\mathcal{O}$ of $x \in \mathbb{R}^d$ and new orthogonal coordinates $y = (y', y_d)$ where $y' = (y_1, \cdots, y_{d-1})$ such that:*

(i) *$\mathcal{O}$ is a hypercube in the new coordinates:*

$$\mathcal{O} = \{y|\ -a_i < y_i < a_i,\ 1 \le i \le d\}.$$

(ii) *There exists a continuous (respectively Lipschitz-continuous, C^k, $C^{k,1}$) function f defined in*

$$\mathcal{O}' = \{y'|\ -a_i < y_i < a_i,\ 1 \le i \le d-1\}$$

that satisfies

$$|f(y')| \le \frac{a_d}{2}, y' \in \mathcal{O}',\ \Omega \cap \mathcal{O} = \{y|\ y_d < f(y')\},\ \Gamma \cap \mathcal{O} = \{y|\ y_d = f(y')\}.$$

Theorem 1.4 (**Trace theorem**). *Let Ω be a bounded open subset of $\mathbb{R}^d$ with a $C^{k,1}$ boundary $\partial\Omega$. Assume that $s - 1/p$ is not an integer, $s \le k+1$, $s - 1/p = l + t$, $l \in \mathbb{N}$, $0 < t < 1$. Then the mapping*

$$u \to \{\gamma_0 u, \gamma_0 \frac{\partial u}{\partial \mathbf{n}}, \cdots, \gamma_0 \frac{\partial^l u}{\partial \mathbf{n}^l}\},$$

which is defined for $u \in C^{k,1}(\bar{\Omega})$, has a unique continuous extension as an operator from

$$W^{s,p}(\Omega) \text{ onto } \prod_{j=0}^{l} W^{s-j-1/p,p}(\partial\Omega).$$

This operator has a right continuous inverse which does not depend on p.

Of special interest for the higher order mortar method are the trace theorems given in [**30, 31**], which will be used in the a priori analysis, see also [**84, 83**]. Let $H^{1/2}(\partial\Omega)$ be the trace space of $H^1(\Omega)$ on $\partial\Omega$. Then the K-method of interpolation yields the equivalent definition

$$H^{1/2}(\partial\Omega) = [L^2(\partial\Omega), H^1(\partial\Omega)]_{1/2}.$$

This space can also be characterized by some other equivalent semi-norms. One of them is

$$|u|^2_{H^{1/2}(\partial\Omega)} = \min_{\tilde{u}|_{\partial\Omega}=u} |\tilde{u}|^2_{H^1(\Omega)}.$$

Another equivalent semi-norm comes from the intrinsic norm (1.2.1) on $W^{s,p}(\Omega)$. The norm on the space $H^{1/2}(\partial\Omega)$ using one of the semi-norms above with K-method of interpolation is given by

$$\|u\|^2_{H^{1/2}(\partial\Omega)} = |u|^2_{H^{1/2}(\partial\Omega)} + \|u\|^2_{L^2(\partial\Omega)}.$$

The space $H^{1/2}_{00}(\gamma')$ is of special interest in the mortar method with $\gamma' \subset \partial\Omega$, which is isomorphic to the interpolation space $[L^2(\gamma'), H^1_0(\gamma')]_{1/2}$, see [**114**, Lemma 11.7]. This space $H^{1/2}_{00}(\gamma')$ is formed by all functions $v \in H^{1/2}(\partial\Omega)$ that vanish outside γ' with an equivalent norm defined by

$$\|u\|^2_{H^{1/2}_{00}(\gamma')} = |u|^2_{H^{1/2}(\gamma')} + \int_{\gamma'} \frac{v(x)^2}{\operatorname{dist}(x, \partial\gamma')}\, d\sigma(x),$$

where $\operatorname{dist}(x, \partial\gamma')$ is the function giving distance between the point x and the set $\partial\gamma'$. The space $H^{1/2}_{00}(\gamma')$ can also be equivalently defined as

$$H^{1/2}_{00}(\gamma') = \{u \in H^{1/2}(\gamma') |\ \tilde{u} \in H^{1/2}(\partial\Omega)\},$$

where $\tilde{u}$ is the trivial extension of u to $\partial\Omega$, see [**44**]. We note that $\mathcal{D}(\Omega)$ is dense in $H^s(\Omega)$ if and only if $0 \le s \le \frac{1}{2}$, and in this case $H^s_0(\Omega) = H^s(\Omega)$, see [**114**, Theorem 11.1]. If $s > \frac{1}{2}$, $H^s_0(\Omega)$ is strictly contained in $H^s(\Omega)$. The dual space of Sobolev space $H^s_0(\Omega)$, $s > 0$ will be denoted by $H^{-s}(\Omega)$ except when $s \neq \mathbb{N} + \frac{1}{2}$. We will denote by $H^{-1/2}(\Omega)$ the dual space of $H^{1/2}_{00}(\Omega)$, and the dual space of $H^{1/2}_0(\Omega)$ will be denoted by $(H^{1/2}_0(\Omega))'$. The Poincaré inequality tells us that the semi-norm in $H^1_0(\Omega)$ is equivalent to the norm itself [**136**].

THEOREM 1.5 (**Poincaré inequality**). *Let Ω be contained in the strip $|x_1| \le r < \infty$. Then there is a constant c, depending only on k and r, such that*

$$\|u\|^2_{H^k(\Omega)} \le c \sum_{|\alpha|=k} \|D^\alpha u\|^2_{L^2(\Omega)}$$

for every $u \in H^k_0(\Omega)$.

1.3. The variational formulation of elliptic equations

The finite element methods are fundamentally based on a variational formulation of partial differential equations, see, e.g., [**63, 50, 40**]. To make our exposition simple, we consider the following elliptic second order boundary value problem

$$-\operatorname{div}(a\nabla u) + cu = f \quad \text{in } \Omega \quad \text{with} \quad u = 0 \quad \text{on } \partial\Omega, \tag{1.3.1}$$

where $\Omega \subset \mathbb{R}^d$, $d = \{2, 3\}$, is a bounded d-polytope, $a, c \in L^\infty(\Omega)$, $a > a_0 > 0$ and $c \geq 0$. The variational form of this equation is obtained by multiplying both sides of (1.3.1) by a test function $v \in H_0^1(\Omega)$, integrating over Ω and using Green's formula so that our variational problem is: find $u \in H_0^1(\Omega)$ so that

$$B(u, v) = l(v), \quad v \in H_0^1(\Omega), \tag{1.3.2}$$

where $B(u, v) := \int_\Omega a\nabla u \cdot \nabla v + cuv\, dx$ and $l(v) := \int_\Omega fv\, dx$. A solution u of (1.3.2) is called a weak solution of problem (1.3.1). We get the coercivity of the bilinear form $B(\cdot, \cdot)$ by using the Poincaré inequality. Since the bilinear form $B(\cdot, \cdot)$ and the linear form $l(\cdot)$ are continuous, the Lax-Milgram Lemma guarantees the existence and uniqueness of the solution of the variational equation (1.3.2).

LEMMA 1.6 (**Lax-Milgram**[**130**]). *Let H be a Hilbert space and let*

$$B : H \times H \to \mathbb{R}$$

be a bilinear mapping. Suppose there exist positive constants c_1 and c_2 such that

$$|B(v, w)| \leq c_1 \|v\|_H \|w\|_H, \quad v, w \in H$$

and

$$|B(v, v)| \geq c_2 \|v\|_H^2, \quad v \in H.$$

Then for every $l \in H'$ there exists a unique $u \in H$ such that

$$B(u, v) = l(v), \quad v \in H.$$

Furthermore, there exists a constant C, independent of l, such that

$$\|u\|_H \leq C \|l\|_{H'}.$$

1.4. Mortar finite element methods

We start with decomposing the domain Ω into K non-overlapping d-polytopes Ω_k, $k = 1, \cdots, K$, such that

$$\overline{\Omega} = \bigcup_{k=1}^{K} \overline{\Omega}_k \quad \text{with} \quad \Omega_i \cap \Omega_j = \emptyset \quad \text{for} \quad i \neq j.$$

For each pair $\{k, l\}$ with $1 \leq k, l \leq K$, we define $\bar{\Gamma}_{kl} := \partial\Omega_k \cap \partial\Omega_l$, the intersection of the boundaries of two subdomains, and select only disjoint and non-empty interfaces $\gamma_k, 1 \leq k \leq N$. Moreover, each γ_k can be associated with a couple $\{k_1, k_2\}$, $1 \leq k_1 < k_2 \leq K$, such that $\bar{\gamma}_k = \partial\Omega_{k_1} \cap \partial\Omega_{k_2}$. On each subdomain, we define

$$H_*^1(\Omega_k) := \{v \in H^1(\Omega_k), v_{|\partial\Omega \cap \partial\Omega_k} = 0\}, \quad k = 1, \cdots, K$$

and consider the unconstrained product space $X := \prod_{k=1}^K H_*^1(\Omega_k)$. The weak matching condition on the skeleton $\Gamma := \bigcup_{k=1}^N \gamma_k$ is realized by means of the $H^{1/2}$-duality pairing. The

mortar method is based on introducing the Lagrange multiplier space $M := \prod_{k=1}^{N} H^{-1/2}(\gamma_k)$ on Γ so that for $v \in H_0^1(\Omega)$

$$\int_\Gamma [v]\ \mu\, d\sigma = 0, \quad \mu \in \prod_{k=1}^{N} H^{-1/2}(\gamma_k).$$

This observation is the motivation for the discrete mortar formulation. Each subdomain Ω_k is associated with a shape regular and locally quasi-uniform family of triangulations $\mathcal{T}_k$, the meshsize of which is bounded by h_k, i.e., $h_k := \max_{T\in\mathcal{T}_k} \operatorname{diam} T$. We denote the discrete space of conforming finite elements of order p_k, $p_k \in \mathbb{N}$, on Ω_k associated with $\mathcal{T}_k$ by $X_k \subset H_*^1(\Omega_k)$. Thus the space X_k is spanned by piecewise polynomials of degree p_k for the simplicial triangulation and piecewise polynomials of degree p_k in each dimension for the quadrilateral or hexahedral triangulation and satisfy the homogeneous Dirichlet boundary condition on $\partial\Omega$. Each interface γ_k, $1 \le k \le N$, inherits a $(d-1)$-dimensional triangulation $\mathcal{S}_k$ either from $\mathcal{T}_{k_1}$ or $\mathcal{T}_{k_2}$. The subdomain from which the interface inherits its triangulation is called slave or non-mortar side, the opposite one master or mortar side. In the following, we denote the index of the slave side of γ_k by $s(k)$ and the one of the master side by $m(k)$. Hence, the elements of $\mathcal{S}_k$ are boundary faces of $\mathcal{T}_{s(k)}$ with a meshsize bounded by $h_{s(k)}$. Here, we do not insist that our decomposition is geometrically conforming. However, to avoid the technicality in the construction of a Lagrange multiplier space, we impose the following assumption on the decomposition of the domain.

ASSUMPTION 1. *γ_k is the union of complete $(d-1)$-dimensional faces of elements at the slave side and lies entirely in a $(d-1)$-dimensional hyperplane for $1 \le k \le N$.*

Note that Assumption 1 does allow the partition into subdomains to be geometrically non-conforming; γ_k needs not to be a full face of both $\Omega_{m(k)}$ and $\Omega_{s(k)}$, or even not to be a full face of either $\Omega_{m(k)}$ or $\Omega_{s(k)}$, see Figure 1.1.

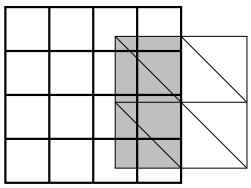

Figure 1.1: A two-dimensional interface that is not a full face of either $\Omega_{m(k)}$ or $\Omega_{s(k)}$; it satisfies Assumption 1 when the square partitioned into triangles is a face of $\Omega_{s(k)}$, but not when this is a face of $\Omega_{m(k)}$, $d = 3$.

Furthermore, we assume that each element in $\mathcal{S}_k$, $1 \le k \le N$, can be affinely mapped to a reference face $\hat{F}$. We point out that the reference face $\hat{F}$ is the $(d-1)$-dimensional reference element. The discrete Lagrange multiplier space M_h on Γ is defined as $M_h := \prod_{k=1}^{N} M_k$, where M_k is the discrete Lagrange multiplier space on γ_k and is assumed that $M_k \subset L^2(\gamma_k)$. Then, the discrete weak matching condition for $v_h \in X_h$ can be written as

$$\int_{\gamma_k} [v_h]\ \mu_i\, d\sigma = 0, \quad 1 \le i \le n_k,\ 1 \le k \le N, \tag{1.4.1}$$

where $n_k := \dim M_k$ and $\{\mu_i\}_{1\le i\le n_k}$ forms a basis of M_k. Here, $[v_h]$ is the jump of the function v_h on γ_k from the master side to the slave side. As usual, we denote the $H^s(\Omega)$ norm and semi-norm by $\|\cdot\|_{s,\Omega}$ and $|\cdot|_{s,\Omega}$, respectively, and the norm on $H^{1/2}_{00}(\gamma)$ and on its dual $H^{-1/2}(\gamma)$ for a $(d-1)$-dimensional polytope γ will be denoted by $\|\cdot\|_{H^{1/2}_{00}(\gamma)}$ and $\|\cdot\|_{-1/2,\gamma}$, respectively. We define the broken norm $\|\cdot\|_s$ on X and the broken dual norm $\|\cdot\|_M$ on M by

$$\|u\|_s^2 := \sum_{k=1}^{K} \|u\|_{s,\Omega_k}^2, \quad \text{and} \quad \|\mu\|_M^2 := \sum_{k=1}^{N} \|\mu\|_{-1/2,\gamma_k}^2, \quad \text{respectively.}$$

There are two main approaches to obtain the mortar solution $u_h \in X_h$ of a discrete variational problem. The first one is based on the positive definite variational problem on the constrained finite element space which is given by means of the global Lagrange multiplier space M_h

$$V_h := \{v_h \in X_h \mid b(v_h, \mu_h) = 0,\ \mu_h \in M_h\},$$

where $b(v_h, \mu_h) := \sum_{k=1}^{N} \int_{\gamma_k} [v_h]\, \mu_h \, d\sigma$, and $X_h := \prod_{k=1}^{K} X_k$. We remark that the elements of the space V_h satisfy a weak continuity condition on the skeleton Γ in terms of the discrete Lagrange multiplier space M_h, and the nodal basis functions of X_h have to be modified appropriately to obtain the basis functions of V_h. However, V_h is, in general, not a subspace of $H^1_0(\Omega)$. The positive definite formulation of the mortar method can be given in terms of the constrained space V_h: find $u_h \in V_h$ such that

$$a(u_h, v_h) = (f, v_h)_0, \quad v_h \in V_h, \tag{1.4.2}$$

where, the bilinear form $a(\cdot,\cdot)$ is defined as $a(v,w) := \sum_{k=1}^{K} \int_{\Omega_k} a\nabla v \cdot \nabla w + cv\, w\, dx$. We assume that a and c are *piecewise smooth with respect to the subdivision into subdomains*, but allow that they have jumps over the interfaces, and $f \in \prod_{k=1}^{K} (H^1_*(\Omega_k))'$. The second approach is based on enforcing the weak continuity condition on the skeleton Γ as an additional variational equation which leads to a saddle point problem on the unconstrained product space X_h, see [**22**]: find $(u_h, \lambda_h) \in X_h \times M_h$ such that

$$\begin{array}{lcll} a(u_h, v_h) + & b(v_h, \lambda_h) & = & (f, v_h)_0, \qquad v_h \in X_h, \\ & b(u_h, \mu_h) & = & 0, \qquad\quad \mu_h \in M_h. \end{array} \tag{1.4.3}$$

It is clear that the choice of the discrete Lagrange multiplier space M_h plays an essential role for the stability of the saddle point problem and the optimality of the discretization scheme. In the next section, we state sufficient conditions on the Lagrange multiplier space to get optimal a priori estimates. We point out that we do not assume the meshes from the slave and master side are matching on $\partial\gamma_k$, see Figure 1.1. The trace space, $X_{s(k)}$ restricted to γ_k, and with zero boundary conditions on $\partial\gamma_k$ will be denoted by W_k, i.e., $W_k := \{w \mid w = v_{|_{\gamma_k}},\ v \in X_{s(k)}\} \cap H^1_0(\gamma_k)$.

We define the product space W_h and the broken $H^{1/2}_{00}$-norm on it as

$$W_h := \prod_{k=1}^{N} W_k, \quad \text{and} \quad \|w\|_W^2 := \sum_{k=1}^{N} \|w\|^2_{H^{1/2}_{00}(\gamma_k)},\ w \in W_h, \quad \text{respectively.}$$

For $1 \leq k \leq K$, if the underlying finite element mesh of X_k is *shape regular* and *quasi-uniform* then we define $\underline{h}_k$ as the constant function of the maximum of the diameters of the elements. If it is only *locally quasi-uniform* instead of quasi-uniform, meaning that any two elements that have non-empty intersection have uniformly comparable diameters, we define $\underline{h}_k$ as the piecewise constant function equal to the diameter of the underlying element, see, e.g., [**65, 139**] so that $h_k = \|\underline{h}_k\|_{L^\infty(\Omega_k)}$. Then we have the following well known inverse inequality on W_k, $1 \leq k \leq N$,

$$\|w\|_{1,\gamma_k} \leq C\|(\underline{h}_{s(k)})^{-1}w\|_{0,\gamma_k}, \quad w \in W_k. \tag{1.4.4}$$

In [**68**], a similar but smoother mesh indicator function is used to deal with inverse inequalities on non-quasi-uniform meshes.

Throughout this thesis the different finite element spaces will be denoted by Roman letters, whereas the matrix will be denoted by the typewriter styled letter. As usual, vector- and tensor-valued functions will be written in boldface letters. A generic but unspecified constant C will be used, which is independent of the meshsize and number of subdomains.

1.5. A priori estimates

In this section, we establish optimal a priori estimates for mortar finite elements without assuming $\dim W_i = \dim M_i$. The assumption $\dim W_i = \dim M_i$ is very often imposed, see, e.g., [**99, 163**]. The relaxation of this assumption will be of great importance to construct dual Lagrange multiplier spaces in the three-dimensional case. In order to guarantee the well-posedness and the optimality of the mortar approach, we impose the following assumptions on our discrete Lagrange multiplier spaces.

ASSUMPTION 2. $\dim M_k \leq \dim W_k, \quad 1 \leq k \leq N.$

ASSUMPTION 3. *There is a constant $\beta_k > 0$ independent of the triangulation such that*

$$\sup_{\theta \in W_k \setminus \{0\}} \frac{(\mu, \theta)_{0,\gamma_k}}{\|\theta\|_{0,\gamma_k}} \geq \beta_k \|\mu\|_{0,\gamma_k}, \quad \mu \in M_k, \quad 1 \leq k \leq N.$$

ASSUMPTION 4. *There is a constant C independent of the triangulation such that*

$$\inf_{\mu \in M_k} \|\lambda - \mu\|_{0,\gamma_k} \leq C h_{s(k)}^{p_{s(k)}} |\lambda|_{p_{s(k)},\gamma_k}, \ \lambda \in H^{p_{s(k)}}(\gamma_k), \ 1 \leq k \leq N.$$

We note that Assumption 4 is satisfied if and only if M_k contains all polynomials of degree $p_{s(k)} - 1$. The natural norm in the mortar setting for the Lagrange multiplier is the broken $H^{-1/2}$-norm on the interior interfaces. Thus to obtain an order $h_{s(k)}^{p_{s(k)}}$ a priori results, it is sufficient to reproduce polynomials of order $p_{s(k)} - 1$ in the Lagrange multiplier space. For each γ_k, the mortar projection $\Pi_k : L^2(\gamma_k) \to W_k$ is defined as

$$\int_{\gamma_k} \Pi_k v \, \mu \, d\sigma := \int_{\gamma_k} v \, \mu \, d\sigma, \quad \mu \in M_k. \tag{1.5.1}$$

The stability of the mortar projection is essential for the optimality of the best approximation error. Under Assumptions 2 and 3, the existence and the stability of the mortar projection follows from the following lemma.

LEMMA 1.7. *Let M, W be closed subspaces of some Hilbert space H, with scalar product $\langle\cdot,\cdot\rangle$ and associated norm $\|\cdot\|$. Then*

$$\beta := \inf_{\mu\in M\setminus\{0\}} \sup_{w\in W\setminus\{0\}} \frac{\langle \mu, w\rangle}{\|\mu\|\|w\|} > 0,$$

if and only if there exists a bounded projector Π from H onto W for which

$$\langle \Pi v, \mu\rangle = \langle v, \mu\rangle, \quad v \in H,\ \mu \in M.$$

Moreover, $\beta^{-1} \le \|\Pi\| \le 1 + 2\beta^{-1}$.

PROOF. Assuming the existence of the bounded projector Π, for any $\mu \in M\setminus\{0\}$ we have

$$\sup_{w\in W\setminus\{0\}} \frac{\langle \mu, w\rangle}{\|\mu\|\|w\|} \ge \frac{\langle \mu, \Pi\mu\rangle}{\|\mu\|\|\Pi\mu\|} \ge \|\Pi\|^{-1}.$$

On the other hand, when $\beta > 0$, given $v \in H$, define $(w, \lambda) \in W \times M$ to be the solution of

$$\begin{array}{lcll} \langle w, z\rangle + & \langle \lambda, z\rangle & = & \langle v, z\rangle, \qquad z \in W, \\ \langle w, \mu\rangle & & = & \langle v, \mu\rangle, \qquad \mu \in M. \end{array}$$

It is well known (see e.g. [**52**, II.1, Proposition 1.3]) that this saddle point problem has a unique solution with $\|w\| \le (1 + 2\beta^{-1})\|v\|$. The second equation yields $w = \Pi v$. □

For the case that we do not have globally quasi-uniform mesh but have only shape regular and locally quasi-uniform mesh, we make an additional assumption that the mortar projections can be selected so that

ASSUMPTION 5. $\|(\underline{h}_{s(k)})^{-1}\Pi_k w\|_{0,\gamma_k} \le C\|(\underline{h}_{s(k)})^{-1} w\|_{0,\gamma_k}, \quad w \in L^2(\gamma_k).$

Under the assumption that the mesh underlying W_k is shape regular and locally quasi-uniform, Assumption 5 is valid when the Π_k are *local* in the sense that $\Pi_k v$ vanishes on an element T whenever v vanishes on all elements that have distance to T less than some absolute multiple of $\mathrm{diam}(T)$. This assumption can easily be verified if the Lagrange multiplier basis functions and the finite element basis functions on the slave side of the interface satisfy the condition of biorthogonality, see [**43, 99, 68, 103**]. However, this assumption may not hold in general without further restriction on the triangulation, see [**99**, A.5].

LEMMA 1.8. *$\Pi_k : L^2(\gamma_k) \to L^2(\gamma_k)$ and $\Pi_k : H^1_0(\gamma_k) \to H^1_0(\gamma_k)$ are uniformly bounded for all $1 \le k \le N$.*

PROOF. We have seen that the first statement is a consequence of Assumption 3 and Lemma 1.7 with $H = L^2(\gamma_k)$. Since the mesh is assumed to be locally quasi-uniform, we can define an operator $Q_k : H^1_0(\gamma_k) \to W_k$ so that for a $w \in H^1_0(\gamma_k)$ we have

$$\|(\underline{h}_{s(k)})^{-1}(w - Q_k w)\|_{0,\gamma_k} \le C\|w\|_{1,\gamma_k} \quad \text{and} \quad \|Q_k w\|_{1,\gamma_k} \le C\|w\|_{1,\gamma_k},$$

see [**65, 139, 68**]. Since Π_k is a projector onto W_k, by Assumption 5 and the inverse inequality (1.4.4) we get

$$\begin{aligned}\|\Pi_k w\|_{1,\gamma_k} &\le \|\Pi_k w - Q_k w\|_{1,\gamma_k} + \|Q_k w\|_{1,\gamma_k}\\ &\le C\|(\underline{h}_{s(k)})^{-1}\Pi_k(w - Q_k w)\|_{0,\gamma_k} + \|Q_k w\|_{1,\gamma_k}\\ &\le C\|(\underline{h}_{s(k)})^{-1}(w - Q_k w)\|_{0,\gamma_k} + \|w\|_{1,\gamma_k}\\ &\le C\|w\|_{1,\gamma_k},\end{aligned}$$

which shows the second statement. □

Interpolating between the L^2- and H^1_0-stability of Π_k, we obtain the $H^{1/2}_{00}$-stability of Π_k so that for $w \in H^{1/2}_{00}(\gamma_k)$, we have

$$\|\Pi_k w\|_{H^{1/2}_{00}(\gamma_k)} \le C\|w\|_{H^{1/2}_{00}(\gamma_k)}. \tag{1.5.2}$$

A simple consequence of the L^2-stability of Π_k and the estimate (1.4.4) is the following corollary.

COROLLARY 1.9. *For $v \in L^2(\gamma_k)$, we have*

$$\|\Pi_k v\|_{H^{1/2}_{00}(\gamma_k)} \le C\|(\underline{h}_{s(k)})^{-\frac{1}{2}} v\|_{0,\gamma_k}. \tag{1.5.3}$$

PROOF. If $w \in W_k$ using an interpolation argument with (1.4.4), see [**152**, Chapter 1], we infer that

$$\|w\|_{H^{1/2}_{00}(\gamma_k)} \le C\|(\underline{h}_{s(k)})^{-\frac{1}{2}} w\|_{0,\gamma_k}. \tag{1.5.4}$$

The estimates of the form (1.5.4) are also established in [**68**]. Again using the interpolation between the L^2-stability of Π_k and Assumption 5, we have

$$\|(\underline{h}_{s(k)})^{-\frac{1}{2}}\Pi_k v\|_{0,\gamma_k} \le \|(\underline{h}_{s(k)})^{-\frac{1}{2}} v\|_{0,\gamma_k}. \tag{1.5.5}$$

Since $\Pi_k v \in W_k \subset H^{1/2}_{00}(\gamma_k)$, we can use (1.5.4) and (1.5.5) to find

$$\|\Pi_k v\|_{H^{1/2}_{00}(\gamma_k)} \le C\|(\underline{h}_{s(k)})^{-\frac{1}{2}}\Pi_k v\|_{0,\gamma_k} \le C\|(\underline{h}_{s(k)})^{-\frac{1}{2}} v\|_{0,\gamma_k}.$$

□

For the solution of the boundary value problem (1.3.2), we assume that

ASSUMPTION 6. *$u \in \prod_{k=1}^K H^{r_k+1}(\Omega_k) \cap H^1_0(\Omega)$ with $r_k > \frac{1}{2}, 1 \le k \le K$.*

Then by using the nodal Lagrange interpolant, we can verify that

$$\begin{aligned}\inf_{v\in X_k} \|u - v\|_{1,\Omega_k} &\le C h_k^{t_k}|u|_{t_k+1,\Omega_k},\\ \inf_{v\in X_k} \|(\underline{h}_k)^{-\frac{1}{2}}(u - v)|_{\partial\Omega_k}\|_{0,\partial\Omega_k} &\le C h_k^{t_k}|u|_{t_k+1,\Omega_k},\ 1 \le k \le K,\end{aligned} \tag{1.5.6}$$

where $t_k := \min(p_k, r_k)$. If we have only $0 < r_k \le \frac{1}{2}$ in Assumption 6, then also the estimates (1.5.6) can easily be verified by using the Scott-Zhang interpolation operator as in [**139**]. If Assumption 6 is satisfied and if a is smooth enough on Ω_k we have $a\frac{\partial u}{\partial \mathbf{n}_k} \in L^2(\gamma_k)$, where $\frac{\partial u}{\partial \mathbf{n}_k}$ is the outer normal derivative of u on γ_k from the master side. Using the ideas

and techniques introduced in [**33, 34, 26**], we prove the best approximation property of the constrained space V_h.

LEMMA 1.10. *Under Assumptions 2–6, there exists a constant C independent of the meshsize such that*

$$\inf_{v_h \in V_h} \|u - v_h\|_1^2 \leq C(1 + h_{mr}) \sum_{k=1}^{K} h_k^{2t_k} \|u\|_{t_k+1,\Omega_k}^2,$$

where

$$h_{mr} := \max_{1 \leq k \leq N} \|\frac{\underline{h}_{m(k)}}{\underline{h}_{s(k)}}\|_{L^\infty(\gamma_k)}.$$

PROOF. Since $W_k \subset H_{00}^{1/2}(\gamma_k)$, each $v_h \in W_k$ can trivially be extended to a function $\tilde{v}_h \in H^{1/2}(\partial\Omega_{s(k)})$. Let $\mathcal{H}_h\tilde{v}_h \in H^1(\Omega_{s(k)})$ be the discrete harmonic extension of $\tilde{v}_h$ on $\Omega_{s(k)}$. Then, $\|\mathcal{H}_h\tilde{v}_h\|_{1,\Omega_{s(k)}} \leq C\|\tilde{v}_h\|_{H^{1/2}(\partial\Omega_{s(k)})} \leq C\|v_h\|_{H_{00}^{1/2}(\gamma_k)}$. By means of this discrete harmonic extension, we define a discrete extension operator $E_k : W_k \to X_h$ for each γ_k as $E_k v_h := \mathcal{H}_h\tilde{v}_h$ on $\Omega_{s(k)}$, and $E_k v_h := 0$ elsewhere. Then

$$\|E_k v_h\|_1 \leq C\|v_h\|_{H_{00}^{1/2}(\gamma_k)}, \quad v_h \in W_k. \tag{1.5.7}$$

Let $I_h u \in X_h$ be the Lagrange interpolant of u in X_h. It is easy to see that $v_h := I_h u + \sum_{k=1}^{N} E_k \Pi_k [I_h u]$ is an element of V_h. Then, we find

$$\|u - v_h\|_1 \leq \|u - I_h u\|_1 + \|\sum_{k=1}^{N} E_k \Pi_k [I_h u]\|_1.$$

By using (1.5.7) and a coloring argument, we have

$$\|\sum_{k=1}^{N} E_k \Pi_k [I_h u]\|_1^2 = \sum_{l=1}^{K} \|\sum_{k=1}^{N} E_k \Pi_k [I_h u]\|_{1,\Omega_l}^2 \leq C \sum_{k=1}^{N} \|\Pi_k [I_h u]\|_{H_{00}^{1/2}(\gamma_k)}^2. \tag{1.5.8}$$

We note that the constant C does not depend on the number of subdomains. Using the result of Corollary 1.9, we get

$$\begin{aligned}
&\|\Pi_k [I_h u]\|_{H_{00}^{1/2}(\gamma_k)}^2 \leq C\|(\underline{h}_{s(k)})^{-\frac{1}{2}} [I_h u]\|_{0,\gamma_k}^2 \\
\leq\ & C\left(\|(\underline{h}_{s(k)})^{-\frac{1}{2}}(u - I_h u)_{|\Omega_{m(k)}}\|_{0,\gamma_k}^2 + \|(\underline{h}_{s(k)})^{-\frac{1}{2}}(u - I_h u)_{|\Omega_{s(k)}}\|_{0,\gamma_k}^2\right) \\
\leq\ & C\left(\|\left(\frac{\underline{h}_{m(k)}}{\underline{h}_{s(k)}}\right)^{\frac{1}{2}} (\underline{h}_{m(k)})^{-\frac{1}{2}}(u - I_h u)_{|\Omega_{m(k)}}\|_{0,\gamma_k}^2 + \|(\underline{h}_{s(k)})^{-\frac{1}{2}}(u - I_h u)_{|\Omega_{s(k)}}\|_{0,\gamma_k}^2\right) \\
\leq\ & C\left(\|\frac{\underline{h}_{m(k)}}{\underline{h}_{s(k)}}\|_{L^\infty(\gamma_k)}\|(\underline{h}_{m(k)})^{-\frac{1}{2}}(u - I_h u)_{|\Omega_{m(k)}}\|_{0,\gamma_k}^2 + \|(\underline{h}_{s(k)})^{-\frac{1}{2}}(u - I_h u)_{|\Omega_{s(k)}}\|_{0,\gamma_k}^2\right).
\end{aligned}$$

Summing over all $k = 1, \cdots, N$, and applying the second estimate of (1.5.6), we obtain

$$\|\sum_{k=1}^{N} E_k \Pi_k [I_h u]\|_1^2 \leq C\left(h_{mr} \sum_{k=1}^{N} h_{m(k)}^{2t_{m(k)}} \|u\|_{t_{m(k)}+1,\Omega_{m(k)}}^2 + \sum_{k=1}^{N} h_{s(k)}^{2t_{s(k)}} \|u\|_{t_{s(k)}+1,\Omega_{s(k)}}^2\right).$$

Finally, the lemma follows by using the interpolation property of $I_h u$. $\square$

THEOREM 1.11. *Let u and u_h be the solutions of the problems* (1.3.2) *and* (1.4.2), *respectively. If Assumptions 1–6 are satisfied, and $[a\frac{\partial u}{\partial \mathbf{n}}] = 0$ on Γ, there exists a constant C independent of the meshsize such that*

$$\|u - u_h\|_1^2 \le C(1 + h_{mr}) \sum_{k=1}^{K} h_k^{2t_k} \|u\|_{t_k+1,\Omega_k}^2$$

with h_{mr} as defined in Lemma 1.10.

PROOF. The bilinear form $a(\cdot,\cdot)$ is continuous on X, and it is coercive on

$$B^* := \left\{ v \,|\, v \in H_*^1(\Omega_k), 1 \le k \le K, \text{ and } \int_{\gamma_k} [v]\, d\sigma = 0,\ 1 \le k \le N \right\},$$

see [**33**]. Assumption 4 assures that $V_h \subset B^*$. Thus, Strang's Lemma [**50**] can be applied, and we get

$$\|u - u_h\|_1 \le C \left(\inf_{v_h \in V_h} \|u - v_h\|_1 + \sup_{v_h \in V_h \setminus \{0\}} \frac{|a(u - u_h, v_h)|}{\|v_h\|_1} \right). \tag{1.5.9}$$

The first term in the right side of (1.5.9) denotes the best approximation error and the second one stands for the consistency error. Lemma 1.10 guarantees the required order for the best approximation error. Thus it is sufficient to consider the consistency error in more detail. Now, $a(u - u_h, v_h)$ can be written as

$$a(u - u_h, v_h) = \int_\Gamma a \frac{\partial u}{\partial \mathbf{n}} [v_h]\, d\sigma = \sum_{k=1}^{N} \left(a \frac{\partial u}{\partial \mathbf{n}_k}, [v_h] \right)_{0,\gamma_k}, \quad v_h \in V_h,$$

where $\frac{\partial u}{\partial \mathbf{n}}$ is the outward normal derivative of u on Γ from the master side, and $\frac{\partial u}{\partial \mathbf{n}} = \frac{\partial u}{\partial \mathbf{n}_k}$ on γ_k. We take $\mu \in M_k$, then the definition of V_h yields

$$\left(a \frac{\partial u}{\partial \mathbf{n}_k}, [v_h] \right)_{0,\gamma_k} = \left(a \frac{\partial u}{\partial \mathbf{n}_k} - \mu, [v_h] \right)_{0,\gamma_k}.$$

Since $\mu \in M_k$ is arbitrary, we can bound the consistency error by

$$\left(a \frac{\partial u}{\partial \mathbf{n}_k}, [v_h] \right)_{0,\gamma_k} \le \inf_{\mu \in M_k} \|a \frac{\partial u}{\partial \mathbf{n}_k} - \mu\|_{\left(H^{1/2}(\gamma_k)\right)'} \|[v_h]\|_{1/2,\gamma_k}.$$

Let $P : L^2(\gamma_k) \to M_k$ be the L^2-projection onto M_k. Using Assumption 4 and interpolation between $L^2(\gamma_k)$ and $H^{t_{s(k)}}(\gamma_k)$, we obtain

$$\|w - Pw\|_{0,\gamma_k} \le C h_{s(k)}^{t_{s(k)} - \frac{1}{2}} \|w\|_{t_{s(k)} - \frac{1}{2}, \gamma_k}, \quad w \in H^{t_{s(k)} - \frac{1}{2}}(\gamma_k).$$

In terms of the standard Aubin–Nitsche trick and the previous estimate, we get

$$\|w - Pw\|_{\left(H^{1/2}(\gamma_k)\right)'} \le C h_{s(k)}^{1/2} \|w - Pw\|_{0,\gamma_k} \le C h_{s(k)}^{t_{s(k)}} \|w\|_{t_{s(k)} - \frac{1}{2}, \gamma_k}.$$

Using the above estimate, we have

$$\left(a\frac{\partial u}{\partial \mathbf{n}_k},[v_h]\right)_{0,\gamma_k} \leq Ch_{s(k)}^{t_{s(k)}}\left\|\frac{\partial u}{\partial \mathbf{n}_k}\right\|_{t_{s(k)}-\frac{1}{2},\gamma_k}\|[v_h]\|_{1/2,\gamma_k}. \tag{1.5.10}$$

Finally, the trace theorem [**84, 30, 31**] yields

$$\left(a\frac{\partial u}{\partial \mathbf{n}_k},[v_h]\right)_{0,\gamma_k} \leq Ch_{s(k)}^{t_{s(k)}}\|u\|_{t_{s(k)}+1,\Omega_{s(k)}}\left(\|v_h\|_{1,\Omega_{m(k)}}+\|v_h\|_{1,\Omega_{s(k)}}\right).$$

Now, summing over all $k=1,\cdots,N$ and using the Cauchy–Schwarz inequality, we obtain

$$|a(u-u_h,v_h)|\leq C\|v_h\|_1\left(\sum_{k=1}^{K}h_k^{2t_k}\|u\|_{t_k+1,\Omega_k}^2\right)^{1/2}. \tag{1.5.11}$$

□

Remark 1.12. *Assumption 6 requires that the exact solution*

$$u\in\prod_{k=1}^{K}H^{r_k+1}(\Omega_k)\cap H_0^1(\Omega) \text{ with } r_k>\frac{1}{2} \text{ for } 1\leq k\leq K.$$

Then the nodal Lagrange interpolant I_hu is well-defined, and the normal derivative $\frac{\partial u}{\partial \mathbf{n}_k}\in L^2(\gamma_k)$, which allows us to use the trace theorem. If we have only $0<r_k\leq\frac{1}{2}$, we can replace the Lagrange interpolant I_hu by an interpolation operator of Scott-Zhang type [**139**]. *The proof of Lemma 1.10 also goes analogously as above also in this case. However, the general trace theorem cannot be applied. If we assume that the normal derivative $\frac{\partial u}{\partial \mathbf{n}_k}\in H^{r_{s(k)}-\frac{1}{2}}(\gamma_k)$, then the estimate* (1.5.10) *of Theorem 1.11 is still true. As $p_k\geq 1$ for $1\leq k\leq K$, we have $r_k=t_k$ in this case. Since we cannot apply the trace theorem in this case, instead of the estimate* (1.5.11), *we obtain*

$$|a(u-u_h,v_h)|\leq C\|v_h\|_1\left(\sum_{k=1}^{N}h_{s(k)}^{2r_{s(k)}}\|\frac{\partial u}{\partial \mathbf{n}_k}\|_{r_{s(k)}-\frac{1}{2},\gamma_k}^2\right)^{1/2}.$$

However, under the assumption that $f\in L^2(\Omega_{s(k)})$ and $u\in H^{r_{s(k)}+1}(\Omega_{s(k)})$, $r_{s(k)}\neq\frac{1}{2}$, the normal trace $\frac{\partial u}{\partial \mathbf{n}_k}\in H^{r_{s(k)}-\frac{1}{2}}(\gamma_k)$, and it holds that [**67, 83, 13**]

$$\|\frac{\partial u}{\partial \mathbf{n}_k}\|_{r_{s(k)}-\frac{1}{2},\gamma_k}^2\leq C\left(\|f\|_{0,\Omega_{s(k)}}^2+\|u\|_{r_{s(k)}+1,\Omega_{s(k)}}^2\right).$$

Hence, the L^2-norm of f enters into the a priori estimate of Theorem 1.11 in this case. The case $r_{s(k)}=\frac{1}{2}$ can be treated by using an operator interpolation theory or by improving the result of [**67**]. *Similar estimates are obtained in* [**27**] *in the context of hp mortar finite elements by using an operator interpolation theory.*

We remark that in the two-dimensional mortar situation if the underlying decomposition of the domain Ω is geometrically conforming, where the intersection between the boundaries of any two different subdomains is either empty, a vertex or a common edge, the constant in the right hand side does not depend on the ratio of meshsizes of master and slave sides. In the three-dimensional case, even if the decomposition of the domain

is geometrically conforming the constant depends on the ratio of meshsizes of master and slave sides if the mesh on the wirebasket is non-conforming. However, if the mesh on the wirebasket is conforming and u is continuous, we find $[I_h u] \in H_{00}^{1/2}(\gamma_k)$ on γ_k, and thus the $H_{00}^{1/2}$-stability of Π_k can be directly applied exactly as in the two-dimensional geometrically conforming decomposition setting. In that case, the ratio does not enter in the upper bound, see [**99**].

COROLLARY 1.13. *Suppose that the Lagrange interpolant $I_h u$ of u in X with respect to the underlying mesh satisfies $[I_h u] \in H_{00}^{1/2}(\gamma_k)$ on γ_k. Then under the assumptions of Lemma 1.10 there exists a constant C independent of the meshsize such that*

$$\inf_{v_h \in V_h} \|u - v_h\|_1^2 \leq C \sum_{k=1}^{K} h_k^{2t_k} \|u\|_{t_k+1,\Omega_k}^2,$$

PROOF. Proceeding exactly as in Lemma 1.10, we obtain (1.5.8), and we use the $H_{00}^{1/2}$-stability of Π_k to get

$$\begin{aligned} \|\Pi_k [I_h u]\|_{H_{00}^{1/2}(\gamma_k)} &\leq C \|[I_h u]\|_{H_{00}^{1/2}(\gamma_k)} \\ &\leq C \|(u - I_h u)_{|\Omega_{m(k)}}\|_{H_{00}^{1/2}(\gamma_k)} + \|(u - I_h u)_{|\Omega_{s(k)}}\|_{H_{00}^{1/2}(\gamma_k)}. \end{aligned}$$

Summing over all $k = 1, \cdots, N$, and using the approximation property of the Lagrange interpolant $I_h u$, we have

$$\|\sum_{k=1}^{N} E_k \Pi_k [I_h u]\|_1^2 \leq C \left(\sum_{k=1}^{N} h_{m(k)}^{2t_{m(k)}} \|u\|_{t_{m(k)}+1,\Omega_{m(k)}}^2 + \sum_{k=1}^{N} h_{s(k)}^{2t_{s(k)}} \|u\|_{t_{s(k)}+1,\Omega_{s(k)}}^2 \right).$$

The rest of the proof follows exactly as in Lemma 1.10. □

On the other hand, assuming *quasi-uniform meshes* on each subdomain without imposing the matching condition, we will demonstrate a new result that the factor h_{mr} can be replaced by the logarithm of it if $h_{mr} > 1$. Although, when having quasi-uniform meshes on each subdomain, for each interface the slave and master sides can be selected such that the mesh size at the master side is less than or equal to that at the slave side, it shows that a different choice of master and slave sides do not affect the bound for the errors. It is well known that the interpolation space $[H_0^1(\gamma_k), L^2(\gamma_k)]_\theta$ is equal to $H_0^{1-\theta}(\gamma_k)$ for $\theta \in [0, \frac{1}{2})$, and that it is equal to $H^{1-\theta}(\gamma_k)$ for $\theta \in (\frac{1}{2}, 1]$, meaning that the corresponding spaces are equal as sets and have equivalent norms. The space $[H_0^1(\gamma_k), L^2(\gamma_k)]_{1/2}$ is strictly contained in $H_0^{1/2}(\gamma_k)$ with a strictly finer topology. In the following, we will consider these interpolation spaces for $\theta \downarrow \frac{1}{2}$. Since norm equivalences stated earlier do not hold uniformly in $\theta \in (\frac{1}{2}, 1]$ we need a lemma, which is proved in [**103**]. We state and prove this lemma for completeness.

LEMMA 1.14. *For $1 \leq k \leq N$ and $\theta \in [0,1] \backslash \{\frac{1}{2}\}$, we have*

$$\sup_{v \in [H_0^1(\gamma_k), L^2(\gamma_k)]_\theta \backslash \{0\}} \frac{\|v\|_{[H_0^1(\gamma_k), L^2(\gamma_k)]_\theta}}{\|v\|_{H^{1-\theta}(\gamma_k)}} \leq C \left| \tfrac{1}{2} - \theta \right|^{-1}.$$

PROOF. Consider γ_k as being a polytope in $\mathbb{R}^{d-1}$. For any function v on γ_k, let $\tilde{v}$ denotes its extension on $\mathbb{R}^{d-1}$ with zero. Then we have $\|v\|_{[H_0^1(\gamma_k),L^2(\gamma_k)]_\theta} \leq C\|\tilde{v}\|_{H^{1-\theta}(\mathbb{R}^{d-1})}$ uniformly in $v \in [H_0^1(\gamma_k), L^2(\gamma_k)]_\theta$ and $\theta \in [0,1]$. From [**83**, Lemma 1.3.2.6 and Theorem 1.4.4.4] it follows that for any $\theta \in [0,1]\backslash\{\frac{1}{2}\}$, there exists a constant $C_\theta > 0$ such that $\|\tilde{v}\|_{H^{1-\theta}(\mathbb{R}^{d-1})} \leq C_\theta \|v\|_{H^{1-\theta}(\gamma_k)}$ for all $v \in [H_0^1(\gamma_k), L^2(\gamma_k)]_\theta$. Inspection of the proof of Theorem 1.4.4.4 in [**83**] reveals that C_θ is a result of the application of Hardy's inequality, and that it can be bounded by some absolute multiple of $\left|\frac{1}{2}-\theta\right|^{-1}$. □

THEOREM 1.15. *Let u and u_h be the solutions of the problems* (1.3.2) *and* (1.4.2)*, respectively. Assume that Assumptions 1–6 are satisfied, and $[a\frac{\partial u}{\partial \mathbf{n}}] = 0$ on Γ. If $h_{mr} >$ $\exp(2)$, there exists a constant C independent of the meshsize such that*

$$\|u - u_h\|_1^2 \leq C(1 + \log^2 h_{mr}) \sum_{k=1}^{K} h_k^{2t_k} \|u\|_{t_k+1,\Omega_k}^2.$$

PROOF. Starting from (1.5.8) and using the inverse estimate, we have

$$\|\Pi_k[I_h u]\|_{H_{00}^{1/2}(\gamma_k)}^2 \leq \frac{C}{h_{s(k)}} \|[I_h u]\|_{0,\gamma_k}^2.$$

Now, by Assumption 5, Lemma 1.8 and interpolation, we have that $\Pi_k : [H_0^1(\gamma_k), L^2(\gamma_k)]_\theta \to [H_0^1(\gamma_k), L^2(\gamma_k)]_\theta$ is bounded uniformly for $\theta \in [0,1]$. So by interpolation and the reiteration theorem [**152**], we have $\|\Pi_k[I_h u]\|_{H_{00}^{1/2}(\gamma_k)} \leq C(h_{s(k)})^{-\epsilon} \|[I_h u]\|_{[H_0^1(\gamma_k),L^2(\gamma_k)]_{\frac{1}{2}+\epsilon}}$ for $\epsilon \in (0, \frac{1}{2}]$.

Now, we can apply Lemma 1.14 with $\theta = \frac{1}{2} + \epsilon$ to find that

$$\begin{aligned}
\|\Pi_k[I_h u]\|_{H_{00}^{\frac{1}{2}}(\gamma_k)} &\leq C(h_{s(k)})^{-\epsilon}\epsilon^{-1}\big(\|(u - I_h u)|_{\Omega_{m(k)}}\|_{H^{\frac{1}{2}-\epsilon}(\gamma_k)} + \|(u - I_h u)|_{\Omega_{s(k)}}\|_{H^{\frac{1}{2}-\epsilon}(\gamma_k)}\big) \\
&\leq C(h_{s(k)})^{-\epsilon}\epsilon^{-1}\{\|u - I_h u\|_{H^{1-\epsilon}(\Omega_{m(k)})} + \|u - I_h u\|_{H^{1-\epsilon}(\Omega_{s(k)})}\},
\end{aligned}$$

where we have used the fact that the trace operator is bounded from $H^{1-\epsilon}(\Omega_k) \to H^{\frac{1}{2}-\epsilon}(\partial\Omega_k)$ uniformly in $\epsilon \in (0, \frac{1}{2})$. Now, using the best approximation property of X_h we obtain

$$\begin{aligned}
\|\Pi_k[I_h u]\|_{H_{00}^{\frac{1}{2}}(\gamma_k)}^2 \leq & \quad \frac{C}{h_{s(k)}^{2\epsilon}\epsilon^2}\left(h_{m(k)}^{2t_{m(k)}+2\epsilon}\|u\|_{t_{m(k)}+1,\Omega_{m(k)}}^2 + h_{s(k)}^{2t_{s(k)}+2\epsilon}\|u\|_{t_{s(k)}+1,\Omega_{s(k)}}^2\right) \\
\leq & \quad \frac{C}{\epsilon^2}\left(\left(\frac{h_{m(k)}}{h_{s(k)}}\right)^{2\epsilon} h_{m(k)}^{2t_{m(k)}}\|u\|_{t_{m(k)}+1,\Omega_{m(k)}}^2 + h_{s(k)}^{2t_{s(k)}}\|u\|_{t_{s(k)}+1,\Omega_{s(k)}}^2\right)
\end{aligned}$$

Summing over all $k = 1, \cdots, N$, we obtain

$$\|\sum_{k=1}^{N} E_k\Pi_k[I_h u]\|_1^2 \leq \frac{C}{\epsilon^2}\left(h_{mr}^{2\epsilon}\sum_{k=1}^{N} h_{m(k)}^{2t_{m(k)}}\|u\|_{t_k+1,\Omega_{m(k)}}^2 + \sum_{k=1}^{N} h_{s(k)}^{2t_{s(k)}}\|u\|_{t_k+1,\Omega_{s(k)}}^2\right).$$

We minimize the expression $\frac{h_{mr}^\epsilon}{\epsilon}$ by choosing $\epsilon = \frac{1}{\log h_{mr}}$, and hence

$$\|\sum_{k=1}^{N} E_k\Pi_k[I_h u]\|_1^2 \leq C(\log h_{mr})^2\left(\exp(2)\sum_{k=1}^{N} h_{m(k)}^{2t_{m(k)}}\|u\|_{t_{m(k)}+1,\Omega_{m(k)}}^2 + \sum_{k=1}^{N} h_{s(k)}^{2t_{s(k)}}\|u\|_{t_{s(k)}+1,\Omega_{s(k)}}^2\right).$$

Since $\epsilon \in (0, \frac{1}{2})$, we require that $h_{mr} > \exp(2)$. Finally, the lemma follows by using the interpolation property of $I_h u$. □

To obtain an a priori estimate for the Lagrange multipliers, we follow exactly the same procedures as in [**22**].

LEMMA 1.16. *Assume that the Lagrange multiplier space M_h satisfies Assumptions 2 and 3. Then, for every $\mu \in M_h$, there exists a $v_\mu \in X_h$ such that*

$$\|v_\mu\|_1 \leq C\|\mu\|_M, \quad \|\mu\|_M^2 \leq Cb(v_\mu, \mu) \quad \textit{and} \quad \|[v_\mu]\|_W \leq C\|\mu\|_M.$$

PROOF. By means of the stability of the mortar projection, we get for $\mu \in M_k$

$$\begin{aligned} \|\mu\|_{-1/2,\gamma_k} &= \sup_{\varphi \in H_{00}^{1/2}(\gamma_k)\setminus\{0\}} \frac{(\mu,\varphi)_{0,\gamma_k}}{\|\varphi\|_{H_{00}^{1/2}(\gamma_k)}} \leq C \sup_{\varphi \in H_{00}^{1/2}(\gamma_k)\setminus\{0\}} \frac{(\mu,\Pi_k\varphi)_{0,\gamma_k}}{\|\Pi_k\varphi\|_{H_{00}^{1/2}(\gamma_k)}} \\ &= C \sup_{\varphi \in W_k\setminus\{0\})} \frac{(\mu,\varphi)_{0,\gamma_k}}{\|\varphi\|_{H_{00}^{1/2}(\gamma_k)}} \leq C(\mu,\tilde{\varphi}_k)_{0,\gamma_k} \end{aligned} \tag{1.5.12}$$

for some $\tilde{\varphi}_k \in W_k$ with $\|\tilde{\varphi}_k\|_{H_{00}^{1/2}(\gamma_k)} = 1$. Now, we extend $\tilde{\varphi}_k \in W_k$ to X_h by using the extension operator E_k as defined in Lemma 1.10 to get $E_k\tilde{\varphi}_k =: v_k \in X_h$. Then, we have

$$\|v_k\|_1 \leq C\|\tilde{\varphi}_k\|_{H_{00}^{1/2}(\gamma_k)} \quad \text{and} \quad 0 \leq (\mu,\tilde{\varphi}_k)_{0,\gamma_k} = b(v_k,\mu).$$

Setting $v_\mu := \sum_{k=1}^N b(v_k,\mu)v_k$ and using the fact that $\|v_k\|_1 \leq C$, we get

$$\begin{aligned} \|v_\mu\|_1^2 &= \|\sum_{k=1}^N b(v_k,\mu)v_k\|_1^2 = \sum_{l=1}^K \|\sum_{k=1}^N b(v_k,\mu)v_k\|_{1,\Omega_l}^2 \\ &\leq C\sum_{k=1}^N b(v_k,\mu)^2 \leq C\sum_{k=1}^N \|\mu\|_{-1/2,\gamma_k}^2 = C\|\mu\|_M^2. \end{aligned}$$

This proves the first assertion. Using a coloring argument, the constant C does not depend on the number of subdomains. Furthermore, summing the equation (1.5.12) over all interfaces γ_k, $k = 1, \cdots, N$, we obtain the second assertion

$$\|\mu\|_M^2 \leq C\sum_{k=1}^N b(v_k,\mu)^2 = Cb(v_\mu,\mu).$$

Finally, the third assertion follows from

$$\|[v_\mu]\|_W^2 = \sum_{k=1}^N b(v_k,\mu)^2\|[v_k]\|_{H_{00}^{1/2}(\gamma_k)}^2 = \sum_{k=1}^N b(v_k,\mu)^2 \leq \sum_{k=1}^N \|\mu\|_{-1/2,\gamma_k}^2\|[v_k]\|_{H_{00}^{1/2}(\gamma_k)}^2 = \|\mu\|_M^2.$$

□

We note that the bilinear form $b(\cdot,\cdot)$ on $X_h \times M_h$ is not continuous with respect to the $\|\cdot\|_1$ and $\|\cdot\|_M$ norms. However the uniform inf-sup condition for $\mu_h \in M_h$ can be established on a subspace of X_h. Restricted to this subspace the bilinear form $b(\cdot,\cdot)$ is continuous and thus the standard saddle point theory can be applied, see, e.g., [**52**]. The best approximation property, Lemma 1.16, Assumptions 2–4 and the first equation of the saddle point problem give an a priori estimate for the Lagrange multiplier, see also [**22, 163**].

LEMMA 1.17. *Assume that* (u_h, λ_h) *is the solution of* (1.4.3) *and* $\lambda = a\frac{\partial u}{\partial \mathbf{n}}$. *Then under the assumptions of Theorem 1.11, there exists a constant* C *independent of the meshsize such that*

$$\|\lambda - \lambda_h\|_M^2 \leq C(1 + h_{mr}) \sum_{k=1}^{K} h_k^{2t_k} \|u\|_{t_k+1,\Omega_k}^2$$

with h_{mr} *as defined in Lemma 1.10*

PROOF. Let $\mu_h \in M_h$. Using the triangle inequality we can write

$$\|\lambda - \lambda_h\|_M \leq \|\lambda - \mu_h\|_M + \|\mu_h - \lambda_h\|_M. \tag{1.5.13}$$

The first equation of saddle point problem (1.4.3) yields

$$b(v_h, \mu_h - \lambda_h) = a(u_h - u, v_h) + b(v_h, \mu_h - \lambda), \quad v_h \in X_h.$$

Choosing $v_{\mu_h - \lambda_h}$ as in Lemma 1.16, we obtain

$$\begin{aligned} \|\mu_h - \lambda_h\|_M^2 &\leq Cb(v_{\mu_h-\lambda_h}, \mu_h - \lambda_h) \\ &= Ca(u_h - u, v_{\mu_h-\lambda_h}) + b(v_{\mu_h-\lambda_h}, \mu_h - \lambda) \\ &\leq C(\|u - u_h\|_1 + \|\mu_h - \lambda\|_M)\|\mu_h - \lambda_h\|_M, \end{aligned}$$

and hence

$$\|\mu_h - \lambda_h\|_M \leq C(\|u - u_h\|_1 + \|\mu_h - \lambda\|_M).$$

Using this estimate in (1.5.13), we have

$$\begin{aligned} \|\lambda - \lambda_h\|_M &\leq \|\lambda - \mu_h\|_M + C(\|u - u_h\|_1 + \|\mu_h - \lambda\|_M) \\ &\leq (1 + C)\|\lambda - \mu_h\|_M + C\|u - u_h\|_1. \end{aligned}$$

Finally, the result follows by using the best approximation property of M_h (Assumption 4) and Theorem 1.11. □

REMARK 1.18. *Assuming quasi-uniform meshes, the factor* h_{mr} *can be replaced by only the log of the quotient of the mesh sizes at the master and the slave sides as in Theorem 1.15.*

1.6. Lagrange multiplier spaces

We have seen in the a priori analysis that the discrete Lagrange multiplier space M_h plays a fundamental role for the stability of the saddle point problem and the optimality of the discretization scheme. The Lagrange multiplier space has to be large enough to obtain an optimal consistency error, and it has to be small enough to get an optimal best approximation error and a suitable discrete inf-sup condition. Here, formally we will see that the choice of discrete Lagrange multiplier space also plays an essential role in the numerical efficiency of the mortar approach. In general, the Lagrange multiplier basis functions are defined locally and are associated with some interior nodes of the mesh on $\gamma_k, 1 \leq k \leq N$. We recall that in contrast to the standard literature on mortar finite elements, see, e.g., [**33, 34, 163, 99**], where the assumption

ASSUMPTION 7. $\dim W_k = \dim M_k, 1 \leq k \leq N$

is imposed on Lagrange multiplier spaces, we work with the more flexible Assumption 2. We refer to [**87, 88, 24**] for the relevant work on stabilized mortar finite elements satisfying Assumption 2 but not 7.

In a first step, we briefly discuss Lagrange multiplier spaces satisfying Assumption 7. We group the degrees of freedom of X_h associated with the skeleton Γ into three groups $u_{h|_\Gamma} := (u_m, u_s, u_c)$, where u_m contains all nodal values of u_h on the master sides, u_s consists of all nodal values of u_h at the interior nodes of γ_k on the slave sides, and u_c contains all nodal values at the nodes on the boundary of the interface γ_k on the slave sides, $1 \leq k \leq N$, see Figure 1.2. The associated sets of nodes are called $\mathcal{N}_m$, $\mathcal{N}_s$ and $\mathcal{N}_c$, respectively. Furthermore, we denote by $\mathcal{N}_h$ the set of all nodes in X_h and we set $\mathcal{N}_i := \mathcal{N}_h \backslash (\mathcal{N}_m \cup \mathcal{N}_s \cup \mathcal{N}_c)$. The corresponding nodal values of u_h in $\mathcal{N}_i$ will be denoted by a block vector u_i. Each $j \in \mathcal{N}_h$ will be associated with its geometrical coordinates x_j. Defining $\mathcal{N}_{mc} := \mathcal{N}_m \cup \mathcal{N}_c$, and the corresponding finite element solution u_{mc} the matching condition (1.4.1) can be written in its algebraic form as

$$\mathtt{M}_s u_s + \mathtt{M}_{mc} u_{mc} = 0. \tag{1.6.1}$$

The entries of the mass matrices $\mathtt{M}_s$ and $\mathtt{M}_{mc}$ are given by $m_{ij} := \int_{\gamma_k} [\phi_j]\, \mu_i \, d\sigma$, where

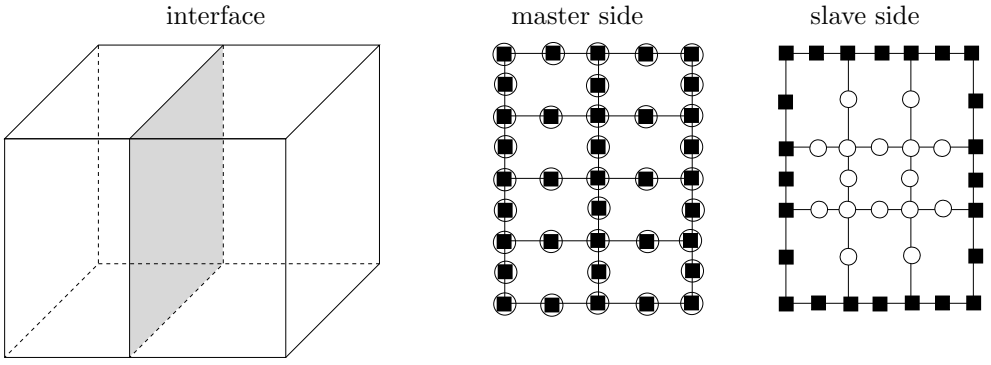

$$\mathcal{N}_m = \{\blacksquare\},\ \mathcal{N}_s = \{\bigcirc\} \text{ and } \mathcal{N}_c = \{\blacksquare\}$$

Figure 1.2: Decomposition of interior degree of freedom at an interface of the master and the slave side for serendipity elements

ϕ_j are the finite element basis functions corresponding to the different groups of nodes, and μ_i denote the basis functions of M_h. Since the basis functions have a local support, the mass matrices are sparse. Formally, we can obtain the values on the slave side as $u_s = -\mathtt{M}_s^{-1} \mathtt{M}_{mc} u_{mc}$. Although $\mathtt{M}_s$ is a sparse matrix, the inverse of $\mathtt{M}_s$ is dense. This observation motivates our interest in Lagrange multiplier spaces which yield a sparse inverse of the mass matrix $\mathtt{M}_s$. A natural choice is a dual Lagrange multiplier space, see, e.g., [**163**], having a diagonal mass matrix $\mathtt{M}_s$. Due to the biorthogonality, the arising mass matrices on the slave side of the mortar formulation are diagonal, and a local static condensation can be carried out. This corresponds physically to a lumping of the mass matrix, and the locality reflects the fact that a local perturbation influences the solution only in a small neighborhood. Therefore, these dual Lagrange multiplier spaces are very attractive from computational and physical points of view. Such a biorthogonal basis was introduced in

[**161**] for lowest order and two-dimensional mortar finite elements, and was called the dual Lagrange multiplier base. The idea has also been extended to higher order elements, see [**104, 103, 124**]. We refer to [**69, 147**] for related work in biorthogonal multi-resolution analysis. However, the construction of biorthogonal bases is not straightforward and preserving the locality of the support is not trivial. In [**124**], one-dimensional higher order dual finite element bases are considered. The drawback of this technique is that the support of the Lagrange multiplier basis has to be extended resulting in more complex assembling routine. Here, we focus on the construction of biorthogonal basis functions having the same support as the nodal basis functions.

Because of the diagonal structure of the mass matrix on the slave side of the interface the degrees of freedom associated to Lagrange multipliers can be locally eliminated leading to a sparse, positive definite formulation based on the unconstrained product space. The modification of the saddle point system arising from mortar finite elements with dual Lagrange multiplier spaces is carried out in [**166**], and a multigrid method based on the new positive definite system is proposed, see also [**163**]. To apply the standard multigrid theory, the transfer operators have to be locally modified. The introduced multigrid has a level-independent convergence rate and is of optimal complexity. Unless otherwise specified, our iterative solver is based on the multigrid approach introduced in [**166**].

Before going to the explicit construction in Chapters 2 and 3, we consider an abstract framework. As in Lemma 1.7, let W and M be finite dimensional subspaces of a Hilbert space H with inner product $\langle \cdot, \cdot \rangle$. We assume that $\dim W = \dim M$ and associate the space W with the basis $\mathbf{\Phi} := \{\phi_1, \cdots, \phi_n\}$ and M with the basis $\mathbf{\Lambda} := \{\lambda_1, \cdots, \lambda_n\}$. To make a consistent matrix notation, basis sets are also thought of as column vectors. We denote by $G_{\mathbf{\Phi},\mathbf{\Lambda}} = (\mathbf{\Phi}, \mathbf{\Lambda}^T)$ the Gram matrix associated with the two finite systems $\mathbf{\Phi}$ and $\mathbf{\Lambda}$ based on the inner product $\langle \cdot, \cdot \rangle$, i.e., $G_{\mathbf{\Phi},\mathbf{\Lambda}}$ is a $n \times n$ matrix with $(G_{\mathbf{\Phi},\mathbf{\Lambda}})_{ij} = \langle \phi_i, \lambda_j \rangle$.

DEFINITION 1.19. *The set $\mathbf{\Lambda}$ will be called a dual basis with respect to $\mathbf{\Phi}$ if and only if $G_{\mathbf{\Phi},\mathbf{\Lambda}} = D_n$, where D_n is a non-singular $n \times n$ diagonal matrix. Equivalently, the bases $\mathbf{\Lambda}$ and $\mathbf{\Phi}$ will be called biorthogonal bases, and the space M spanned by the basis $\mathbf{\Lambda}$ will be called the dual space.*

Hence, if we work with a dual Lagrange multiplier space M_k satisfying Assumption 7, the basis functions $\{\mu_i\}_{1 \le i \le n_k}$ of M_k and $\{\varphi_i\}_{1 \le i \le n_k}$ of the trace space W_k having the zero boundary condition on $\partial\gamma_k$ satisfy the biorthogonality relation

$$\int_{\gamma_k} \mu_i \, \varphi_j \, d\sigma = c_j \delta_{ij}, \; c_j \neq 0, \; 1 \le i, j \le n_k, \tag{1.6.2}$$

where $n_k := \dim W_k = \dim M_k$, and δ_{ij} is the Kronecker symbol. Here, we can take $c_j = \int_{\gamma_k} \varphi_j \, d\sigma$ for the two-dimensional case, and for the three-dimensional case with a hexahedral triangulation. In case of quadratic simplicial finite elements, $\int_{\gamma_k} \varphi_j \, d\sigma = 0$ if φ_j is a vertex basis function. In this case, we can simply set $c_j = |\mathrm{supp}\, \varphi_j|$. A more general definition of the dual Lagrange multiplier space will be provided in the next paragraph. To obtain more flexibility, we focus on constructing optimal and numerically efficient Lagrange multiplier bases. In comparison to the two-dimensional case, the situation is more complicated in the three-dimensional case. As we will see in Chapter 3, the construction of dual Lagrange

multiplier spaces preserving the optimality and the flexibility of the approach in the three-dimensional case is not at all trivial. On the other hand, it is enough to work with a Lagrange multiplier space which yields a sparse mass matrix $\mathtt{M}_s$, whose inverse will be sparse. This observation motivates our interest in a quasi-dual Lagrange multiplier space.

DEFINITION 1.20. *The Lagrange multiplier basis functions* $\{\mu_i\}_{1\le i\le n_k}$ *of* M_k *and the nodal basis functions* $\{\varphi_i\}_{1\le i\le n_k}$ *of the trace space* W_k *are called quasi-biorthogonal and the Lagrange multiplier space quasi-dual if the mass matrix* $\mathtt{M}_s$ *restricted to the slave side of the interface* γ_k *is of the form*

$$\mathtt{M}_s = \begin{bmatrix} \mathtt{D}_1 & 0 \\ \mathtt{R} & \mathtt{D}_2 \end{bmatrix},$$

where $\mathtt{D}_1$ *and* $\mathtt{D}_2$ *are diagonal matrices and* $\mathtt{R}$ *is a rectangular matrix.*

REMARK 1.21. *The idea of the quasi-biorthogonal bases is a natural generalization of the biorthogonal base. If the bases* W_k *and* M_k *are biorthogonal, the rectangular matrix* $\mathtt{R} = 0$. *Thus biorthogonal bases are also quasi-biorthogonal.*

In a second step, we discuss the Lagrange multiplier space which may not satisfy Assumption 7. Assumption 4 requires that the Lagrange multiplier space contains piecewise or continuous piecewise polynomial of degree less than or equal to $p_{s(k)}-1$ on each interface γ_k, $1 \le k \le N$, if finite element space of order $p_{s(k)}$ is used in $\Omega_{s(k)}$. This observation leads to consider a Lagrange multiplier space only satisfying Assumption 2 and not 7. For the Lagrange multiplier space which spans only piecewise *discontinuous* polynomials of degree $p_{s(k)} - 1$ on γ_k, we refer to [**87, 88, 24**]. The drawback of this approach is that the slave side of the interface γ_k should be augmented by some bubble functions to get a stable formulation. The advantage is that the modification of the Lagrange multipliers along the boundary is not necessary. Here, we consider the Lagrange multiplier space which spans piecewise *continuous* polynomials of degree $p_{s(k)} - 1$ for $p_{s(k)} > 1$. Recalling the decomposition of the set of nodes in X_h, we extract a set $\mathcal{N}_l \subset \mathcal{N}_s$ and associate our Lagrange multipliers with the nodes in $\mathcal{N}_l$ with the corresponding finite element solution u_l. Now we give a general definition of the dual Lagrange multiplier space.

DEFINITION 1.22. *The Lagrange multiplier space* M_k *will be called a dual Lagrange multiplier space if the basis functions* $\{\mu_i\}_{1\le i\le l_k}$ *of* M_k *and* $\{\varphi_i\}_{1\le i\le l_k}$ *of the subset* $\mathcal{S}_k$ *of the trace space* W_k *having the zero boundary condition on* $\partial\gamma_k$ *satisfy the biorthogonality condition* (1.6.2)*, where* l_k *is the number of nodes in* $\mathcal{N}_l$.

Examples for quadratic serendipity and simplicial quadratic finite elements in two-dimensional interface at the slave side are shown in Figure 1.3. Defining $\mathcal{N}_r := \mathcal{N}_{mc} \cup (\mathcal{N}_s \backslash \mathcal{N}_l)$, and the associated nodal finite element solution u_r, the equation (1.4.1) can be similarly written in its algebraic form as (1.6.1)

$$\mathtt{M}_l u_l + \mathtt{M}_r u_r = 0,$$

where $\mathtt{M}_l$ is a non-singular diagonal matrix, and $\mathtt{M}_r$ is the rectangular matrix, and hence the static condensation of the Lagrange multiplier can easily be done. The entries of the mass matrices $\mathtt{M}_l$ and $\mathtt{M}_r$ are given by $m_{ij} := \int_{\gamma_k} [\phi_j]\, \mu_i \, d\sigma$ as before. The more detailed discussion and explicit construction can be found in the following chapters.

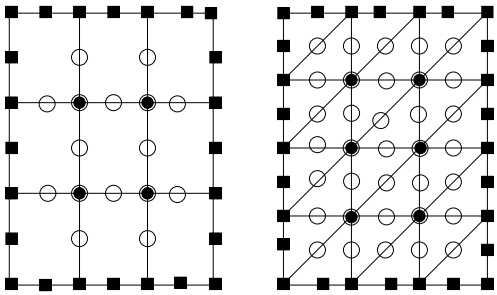

$$\mathcal{N}_s = \{\circledcirc\} \cup \{\bigcirc\},\ \mathcal{N}_l = \{\circledcirc\},\ \mathcal{N}_r = \{\bigcirc\} \cup \mathcal{N}_{mc}$$

Figure 1.3: Decomposition of interior degree of freedom inside a slave side of the interface, quadratic serendipity (left) and simplicial quadratic (right), $d = 3$

In all our forthcoming numerical results for two- and three-dimensional mortar finite elements, we use a mesh dependent L^2-norm to measure the error in the Lagrange multiplier, which is defined as

$$\|\mu - \mu_h\|_h^2 := \sum_{k=1}^{N} \sum_{F \in \mathcal{S}_k} h_F \|\mu - \mu_h\|_{0,F}^2, \tag{1.6.3}$$

where h_F is the length of the edge F on the slave side in the two-dimensional case, and the diameter of the face F on the slave side in the three-dimensional case. This norm will also be called a weighted L^2-norm or a weighted Lagrange multiplier norm.

CHAPTER 2

Lagrange Multiplier Spaces in 2D

2.1. Introduction

We construct basis functions which are biorthogonal to nodal conforming one-dimensional finite element basis functions of order p with respect to the L^2-norm, see the definition of biorthogonality 1.19. The *newly* constructed basis functions have the same support as the conforming nodal basis functions and satisfy Assumption 7. However, as the Lagrange multiplier space satisfying only Assumption 2 can yield optimal results we also provide a result for constructing such a Lagrange multiplier space in Theorem 2.8. The *new* idea is to use Gauß-Lobatto nodes to define the conforming nodal basis functions. Using the finite element basis functions based on Gauß-Lobatto of order p, our biorthogonal basis functions span a non-conforming finite element space which includes the conforming finite element space of order $p-1$, $p>1$. Dual spaces with optimal approximation properties are also considered in [**124**] for higher order finite elements. In contrast to [**124**], our basis functions have the same support as the nodal finite element basis functions. Using this type of non-conforming space as a Lagrange multiplier space for two-dimensional mortar finite elements results in an optimal discretization scheme. The reproduction property of the Lagrange multiplier space is based on an interesting relation between biorthogonality and quadrature formulas. We note that the Lagrange multiplier space has to be modified in a suitable way in the neighborhood of the crosspoints to satisfy a uniform inf-sup condition.

This chapter is organized as follows. In the next section, we construct our dual basis starting from a given set of nodal basis functions on a reference element. In particular, the reproduction property of the dual basis functions is verified. In Section 2.3, we consider the application to mortar finite elements. We work out the required modification at the endpoints of the interfaces. Numerical results for linear, quadratic and cubic finite elements are presented in 2.4. Starting from discontinuous quadratic dual Lagrange multiplier basis functions, we show different ways of constructing continuous dual Lagrange multiplier basis functions in Section 2.5, and finally we compare the numerical results from different Lagrange multipliers in the quadratic case.

2.2. Dual basis in one dimension

Let $\mathcal{Z}_p := \{-1 =: x_1^p < x_2^p < \cdots < x_{p+1}^p := 1\}$ be a set of distinct points in the reference interval $\bar{I} := [-1,1]$, and $\hat{\mathbf{\Phi}}_p := \{\phi_1^p, \phi_2^p, \cdots, \phi_{p+1}^p\}$, $\phi_i^p \in \mathcal{P}_p(I)$, $1 \le i \le p+1$, be the associated set of nodal finite element basis functions, i.e., $\phi_i^p(x_j^p) = \delta_{ij}$, where δ_{ij} is the Kronecker symbol. Here, $\mathcal{P}_p(I)$ denotes the $(p+1)$-dimensional space of polynomials of degree less than or equal to p. From now on, the basis $\hat{\mathbf{\Phi}}_p$ will be called a finite element basis on I of order p based on $\mathcal{Z}_p$. Associated with $\hat{\mathbf{\Phi}}_p$ is the dual basis $\hat{\mathbf{\Lambda}}_p := \{\lambda_1^p, \lambda_2^p, \cdots, \lambda_{p+1}^p\}$,

where the $\lambda_i^p \in \mathcal{P}_p(I)$, $1 \le i \le p+1$, are uniquely defined by

$$\int_I \lambda_i^p(\hat{s})\phi_j^p(\hat{s})\ d\hat{s} = d_i^p\delta_{ij}, \quad d_i^p \neq 0. \tag{2.2.1}$$

We set $d_i^p := \int_I \phi_i^p(\hat{s})\ d\hat{s}$ if the integral is non-zero, and $d_i^p := \int_I d\hat{s}$ otherwise. It is trivial to see that the spaces spanned by $\hat{\mathbf{\Phi}}_p$ and $\hat{\mathbf{\Lambda}}_p$ are the same. Moreover for $q \le p$ there exists a unique $(q+1)\times(p+1)$ matrix $\mathtt{N}^{q;p}$ such that

$$\hat{\mathbf{\Phi}}_q = \mathtt{N}^{q;p}\hat{\mathbf{\Lambda}}_p, \tag{2.2.2}$$

where basis sets $\hat{\mathbf{\Phi}}_q$ and $\hat{\mathbf{\Lambda}}_p$ are thought of as column vectors. To define our global spaces, we introduce a locally quasi-uniform finite element mesh $\mathcal{T}_h$ which is formed by partitioning a segment γ into K subintervals (elements), I_k, $1 \le k \le K$, with $\bar{\gamma} = \cup_{k=1}^K \bar{I}_k$. The ordering of the I_k is done in a lexicographical way from the left to the right. Associated with each element I_k is a unique affine mapping $F_k : \bar{I} \longrightarrow \bar{I}_k$ which maps -1 to the left and 1 to the right endpoint of I_k. Due to the ordering, we find that $F_k(x_1^p) = F_{k-1}(x_{p+1}^p)$, $2 \le k \le K$. We transform the basis functions ϕ_i^p and λ_i^p on I in the standard way, and set $\mathbf{\Phi}_p^k := \{\phi_{k;1}^p, \phi_{k;2}^p, \cdots, \phi_{k;p+1}^p\}$ and $\mathbf{\Lambda}_p^k := \{\lambda_{k;1}^p, \lambda_{k;2}^p, \cdots, \lambda_{k;p+1}^p\}$, where $\phi_{k;i}^p := \phi_i^p \circ F_k^{-1}$ and $\lambda_{k;i}^p := \lambda_i^p \circ F_k^{-1}$. Then it is easy to see that the following biorthogonality relation holds

$$\int_{I_k} \lambda_{k;i}^p(s)\phi_{k;j}^p(s)\ ds = \frac{|I_k|}{2} d_i^p\delta_{ij},$$

and we have $\mathbf{\Phi}_q^k = \mathtt{N}^{q;p}\mathbf{\Lambda}_p^k$ with the same $\mathtt{N}^{q;p}$ as in (2.2.2). Associated with each node $x_j \in \bar{\gamma}$, $1 \le j \le pK+1$, $x_1 := F_1(-1)$, $x_{p(k-1)+j} := F_k(x_j^p)$, $1 \le k \le K$, $2 \le j \le p+1$, is exactly one basis function in $\mathbf{\Phi}_p$ and $\mathbf{\Lambda}_p$. We define

$$\phi_j^p := \begin{cases} \phi_{k;i}^p, & j = p(k-1)+i, 2 \le i \le p, 1 \le k \le K, \\ \phi_{1;1}^p, & j = 1, \\ \phi_{K;p+1}^p, & j = pK+1, \\ \phi_{k;p+1}^p + \phi_{k+1;1}^p, & j = pk+1, 1 \le k < K, \end{cases}$$

where all basis functions $\phi_{k;j}^p$ are extended by zero outside of $\bar{I}_k$, and the addition of two basis functions "$\phi_{k;p+1}^p + \phi_{k+1;1}^p$" has to be interpreted such that $\phi_j^p|_{\bar{I}_k} = \phi_{k;p+1}^p$ and $\phi_j^p|_{\bar{I}_{k+1}} = \phi_{k+1;1}^p$ for $j = pk+1, 1 \le k < K$. We note that this is well defined because $\phi_{k;p+1}^p(x_{pk+1}) = \phi_{k+1;1}^p(x_{pk+1})$. It is well known that the basis $\mathbf{\Phi}_p := \{\phi_1^p, \ldots, \phi_{pK+1}^p\}$ spans the conforming finite element space W_h^p of order p associated with the one-dimensional mesh $\mathcal{T}_h$. Now we define a dual basis of $\mathbf{\Phi}_p$ as $\mathbf{\Lambda}_p := \{\lambda_1^p, \ldots, \lambda_{pK+1}^p\}$, where

$$\lambda_j^p := \begin{cases} \lambda_{k;i}^p, & j = p(k-1)+i, 2 \le i \le p, 1 \le k \le K, \\ \lambda_{1;1}^p, & j = 1, \\ \lambda_{K;p+1}^p, & j = pK+1, \\ \lambda_{k;p+1}^p + \lambda_{k+1;1}^p, & j = pk+1, 1 \le k < K, \end{cases}$$

where the basis functions $\lambda_{k;j}^p$ are extended by zero outside of $\bar{I}_k$ as before, and the sum $\lambda_{k;p+1}^p + \lambda_{k+1;1}^p$ has to be interpreted as an element-wise addition, which gives a well defined function in the L^2-sense. We note that the global basis functions λ_j^p are in general discontinuous at the endpoints of the elements. As a result the space M_h^p spanned by the

basis functions in $\mathbf{\Lambda}_p$ is a non-conforming finite element space. Moreover, we will find that the finite element space of order less than or equal to p on γ will not be included in M_h^p. A first result in this direction is provided by the following lemma.

LEMMA 2.1. *$W_h^q \subset M_h^p$ if and only if*

$$\begin{array}{rcl} n_{1,1}^{q;p} & = & n_{q+1,p+1}^{q;p} \quad \textit{and} \quad n_{q+1,1}^{q;p} = n_{1,p+1}^{q;p} = 0, \\ n_{i,1}^{q;p} & = & n_{i,p+1}^{q;p} = 0 \quad \textit{for all} \quad 2 \leq i \leq q, \end{array} \tag{2.2.3}$$

where $n_{i,j}^{q;p}$ is the (i,j)-th entry of the matrix $\mathbb{N}^{q;p}$.

PROOF. The dimension of W_h^q is given by $qK+1$. In a first step, we consider the basis functions ϕ_j^q, $j = q(k-1)+i$, $2 \leq i \leq q$, $1 \leq k \leq K$, in more detail. Using the definition of the global basis functions, we find

$$\phi_j^q = \phi_{k;i}^q = (\mathbb{N}^{q;p} \mathbf{\Lambda}_p^k)_i = \sum_{l=1}^{p+1} n_{i,l}^{q;p} \lambda_{k;l}^p = n_{i,1}^{q;p} \lambda_{k;1}^p + \sum_{l=2}^{p} n_{i,l}^{q;p} \lambda_{p(k-1)+l}^p + n_{i,p+1}^{q;p} \lambda_{k;p+1}^p.$$

As a result, we obtain that $\phi_j^q \in M_h^p$, $j = q(k-1)+i$, $2 \leq i \leq q$, $1 \leq k \leq K$, if and only if $n_{i,1}^{q;p} = n_{i,p+1}^{q;p} = 0$, $2 \leq i \leq q$. Secondly, we consider the basis functions of W_h^q which are associated with an endpoint of one element. We do not work out the details for ϕ_1^q and ϕ_{qK+1}^q but concentrate on ϕ_{qk+1}^q, $1 \leq k < K$. Each ϕ_{qk+1}^q can be written as an element-wise sum of two local basis functions

$$\begin{array}{rcl} \phi_{qk+1}^q & = & \phi_{k;q+1}^q + \phi_{k+1;1}^q, = (\mathbb{N}^{q;p} \mathbf{\Lambda}_p^k)_{q+1} + (\mathbb{N}^{q;p} \mathbf{\Lambda}_p^{k+1})_1 \\ & = & \displaystyle\sum_{l=1}^{p+1} (n_{q+1,l}^{q;p} \lambda_{k;l}^p + n_{1,l}^{q;p} \lambda_{k+1;l}^p) \\ & = & n_{q+1,1}^{q;p} \lambda_{k;1}^p + (n_{q+1,p+1}^{q;p} - n_{1,1}^{q;p}) \lambda_{k;p+1}^p + n_{1,p+1}^{q;p} \lambda_{k+1;p+1}^p \\ & & + n_{1,1}^{q;p} \lambda_{pk+1}^p + \displaystyle\sum_{l=2}^{p} (n_{q+1,l}^{q;p} \lambda_{p(k-1)+l}^p + n_{1,l}^{q;p} \lambda_{pk+l}^p). \end{array}$$

Now, it is easy to see that $\phi_{qk+1}^q \in M_h^p$, $1 \leq k < K$, if and only if $n_{q+1,p+1}^{q;p} - n_{1,1}^{q;p} = n_{q+1,1}^{q;p} = n_{1,p+1}^{q;p} = 0$. □

The case, $q = p-1$ will be of special interest for mortar finite elements. For simplicity of notation, we denote from now on $\mathbb{N}^{p-1;p}$ by $\mathbb{N}^p$ and $n_{i,j}^{p-1;p}$ by $n_{i,j}^p$. Therefore, we rewrite the general condition (2.2.3) and obtain that $W_h^{p-1} \subset M_h^p$ if and only if

$$\begin{array}{rcl} n_{1,1}^p & = & n_{p,p+1}^p \quad \text{and} \quad n_{p,1}^p = n_{1,p+1}^p = 0 \\ n_{i,1}^p & = & n_{i,p+1}^p = 0 \quad \text{for all} \quad 2 \leq i \leq p-1. \end{array} \tag{2.2.4}$$

To get a better feeling, we consider the case $p = 2$ in more detail. Then the conditions (2.2.4) can be simply written as

$$n_{1,1}^p = n_{2,3}^p \quad \text{and} \quad n_{2,1}^p = n_{1,3}^p = 0. \tag{2.2.5}$$

Let us consider $x_1^p := -1$, $x_2^p := 0$ and $x_3^p := 1$. Then the basis functions of $\hat{\mathbf{\Lambda}}_p$ are given by

$$\lambda_1^p = \frac{5}{4}x^2 - \frac{1}{2}x - \frac{1}{4}, \quad \lambda_2^p = -\frac{5}{2}x^2 + \frac{3}{2}, \quad \lambda_3^p = \frac{5}{4}x^2 + \frac{1}{2}x + \frac{1}{4},$$
$$\lambda_1^p = \phi_1^p - \frac{3}{4}\phi_2^p + \frac{1}{2}, \quad \lambda_2^p = \frac{5}{2}\phi_2^p - 1, \quad \lambda_3^p = \phi_3^p - \frac{3}{4}\phi_2^p + \frac{1}{2},$$

see [**104**]. Using $\phi_1^{p-1} = \phi_1^p + \frac{1}{2}\phi_2^p$ and $\phi_2^{p-1} = \phi_3^p + \frac{1}{2}\phi_2^p$, we find for the entries of the 2×3 matrix $\mathtt{N}^2$

$$n_{1,1}^p = 1, \quad n_{1,2}^p = \frac{1}{2}, \quad n_{1,3}^p = 0,$$
$$n_{2,1}^p = 0, \quad n_{2,2}^p = \frac{1}{2}, \quad n_{2,3}^p = 1,$$

and thus (2.2.5) is satisfied. Unfortunately for $p = 3$ and $x_1^p := -1$, $x_2^p := -1/3$, $x_3^p := 1/3$ and $x_4^p := 1$, (2.2.4) is not satisfied. A straightforward calculation shows that the matrix $\mathtt{N}^p$ for $p = 3$ is given by

$$\mathtt{N}^3 = \begin{bmatrix} \frac{11}{15} & \frac{2}{5} & -\frac{1}{5} & 0 \\ \frac{4}{15} & \frac{4}{5} & \frac{4}{5} & \frac{4}{15} \\ 0 & -\frac{1}{5} & \frac{2}{5} & \frac{11}{15} \end{bmatrix}.$$

Although the conditions $n_{1,1}^3 = n_{3,4}^3$ and $n_{3,1}^3 = n_{1,4}^3 = 0$ are satisfied, we find $n_{2,1}^3 = n_{2,4}^3 = \frac{4}{15} \neq 0$. As a result, working with cubic Lagrange finite elements and dual Lagrange multipliers does not yield optimal a priori results for the mortar discretization. We refer to Section 2.4 for numerical results.

In the rest of this section, we construct for general p, a set of nodal points $\{x_1^p, \ldots, x_{p+1}^p\}$ such that (2.2.4) holds. To start with, we consider $\mathtt{N}^p$ in more detail. The Gram matrix of the finite element base $\hat{\mathbf{\Phi}}_p$ is given by $\mathtt{M}_p = G_{\hat{\mathbf{\Phi}}_p, \hat{\mathbf{\Phi}}_p}$ with the (i,j)-th entry $m_{i,j}^p = \int_I \phi_i(\hat{s})\phi_j(\hat{s})\, d\hat{s}$. We note that $\mathtt{M}_p \in \mathbb{R}^{(p+1)\times(p+1)}$ is positive-definite and symmetric. The set of biorthogonal basis functions satisfying (2.2.1) can be formally given by

$$\hat{\mathbf{\Lambda}}_p = \mathtt{D}_{p+1}\mathtt{M}_p^{-1}\hat{\mathbf{\Phi}}_p \quad \text{with} \quad G_{\hat{\mathbf{\Phi}}, \hat{\mathbf{\Lambda}}} = \mathtt{D}_{p+1}, \tag{2.2.6}$$

where the entries of the diagonal matrix $\mathtt{D}_{p+1}$ are given by $d_i^p \neq 0$. Moreover, we can find a unique restriction matrix $\mathtt{P}_p$ such that $\hat{\mathbf{\Phi}}_{p-1} = \mathtt{P}_p\hat{\mathbf{\Phi}}_p$ yielding

$$\mathtt{P}_p\mathtt{M}_p\mathtt{D}_{p+1}^{-1}\hat{\mathbf{\Lambda}}_p = \hat{\mathbf{\Phi}}_{p-1},$$

and thus $\mathtt{N}^p = \mathtt{P}_p\mathtt{M}_p\mathtt{D}_{p+1}^{-1}$. We recall that the set $\hat{\mathbf{\Phi}}_p$ forms a nodal basis associated with the nodes x_i^p, $1 \leq i \leq p+1$. Then the entries p_{ij}^p of the restriction matrix $\mathtt{P}_p$ are given by $p_{ij}^p = \phi_i^{p-1}(x_j^p)$, $1 \leq i \leq p$, $1 \leq j \leq p+1$. Using the product form of $\mathtt{N}^p$, we find

$$n_{i,j}^p = \frac{1}{d_j^p}\sum_{k=1}^{p+1} \phi_i^{p-1}(x_k^p) \int_I \phi_k^p(\hat{s})\phi_j^p(\hat{s})\, d\hat{s} = \frac{1}{d_j^p}\int_I \phi_i^{p-1}(\hat{s})\phi_j^p(\hat{s})\, d\hat{s}. \tag{2.2.7}$$

LEMMA 2.2. *If the nodal points in $\mathcal{Z}_p$ are symmetric with respect to the origin then*

$$n^p_{1,1} = n^p_{p,p+1}.$$

PROOF. Since the nodal points are symmetric with respect to the origin, we have

$$x^p_i = -x^p_{p+2-i}, \quad 1 \le i \le p+1.$$

Then $\int_I \phi^p_i(\hat{s})\, d\hat{s} = \int_I \phi^p_{p+2-i}(\hat{s})\, d\hat{s}$, and moreover

$$\int_I \phi^{p-1}_1(\hat{s})\phi^p_1(\hat{s})\, d\hat{s} = \int_I \phi^{p-1}_p(\hat{s})\phi^p_{p+1}(\hat{s})\, d\hat{s}.$$

□

Combining (2.2.4) and Lemma 2.2, we obtain the following corollary.

COROLLARY 2.3. *Under the assumption that the nodal points are symmetric with respect to the origin, $W^{p-1}_h \subset M^p_h$ if and only if*

$$\begin{array}{rcll} \int_I \phi^p_1(\hat{s})\phi^{p-1}_i(\hat{s})\, d\hat{s} & = & 0, & 2 \le i \le p, \\ \int_I \phi^p_{p+1}(\hat{s})\phi^{p-1}_i(\hat{s})\, d\hat{s} & = & 0, & 1 \le i \le p-1. \end{array} \tag{2.2.8}$$

We remark that (2.2.8) is equivalent to the condition that ϕ^p_1 and ϕ^p_{p+1} are in a suitable orthogonal subspace of dimension two, i.e.,

$$\phi^p_1 \in \operatorname{span}\{\phi^{p-1}_2, \ldots, \phi^{p-1}_p\}^\perp \subset \mathcal{P}_p(I), \qquad \phi^p_{p+1} \in \operatorname{span}\{\phi^{p-1}_1, \ldots, \phi^{p-1}_{p-1}\}^\perp \subset \mathcal{P}_p(I).$$

Observing $x^{p-1}_1 = x^p_1$ and $x^{p-1}_p = x^p_{p+1}$, we find

$$\phi^p_l(x^p_j)\phi^{p-1}_i(x^p_j) = 0, \quad l = 1, 2 \le i \le p, \text{and } l = p+1, 1 \le i \le p-1.$$

Now, we can easily relate the condition (2.2.8) to a quadrature formula. Let us assume for the moment that associated with the symmetric set of nodal points $-1 = x^p_1 < \ldots < x^p_{p+1} = 1$ is a quadrature formula which is exact for all polynomials of order less than or equal to $2p-1$, then

$$\int_I \phi^p_l(\hat{s})\phi^{p-1}_i(\hat{s})\, d\hat{s} = \sum_{j=1}^{p+1} w^p_j \phi^p_l(x^p_j)\phi^{p-1}_i(x^p_j) = 0 \tag{2.2.9}$$

for $l = 1$, $2 \le i \le p$ and $l = p+1$, $1 \le i \le p-1$. Here, w^p_j denote the weights of the quadrature formula. It is well known that there exists a unique quadrature formula on $\bar{I}$ with $p+1$ nodes satisfying $x^p_1 = -1$ and $x^p_{p+1} = 1$, and being exact for all polynomials of order less than or equal to $2p-1$. This is the family of Gauß-Lobatto quadrature formulas. The nodes are based on Legendre polynomials and satisfy that the set of nodes is symmetric and all weights w^p_j are positive. We note that

$$w^p_j = \int_I \phi^p_j(\hat{s})\, d\hat{s}, \quad 1 \le j \le p+1,$$

and thus we have $d^p_j = \int_I \phi^p_j(\hat{s})\, d\hat{s}$ for all $1 \le j \le p+1$. For convenience of the reader, we recall some characteristic properties of the Legendre polynomials $L_n(x)$ and of the Gauß-Lobatto points which are relevant to our applications, see, e.g., [**70**].

L1 For some $N \in \mathbb{N}$, the set $\{L_0(x), L_1(x), \cdots, L_N(x)\}$ forms a set of orthogonal system on $(-1,1)$ with respect to the L^2-inner product.

L2 The Legendre polynomial of degree n has exactly n distinct real zeros in $(-1,1)$.

L3 If $\{x_1^n < x_2^n < \cdots < x_n^n\}$ be the set of n-zeros of the Legendre polynomial $L_n(x)$, then the identity $\int_{-1}^{1} f(x)\,dx = \sum_{k=1}^{n} w_k^n f(x_k^n)$ holds for all $f \in \mathcal{P}_{2n-1}(-1,1)$ with $w_k^n = \frac{2}{nL_{n-1}(x_k^n)L_n'(x_k^n)}$ for $1 \le k \le n$, where $L_n'(x) = \frac{dL_n(x)}{dx}$.

L4 The polynomial $(1-x^2)L_n'(x)$ is orthogonal to all polynomials of degree less than $n-1$ and has $(n+1)$-distinct zeros in $[-1,1]$. If $\mathcal{Z}_n := \{-1 =: x_1^n < x_2^n < \cdots < x_{n+1}^n =: 1\}$ be the zeros of polynomial $(1-x^2)L_n'(x)$, then $\mathcal{Z}_n$ is the set of Gauß-Lobatto nodes of order n.

L5 If $\mathcal{Z}_n := \{x_1^n < x_2^n < \cdots < x_{n+1}^n\}$ is the set of Gauß-Lobatto nodes of order n, then $\int_{-1}^{1} f(x)\,dx = \sum_{k=1}^{n+1} w_k^n f(x_k^n)$ for all $f \in \mathcal{P}_{2n-1}(-1,1)$ with $w_1^n = w_{n+1}^n = \frac{2}{n(n+1)}$ and $w_k^n = \frac{2}{n(n+1)(L_n(x_k^n))^2}$ for $2 \le k \le n$.

By construction, we specified a set of nodal points such that $W_h^{p-1} \subset M_h^p$. The following theorem shows that this set is unique.

THEOREM 2.4. *$W_h^{p-1} \subset M_h^p$ if and only if the finite element basis $\hat{\mathbf{\Phi}}_p$ which defines M_h^p is based on the set of Gauß-Lobatto points $\mathcal{Z}_p := \{-1 =: x_1^p < \ldots < x_{p+1}^p := 1\}$.*

PROOF. Let $\mathcal{Z}_p := \{-1 =: x_1^p < x_2^p < \cdots < x_{p+1}^p := 1\}$ be the Gauß-Lobatto points, then the nodal points are symmetric with respect to the origin, and moreover (2.2.9) holds. Thus, we are in the setting of Corollary 2.3, and we find $W_h^{p-1} \subset M_h^p$. Now, let us assume that we have $\hat{\mathbf{\Phi}}_p$ such that the associated space M_h^p satisfies $W_h^{p-1} \subset M_h^p$. We observe that the zeros of the polynomial $(\hat{s}+1)\phi_1^p(\hat{s})$ are exactly the nodes in $\mathcal{Z}_p$. In a next step, we show that the polynomial $(\hat{s}+1)\phi_1^p(\hat{s})$ is orthogonal to the polynomial space $\mathcal{P}_{p-2}(I)$. Let $R(\hat{s})$ be in $\mathcal{P}_{p-2}(I)$, we find that $T(\hat{s}) := (\hat{s}+1)R(\hat{s})$ is in $\mathcal{P}_{p-1}(I)$ and $T(-1) = 0$, and thus it can be written as $T(\hat{s}) = \sum_{k=2}^{p} T(x_k^p)\,\phi_k^{p-1}(\hat{s})$. In terms of (2.2.4) and (2.2.7), we find

$$\int_I (\hat{s}+1)\phi_1^p(\hat{s})R(\hat{s})\,d\hat{s} = \int_I \phi_1^p(\hat{s}) \sum_{k=2}^{p} T(x_k^p)\,\phi_k^{p-1}(\hat{s})\,d\hat{s} = 0.$$

Since $(1-\hat{s}^2)L_p'(\hat{s})$ is the unique polynomial (up to a factor) orthogonal to the polynomial space $\mathcal{P}_{p-2}(I)$ in I we obtain that the zeros of $(\hat{s}+1)\phi_1^p(\hat{s})$ are the same as those of $(1-\hat{s}^2)L_p'(\hat{s})$. □

We note that Theorem 2.4 guarantees the existence and uniqueness of the set of points. Now, we reconsider the cases $p=2$ and $p=3$. For $p=2$, we find for the Gauß-Lobatto nodes $\mathcal{Z}_2 := \{-1, 0, 1\}$ which corresponds to the case of Lagrange finite elements. However for $p=3$ the Gauß-Lobatto nodes are given by $\mathcal{Z}_3 := \{-1, -\frac{\sqrt{5}}{5}, \frac{\sqrt{5}}{5}, 1\}$. This set of nodes is not equidistributed. A simple calculation shows that

$$\mathtt{N}^3 := \begin{bmatrix} \frac{1}{6} & \frac{1+\sqrt{5}}{12} & \frac{1-\sqrt{5}}{12} & 0 \\ 0 & \frac{2}{3} & \frac{2}{3} & 0 \\ 0 & \frac{1-\sqrt{5}}{12} & \frac{1+\sqrt{5}}{12} & \frac{1}{6} \end{bmatrix} \mathtt{D}_4^{-1} = \begin{bmatrix} 1 & \frac{1+\sqrt{5}}{10} & \frac{1-\sqrt{5}}{10} & 0 \\ 0 & \frac{4}{5} & \frac{4}{5} & 0 \\ 0 & \frac{1-\sqrt{5}}{10} & \frac{1+\sqrt{5}}{10} & 1 \end{bmatrix}.$$

Having computed $\mathbb{N}^3$, we can directly verify the conditions (2.2.4) and find $W_h^{p-1} \subset M_h^p$. Figures 2.1 and 2.2 show the cubic and quartic nodal basis functions on the reference element associated with the Gauß-Lobatto nodes and the corresponding biorthogonal basis functions

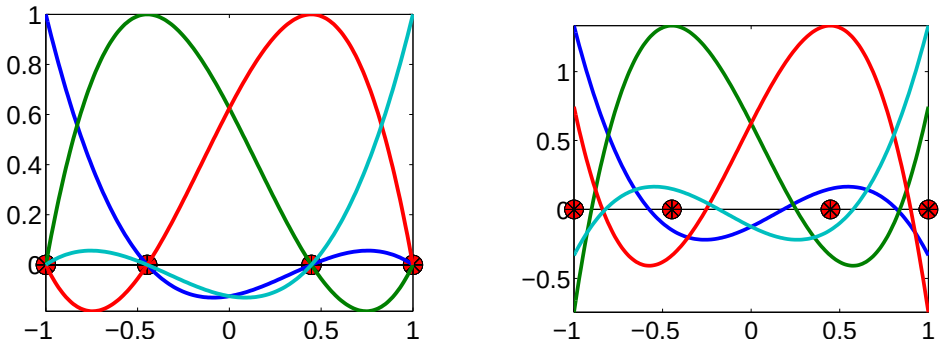

Figure 2.1: The finite element basis functions based on Gauß-Lobatto nodes $\mathcal{Z}_3$ (left) and the corresponding biorthogonal basis functions (right)

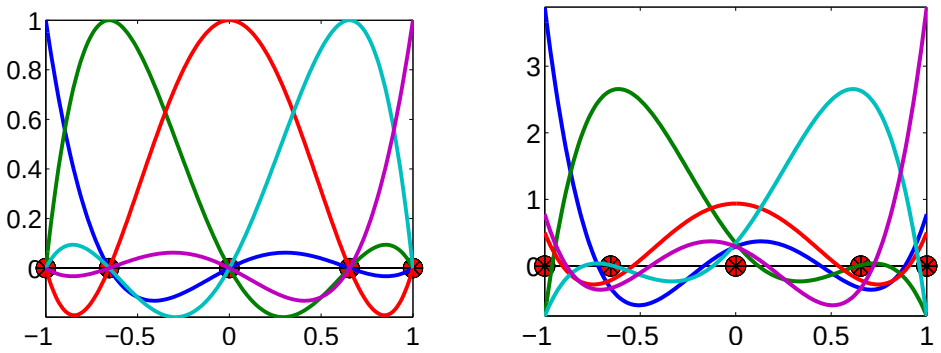

Figure 2.2: The finite element basis functions based on Gauß-Lobatto nodes $\mathcal{Z}_4$ (left) and the corresponding biorthogonal basis functions (right)

REMARK 2.5. *Recently, spectral element methods with nodal polynomial interpolation have been of research interest, see, e.g.,* [**155, 91**]. *Most often Gauß-Lobatto quadrature nodes are used to get a set of interpolation points for the approximation of smooth functions on rectangular meshes. On simplicial meshes such type of nodes are not known. In this case, Fekete points seem to be a natural and good choice, see, e.g.,* [**149, 125**]. *Computational results,* [**149**]*, support the conjecture of Bos* [**36**] *that Fekete points along the one-dimensional boundary of the triangle are the one-dimensional Gauß-Lobatto points. Additionally, it has been shown in* [**37**] *that tensor product Gauß-Lobatto points are Fekete points. Hence, working with Fekete points in two-dimensional finite elements one obtains the Gauß-Lobatto nodes along the boundary of a triangle or a quadrilateral and the biorthogonal base can easily be formed for the Lagrange multiplier space leading to an optimal scheme for the mortar finite elements in two dimensions.*

The next remark is concerned with the quality of convergence of the finite element interpolant based on Gauß-Lobatto and Fekete points.

REMARK 2.6. *It is well known that working with equally spaced interpolation points, uniform convergence in p of the polynomial interpolation cannot be obtained. The so-called Lebesgue constant $C_L(p)$, see, e.g.,* [**57, 149**]*, characterizes the quality of the approximation of the polynomial interpolant. In case of equally spaced points, $C_L(p)$ grows exponentially in p. Although the construction of best approximation polynomials are, in general, not known, it can be shown that working with Fekete points reduces the exponential growth of $C_L(p)$ to a linear growth* [**149**]*. Moreover, numerical results suggest that $C_L(p)$ grows like $\sqrt{p}$ on triangles. In the univariate case, the bound for the Gauß-Lobatto nodes is well known to be logarithmic in p, see* [**57**].

As shown in the first chapter, we can find optimal a priori estimates for mortar finite elements even if the Lagrange multiplier space has a smaller dimension than the trace space of the finite elements on the slave interface side with zero boundary condition, see also [**103**]. However, working with a standard finite element space of order p the Lagrange multiplier space has to reproduce the polynomial space of order $p-1$ to get optimal error estimates. In this section, we consider the construction of a biorthogonal basis of smaller dimension. This construction will also be useful for the modification of Lagrange multipliers around some crosspoint. Let $\mathcal{R}_q := \{y_1 < y_2 < \ldots < y_q\}$ be a proper subset of $\mathcal{Z}_p$ consisting of q distinct points of $\mathcal{Z}_p$ with $q \leq p$, and $\hat{\Phi}_q := \{\phi^p_{l(1)}, \ldots, \phi^p_{l(q)}\}$, $1 \leq l(k) \leq p+1$, be the subset of $\hat{\mathbf{\Phi}}_p$ associated with the nodes in $\mathcal{R}_q$, i.e., $x^p_{l(k)} = y_k$, $1 \leq k \leq q$. We note that $\hat{\Phi}_q$ spans a q-dimensional space and that the set $\hat{\Psi}_q := \{\psi_1, \ldots, \psi_q\}$ with the property $\psi_i \in \mathcal{P}_{q-1}(I)$, $\psi_i(y_j) = \delta_{ij}$ spans the polynomial space of order $q-1$. The following lemma states the biorthogonality between the elements of $\hat{\Phi}_q$ and $\hat{\Psi}_q$.

LEMMA 2.7. *If $\mathcal{Z}_p$ is the set of $(p+1)$-Gauß-Lobatto nodes in $[-1,1]$, then the basis $\hat{\Phi}_q$ is biorthogonal to $\hat{\Psi}_q$.*

PROOF. Using $\phi_{l(k)} \in \mathcal{P}_p(I)$, $1 \leq k \leq q$, $\psi_j \in \mathcal{P}_{q-1}(I)$, $1 \leq j \leq q$ and $q \leq p$ and applying an exact quadrature formula based on the set of $(p+1)$ Gauß-Lobatto nodes $\mathcal{Z}_p$, we find

$$\begin{aligned}\int_I \phi_{l(k)}(\hat{s})\psi_j(\hat{s})\,d\hat{s} &= \sum_{i=1}^{p+1} w_i^p \phi_{l(k)}(x_i^p)\psi_j(x_i^p) = \sum_{i=1}^{p+1} w_i^p \delta_{il(k)}\psi_j(x_i^p) \\ &= w^p_{l(k)}\psi_j(x^p_{l(k)}) = w^p_{l(k)}\psi_j(y_k) = w^p_{l(k)}\delta_{jk}.\end{aligned}$$

□

Of special interest for our crosspoint modifications is the choice $q = p$, and

$$\mathcal{R}_p^{\mathrm{l}} := \{x_2^p < x_3^p < \ldots < x_{p+1}^p\}, \quad \mathcal{R}_p^{\mathrm{r}} := \{x_1^p < x_2^p < \ldots < x_p^p\}.$$

The associated biorthogonal sets will be denoted by $\hat{\Psi}_p^{\mathrm{l}} = \{\psi_1^{\mathrm{l}}, \ldots, \psi_p^{\mathrm{l}}\}$ and $\hat{\Psi}_p^{\mathrm{r}} = \{\psi_1^{\mathrm{r}}, \ldots, \psi_p^{\mathrm{r}}\}$, respectively.

2.3. Boundary modifications

Unfortunately, we cannot apply directly the results of previous section to the general mortar situation. The crucial points are the so-called crosspoints. In a geometrical conforming decomposition of the domain of interest in non-overlapping subdomains, at least three subdomains meet at an interior crosspoint and several interfaces can have this crosspoint as a common endpoint. On each interface, we use our newly constructed spaces M_h^p as discrete Lagrange multiplier space. Working with the product space of Lagrange multipliers associated with the different interfaces, we obtain too many constraints for the nodal values of the finite element solution at the crosspoints. In other words, the inf-sup condition of the arising saddle point formulation cannot be satisfied uniformly. To obtain a uniform bound for the discretization error, we have to reduce the dimension of the Lagrange multiplier space, and to keep the approach as local as possible we have to reduce the dimension of M_h^p associated with each interface. Roughly speaking, we have to remove the two degrees of freedom of the Lagrange multiplier space associated with the endpoints of each interface. In the rest of this section, we consider the required modifications of the Lagrange multipliers in detail. Using the same notation as before, we find that $\mathbf{\Phi}_{0;p} := \{\phi_2^p, \ldots, \phi_{pK}^p\}$ spans the conforming finite element space $W_{0;h}^p := W_h^p \cap H_0^1(\gamma)$ with zero boundary condition. Here K denotes the number of edges on the slave side. Now we define a $(pK-1)$-dimensional Lagrange multiplier space by $\mathbf{\Lambda}_{0;p} := \{\tilde{\lambda}_2^p, \ldots, \tilde{\lambda}_{pK}^p\}$, where

$$\tilde{\lambda}_j^p := \begin{cases} \psi_{j-1}^{\mathrm{l}} \circ F_1^{-1}, & 2 \le j \le p, \\ \psi_p^{\mathrm{l}} \circ F_1^{-1} + \lambda_{2;1}^p, & j = p+1, \\ \lambda_j^p, & p+2 \le j \le p(K-1), \\ \psi_1^{\mathrm{r}} \circ F_K^{-1} + \lambda_{K-1;p+1}^p, & j = p(K-1)+1, \\ \psi_{j-p(K-1)}^{\mathrm{r}} \circ F_K^{-1}, & p(K-1)+2 \le j \le pK. \end{cases}$$

As before, element-wise addition is applied for the sum of two basis functions.

THEOREM 2.8. *The set $\mathbf{\Lambda}_{0;p}$ is a dual basis with respect to $\mathbf{\Phi}_{0;p}$. Moreover $M_m^p :=$ span $\mathbf{\Lambda}_{0;p}$ satisfies $W_h^{p-1}(\gamma) \subset M_m^p$.*

PROOF. By definition of the elements in $\mathbf{\Lambda}_{0;p}$ and by means of Lemma 2.7, the biorthogonality holds. Following the lines as in the proof of Lemma 2.1, we have to consider the first and the last edge of γ. We only work out the details for the first edge. Observing $\phi_j^{p-1}(F_1(x_{p+1}^p)) = 0$, $1 \le j \le p-1$, we find

$$\phi_j^{p-1} = \sum_{i=1}^{p-1} \phi_j^{p-1}(F_1(x_{i+1}^p))\psi_i^{\mathrm{l}} \circ F_1^{-1} = \sum_{i=1}^{p-1} \phi_j^{p-1}(F_1(x_{i+1}^p))\tilde{\lambda}_{i+1}^p \in M_m^p.$$

A similar consideration for $j = p$ yields that $\phi_p^{p-1} \in M_m^p$ if and only if $n_{1,1}^p = 1$. Using the explicit form (2.2.7) of $n_{1,1}^p$, and $\phi_1^p(-1) = \phi_1^{p-1}(-1) = 1$, we find that

$$\int_I \phi_1^{p-1}(\hat{s})\phi_1^p(\hat{s})\, d\hat{s} = w_1^p = \int_I \phi_1^p(\hat{s})\, d\hat{s},$$

and hence

$$n_{1,1}^p = \frac{1}{d_1^p} \int_I \phi_1^{p-1}(\hat{s})\phi_1^p(\hat{s})\, d\hat{s} = \frac{w_1^p}{\int_I \phi_1^p(\hat{s})\, d\hat{s}} = 1.$$

This completes the proof. □

We have shown the modified Lagrange multiplier basis functions in case of the first and the last edge in Figures 2.3 and 2.4 for cubic and quartic case, respectively.

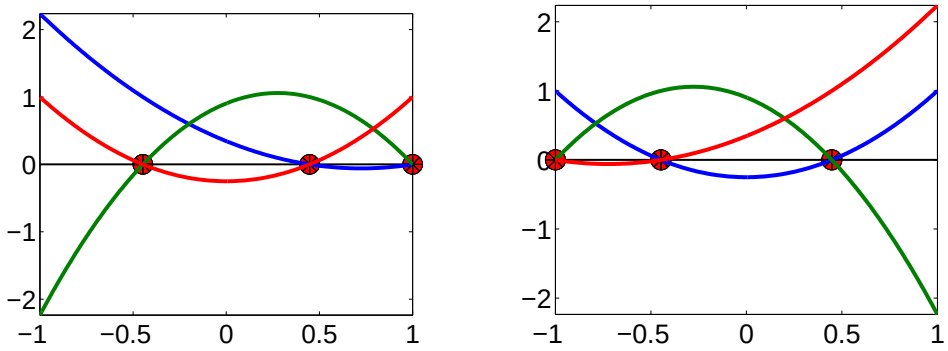

Figure 2.3: The modified Lagrange multiplier basis functions at the crosspoints for the cubic case, the first edge (left) and the last edge (right)

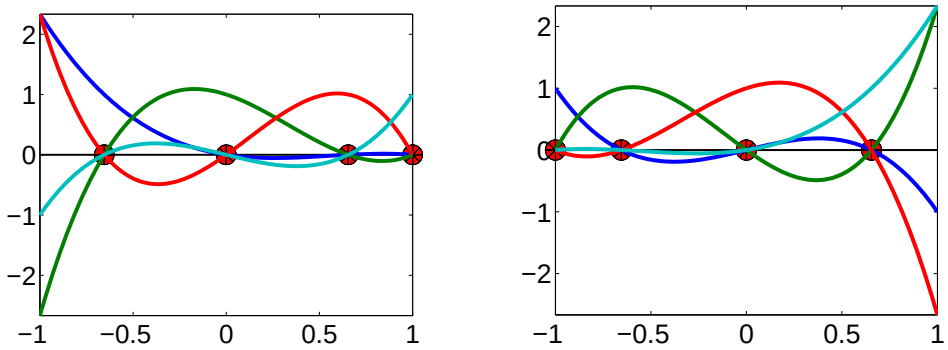

Figure 2.4: The modified Lagrange multiplier basis functions at the crosspoints for the quartic case, the first edge (left) and the last edge (right)

REMARK 2.9. *The Lagrange multiplier basis functions constructed here are, in general, discontinuous. Working with some quadrature formula, it might be advantegous to have continuous Lagrange multiplier basis functions. In Section 2.5, we will demonstrate different possibilities to construct continuous dual Lagrange multiplier basis functions for quadratic mortar finite elements. Similar approach can be adopted for the higher order case.*

Using this type of Lagrange multiplier space in the definition of a mortar finite element method, we obtain optimal a priori estimates and the mass matrix on the slave side is a diagonal one. Now, we briefly discuss the extension of our one-dimensional construction of dual Lagrange multiplier space to the two-dimensional case in a reference element T, where T is the reference square $(-1,1)\times(-1,1)$ or the reference triangle $\{(x,y), x \geq 0, y \geq 0, x+y \leq 1\}$ depending on the quadrangulation or triangulation of the domain. The following remark is concerned with the extension to the two-dimensional case. Unfortunately, in case of a triangle, the straightforward construction as in case of a quadrilateral is not possible.

REMARK 2.10. *Working with a tensor product finite element space from one dimension in quadrilateral meshes, we can apply the idea of one-dimensional construction in a straightforward way. However, since Gauß-Lobatto nodes are, in general, not known for the triangle, the situation with simplicial mesh is much more complicated. The Fekete points in a triangle do not show the nice property of Gauß-Lobatto nodes that any polynomial of degree* $2p-1$ *can be integrated exactly with a suitable choice of weights. A sort of Gauß-Lobatto quadrature formulas of order* 3 *and* 5 *for triangles are constructed in* [**66**]. *However, it is necessary to enrich the finite element space with some bubble functions leading to the requirement of higher order quadrature formulas. Hence one can easily show that a basis biorthogonal to nodal finite element base does not exist for a triangle with optimal approximation property for* $p \geq 2$. *In this case, one can look for a basis biorthogonal to a proper subset of finite element space* $\hat{\mathbf{\Phi}}_p$ *as described above or a basis* $\hat{\mathbf{\Lambda}}_p$ *which leads to a lower or upper triangular mass matrix. We refer to Chapter 3 for the quadratic case, see also* [**103**]. *Although there does not exist a straightforward relation between a quadrature formula and a biorthogonal base in a triangle as in quadrilaterals, from the theory presented above one can figure out that there exists some form of relationship even in this case.*

REMARK 2.11. *It is straightforward to show that the Lagrange multiplier basis functions constructed above satisfy Assumptions 2–4. We note that Assumptions 2 and 4 are trivially satisfied by construction. Now, we verify Assumption 3. Let* $\mu := \sum_{i=1}^{n_k} a_i \mu_i \in M_k$, *and define* $\varphi := \sum_{i=1}^{n_k} a_i \varphi_i \in W_k$. *Assuming* $\underline{h}_{s(k),i}$ *for the local meshsize at* i*-th node, the biorthogonality* (1.6.2) *yields*

$$(\varphi, \mu)_{0,\gamma_k} = \sum_{F \in \mathcal{S}_k} \sum_{i,j=1}^{n_k} a_i a_j (\varphi_i, \mu_j)_{0,F} \equiv \sum_{i=1}^{n_k} \underline{h}^2_{s(k),i} a_i^2 \geq C \|\varphi\|^2_{0,\gamma_k}.$$

Hence, taking into account the fact that $\|\varphi\|^2_{0,\gamma_k} \equiv \|\mu\|^2_{0,\gamma_k} \equiv \sum_{i=1}^{n_k} a_i^2 \underline{h}^2_{s(k),i}$, *we find that Assumption 3 is satisfied.*

2.4. Numerical results

In this section, we present numerical results in two dimensions for various types of domain decompositions. In particular, we demonstrate the performance of our dual Lagrange multiplier spaces by presenting the discretization errors for linear, quadratic and cubic mortar finite elements. For linear finite elements, the dual Lagrange multiplier space introduced in [**161**] is used. The relative errors for the primal solution are measured in the L^2- and H^1-norms, whereas the error in the Lagrange multiplier is measured in the mesh dependent L^2-norm given by (1.6.3).

The flexibility of mortar methods allows us to consider geometrically non-conforming decompositions, non-convex subdomains and crosspoints. Starting with a conforming coarse triangulation on each subdomain, we apply uniform refinement in each step. Here, we choose different exact solutions and different decompositions to illustrate the flexibility and the optimality of mortar approach. The multigrid method based on the unconstrained product space and dual Lagrange multiplier spaces is used for solving the arising linear system, see [**166**]. The implementation is based on the finite element toolbox UG, [**17**].

2.4.1. Problems for Poisson and reaction-diffusion equations.

Example 1: In our first example, we consider a problem with many crosspoints. Here, we consider $-\Delta u = f$ in Ω, where Ω is the unit square $(0,1)^2$. The domain Ω is decomposed into nine squares with $\Omega_{ij} := ((i-1)/3, i/3) \times ((j-1)/3, j/3), 1 \leq i \leq 3, 1 \leq j \leq 3$. The right hand side f and the Dirichlet boundary conditions are chosen such that the exact solution is given by

$$u(x,y) = \sin(3.5\,\pi\,y + x)\, e^{y+(1-x)^2} + \cos(3.5\,\pi\,x + y)\, e^{x+(1-y)^2}.$$

In Figure 2.5, the decomposition of the domain, the initial finite element partition, and the isolines of the solution are shown. Here, we have four interior crosspoints and 12 interfaces, and the master and slave sides are chosen randomly. The discretization errors versus the number of elements along with the order of convergence at each refinement step are given in Figure 2.6. We observe the optimal asymptotic rates of convergence both in the L^2- and H^1-norms. The asymptotic rates confirm the theoretical convergence rates. We find that the energy error is of order h, h^2 and h^3 whereas the errors in the L^2-norm are of order h^2, h^3 and h^4 for the linear, quadratic and cubic case, respectively. The correct order can be observed from the beginning. In the right picture of Figure 2.6, the error in the Lagrange multiplier at the interface is given. The rate of convergence in the weighted Lagrange multiplier norm is of order $h^{3/2}$, $h^{5/2}$ and $h^{7/2}$ for the linear, quadratic and cubic case, respectively.

Although from the theoretical point of view, we can expect that the errors are of order h, h^2 and h^3 in the linear, quadratic and cubic case, respectively, the numerical results show that the convergence is of order $h^{3/2}$ for the linear case, of order $h^{5/2}$ for the quadratic case and of order $h^{7/2}$ for the cubic case. The observed superconvergence behavior can be explained in the same way as in [**164**]. The a priori analysis of the Lagrange multiplier error consists of two terms. The first one is the best approximation property which is of order $h^{p+\frac{1}{2}}$ for the mortar finite elements of order p, whereas the second one involves the energy norm which can only be expected to be of order h^p. However, it is sufficient to take into account the energy error in a small strip of width h on the slave side. If we assume that the error in the energy norm is equidistributed, we find that the error in the strip is bounded by $Ch^{1/2}$ times the error in the slave subdomain. As a consequence, better asymptotic results for the Lagrange multiplier can be observed, see the right picture of Figure 2.6.

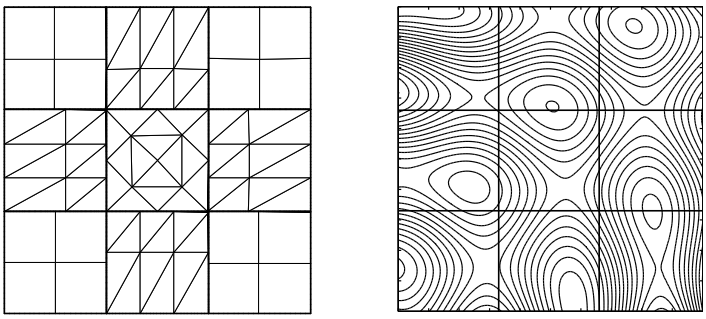

Figure 2.5: Decomposition of the domain and initial partitions (left) and isolines of the solution (right), Example 1

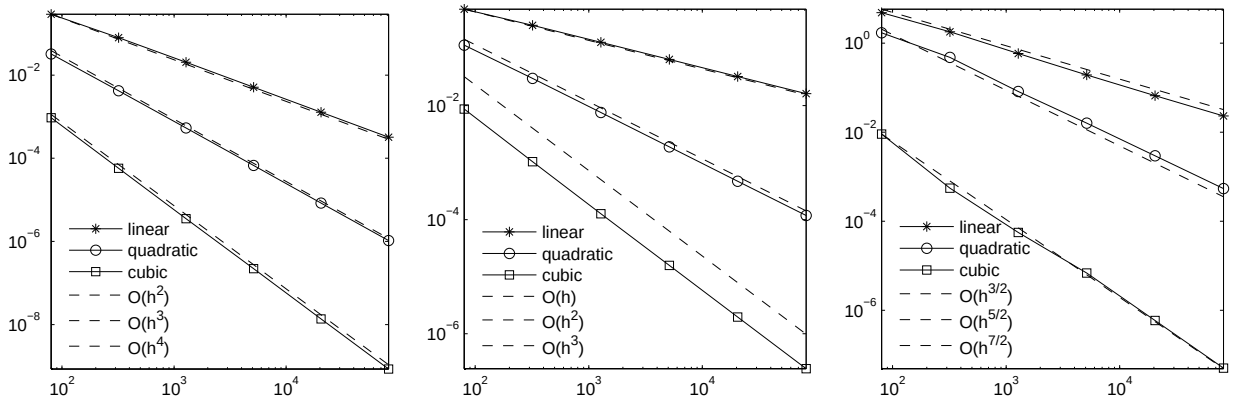

Figure 2.6: Error plot versus number of elements, L^2-norm (left), H^1-norm (middle) and weighted Lagrange multiplier norm (right), Example 1

Example 2: In our next example, we consider a polygonal domain Ω with vertices $(0,0)$, $(1,-1)$, $(2,0)$, $(2,1)$, $(1,2)$ and $(0,1)$ which is decomposed into three subdomains, see Figure 2.7. Here Ω_1 is $(0,2)\times(0,1)$ whereas Ω_2 is a triangle with vertices $(0,0),(1,-1)$ and $(1,0)$, and Ω_3 is also a triangle joining the points $(0,1),(1,2)$ and $(2,1)$. The subdomain Ω_1 is the slave subdomain and Ω_2 and Ω_3 are master subdomains. We have two interior interfaces and four crosspoints. We compute the numerical solution of the Poisson equation $-\Delta u = f$, where the right hand side and the Dirichlet boundary conditions are determined by choosing the exact solution $u(x,y) = \exp(-10(x-y)^2)\cos(x^2+2y^2)+\sin(2x)+\cos(10y)$. Figure 2.7 shows the initial non-matching triangulation and the isolines of the solution.

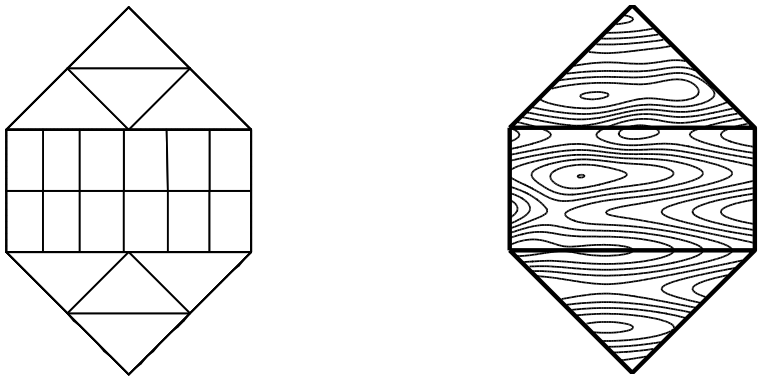

Figure 2.7: Decomposition into three subdomains and initial triangulation (left) and isolines of the solution (right), Example 2

The discretization errors for the different norms versus the number of elements are shown in Figure 2.8. As in the first example, we observe the same asymptotic rates and better convergence rate in the weighted Lagrange multiplier norm. The numerical results confirm the theory.

Example 3: In our third example, we consider a decomposition of the unit square into three subdomains with two non-convex subdomains. The middle subdomain is chosen as the slave side. We have shown the decomposition of the domain and initial non-matching

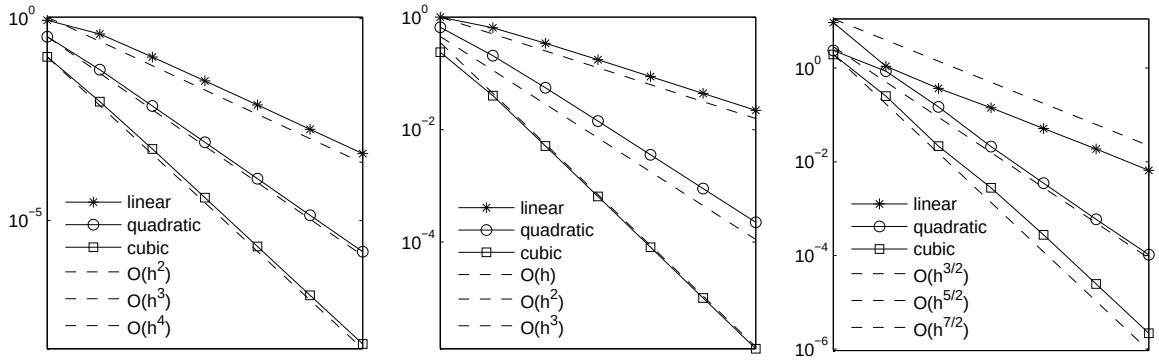

Figure 2.8: Error plot versus number of elements, L^2-norm (left), H^1-norm (middle) and weighted Lagrange multiplier norm (right), Example 2

triangulation in the left picture of Figure 2.9, and the isolines of the solution are shown in the right. The right hand side f and the Dirichlet boundary conditions of $-\Delta u = f$ are chosen from the exact solution, which is given by

$$u(x,y) = x\,(x-y)\,e^{-10.0\,(x-0.5)^2-6.0\,(y-0.5)^2}.$$

The discretization errors in the L^2-, H^1- and in the weighted Lagrange multiplier norms are shown in Figure 2.10. Although two subdomains are non-convex, we observe optimal convergence rates for all considered norms.

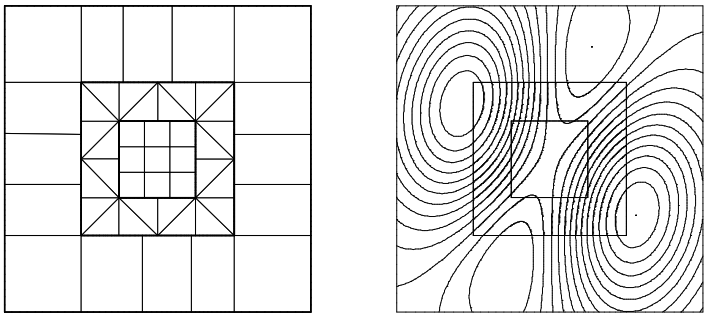

Figure 2.9: Decomposition of the domain and initial partitions (left) and isolines of the solution (right), Example 3

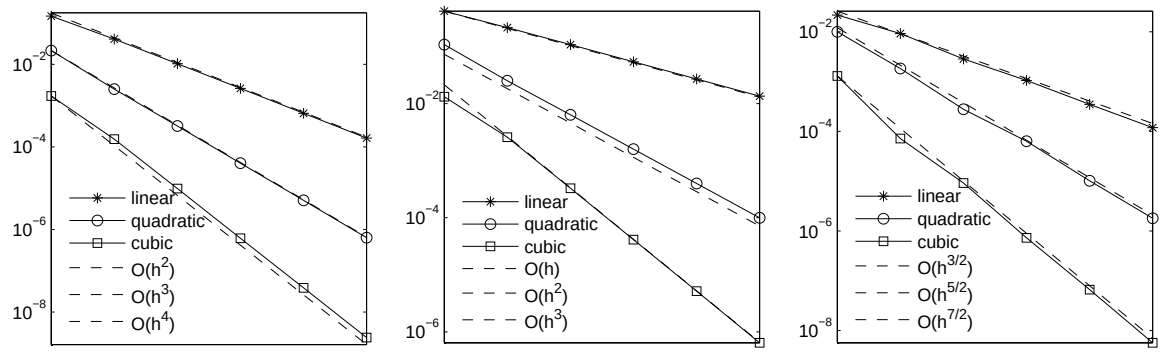

Figure 2.10: Error plot versus number of elements, L^2-norm (left), H^1-norm (middle) and weighted Lagrange multiplier norm (right), Example 3

Example 4: In our fourth example, we consider a decomposition of $\Omega = (0,1) \times (0,1)$ into four subdomains defined by $\Omega_{ij} := ((i-1)/2, i/2) \times ((j-1)/2, j/2), 1 \leq i \leq 2, 1 \leq j \leq 2$, with non-matching triangulations at the interfaces. For this example, we solve a reaction-diffusion equation

$$-\mathrm{div}(a\nabla u) + u = f \quad \text{in} \quad \Omega,$$

and we choose a to be 1 in Ω_{11} and Ω_{22}, and $a = 3$ in Ω_{21} and Ω_{12}. Figure 2.11 shows the decomposition into four subdomains, our initial non-matching triangulation and the isolines of the solution. Here, we choose the exact solution $u(x,y) = (x-1/2)(y-1/2)\exp(-10\,(x-1/2)^2 - 5\,(y-1/2)^2)/a$, see Figure 2.11.

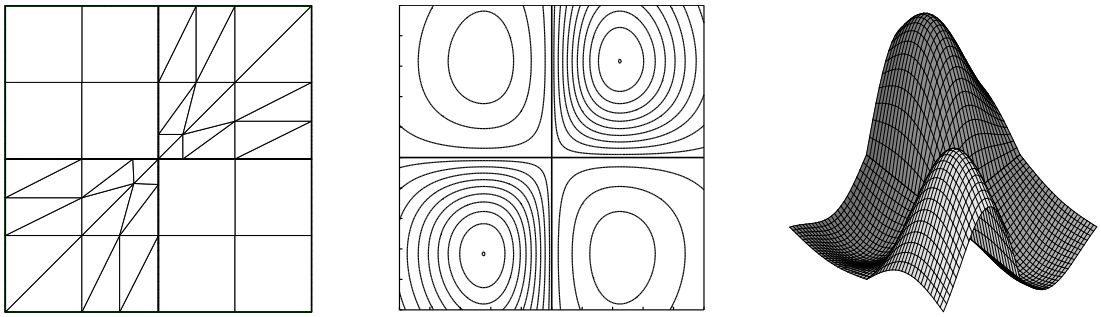

Figure 2.11: Decomposition of the domain and initial triangulation (left), isolines of the solution (middle) and exact solution (right), Example 4

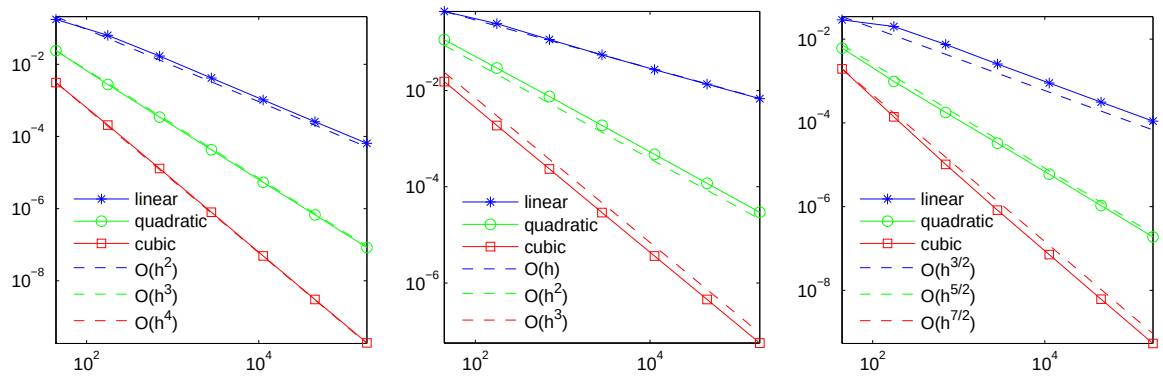

Figure 2.12: Error plot versus number of elements, L^2-norm (left), H^1-norm (middle) and weighted Lagrange multiplier norm (right), Example 4

The discretization errors are shown in Figure 2.12. The solution has a jump in the normal derivative at the interface but not in the flux. As in all previous examples, we observe the optimal asymptotic convergence rates in the L^2- and H^1-norms and a better convergence rate in the weighted Lagrange multiplier norm.

Example 5: In our fifth example, we decompose the domain into three subdomains in a geometrically non-conforming way as shown in right picture of Figure 2.13. The subdomains are given by $\Omega_1 := (1.5, 2.5) \times (0, 1)$, $\Omega_2 := (0, 4) \times (1, 2)$ and $\Omega_3 := (1.5, 2.5) \times (2, 3)$, where the slave sides are set to be on Ω_1 and Ω_3 so that Assumption 1 is satisfied. Our fifth problem is defined by

$$\begin{aligned} -\Delta u &= f \quad \text{in} \quad \Omega \quad \text{with} \\ \frac{\partial u}{\partial \mathbf{n}}|_{\Gamma_N} &= 0, \quad \text{and} \quad u|_{\Gamma_D} = g_D, \end{aligned}$$

where $\Gamma_N = \{(x, 1) \in \mathbb{R}^2 : 0 < x < 1.5\} \cup \{(x, 1) \in \mathbb{R}^2 : 2.5 < x < 4\} \cup \{(x, 2) \in \mathbb{R}^2 : 0 < x < 1.5\} \cup \{(x, 2) \in \mathbb{R}^2 : 2.5 < x < 4\}$ and $\Gamma_D := \partial\Omega \backslash \Gamma_N$. The right hand side and the function g_D of the problem are determined from the exact solution

$$u(x, y) = e^{-1.5\,(y-1.5)^2}\, x\,(x-4)\, y\,(y-3)\,(y-1)^2\,(y-2)^2\,(\sin(5\,x) + \cos(5\,y))\,,$$

which satisfies the homogeneous natural boundary condition on Γ_N. The isolines of the solution are given in the right picture of Figure 2.13, and the discretization errors in the L^2-, H^1- and the weighted Lagrange multiplier norm are given in Figure 2.14. Having a geometrically non-conforming decomposition does not affect the optimality of the method. In this example, we see that the convergence rate in the weighted Lagrange multiplier norm for the linear case is almost the same as for the quadratic case.

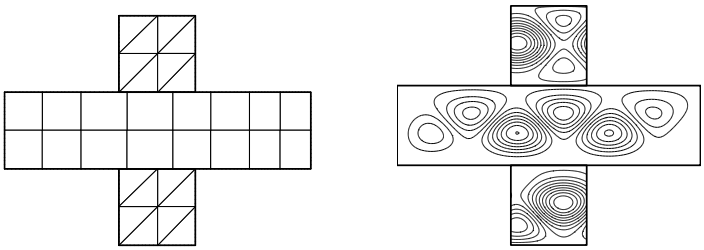

Figure 2.13: Decomposition of the domain and initial partitions (left) and isolines of the solution (right), Example 5

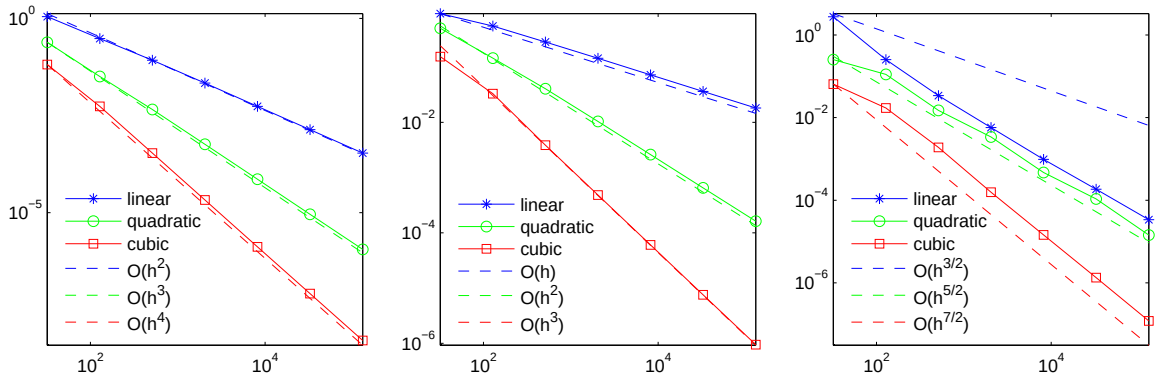

Figure 2.14: Error plot versus number of elements, L^2-norm (left), H^1-norm (middle) and weighted Lagrange multiplier norm (right), Example 5

Example 6: We compare two different mortar situations for cubic finite elements in our last example. In the first case, our finite element basis functions are based on Gauß-Lobatto nodes whereas in the second case, our finite element basis functions are based on equidistant nodes. In both cases, we work with dual Lagrange multiplier spaces so that the mass matrix on the slave side is the same. In this example, we decompose the domain $\Omega = (-1,1) \times (0,1)$ into two squares $\Omega_1 = (-1,0) \times (0,1)$ and $\Omega_2 = (0,1) \times (1,0)$ with the interface $\Gamma = \{0\} \times (0,1)$. The initial non-matching triangulation and decomposition into two subdomains are shown in the left picture of Figure 2.15. The problem for this example is given by

$$\begin{aligned} -\Delta u &= f \quad \text{in} \quad \Omega \quad \text{with} \\ \frac{\partial u}{\partial \mathbf{n}}|_{\Gamma_N} &= g_N, \quad \text{and} \quad u|_{\Gamma_D} = g_D, \end{aligned}$$

where $\Gamma_N := \{(x,0) \in \mathbb{R}^2 : -1 < x < 1\} \cup \{(x,1) \in \mathbb{R}^2 : -1 < x < 1\}$, and $\Gamma_D := \partial\Omega \backslash \Gamma_N$. In a first step, we compute the right hand side function f, and the boundary conditions on Γ_D and Γ_N by using the exact solution

$$u(x,y) = e^x \left(x^2 - 1\right)\left(y^2 - y\right),$$

and compare the errors for the two mortar situations. We have given the errors in three different norms in Table 2.1 for the cubic mortar case with equidistant nodes and in Table 2.2 for the cubic mortar case with Gauß-Lobatto nodes. As can be seen from these tables,

the solution in all three norms for the cubic mortar case with equidistant nodes exhibit suboptimal convergence rates, whereas the cubic mortar case with Gauß-Lobatto nodes yield optimal behavior. In contrast to optimal convergence rates attained by the cubic mortar finite elements with Gauß-Lobatto nodes, we only observe the convergence rate of order 2.5 and 1.5 in the L^2- and H^1-norms, respectively, whereas in the weighted Lagrange multiplier norm convergence of order 1.5 is attained.

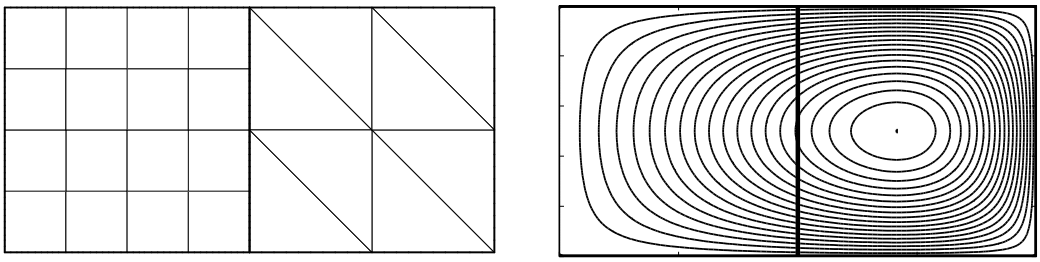

Figure 2.15: Decomposition into two subdomains and initial triangulation and isolines of the solution (right), Example 6

TABLE 2.1. Discretization errors with equidistant nodes, Example 6

level	# elem.	$\|u-u_h\|_{L^2(\Omega)}$		$\|u-u_h\|_1$		$\|\lambda-\lambda_h\|_h$	
0	24	5.538769e-03		1.734019e-02		1.379111e-03	
1	96	3.549887e-04	3.96	2.371300e-03	2.87	4.073067e-03	-1.56
2	384	2.431964e-05	3.87	4.343096e-04	2.45	2.027625e-03	1.01
3	1536	2.521352e-06	3.27	1.285930e-04	1.76	8.196174e-04	1.31
4	6144	3.949683e-07	2.67	4.489307e-05	1.52	3.078777e-04	1.41
5	24576	6.887069e-08	2.52	1.595379e-05	1.49	1.120462e-04	1.46
6	98304	1.217062e-08	2.50	5.662350e-06	1.49	4.017874e-05	1.48

In a next step, we take a cubic polynomial function as our exact solution and define the right hand side f and the boundary conditions on Γ_N and Γ_D by using this function. Now, we define our exact solution by

$$u(x,y) = x^3 - 3\,y^3 + 3\,x^2 + 4\,xy^2 - 5\,yx^2 + 5\,y + 12.$$

With the cubic mortar case based on Gauß-Lobatto nodes, we can compute the exact solution, whereas we can see from Table 2.3 that we cannot solve the problem exactly with the cubic mortar case based on equidistant nodes. The convergence rate in the L^2-norm is of order 2.5, whereas the convergence rate in the H^1-norm is of order 1.5 as in Table 2.1. As can be proved theoretically that the Lagrange multiplier space contains the constant

TABLE 2.2. Discretization errors with Gauß-Lobatto nodes, Example 6

level	# elem.	$\|u-u_h\|_{L^2(\Omega)}$		$\|u-u_h\|_1$		$\|\lambda-\lambda_h\|_h$	
0	24	5.517110e-03		1.734006e-02		1.372373e-03	
1	96	3.485755e-04	3.98	2.231279e-03	2.96	9.338184e-05	3.88
2	384	2.116152e-05	4.04	2.791363e-04	3.00	7.064503e-06	3.72
3	1536	1.290748e-06	4.04	3.476529e-05	3.01	5.729362e-07	3.62
4	6144	7.948833e-08	4.02	4.333049e-06	3.00	4.838724e-08	3.57
5	24576	4.928211e-09	4.01	5.406926e-07	3.00	4.177711e-09	3.53
6	98304	3.069439e-10	4.01	6.752319e-08	3.00	3.648872e-10	3.52

function, the convergence rate for the weighted Lagrange multiplier norm has exactly the same asymptotic as linear mortar finite elements.

TABLE 2.3. Discretization errors with equidistant nodes (cubic exact solution), Example 6

level	# elem.	$\|u-u_h\|_{L^2(\Omega)}$		$\|u-u_h\|_1$		$\|\lambda-\lambda_h\|_h$	
0	24	2.935203e-05		1.970982e-03		9.234661e-02	
1	96	5.862444e-06	2.32	8.170738e-04	1.27	4.589376e-02	1.01
2	384	1.071774e-06	2.45	3.040267e-04	1.43	1.854690e-02	1.31
3	1536	1.916484e-07	2.48	1.097294e-04	1.47	6.966565e-03	1.41
4	6144	3.402984e-08	2.49	3.915526e-05	1.49	2.535323e-03	1.46
5	24576	6.027017e-09	2.50	1.390406e-05	1.49	9.091418e-04	1.48
6	98304	1.067999e-09	2.50	4.926273e-06	1.50	3.236870e-04	1.49

2.4.2. Problems in solid mechanics. In this subsection, we present some numerical examples illustrating the performance of mortar finite elements for problems of linear and nonlinear elasticity. We point out that the theory presented in the first chapter can easily be extended to the case of linear elasticity with standard arguments. First, we recall standard boundary value problems in linear and nonlinear elasticity. The boundary value problem of a linear elastic body clamped on Γ_D without a volume force consists in finding a displacement field $\boldsymbol{u} : \Omega \to \mathbb{R}^d$ so that

$$\begin{aligned} -\nabla \cdot \sigma(\mathbf{u}) &= 0 \quad \text{in} \quad \Omega, \\ \mathbf{u} = 0 \quad \text{on} \quad \Gamma_D \quad \text{and} \quad \sigma(\mathbf{u})\mathbf{n} &= \boldsymbol{g}_N \quad \text{on} \quad \Gamma_N, \end{aligned} \tag{2.4.1}$$

where $\sigma(\mathbf{u})$ is a second order tensor defined as

$$\sigma(\mathbf{u}) = 2\mu\varepsilon(\mathbf{u}) + \lambda \operatorname{trace} \varepsilon(\mathbf{u})\mathbf{1}, \quad \varepsilon(\mathbf{u}) = \frac{1}{2}\left(\nabla\mathbf{u} + [\nabla\mathbf{u}]^T\right).$$

where $\mathbf{1}$ is the identity tensor. However, the linear elastic law is valid only when strains and deformations are small. In order to extend the model to large strains and large deformations one has to work with nonlinear elasticity. The governing boundary value problem for the

nonlinear elastic body clamped on Γ_D without a volume force is given by

$$\begin{aligned} -\nabla \cdot (\boldsymbol{F}(\boldsymbol{u})\boldsymbol{s}(\boldsymbol{u})) &= \mathbf{0} \quad \text{in} \quad \Omega, \\ \mathbf{u} = 0 \quad \text{on} \quad \Gamma_D \quad \text{and} \quad \boldsymbol{F}(\boldsymbol{u})\boldsymbol{s}(\boldsymbol{u})\mathbf{n} &= \boldsymbol{g}_N \quad \text{on} \quad \Gamma_N, \end{aligned} \tag{2.4.2}$$

where $\boldsymbol{s}(\boldsymbol{u})$ is the second Piola-Kirchhoff stress tensor, and $\boldsymbol{F}(\boldsymbol{u})$ is the deformation gradient defined as $\boldsymbol{F}(\boldsymbol{u}) = \mathbf{1} + \nabla \boldsymbol{u}$. In particular, we work with neo-Hookean law, which expresses the second Piola-Kirchhoff stress $\boldsymbol{s}$ in terms of the Cauchy-Green strain tensor $\boldsymbol{C}(\boldsymbol{u}) = \boldsymbol{F}^T(\boldsymbol{u})\boldsymbol{F}(\boldsymbol{u})$ by

$$\boldsymbol{s}(\boldsymbol{u}) = \mu(\mathbf{1} - \boldsymbol{C}(\boldsymbol{u})^{-1}) + \frac{\lambda}{2}(J(\boldsymbol{u})^2 - 1)\boldsymbol{C}(\boldsymbol{u})^{-1}$$

with $J(\boldsymbol{u}) = \det \boldsymbol{F}(\boldsymbol{u})$ denoting the determinant of the deformation gradient.

Example 1: In our first example, we consider a structure occupying a region

$$\Omega := \text{conv}\{(0,0),(48,44),(48,60),(0,44)\},$$

where convξ is the convex hull of the set ξ. The left boundary of Ω is fixed and an in-plane shearing load of 100N is applied along the positive y-direction on the right boundary. Here, the domain Ω is decomposed into two subdomains Ω_1 and Ω_2 with

$$\Omega_2 := \text{conv}\{(12,20.25),(36,38.75),(36,50.25),(12,38.75)\},$$

and $\Omega_1 := \Omega \backslash \bar{\Omega}_2$. The decomposition of the domain Ω and the initial triangulation are given in the left picture of Figure 2.16, and the deformation of the structure is shown in the right. We choose material parameters as $E_1 = 2000$, $E_2 = 200$, $\nu_1 = 0.45$, and $\nu_2 = 0.35$,

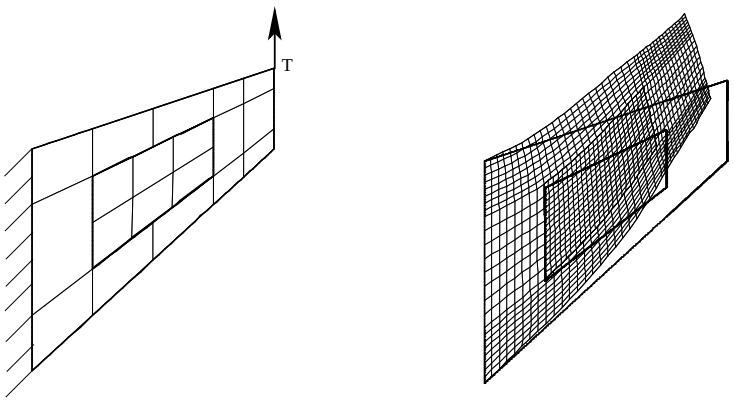

Figure 2.16: Cook's membrane decomposed into two subdomains (left) and the zoomed deformed configuration (right)

where the suffices indicate the corresponding subdomains. We recall that Lamé parameters λ and μ are related to Young's modulus E and Poisson ratio ν by

$$\lambda = \frac{E\nu}{(1+\nu)(1-2\nu)}, \quad \text{and} \quad \mu = \frac{E}{2(1+\nu)}. \tag{2.4.3}$$

The vertical tip displacements of the membrane at different refinement levels using the linear elastic and neo-Hookean law are given in the left and the right pictures of Figure

2.17, where we show the vertical tip displacement against the number of degrees of freedom. The efficiency of higher order mortar finite elements can be easily seen.

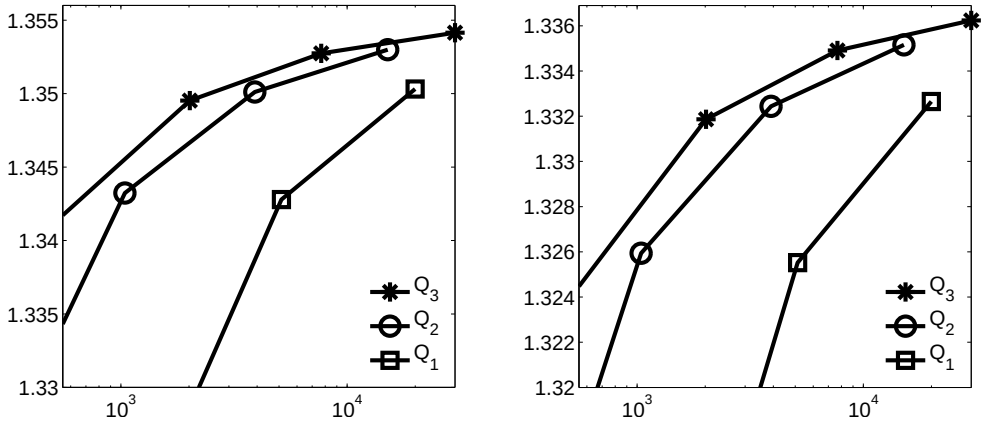

Figure 2.17: Vertical tip displacements versus number of degrees of freedom of the Cook's membrane with linear elastic law (left) and neo-Hookean law (right), zoomed

Example 2: In our second example, we consider an I-beam consisting of three subdomains $\Omega_1 := (0,3) \times (0,1)$, $\Omega_2 := (0.9, 2.1) \times (1,3)$, and $\Omega_3 := (0,3) \times (3,4)$. The lower boundary of Ω_1 is fixed, and we apply $1.8N$ traction force per unit length along the horizontal and vertical directions on the top boundary of Ω_3. As in our first example, we consider the linear elastic model and the nonlinear model with neo-Hookean law with different material parameters in different subdomains, where Young's modulus and Poisson's ratios are set to be $E_1 = 1500, \nu_1 = 0.45, E_2 = 500, \nu_2 = 0.35$ and $E_3 = 150, \nu_3 = 0.34$. In the left picture of Figure 2.18, we show the decomposition of our I-beam and the initial triangulation, and the deformation of the I-beam is shown in the right.

In Figure 2.19, we show the vertical tip displacement against the number of degrees of freedom. As in our first example, we can see the efficiency of higher order mortar finite elements.

In the left and the right pictures of Figure 2.20, we compare the numerical results from the linear elastic model and the nonlinear model with neo-Hookean law for our first and second example, respectively. In case of the first example, we plot the vertical displacement along the line $x = 48$, and in case of the second example we plot the vertical displacement along the line $y = 4$. In both cases, since the deformation is already large, the nonlinear model gives more realistic results.

2.5. Continuous quadratic dual Lagrange multiplier spaces

In this section, starting with the piecewise quadratic biorthogonal basis functions presented in Section 2.2, we construct locally supported continuous biorthogonal basis functions. We do not work it out for the general situation, but we present different possibilities for the quadratic case. However, a similar approach can be adopted for any higher order case. Suppose that $\hat{\varphi}_0, \hat{\varphi}_1$ and $\hat{\varphi}_2$ be the quadratic nodal finite element basis functions on the reference element $(-1, 1)$ in one dimension, where $\hat{\varphi}_0$ is the basis function corresponding to the midpoint of the reference element and $\hat{\varphi}_1$ and $\hat{\varphi}_2$ are the basis functions

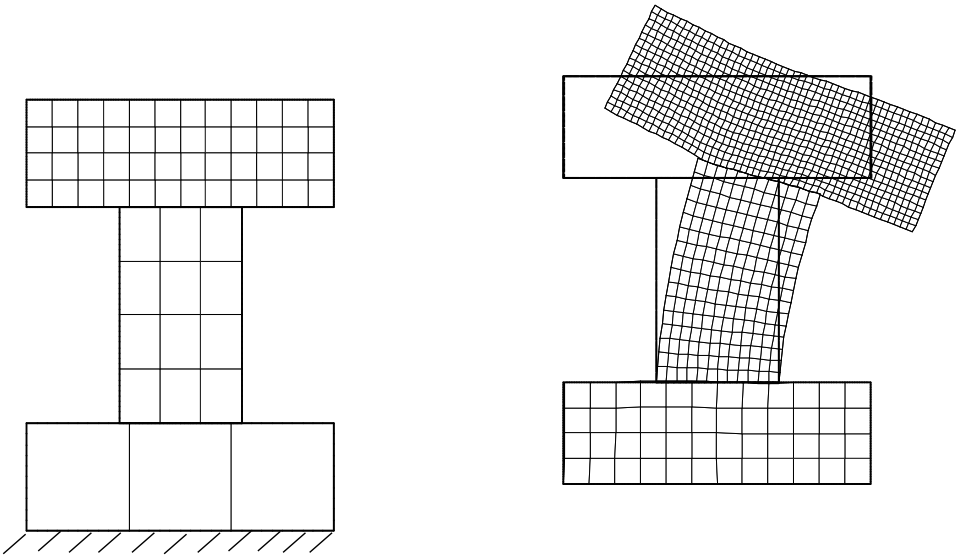

Figure 2.18: I-beam decomposed into three subdomains (left) and the deformed configuration (right)

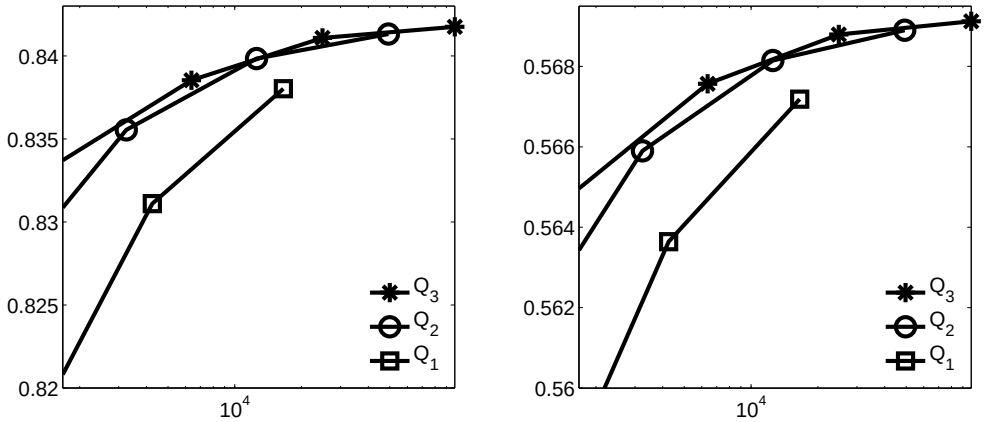

Figure 2.19: Vertical tip displacements versus number of degrees of freedom of I-beam with linear elastic law (left) and neo-Hookean law (right), zoomed

corresponding to the left and the right vertices, respectively. The quadratic dual Lagrange multiplier basis functions in the reference element are defined by

$$\lambda_0 = \frac{5}{2}\hat{\varphi}_0 - 1, \quad \lambda_1 = \hat{\varphi}_1 - \frac{3}{4}\hat{\varphi}_0 + \frac{1}{2}, \quad \lambda_2 = \hat{\varphi}_2 - \frac{3}{4}\hat{\varphi}_0 + \frac{1}{2}, \tag{2.5.1}$$

where λ_0, λ_1 and λ_2 are the quadratic dual basis functions corresponding to the midpoint, left and right vertices of the reference element, respectively. The approximation property of the Lagrange multiplier for quadratic finite elements requires that the constants and the linear functions are contained in the Lagrange multiplier space M_h. To satisfy these conditions, the Lagrange multipliers have to be modified near the crosspoints. If $t = -1$ is

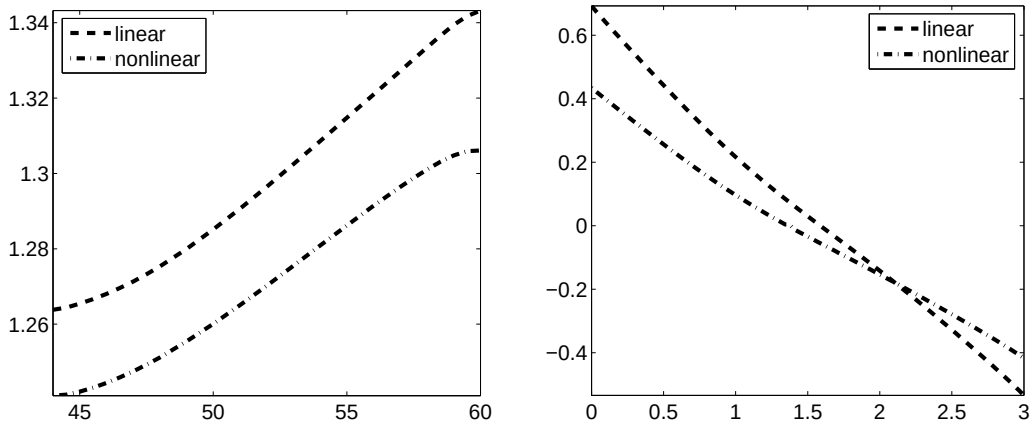

Figure 2.20: Vertical displacements along the line $x = 48$, Example 1 (left) and vertical displacements along the line $y = 4$, Example 2 (right)

the crosspoint, the Lagrange multipliers on the reference edge will be given by

$$\lambda_0(t) = -t + 1, \quad \lambda_1(t) = t, \tag{2.5.2}$$

and if $t = 1$ is the crosspoint we have

$$\lambda_0(t) = 1 + t, \quad \lambda_1(t) = -t. \tag{2.5.3}$$

We note that λ_2 does not exist if $t = -1$ or $t = 1$ is a crosspoint. The global basis functions μ_i are obtained by using an affine mapping and gluing the local ones at the vertices together. The two left pictures of Figure 2.21 illustrate the interior Lagrange multipliers. The left one is associated with the midpoint of an edge and the right one with a vertex. In the two pictures on the right, the situation of a left crosspoint is shown. The left one gives the Lagrange multiplier associated with the interior vertex and the right one shows the one associated with the midpoint of the edge.

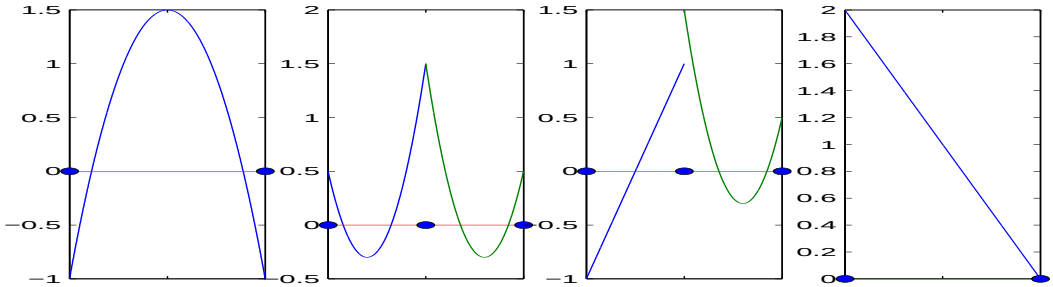

Figure 2.21: Interior dual basis functions (left 1 and 2) and modification at a left crosspoint (right 1 and 2), discontinuous case

Although these dual basis functions are locally supported and optimal a priori bounds hold, the use of discontinuous Lagrange multiplier spaces can be disadvantageous if some inexact quadrature formulas are used. To compute the algebraic form of the matching condition (1.6.1), the mass matrix $\mathtt{M}_{mc}$ is to be assembled, and for that purpose we have to

compute the integral of the product of two discrete functions defined on two completely different meshes. The discontinuities of the Lagrange multipliers which are living on the slave side will lead to a considerable loss of accuracy in the integral computation if the quadrature nodes are not adapted to the discontinuities. Since we have independent meshes on the slave and the master side, the discontinuities of the Lagrange multiplier basis functions are not captured by quadrature points based on the master side. Therefore, it might be better to work with continuous Lagrange multiplier spaces. The idea is to modify locally the piecewise quadratic dual basis functions by adding some local correction functions g, h_1 and h_2, i.e., $\hat{\lambda}_0 = \lambda_0 + g$, $\hat{\lambda}_1 = \lambda_1 + h_1$ and $\hat{\lambda}_2 = \lambda_2 + h_2$. The associated global Lagrange multiplier basis functions $\hat{\mu}_i$ on the slave side of the interface γ_m have to satisfy

[P0] $\hat{\mu}_i$ is continuous
[P1] $\text{supp } \hat{\mu}_i = \text{supp } \mu_i$
[P2] $\sum_{i=1}^{n_m} \hat{\mu}_i = 1$
[P3] $\int_{\gamma_m} \hat{\mu}_i \, \varphi_j \, d\sigma = \delta_{ij} \int_{\gamma_m} \varphi_j \, d\sigma$
[P4] $\|\hat{\mu}_i\|_1 \equiv \|\varphi_i\|_1$.

To do so, we start with the piecewise quadratic dual Lagrange multiplier basis functions on the reference element. We have to find a function g for λ_0 such that the conditions

[g0] $g(1) + \lambda_0(1) = 0$,
[g1] $g(-1) + \lambda_0(-1) = 0$ and
[g2] $\int_{-1}^{1} g\, p \, dt = 0$ for all quadratic functions $p \in \mathcal{P}_2(I)$

are satisfied. Similarly, we have to find functions h_1 for λ_1 and h_2 for λ_2 such that

[h0] $h_1(1) + \lambda_1(1) = 0, \quad h_2(1) + \lambda_2(1) = 1$
[h1] $h_1(-1) + \lambda_1(-1) = 1, \quad h_2(-1) + \lambda_2(-1) = 0$ and
[h2] $\int_{-1}^{1} h_i \, p \, dt = 0$ for all quadratic functions $p \in \mathcal{P}_2(I)$, $i = 1, 2$,

are satisfied. Furthermore, we require that $h_1 + h_2 + g = 0$ on $(-1, 1)$ and that $g, h_1, h_2 \in H^1((-1, 1))$. Then the modified Lagrange multipliers $\hat{\mu}_i$ are obtained by an affine mapping from the ones on the reference edge. We note that we do not modify the definition of a Lagrange multiplier restricted to an edge having one crosspoint.

LEMMA 2.12. *If g satisfies [g0]–[g2], and h_1 and h_2 satisfy [h0]–[h2], then the modified basis functions $\hat{\mu}_i$ satisfy the properties [P0]–[P4].*

The properties [P0]–[P4] follow by construction. Of course, there are many choices for g, h_1 and h_2. Regarding [h0] and [h1], we can choose $h_1 = h_2 = h$. In the following, we discuss different possibilities for h and g. One possibility is to consider the case where g and h are polynomials of minimal degree satisfying the given conditions. Another possibility is to define g and h as piecewise quadratic functions on $(-1, 1)$. Following the first possibility, we get unique quartic polynomials g and h on $(-1, 1)$ such that the modified Lagrange multipliers have all the properties listed above. The polynomial g on $(-1, 1)$ is explicitly given by

$$g(t) := \frac{35}{8}\, t^4 - \frac{15}{4}\, t^2 + \frac{3}{8} \quad \text{and} \quad h := -g/2. \tag{2.5.4}$$

The modified Lagrange multipliers are shown in Figure 2.22, and the correction g is given in the left picture of Figure 2.23. The conditions $[g2]$ and $[h2]$ ensure the biorthogonality, and it can be easily seen that the correction g is reflection invariant on (-1,1), i.e., $g(t) = g(-t)$. The maximum value of the nodal Lagrange multiplier basis function associated with the midpoint is 1.875.

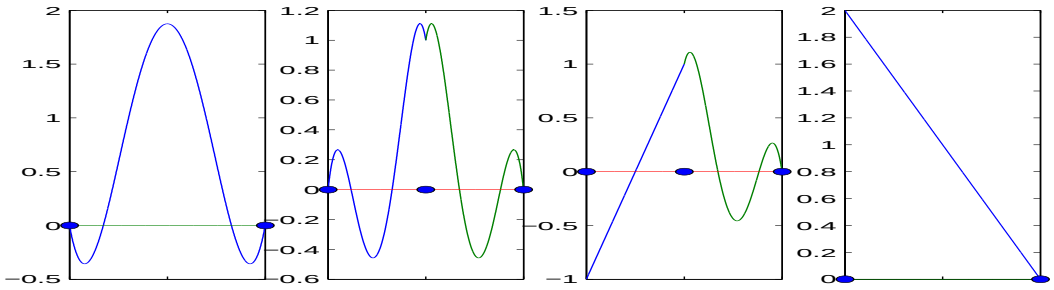

Figure 2.22: Interior dual basis functions (left 1 and 2) and modification at a left crosspoint (right 1 and 2), quartic correction

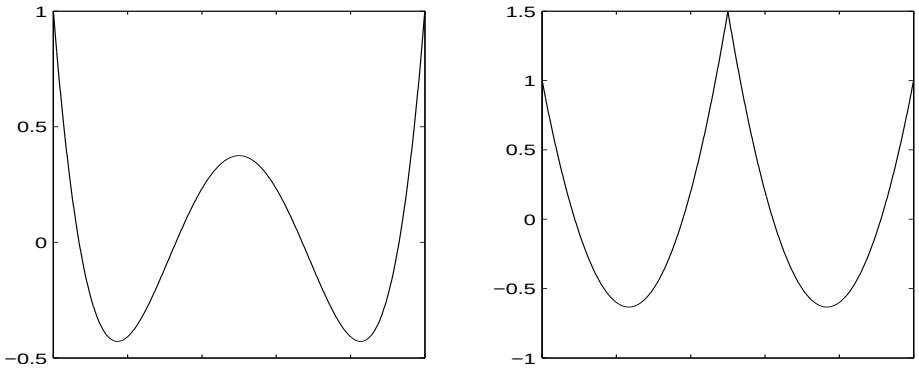

Figure 2.23: The quartic correction g (left) and the piecewise quadratic one (right)

In the following examples, we consider piecewise quadratic corrections in $(-1, 1)$ satisfying the properties $[g0]$–$[g2]$ and $[h0]$–$[h2]$. We have to decompose the unit interval at least into two subintervals. In the case of two subintervals, the correction g is uniquely defined. If we use more than two subintervals, we can impose additional conditions on g. Using only two subintervals, we find

$$g(t) := \begin{cases} \frac{15}{2}\,t^2 + 8\,t + \frac{3}{2}, & -1 \le t < 0\ , \\ \frac{15}{2}\,t^2 - 8\,t + \frac{3}{2}, & 0 \le t \le 1\ , \end{cases} \quad \text{and} \quad h := -g/2. \tag{2.5.5}$$

The correction g is given in the right of Figure 2.23, and the associated dual basis functions are shown in Figure 2.24.

Another possibility is to decompose the unit interval $(-1, 1)$ into three subintervals and consider piecewise linear polynomials in two subintervals and a piecewise quadratic in the third one. Then, we get a unique correction function g. If we choose piecewise

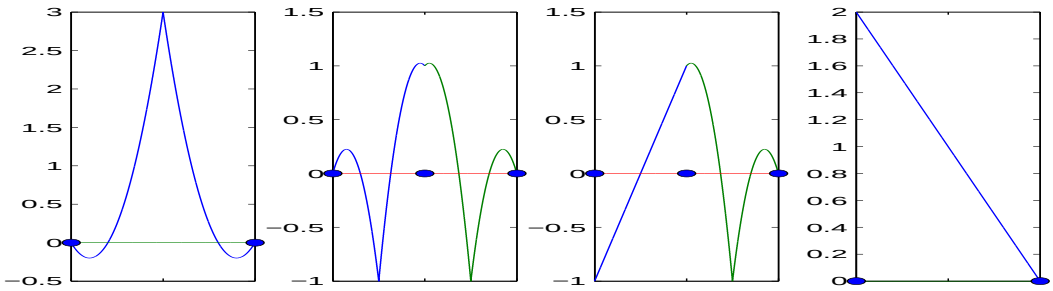

Figure 2.24: Interior dual basis functions (left 1 and 2) and modification at a left crosspoint (right 1 and 2), piecewise quadratic correction

linear functions in the left and right subintervals $(-1, 1/3)$ and $[2/3, 1)$ and a quadratic polynomial in the middle subinterval $[1/3, 2/3)$, g is defined by

$$g(t) := \begin{cases} -\frac{145}{44} - \frac{189}{44}\, t, & -1 \le t < -\frac{1}{3}\ , \\ -\frac{405}{11}\, t^2 + \frac{49}{22}, & -\frac{1}{3} \le t < \frac{1}{3}\ , \\ \frac{189}{44}\, t - \frac{145}{44}, & \frac{1}{3} \le t \le 1, \end{cases} \qquad \text{and} \quad h := -g/2.$$

The correction function g is shown in the left of Figure 2.26 and the associated basis function in Figure 2.25.

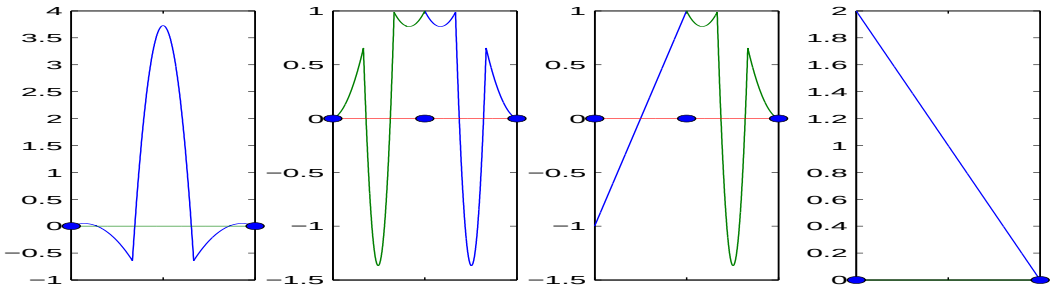

Figure 2.25: Interior dual basis functions (left 1 and 2) and modification at a left crosspoint (right 1 and 2), piecewise linear and quadratic correction

Although there are many possibilities to construct continuous Lagrange multipliers, the numerical experiments show that the Lagrange multipliers with smaller maximum value on the reference element give better results. To get a symmetric Lagrange multiplier which has a smaller maximum, we consider another case with piecewise quadratic functions in $(-1, 1/3)$ and $[2/3, 1)$ and being constant in the middle interval $[1/3, 2/3)$. Then, we get a unique g defined by

$$g(t) := \begin{cases} \frac{405}{38}\, t^2 + \frac{999}{76}\, t + \frac{265}{76}, & -1 \le t < -\frac{1}{3}\ , \\ \frac{11}{38}, & -\frac{1}{3} \le t < \frac{1}{3}\ , \\ \frac{405}{38}\, t^2 - \frac{999}{76}\, t + \frac{265}{76}, & \frac{1}{3} \le t \le 1\ , \end{cases} \qquad \text{and} \quad h := -g/2. \tag{2.5.6}$$

The correction function g is given in the right picture of Figure 2.26, and the associated dual basis functions are shown in Figure 2.27. We note that if we want to minimize the

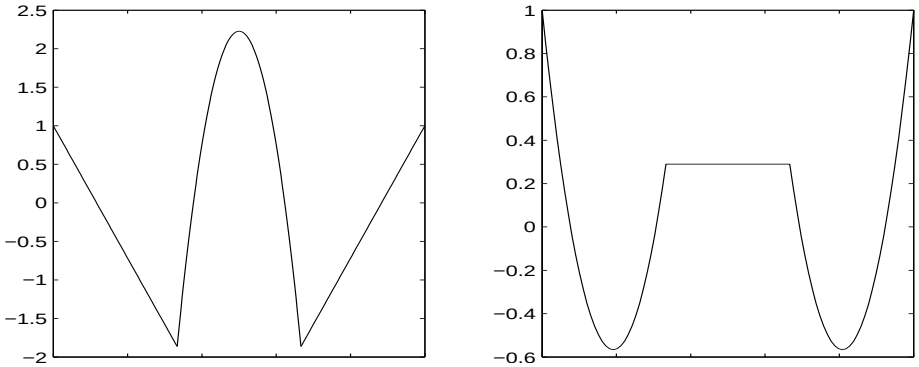

Figure 2.26: The piecewise linear and quadratic correction g (left) and piecewise constant and quadratic one (right)

maximum value of the Lagrange multiplier on the reference element corresponding to the midpoint of the edge by relaxing the condition of symmetry, it is possible to find another Lagrange multiplier with a smaller maximum value. But the difference is very small.

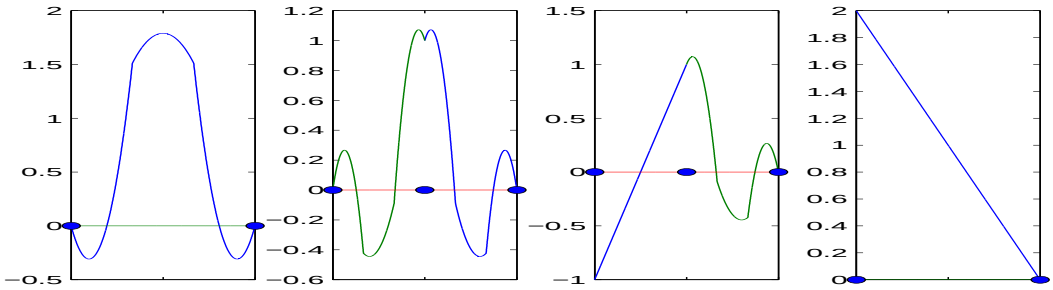

Figure 2.27: Interior dual basis functions (left 1 and 2) and modification at a left crosspoint (right 1 and 2), piecewise quadratic and constant correction

REMARK 2.13. *The Lagrange multiplier space spanned by the discontinuous quadratic functions given by* (2.5.1), (2.5.2) *and* (2.5.3) *will be denoted by* M_h^d, *and the Lagrange multiplier spaces spanned by the continuous functions which are corrected by g and h given in* (2.5.4), (2.5.5) *and* (2.5.6) *will be denoted by* M_h^q, M_h^b *and* M_h^c, *respectively. We will denote by* M_h^l *the dual Lagrange multiplier space for linear finite elements spanned by piecewise linear functions.*

2.6. A comparison of different Lagrange multiplier spaces

In this section, we compare the performance of our new continuous dual Lagrange multiplier spaces M_h^q, M_h^b and M_h^c with the piecewise quadratic but discontinuous dual Lagrange multiplier space M_h^d. Due to the fact that the continuous quartic Lagrange multiplier is locally a fourth order polynomial, we have to use a higher order quadrature formula to compute the integral in the mass matrix and the weighted error norm for the Lagrange multiplier. We denote by u_h^d, u_h^q, u_h^b and u_h^c the mortar finite element solutions associated with the different Lagrange multiplier spaces M_h^d, M_h^q, M_h^b and M_h^c, respectively.

For all our examples, we solve the Poisson problem $-\Delta u = f$ in Ω with different exact solutions, and the right hand side and the Dirichlet boundary conditions are computed so that we get the predefined exact solution. In our first example, we consider a decomposition of a square $\Omega = (0,1) \times (0,1)$ into two subdomains Ω_1 and Ω_2, where Ω_1 is a closed polygonal non-convex subdomain joining the points $(0,0), (1,0), (1/2,1/2), (1,1)$ and $(0,1)$ and Ω_2 is a triangle with the vertices $(1,0), (1,1)$ and $(1/2,1/2)$. A simple exact solution $u(x,y) = xy(1-x)(1-y)$ is chosen to see the influence of different Lagrange multiplier spaces. Figure 2.28 shows the decomposition into two subdomains, the non-matching initial triangulation and the isolines of the solution. We have two interfaces and three crosspoints. The master sides are defined to be on the non-convex subdomain, and the slave subdomain is the triangle.

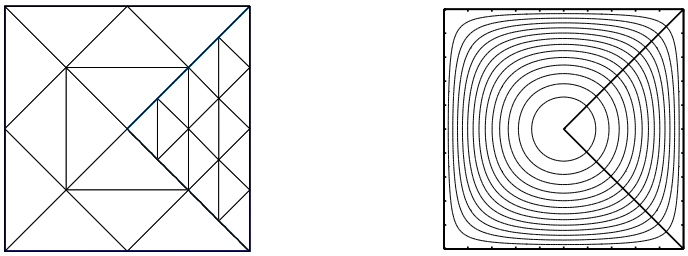

Figure 2.28: Decomposition into two subdomains and initial triangulation (left) and isolines of the solution (right), Example 1

In our second example, we consider the decomposition of $\Omega = (0,1) \times (0,1)$ into six subdomains defined by $\Omega_{ij} := ((i-1)/3, i/3) \times ((j-1)/2, j/2), 1 \leq i \leq 3, 1 \leq j \leq 2$, and the triangulations do not match at the interfaces. We have two interior crosspoints and seven interfaces. The meshes at the interfaces are non-matching and the master sides are chosen randomly. The right hand side f and the Dirichlet boundary conditions are chosen such that the exact solution is given by $u(x,y) = (x-y)\exp(-5(x-0.5)^2 - 5(y-0.5)^2)$. Figure 2.29 shows the decomposition into subdomains, the initial non-matching triangulation and the isolines of the solution. Our last example is the same as the second

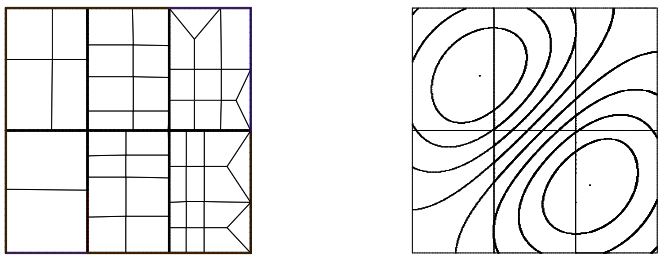

Figure 2.29: Decomposition into six subdomains and initial triangulation (left) and isolines of the solution (right), Example 2

example of Section 2.4, see Figure 2.7. Tables 2.4-2.6 show the numerical results for the three different examples and for the four different choices of Lagrange multipliers. The discretization errors in the L^2- and H^1-norm for the weak solution u were exactly the same for the first example, and in the two other examples the differences were extremely small.

Therefore, we do not give these errors. A small difference can be observed only in the error in the Lagrange multiplier. If we compare the other Lagrange multiplier spaces with the discontinuous Lagrange multiplier space, we observe that the continuous quartic Lagrange multiplier space yields an error of about 3 % higher in the first level and in the final level the difference is about 5 % whereas the error for the broken-quadratic Lagrange multiplier space is about 24 % higher in the first level which goes up to 58 % in the final refinement level. The error for the broken-constant Lagrange multiplier space is about 0.3 % less in the first level and around 2 % in the final refinement level. The bigger error in the Lagrange multiplier norm for M_h^b is due to the fact that the maximum value of the nodal basis function is higher compared to the other Lagrange multiplier basis functions. In fact, the maximum value of the nodal basis function from M_h^b corresponding to the midpoint of the edge is 3 whereas the maximum value of the discontinuous Lagrange multiplier at this node is 1.5. The broken-constant Lagrange multiplier has a maximum value of 1.8.

TABLE 2.4. Discretization errors in the weighted Lagrange multiplier norm, Example 1

level	# elem.	$\|\mu - \mu_h^d\|_h$	$\|\mu - \mu_h^q\|_h$	$\|\mu - \mu_h^b\|_h$	$\|\mu - \mu_h^c\|_h$
0	28	9.470143e-03	9.731379e-03	1.252511e-02	9.435581e-03
1	112	1.620246e-03	1.674903e-03	2.265275e-03	1.604492e-03
2	448	2.767632e-04	2.880399e-04	4.077914e-04	2.728400e-04
3	1792	4.787615e-05	5.007306e-05	7.302227e-05	4.707297e-05
4	7168	8.362299e-06	8.771935e-06	1.300681e-05	8.210304e-06
5	28672	1.468960e-06	1.543415e-06	2.308726e-06	1.441193e-06
6	114688	2.588398e-07	2.721896e-07	4.089964e-07	2.538517e-07

TABLE 2.5. Discretization errors in the weighted Lagrange multiplier norm, Example 2

level	# elem.	$\|\mu - \mu_h^d\|_h$	$\|\mu - \mu_h^q\|_h$	$\|\mu - \mu_h^b\|_h$	$\|\mu - \mu_h^c\|_h$
0	47	3.435663e-02	3.472259e-02	3.746504e-02	3.457403e-02
1	188	6.794099e-03	7.249089e-03	1.011761e-02	7.118611e-03
2	752	1.031815e-03	1.094674e-03	1.515990e-03	1.068923e-03
3	3008	1.829821e-04	1.968839e-04	2.880542e-04	1.904619e-04
4	12032	3.198112e-05	3.459908e-05	5.179677e-05	3.335310e-05
5	48128	5.642177e-06	6.117301e-06	9.213434e-06	5.887483e-06
6	192512	9.928575e-07	1.076081e-06	1.628637e-06	1.034036e-06

TABLE 2.6. Discretization errors in the weighted Lagrange multiplier norm, Example 3

level	# elem.	$\|\mu - \mu_h^d\|_h$	$\|\mu - \mu_h^q\|_h$	$\|\mu - \mu_h^b\|_h$	$\|\mu - \mu_h^c\|_h$
0	20	2.393161e+00	2.515256e+00	3.143823e+00	2.492000e+00
1	80	8.601690e-01	9.046823e-01	1.309716e+00	8.742536e-01
2	320	1.680722e-01	1.488028e-01	2.678213e-01	1.622111e-01
3	1280	2.113279e-02	2.279722e-02	3.357682e-02	2.199264e-02
4	5120	3.480169e-03	3.699532e-03	5.332353e-03	3.548563e-03
5	20480	5.915244e-04	6.262941e-04	8.860717e-04	6.020646e-04
6	81920	1.034967e-04	1.094254e-04	1.542287e-04	1.051368e-04

In all our examples the difference in the errors for the different Lagrange multiplier spaces in the L^2- and in the H^1-norm can be neglected. Only in the weighted Lagrange multiplier norm, we observe some quantitative difference. However, the qualitative results are the same. We note that better results can be obtained if Lagrange multiplier basis functions are used having a small maximum value. The Lagrange multiplier spaces M_h^d and M_h^c yield better results than the space M_h^b. In contrast to the discretization error in the L^2-norm and in the H^1-norm, the weighted L^2-norm for the Lagrange multiplier is sensitive to the choice of the Lagrange multiplier space. It turns out that the quality of the Lagrange multiplier space depends on the maximum value of its nodal basis functions.

CHAPTER 3

Lagrange Multiplier Spaces in 3D

3.1. Introduction

In this chapter, we consider the construction of Lagrange multiplier spaces for three-dimensional mortar finite elements. In a first step, we focus on constructing dual Lagrange multiplier spaces satisfying Assumption 7 as in the two-dimensional case, which also provides a motivation to relax this assumption. Although the construction of a dual Lagrange multiplier space for a finite element space with tensor product structure is trivial, the situation is not so easy for serendipity or a simplicial family of finite elements. For quadratic serendipity elements, we consider a quasi-dual Lagrange multiplier space which generalizes the concept of a dual Lagrange multiplier space, see Section 1.6. In a next step, working with Assumption 2, we show that dual Lagrange multiplier spaces can be constructed for quadratic simplicial and serendipity elements.

This chapter is organized as follows. In the next section, we present different Lagrange multiplier spaces for quadratic hexahedral finite elements satisfying Assumption 7 and provide numerical results in Section 3.3. Dual Lagrange multiplier spaces for linear and quadratic simplicial finite elements satisfying Assumption 7 are discussed in Section 3.4. In Section 3.5, we present a new idea of constructing dual Lagrange multiplier spaces *only* satisfying Assumption 2 for quadratic serendipity hexahedral elements and quadratic simplicial elements. Numerical results using these Lagrange multiplier spaces are presented in the final section.

3.2. Lagrange multiplier spaces for the hexahedral case

In this section, we consider different possibilities for constructing Lagrange multiplier spaces in three dimensions for higher order hexahedral finite elements satisfying Assumption 7 with $\operatorname{supp}\varphi_i = \operatorname{supp}\mu_i$. If we work with a tensor product finite element space in a hexahedral mesh, we can apply the idea of the one-dimensional construction presented in Chapter 2 in a straightforward way by using the tensor product structure of Lagrange multipliers, see Remark 2.10. We do not work out details for the general higher order case but we focus on the standard triquadratic finite elements. Unfortunately, the tensor product construction of dual Lagrange multiplier spaces cannot be adopted in case of the serendipity family of finite element spaces. For quadratic serendipity finite element spaces, we consider standard and quasi-dual Lagrange multiplier spaces. We use standard nodal quadratic serendipity elements as introduced in [**50**]. A higher order case can be defined similarly.

3.2.1. A dual Lagrange multiplier space for standard triquadratic finite elements. Here, we give the explicit construction of the tensor product Lagrange multiplier

space for standard triquadratic finite elements. Let $\hat{\varphi}_0$ be the basis function corresponding to the midpoint of the reference element, and $\hat{\varphi}_1$ and $\hat{\varphi}_2$ are the basis functions corresponding to the left and the right vertices, respectively for the quadratic nodal finite element basis functions on the reference element $(-1,1)$ in one dimension. Then the quadratic dual Lagrange multiplier basis functions on the reference element are defined by equations (2.5.1)-(2.5.3). If we denote a hat function at an interior vertex p by ϕ_p^l, we find

$$\phi_p^l(t) = \mu_p(t) + \frac{1}{2}(\mu_{e1}(t) + \mu_{e2}(t)), \tag{3.2.1}$$

where μ_p is the Lagrange multiplier corresponding to the vertex p and μ_{e1} and μ_{e2} are the basis functions associated with the midpoints of the two adjacent edges. If p is a crosspoint, we have $\phi_p^l(t) = \frac{1}{2}\mu_e(t)$, where μ_e is the Lagrange multiplier basis function corresponding to the midpoint of the edge containing the crosspoint. Then, the Lagrange multiplier basis functions on the reference face $\hat{F} := (-1,1) \times (-1,1)$ having a tensor product structure are defined as

$$\hat{\lambda}_{ij}(x,y) := \hat{\lambda}_i(x)\hat{\lambda}_j(y).$$

Here, $\hat{\lambda}_{11}(x,y)$, $\hat{\lambda}_{21}(x,y)$, $\hat{\lambda}_{22}(x,y)$ and $\hat{\lambda}_{12}(x,y)$ are the Lagrange multipliers corresponding to the four vertices $(-1,-1),(1,-1),(1,1)$ and $(-1,1)$, and $\hat{\lambda}_{01}(x,y)$, $\hat{\lambda}_{20}(x,y)$, $\hat{\lambda}_{02}(x,y)$ and $\hat{\lambda}_{10}(x,y)$ are the ones corresponding to the midpoints $(0,-1),(1,0),(0,1)$ and $(-1,0)$ of the four edges, respectively, and finally $\hat{\lambda}_{00}(x,y)$ is the one corresponding to the center of gravity $(0,0)$ of the reference face. The Lagrange multiplier basis functions are associated with the vertices, midpoints of the edges and the center of gravity of elements in $\mathcal{S}_k, 1 \le k \le N$. The global basis functions μ_i are obtained by using an affine mapping and gluing the local ones together. All nodes on the boundary $\partial\gamma_k$ of γ_k are crosspoints and do not carry a degree of freedom for the Lagrange multiplier space. We note that we have to use the modification at the crosspoints to compute the tensor product for the Lagrange multipliers corresponding to the elements touching $\partial\gamma_k$. Observing (3.2.1), we find that the bilinear hat function at each vertex is contained in the Lagrange multiplier space M_k. We point out that this is also valid on $\partial\gamma_k$, although there are no degrees of freedom. Hence, Assumption 4 is satisfied. Now, we verify Assumption 3. Let $\mu := \sum_{k=1}^{n_k} a_k\mu_k \in M_k$, and set $\varphi := \sum_{k=1}^{n_k} a_k\varphi_k$. Denoting the local meshsize at the i-th node by $\underline{h}_{s(k),i}$, we use the biorthogonality relation (1.6.2) to obtain

$$(\varphi,\mu)_{0,\gamma_k} = \sum_{F\in\mathcal{S}_k}\sum_{i,j=1}^{n_k} a_i a_j(\varphi_i,\mu_j)_{0,F} \equiv \sum_{i=1}^{n_k} \underline{h}_{s(k),i}^2 a_i^2 \ge C\|\varphi\|_{0,\gamma_k}^2.$$

Taking into account the fact that $\|\varphi\|_{0,\gamma_k}^2 \equiv \|\mu\|_{0,\gamma_k}^2 \equiv \sum_{i=1}^{n_k} a_i^2\underline{h}_{s(k),i}^2$, Assumption 3 is satisfied.

3.2.2. A non-existence result for quadratic serendipity elements. Although the construction of dual Lagrange multiplier spaces for higher order tensor product finite element spaces was quite straightforward, the situation is not as simple for serendipity type finite elements. First, we give a non-existence result for a dual Lagrange multiplier space for the quadratic serendipity elements. We denote by W_k^1 the finite element space of piecewise bilinear hat functions on γ_k. In case of standard triquadratic finite elements, the

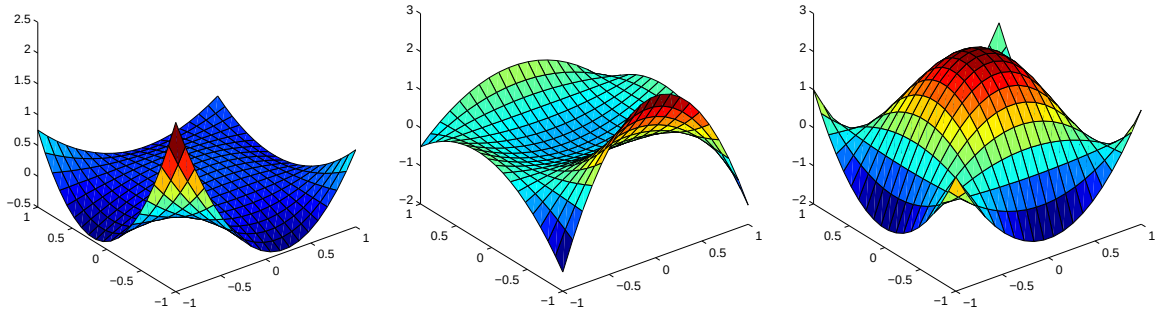

Figure 3.1: The Lagrange multipliers corresponding to a vertex (left), to an edge (middle) and to the center of gravity (right)

dual Lagrange multiplier space with tensor product structure contains W_k^1 for $1 \leq k \leq N$. Unfortunately, under Assumption 7 there exists no dual Lagrange multiplier space yielding optimal a priori estimates with $\operatorname{supp} \varphi_i = \operatorname{supp} \mu_i$, where φ_i are the quadratic serendipity nodal finite element basis functions on the interface γ_k.

LEMMA 3.1. *Under the assumption that* $\operatorname{supp} \varphi_i = \operatorname{supp} \mu_i$ *and Assumption 7, there exists no dual Lagrange multiplier space* M_k *such that* $W_k^1 \subset M_k$.

PROOF. We prove this by contradiction. Assume that

$$\sum_i \alpha_i \mu_i = \phi_p^l, \tag{3.2.2}$$

where ϕ_p^l is the bilinear hat function associated with the interior vertex p having the coordinates $(0,0)$, see Figure 3.2. Suppose the coordinates of the four corners of the face F_1 be $(-1,0),(0,0),(0,1)$ and $(-1,1)$, and of the face F_2 be $(0,0),(1,0),(1,1)$ and $(0,1)$.

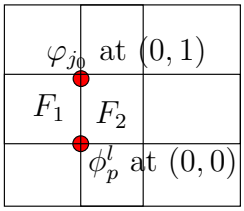

Figure 3.2: 2D interface of 3D hexahedral triangulation

Because of the duality, the functions μ_i are biorthogonal to the finite element basis functions φ_i on the interface. Hence, after multiplying (3.2.2) by some finite element basis function φ_j and integrating over the interface γ_k, we get

$$\alpha_j = \frac{\int_{\gamma_k} \varphi_j \phi_p^l \, d\sigma}{\int_{\gamma_k} \varphi_j \, d\sigma}.$$

Let j_0 be the interior vertex with coordinates $(0,1)$ such that j_0 and p share one edge, see Figure 3.2. Then, we can write

$$\int_{\gamma_k} \varphi_{j_0}\phi_p^l \, d\sigma = \int_{F_1} \varphi_{j_0}\phi_p^l \, d\sigma + \int_{F_2} \varphi_{j_0}\phi_p^l \, d\sigma = -\frac{1}{18}$$

and thus $\alpha_{j_0} \neq 0$. Since the basis functions μ_i are locally linearly independent, we obtain $\operatorname{supp}\mu_{j_0} \subseteq \operatorname{supp}\sum_i \alpha_i\mu_i$. By construction, we find $\operatorname{supp}\mu_{j_0} \not\subset \operatorname{supp}\phi_p^l$, which contradicts (3.2.2). □

3.2.3. The standard Lagrange multiplier space for quadratic serendipity elements. The previous subsection shows that there does not exist a dual Lagrange multiplier space for quadratic serendipity elements containing the bilinear hat function at each vertex and satisfying $\operatorname{supp}\varphi_i = \operatorname{supp}\mu_i$ and Assumption 7. We recall that Assumptions 2–4 are crucial for the Lagrange multiplier space so that the resulting discretization scheme is optimal and stable. The first idea is to choose a standard Lagrange multiplier space, see [**33, 34**]. In this case, the basis functions for each interior face $F \in \mathcal{T}_k$ of the interface γ_k (i.e., $F \in \mathcal{T}_k$ with $\partial F \cap \partial\gamma_k = \emptyset$) are quadratic serendipity basis functions in two dimensions. All nodes on $\partial\gamma_k$ do not carry a degree of freedom for the Lagrange multipliers. Therefore, in order to satisfy Assumption 4, it is necessary to modify the definition of the basis functions for the elements touching the boundary $\partial\gamma_k$ of the interface γ_k. Suppose a face $F \in \mathcal{S}_k$ with $\partial F \cap \partial\gamma_k \neq \emptyset$ has n degrees of freedom for the Lagrange multipliers with $n \geq 3$. Then, the local Lagrange multiplier basis function μ_i at a node x_i of F is chosen to be a polynomial of minimal degree such that $\mu_i(x_j) = \delta_{ij}$ for all x_j, $j = 1, \cdots, n$. These Lagrange multiplier basis functions are continuous. Since, in general, $M_k \subset \left(H^{1/2}(\gamma_k)\right)'$, we can work with discontinuous Lagrange multipliers. Working with a continuous Lagrange multiplier space which locally contains the linear functions has the advantage that Assumption 4 is satisfied. Here too, Assumption 2 is trivially satisfied by construction. To verify Assumption 3, we take $\mu := \sum_{k=1}^{n_k} a_k\mu_k \in M_k$, and define $\varphi := \sum_{k=1}^{n_k} a_k\varphi_k$ in W_k. Then

$$(\varphi,\mu)_{0,\gamma_k} = \sum_{i,j=1}^{n_k} a_i a_j (\varphi_i,\mu_j)_{0,\gamma_k} = \sum_{i,j=1}^{n_k} a_i a_j \int_{\gamma_k} \varphi_i \, \mu_j \, d\sigma.$$

The local mass matrix $\mathtt{M}_{\hat{F}}$ on the reference element $\hat{F}$ for a face having all the vertices in γ_k is given by

$$\mathtt{M}_{\hat{F}} = \begin{bmatrix} \frac{2}{15} & \frac{2}{45} & \frac{1}{15} & \frac{2}{45} & -\frac{2}{15} & -\frac{8}{45} & -\frac{8}{45} & -\frac{2}{15} \\ \frac{2}{45} & \frac{2}{15} & \frac{2}{45} & \frac{1}{15} & -\frac{2}{15} & -\frac{2}{15} & -\frac{8}{45} & -\frac{8}{45} \\ \frac{1}{15} & \frac{2}{45} & \frac{2}{15} & \frac{2}{45} & -\frac{8}{45} & -\frac{2}{15} & -\frac{2}{15} & -\frac{8}{45} \\ \frac{2}{45} & \frac{1}{15} & \frac{2}{45} & \frac{2}{15} & -\frac{8}{45} & -\frac{8}{45} & -\frac{2}{15} & -\frac{2}{15} \\ -\frac{2}{15} & -\frac{2}{15} & -\frac{8}{45} & -\frac{8}{45} & \frac{32}{45} & \frac{4}{9} & \frac{16}{45} & \frac{4}{9} \\ -\frac{8}{45} & -\frac{2}{15} & -\frac{2}{15} & -\frac{8}{45} & \frac{4}{9} & \frac{32}{45} & \frac{4}{9} & \frac{16}{45} \\ -\frac{8}{45} & -\frac{8}{45} & -\frac{2}{15} & -\frac{2}{15} & \frac{16}{45} & \frac{4}{9} & \frac{32}{45} & \frac{4}{9} \\ -\frac{2}{15} & -\frac{8}{45} & -\frac{8}{45} & -\frac{2}{15} & \frac{4}{9} & \frac{16}{45} & \frac{4}{9} & \frac{32}{45} \end{bmatrix}.$$

Similarly, computing the local mass matrices for the different boundary cases, we find that all the eigenvalues of the local mass matrices are greater than $\frac{1}{25}$ and smaller than $\frac{24}{11}$. Then $(\varphi,\mu)_{0,\gamma_k}$, $\|\varphi\|^2_{0,\gamma_k}$ and $\|\mu\|^2_{0,\gamma_k}$ are equivalent to $\sum_{i=1}^{n_k} \underline{h}^2_{s(k),i} a_i^2$, which guarantees Assumption 3. Here, $\underline{h}_{s(k),i}$ is the local meshsize at the i-th node as before. The coupling of the local mass matrices yield a global mass matrix which is sparse and banded. But the inverse of the global mass matrix $\mathtt{M}_s$ on the slave side is dense. As a consequence, we obtain a stiffness matrix associated with the variational problem (1.4.2), which is not sparse. Then we cannot apply static condensation, and the multigrid method discussed in [**166**] cannot be used.

3.2.4. A quasi-dual Lagrange multiplier space for quadratic serendipity elements. To overcome this difficulty arising from the use of standard Lagrange multiplier space, we introduce a new approach for the quadratic serendipity elements. The idea is to use a Lagrange multiplier space which yields a sparse inverse of the global mass matrix $\mathtt{M}_s$ on the slave side. Working with the tensor product dual basis functions associated with the degrees of freedom of quadratic serendipity elements yields a diagonal mass matrix $\mathtt{M}_s$, and Assumptions 2 and 3 are satisfied. However, Assumption 4 is not satisfied, and although the discretization scheme is stable, no optimal a priori bounds can be obtained. Now in a first step, we enrich the Lagrange multiplier space to guarantee Assumption 4. As a result, Assumption 2 is lost and thus the inf-sup condition for the Lagrange multiplier space. Therefore, we have to augment the trace space in a second step. The second step can be viewed as a stabilization technique and is well known within the framework of three-field approaches, see, e.g., [**54, 55, 58, 24**]. This step guarantees that after enriching the Lagrange multiplier space, Assumptions 2–3 are satisfied. To perform the second step, we enrich each non-empty face $F \subseteq \partial T \cap \Gamma$ of the element T of the slave side with a bubble function. The bubble function $b \in H^1(T)$ corresponding to the face F of T has the property that $b_{|\partial T\setminus F} = 0$, and $\int_F b\, d\sigma \neq 0$. Although we need only the restriction of the bubble functions to the associated face to satisfy Assumption 2, each bubble function is supported on the whole element. In general, such a bubble function can be defined in many different ways. Using the triquadratic nodal finite element function associated with the center of gravity of the face as a bubble function corresponding to this face, we obtain the mass matrix $\mathtt{M}_s$ on the slave side having a special structure.

Suppose $\hat{\varphi}_i$ and $\hat{\lambda}_i$, $1 \le i \le 9$, be the local basis functions of the standard triquadratic finite elements and their dual Lagrange multipliers on the reference face $\hat{F}$, respectively. Here, the first four basis functions correspond to the vertices, the second four ones correspond to the midpoints of the edges, and the last one corresponds to the center of gravity of the reference face $\hat{F}$. Then, the local basis functions of the quadratic serendipity elements can be written as $\hat{\varphi}_i^s = \hat{\varphi}_i + \alpha_i \hat{\varphi}_9$, $(1 \le i \le 8)$, where $\alpha_i = -\frac{1}{4}$ for $(1 \le i \le 4)$ and $\alpha_i = \frac{1}{2}$ for $(5 \le i \le 8)$. Using the biorthogonality of $\hat{\varphi}_i$ and $\hat{\lambda}_i$, we have

$$\int_{\hat{F}} \hat{\varphi}_i^s\, \hat{\lambda}_j\, d\sigma = \int_{\hat{F}} (\hat{\varphi}_i + \alpha_i \hat{\varphi}_9)\, \hat{\lambda}_j\, d\sigma = \delta_{ij} \int_{\hat{F}} \hat{\varphi}_i\, d\sigma + \alpha_i \delta_{9j} \int_{\hat{F}} \hat{\varphi}_9\, d\sigma.$$

In fact, the mass matrix on the reference face $\hat{F}$ is

$$\mathtt{M}_{\hat{F}} = \begin{bmatrix} \frac{1}{9} & 0 & 0 & 0 & 0 & 0 & 0 & 0 & 0 \\ 0 & \frac{1}{9} & 0 & 0 & 0 & 0 & 0 & 0 & 0 \\ 0 & 0 & \frac{1}{9} & 0 & 0 & 0 & 0 & 0 & 0 \\ 0 & 0 & 0 & \frac{1}{9} & 0 & 0 & 0 & 0 & 0 \\ 0 & 0 & 0 & 0 & \frac{4}{9} & 0 & 0 & 0 & 0 \\ 0 & 0 & 0 & 0 & 0 & \frac{4}{9} & 0 & 0 & 0 \\ 0 & 0 & 0 & 0 & 0 & 0 & \frac{4}{9} & 0 & 0 \\ 0 & 0 & 0 & 0 & 0 & 0 & 0 & \frac{4}{9} & 0 \\ -\frac{4}{9} & -\frac{4}{9} & -\frac{4}{9} & -\frac{4}{9} & \frac{8}{9} & \frac{8}{9} & \frac{8}{9} & \frac{8}{9} & \frac{16}{9} \end{bmatrix}. \tag{3.2.3}$$

We define $\mathcal{K}_s := \{T \in \mathcal{T}_{s(k);h_{s(k)}}, 1 \leq k \leq N \mid \partial T \cap \Gamma \text{ contains at least one face of } T\}$. Now, the space of bubble functions B_h is formed by N_s bubbles, where N_s is the number of faces in $\cup_{k=1}^{N} \mathcal{S}_{k;h_k}$, and each of them is associated with a face F of an element $T \in \mathcal{K}_s$, where $F \subseteq \partial T \cap \Gamma$. This leads to one additional degree of freedom for each non-empty face $F \subseteq \partial T \cap \Gamma$ of $T \in \mathcal{K}_s$. Now, the modified unconstrained product space X_h^t can be written as $X_h^t = X_h^s \oplus B_h$, where X_h^s is the unconstrained product space associated with quadratic serendipity elements. In the sequel, the space X_h^t will be called augmented quadratic serendipity space and the corresponding elements augmented quadratic serendipity elements.

In a next step, we consider the global mass matrix $\mathtt{M}_s$ on the slave side in more detail. In the following, we use the same notation for the vector representation of the solution and the solution as an element in X_h^t and M_h. The matrix $\mathtt{A}$ is the stiffness matrix associated with the bilinear form $a(\cdot,\cdot)$ on $X_h^t \times X_h^t$, and the matrices $\mathtt{B}$ and $\mathtt{B}^T$ are associated with the bilinear form $b(\cdot,\cdot)$ on $X_h^t \times M_h$. Then, the algebraic formulation of the saddle point problem (1.4.3) is given by

$$\begin{bmatrix} \mathtt{A} & \mathtt{B}^T \\ \mathtt{B} & 0 \end{bmatrix} \begin{bmatrix} u_h \\ \lambda_h \end{bmatrix} = \begin{bmatrix} f_h \\ 0 \end{bmatrix}. \tag{3.2.4}$$

We recall the grouping of the degrees of freedom of X_h^t introduced in Section 1.6 and redefine the group $\mathcal{N}_m$ and the block vector u_m with $\mathcal{N}_m \cup \mathcal{N}_c \to \mathcal{N}_m$, and $(u_m^T, u_c^T) \to u_m^T$, respectively. After augmenting the quadratic serendipity space with the space of bubble functions B_h and redefining the group $\mathcal{N}_m$ and the block vector u_m, we further decompose the degrees of freedom associated with the interior nodes of $\gamma_k, 1 \leq k \leq N$, on the slave side into two groups (u_s, u_b). Here, the block vector u_s contains nodal values of u at the interior nodes of γ_k, $1 \leq k \leq N$, corresponding to the vertices and edges on the slave side, and u_b stands for all nodal values corresponding to the bubble functions on the slave side. With this decomposition, we can write $u_h^T = (u_i^T, u_m^T, u_s^T, u_b^T)$. The block vector λ_h containing the nodal values of the Lagrange multiplier is similarly decomposed with $\lambda_h^T = (\lambda_s^T, \lambda_b^T)$. In terms of this decomposition, we can rewrite the algebraic form of the saddle point problem

(3.2.4) as

$$
\begin{bmatrix}
\mathtt{A}_{ii} & \mathtt{A}_{im} & \mathtt{A}_{is} & \mathtt{A}_{ib} & 0 & 0 \\
\mathtt{A}_{mi} & \mathtt{A}_{mm} & \mathtt{A}_{ms} & \mathtt{A}_{mb} & \mathtt{M}_m^T & \mathtt{M}_{bm}^T \\
\mathtt{A}_{si} & \mathtt{A}_{sm} & \mathtt{A}_{ss} & \mathtt{A}_{sb} & \mathtt{D}_s & \mathtt{M}_{bs}^T \\
\mathtt{A}_{bi} & \mathtt{A}_{bm} & \mathtt{A}_{bs} & \mathtt{A}_{bb} & 0 & \mathtt{D}_b \\
0 & \mathtt{M}_m & \mathtt{D}_s & 0 & 0 & 0 \\
0 & \mathtt{M}_{bm} & \mathtt{M}_{bs} & \mathtt{D}_b & 0 & 0
\end{bmatrix}
\begin{bmatrix} u_i \\ u_m \\ u_s \\ u_b \\ \lambda_s \\ \lambda_b \end{bmatrix}
=
\begin{bmatrix} f_i \\ f_m \\ f_s \\ f_b \\ 0 \\ 0 \end{bmatrix}. \tag{3.2.5}
$$

Recalling the algebraic structure (1.6.1) of the bilinear form $b(\cdot,\cdot)$ restricted to $X_h^t \times M_h$, we have

$$
\mathtt{B} = \begin{bmatrix} 0 & \mathtt{M}_m & \mathtt{D}_s & 0 \\ 0 & \mathtt{M}_{bm} & \mathtt{M}_{bs} & \mathtt{D}_b \end{bmatrix},
$$

where $\mathtt{D}_b$ and $\mathtt{D}_s$ are diagonal matrices, and $\mathtt{M}_{bs}$, $\mathtt{M}_m$ and $\mathtt{M}_{bm}$ are rectangular matrices. The matrix $\mathtt{D}_b$ is diagonal due to the fact that the bubble functions are supported only in one element, and the diagonal form of $\mathtt{D}_s$ follows from the structure of the local mass matrix, see (3.2.3). Hence, the global mass matrix $\mathtt{M}_s$ on the slave side can be written as

$$
\mathtt{M}_s = \begin{bmatrix} \mathtt{D}_s & 0 \\ \mathtt{M}_{bs} & \mathtt{D}_b \end{bmatrix}.
$$

Comparing the mass matrix $\mathtt{M}_s$ from the definition (1.20) of the quasi-dual Lagrange multiplier space, we conclude that this is a quasi-dual Lagrange multiplier space. The great benefit of this Lagrange multiplier space is that the inverse of the mass matrix $\mathtt{M}_s$ can be computed very easily, and the inverse is sparse. In fact, the inverse of the mass matrix $\mathtt{M}_s$ is

$$
\mathtt{M}_s^{-1} = \begin{bmatrix} {\mathtt{D}_s}^{-1} & 0 \\ -\mathtt{D}_b^{-1}\mathtt{M}_{bs}\mathtt{D}_s^{-1} & {\mathtt{D}_b}^{-1} \end{bmatrix}.
$$

Thus the solution at the slave side depends locally on the solution at the master side. Here, we have to invert only two diagonal matrices and scale $\mathtt{M}_{bs}$ to compute the inverse of the mass matrix $\mathtt{M}_s$. The stiffness matrix associated with the variational problem (1.4.2) is sparse, and efficient iterative solver like multigrid can easily be adapted to the non-conforming situation. Furthermore, the degree of freedom corresponding to the bubble functions can locally be eliminated by static condensation. Since the matrix $\mathtt{D}_b$ is diagonal, the sixth and the fourth line of the system (3.2.5) give

$$
\begin{aligned}
u_b &= -\mathtt{D}_b^{-1}(\mathtt{M}_{bm}u_m + \mathtt{M}_{bs}u_s), \quad \text{and} \\
\lambda_b &= \mathtt{D}_b^{-1}\left[f_b - \mathtt{A}_{bi}u_i - (\mathtt{A}_{bm} - \mathtt{A}_{bb}\mathtt{D}_b^{-1}\mathtt{M}_{bm})u_m - (\mathtt{A}_{bs} - \mathtt{A}_{bb}\mathtt{D}_b^{-1}\mathtt{M}_{bs})u_s\right].
\end{aligned}
$$

Now, we eliminate u_b and λ_b from the system (3.2.5) and obtain a new system

$$
\hat{\mathtt{A}}\hat{u}_h = \hat{f}_h,
$$

where $\hat{u}_h^T = (u_i^T, u_m^T, u_s^T, \lambda_s^T)$. Defining $\mathtt{M}_1 := \mathtt{D}_b^{-1}\mathtt{M}_{bm}$, and $\mathtt{M}_2 := \mathtt{D}_b^{-1}\mathtt{M}_{bs}$, we have

$$\hat{\mathtt{A}} = \begin{bmatrix} \mathtt{A}_{ii} & \mathtt{A}_{im} - \mathtt{A}_{ib}\mathtt{M}_1 & \mathtt{A}_{is} - \mathtt{A}_{ib}\mathtt{M}_2 & 0 \\ \mathtt{A}_{mi} - \mathtt{M}_1^T\mathtt{A}_{bi} & \mathtt{A}_{mm} - \mathtt{A}_{mb}\mathtt{M}_1 - \mathtt{M}_1^T(\mathtt{A}_{bm} - \mathtt{A}_{bb}\mathtt{M}_1) & \mathtt{A}_{ms} - \mathtt{A}_{mb}\mathtt{M}_2 - \mathtt{M}_1^T(\mathtt{A}_{bs} - \mathtt{A}_{bb}\mathtt{M}_2) & \mathtt{M}_m^T \\ \mathtt{A}_{si} - \mathtt{M}_2^T\mathtt{A}_{bi} & \mathtt{A}_{sm} - \mathtt{A}_{sb}\mathtt{M}_1 - \mathtt{M}_2^T(\mathtt{A}_{bm} - \mathtt{A}_{bb}\mathtt{M}_1) & \mathtt{A}_{ss} - \mathtt{A}_{sb}\mathtt{M}_2 - \mathtt{M}_2^T(\mathtt{A}_{bs} - \mathtt{A}_{bb}\mathtt{M}_2) & \mathtt{D}_s \\ 0 & \mathtt{M}_m & \mathtt{D}_s & 0 \end{bmatrix},$$

and the right hand side can be written as

$$\hat{f}_h = \begin{bmatrix} f_i \\ f_m - \mathtt{M}_1^T f_b \\ f_s - \mathtt{M}_2^T f_b \\ 0 \end{bmatrix}.$$

We observe that the matrix $\hat{\mathtt{A}}$ is symmetric, if $\mathtt{A}$ is symmetric and it has exactly the same structure as the saddle point matrix arising from mortar finite element method with a dual Lagrange multiplier space, see [**163**]. Because of this structure of the algebraic system, we can apply the multigrid method proposed in [**166**].

REMARK 3.2. *There is also a possibility to use wavelets to get a mass matrix of special structure so that the inversion can be cheaper, and the inverse is sparse. In* [**147**]*, locally supported and piecewise polynomial wavelets are studied on non-uniform meshes which give a lower triangular mass matrix with higher order finite elements in triangular meshes.*

3.3. Numerical results

We consider three different cases for quadratic mortar finite elements. The first one is the standard triquadratic finite element space with the dual Lagrange multiplier space. The second one is the quadratic serendipity space with a standard Lagrange multiplier space. Finally, the third one is the augmented quadratic serendipity space associated with the tensor product Lagrange multiplier space. These Lagrange multiplier spaces are introduced in Section 3.2. The dual Lagrange multiplier space introduced in [**163**] is used for the lowest order case. Our numerical results show the same asymptotic behavior as predicted by the theory. As in the two-dimensional case, the implementation is based on the finite element toolbox UG, [**17**]. We do not discuss and analyze an iterative solver for the arising linear systems. As noted in the first chapter, an optimal multigrid solver can be applied when working with dual Lagrange multiplier spaces. Unfortunately, in the case of a standard Lagrange multiplier space no local elimination of the flux can be carried out. Following the approach in [**166**], the sparsity of the modified system and the efficiency of the multigrid solver is lost. In that case, we apply a multigrid method for saddle point problems. This technique has been considered for mortar elements in [**159**] and further analyzed in [**44, 160**]. It turns out that we do not have to work in a positive definite subspace, and the smoother can be realized by an inner and outer iteration scheme. As in the other approach, level-independent multigrid convergence rates can be established. However, the numerical solution process is slower if we have to work with the saddle point approach. We point out that the more efficient multigrid method for the modified positive definite system can only be applied when the inverse of $\mathtt{M}_s$ is sparse, whereas the saddle point multigrid method is more general. Although we do not have a dual Lagrange

multiplier space for the quadratic serendipity elements satisfying Assumption 7, the tensor product Lagrange multiplier space in combination with the introduction of bubble functions on the slave side of the interface yield an optimal discretization scheme. We present some numerical results in three dimensions illustrating the performance of the different Lagrange multiplier spaces. In particular, we compare the discretization errors in the L^2- and H^1-norms for the solution computed with linear and quadratic mortar finite elements. The discretization errors in the flux across the interface are compared in the mesh-dependent Lagrange multiplier norm given by 1.6.3. For all our examples, we have used uniform refinement. In each refinement step, one element is refined into eight subelements. We denote by X_h^l and X_h^f the unconstrained finite element spaces associated with the standard finite element spaces for the trilinear and the triquadratic case, respectively. Similarly, X_h^s and X_h^t are the unconstrained finite element spaces associated with the quadratic serendipity elements and the augmented quadratic serendipity elements as defined in the previous section, respectively. The corresponding finite element solutions are denoted by u_h^l, u_h^f, u_h^s and u_h^t, respectively. The Lagrange multiplier solution will be similarly denoted by $\lambda_h^l, \lambda_h^f, \lambda_h^s$ and λ_h^t, respectively.

REMARK 3.3. *We note that the concept of dual Lagrange multiplier spaces can be generalized to distorted hexahedral meshes. In that case, the mapping between the actual element and the reference element has a non-constant Jacobian. As a consequence, we have to compute for each face on the interface a biorthogonal basis with respect to the local nodal one. This can be easily done by solving a local mass matrix system. By construction, the sum of the local dual Lagrange multiplier basis functions is one. Defining the global Lagrange multiplier basis functions by gluing the local ones together, we find that the constants are included in the Lagrange multiplier space. As a consequence, it is easy to verify that the discretization error is of order h for lowest order finite elements, see* [**78**].

Example 1: Our first example is given by $-\Delta u = f$ on $\Omega := (0,1)^2 \times (0,2)$, where Ω is decomposed into two subdomains $\Omega_1 := (0,1)^3$ and $\Omega_2 := (0,1)^2 \times (1,2)$. The right hand side f and the boundary conditions are chosen such that the exact solution is given by $u(x,y,z) = 2\exp(-x^2-y^2-z^2)\sin(12\,yx)\,(x+y+z)\,(x-y-z)$. In Figure 3.3, the decomposition of the domain, the initial triangulation and the isolines of the solution at the interface $z = 1$ are shown. We have used a non-conforming initial triangulation, where the lower cube is refined once, and the upper cube is left as it is. The errors in the L^2-, H^1- and the weighted Lagrange multiplier norms are given in Tables 3.1–3.3. The tables show that we get the predicted asymptotic convergence rates. For the quadratic case, the errors in the L^2- and H^1-norms are of order h^3 and h^2, whereas they are of order h^2 and h for the linear case. The errors in the weighted Lagrange multiplier norm for the quadratic and linear cases are of order $h^{5/2}$ and $h^{3/2}$, respectively. Theoretically, the errors in the weighted Lagrange multiplier norm for quadratic and linear case are expected to be of order h^2 and h, respectively. The better convergence rates are due to the fact that the error in the H^1-norm is equally distributed and the Lagrange multiplier space has an $O(h^{5/2})$ and $O(h^{3/2})$ approximation property in the considered norm. For the three different second order approaches, the quantitative results are asymptotically almost the same in the L^2- and H^1-norms. Only in the weighted Lagrange multiplier norm, the full

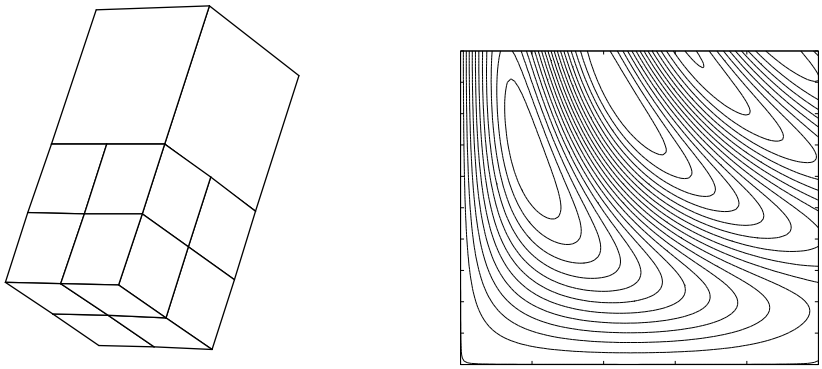

Figure 3.3: Decomposition of the domain and initial triangulation (left), isolines of the solution at the interface (right), Example 1

triquadratic case yields better results. However, there is not any essential difference between the quadratic serendipity elements with the standard Lagrange multiplier space and the augmented quadratic serendipity elements with the tensor product Lagrange multiplier space.

TABLE 3.1. Discretization errors in the L^2-norm, Example 1

level	# elem.	$\|u-u_h^l\|_0$	$\|u-u_h^f\|_0$	$\|u-u_h^s\|_0$	$\|u-u_h^t\|_0$
0	9	1.004794e+00	8.867203e-01	9.145121e-01	9.125653e-01
1	72	9.091292e-01	3.187528e-01	4.650386e-01	4.574443e-01
2	576	4.363422e-01	3.705310e-02	4.563530e-02	4.558460e-02
3	4608	1.033778e-01	7.450696e-03	7.649595e-03	7.611510e-03
4	36864	2.640337e-02	9.606873e-04	9.654041e-04	9.639183e-04

TABLE 3.2. Discretization errors in the H^1-norm, Example 1

level	# elem.	$\|u-u_h^l\|_1$	$\|u-u_h^f\|_1$	$\|u-u_h^s\|_1$	$\|u-u_h^t\|_1$
0	9	1.000886e+00	9.356647e-01	9.705044e-01	9.671180e-01
1	72	9.446222e-01	6.608442e-01	7.237820e-01	7.076152e-01
2	576	6.449633e-01	1.353106e-01	1.490407e-01	1.485072e-01
3	4608	3.005969e-01	4.988503e-02	5.140438e-02	5.108725e-02
4	36864	1.508831e-01	1.261993e-02	1.269328e-02	1.267161e-02

For the next three examples, we consider only the quadratic serendipity elements.

Example 2: In our second example, the domain $\Omega := (0,1)^2 \times (0,2.5)$ is decomposed into three subdomains $\Omega_1 := (0,1)^3$, $\Omega_2 := (0,1)^2 \times (1,2)$, and $\Omega_3 := (0,1)^2 \times (2,2.5)$. The right hand side f and the boundary conditions of $-\Delta u = f$ are chosen such that the exact solution is given by $u(x,y,z) = 5(z-1.4)((x-0.5)^2+4(y-0.3)^3)+z(z-1)\sin(4\pi xy)(2(x-y)^2+(y+x-1)^2)$. In Figure 3.4, we have shown the decomposition of the domain, the initial non-matching triangulation and the isolines of the solution at the interface $z = 2$.

TABLE 3.3. Discretization errors in the weighted Lagrange multiplier norm, Example 1

level	# elem.	$\|\lambda - \lambda_h^l\|_h$	$\|\lambda - \lambda_h^f\|_h$	$\|\lambda - \lambda_h^s\|_h$	$\|\lambda - \lambda_h^t\|_h$
0	9	4.685044e-01	5.949429e+00	6.980608e+00	8.650037e+00
1	72	3.072290e+00	4.254093e+00	4.300310e+00	5.528655e+00
2	576	1.824458e+00	4.052985e-01	6.517151e-01	7.399415e-01
3	4608	6.300125e-01	1.071732e-01	1.493473e-01	1.466488e-01
4	36864	2.246235e-01	1.669782e-02	2.047104e-02	2.410364e-02

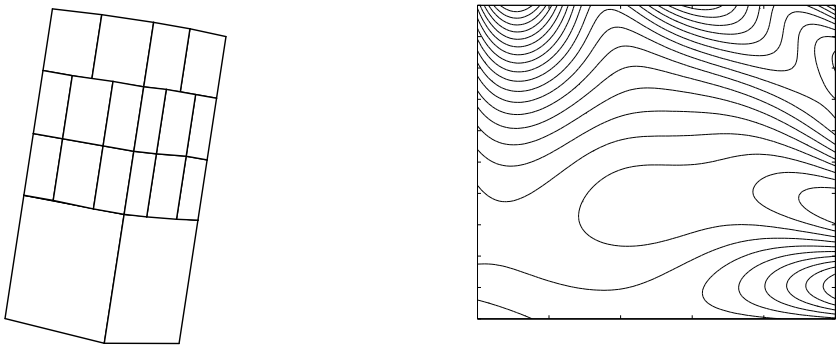

Figure 3.4: Decomposition of the domain and initial triangulation (left), isolines of the solution at the interface $z = 2$ (right), Example 2

Here, we have three subdomains and two interfaces. The middle cube is taken as the slave side. We start with a non-conforming coarse initial triangulation having 23 elements. The errors along with their order of convergence at every step of refinement in different norms are given in Tables 3.4–3.6. As before, we get the correct asymptotic rates for both cases of the quadratic serendipity elements. The errors in the L^2- and H^1-norms are almost the same for both approaches. In the weighted Lagrange multiplier norm, the quadratic serendipity elements yield less errors than the augmented quadratic serendipity elements. However, the difference is quite negligible, and the asymptotic rate of convergence is optimal in both cases.

TABLE 3.4. Discretization errors in the L^2-norm, Example 2

level	# elem.	$\|u - u_h^l\|_0$		$\|u - u_h^s\|_0$		$\|u - u_h^t\|_0$	
0	23	8.911337e-01		1.745670e-01		1.760480e-01	0
1	184	2.582954e-01	1.79	2.997997e-02	2.54	3.010899e-02	2.55
2	1472	6.366337e-02	2.02	3.664595e-03	3.03	3.671731e-03	3.04
3	11776	1.607229e-02	1.99	4.466631e-04	3.04	4.462098e-04	3.04
4	94208	4.031862e-03	2.00	5.393667e-05	3.05	5.391429e-05	3.05

TABLE 3.5. Discretization errors in the H^1-norm, Example 2

level	# elem.	$\|u-u_h^l\|_1$		$\|u-u_h^s\|_1$		$\|u-u_h^t\|_1$	
0	23	8.170532e-01		5.517577e-01		5.290887e-01	0
1	184	5.643329e-01	0.53	1.478160e-01	1.90	1.482833e-01	1.84
2	1472	2.626420e-01	1.10	3.915936e-02	1.92	3.920488e-02	1.92
3	11776	1.293053e-01	1.02	9.352708e-03	2.07	9.332480e-03	2.07
4	94208	6.446694e-02	1.00	2.295583e-03	2.03	2.293897e-03	2.02

TABLE 3.6. Discretization errors in the weighted Lagrange multiplier norm, Example 2

level	# elem.	$\|\lambda-\lambda_h^l\|_h$		$\|\lambda-\lambda_h^s\|_h$		$\|\lambda-\lambda_h^t\|_h$	
0	23	7.433164e+00		2.762317e+01		2.758347e+01	0
1	184	5.657720e+00	0.39	2.006842e+00	3.78	3.320707e+00	3.05
2	1472	1.855735e+00	1.61	7.048806e-01	1.51	8.042462e-01	2.05
3	11776	4.868778e-01	1.93	1.001359e-01	2.82	1.151919e-01	2.80
4	94208	1.832775e-01	1.41	1.564914e-02	2.68	1.879805e-02	2.62

Example 3: In our third example, we have used a U-shaped domain Ω decomposed into five subdomains Ω_k, $k = 1, \cdots, 5$, and the problem is given by a Poisson equation $-\Delta u = f$. Here, $\Omega_1 := (0,1)^3$, $\Omega_2 := (0,1)^2 \times (1,2.4)$, $\Omega_4 := (2,3) \times (-0.2,1.2) \times (0,1)$, $\Omega_5 := (2,3) \times (-0.2,1.2) \times (1,2)$, and Ω_3 is a hexahedral pyramidal frustum joining the domain Ω_1 and Ω_4, see the left picture of Figure 3.5. Here, we choose the right hand side function f and Dirichlet boundary condition on $\partial\Omega$ so that we obtain the exact solution

$$u(x,y,z) = \exp\left(-\frac{1}{4}(x^2+y^2+z^2)\right)\left(\cos(5\,x+z) + 3\,\sin(4\,y+z)\right).$$

The isolines of the solution at the plane $z = 1$ are given in the right picture of Figure 3.5. We have given the discretization errors in different norms in Tables 3.7–3.9. As before, we get optimal convergence rates in the L^2- and H^1-norms for both quadratic approaches and better convergence behavior in the weighted Lagrange multiplier norm.

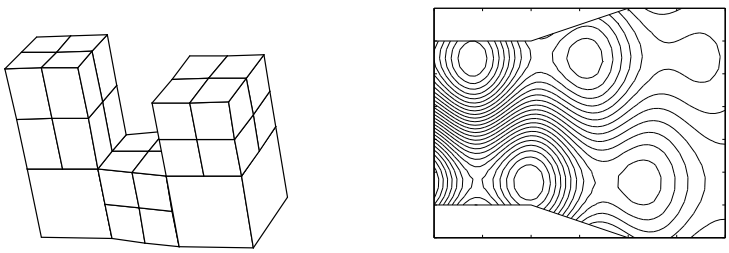

Figure 3.5: Decomposition of the domain and initial triangulation (left) and isolines of the solution at the plane $z = 1$ (right), Example 3

TABLE 3.7. Discretization errors in the L^2-norm, Example 3

level	# elem.	$\|u-u_h^l\|_0$		$\|u-u_h^s\|_0$		$\|u-u_h^t\|_0$	
0	26	7.310111e-01		3.478550e-01		3.166037e-01	
1	208	3.398657e-01	1.10	4.304959e-02	3.01	4.209598e-02	2.91
2	1664	8.175747e-02	2.06	5.991830e-03	2.84	5.949794e-03	2.82
3	13312	2.027467e-02	2.01	7.579318e-04	2.98	7.564277e-04	2.98
4	106496	5.037341e-03	2.01	9.456858e-05	3.00	9.451905e-05	3.00

TABLE 3.8. Discretization errors in the H^1-norm, Example 3

level	# elem.	$\|u-u_h^l\|_1$		$\|u-u_h^s\|_1$		$\|u-u_h^t\|_1$	
0	26	8.982209e-01		5.699839e-01		4.440725e-01	
1	208	5.597470e-01	0.68	1.391079e-01	2.03	1.308973e-01	1.76
2	1664	2.683965e-01	1.06	3.643727e-02	1.93	3.576211e-02	1.87
3	13312	1.327426e-01	1.02	9.024865e-03	2.01	8.980617e-03	1.99
4	106496	6.597358e-02	1.01	2.239350e-03	2.01	2.236550e-03	2.01

TABLE 3.9. Discretization errors in the weighted Lagrange multiplier norm, Example 3

level	# elem.	$\|\lambda-\lambda_h^l\|_h$		$\|\lambda-\lambda_h^s\|_h$		$\|\lambda-\lambda_h^t\|_h$	
0	26	8.792140e+00		1.351765e+01		1.416514e+01	
1	208	5.592290e+00	0.65	2.113658e+00	2.68	1.567016e+00	3.18
2	1664	1.963516e+00	1.51	3.166530e-01	2.74	3.365031e-01	2.22
3	13312	7.490561e-01	1.39	4.610005e-02	2.78	5.699660e-02	2.56
4	106496	2.745105e-01	1.45	7.388080e-03	2.64	9.779245e-03	2.54

Example 4: In our last example, we consider a domain $\Omega := (0,2)\times(0,1)\times(0,2)$, which is decomposed into four subdomains $\Omega_1 := (0,1)^3, \Omega_2 := (0,1)^2\times(1,2), \Omega_3 := (1,2)\times(0,1)^2$ and $\Omega_4 := (1,2)\times(0,1)\times(1,2)$. We have shown the decomposition of the domain and the initial triangulation in the left picture of Figure 3.6, the isolines of the solution on the plane $y = \frac{1}{2}$ in the middle, and the flux of the exact solution at the interface $x = 1$ is shown in the right one. Here, Ω_2 and Ω_3 are taken to be the slave sides and the rest are the master sides. The problem for this example is given by a reaction-diffusion equation

$$-\mathrm{div}(a\nabla u) + u = f \quad \text{in} \quad \Omega,$$

where a is chosen to be 1 in Ω_1 and Ω_4, and $a = 10$ in Ω_2 and Ω_3. We have chosen the exact solution $u(x,y,z) = (x-1)\,y\,(z-1)\exp(-(x-1)^2 - y^2 - (z-1)^2)\cos(2\,x + 2\,y + 2\,z)/a$ and the right hand side f and the Dirichlet boundary conditions are determined from the exact solution. We remark that the exact solution u has a jump in the normal derivative across the interface, whereas the flux is continuous. We have given the errors together with

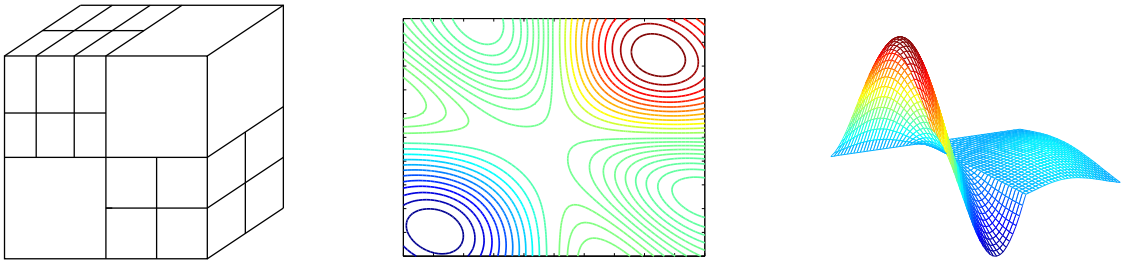

Figure 3.6: Decomposition of the domain and initial triangulation (left), isolines of the solution at the plane $y = \frac{1}{2}$ (middle) and flux of the exact solution at the interface $x = 1$ (right), Example 4

their order of convergence in every step of refinement in different norms in Tables 3.10–3.12. As in other examples, we get the same asymptotic rates for the L^2- and H^1-norm and better convergence rates in the weighted Lagrange multiplier norm. In contrast to other examples, we see that the asymptotic rate in the weighted Lagrange multiplier norm for the quadratic case is even better than $O(h^3)$, and the augmented quadratic serendipity elements show the better order of convergence in this norm.

TABLE 3.10. Discretization errors in the L^2-norm, Example 4

level	# elem.	$\|u - u_h^l\|_0$		$\|u - u_h^s\|_0$		$\|u - u_h^t\|_0$	
0	22	4.636300e-01		1.237718e-01		1.233229e-01	
1	176	1.218875e-01	1.93	1.220035e-02	3.34	1.220072e-02	3.34
2	1408	3.082112e-02	1.98	1.164306e-03	3.39	1.164276e-03	3.39
3	11264	7.712933e-03	2.00	1.422899e-04	3.03	1.422876e-04	3.03
4	90112	1.928288e-03	2.00	1.773015e-05	3.00	1.773010e-05	3.00

TABLE 3.11. Discretization errors in the H^1-norm, Example 4

level	# elem.	$\|u - u_h^l\|_1$		$\|u - u_h^s\|_1$		$\|u - u_h^t\|_1$	
0	22	6.295650e-01		2.218643e-01		2.205473e-01	
1	176	3.009651e-01	1.06	4.609256e-02	2.27	4.607911e-02	2.26
2	1408	1.482825e-01	1.02	1.029429e-02	2.16	1.029336e-02	2.16
3	11264	7.379459e-02	1.01	2.523696e-03	2.03	2.523642e-03	2.03
4	90112	3.684966e-02	1.00	6.289388e-04	2.00	6.289362e-04	2.00

TABLE 3.12. Discretization errors in the weighted Lagrange multiplier norm, Example 4

level	# elem.	$\|\lambda - \lambda_h^l\|_h$		$\|\lambda - \lambda_h^s\|_h$		$\|\lambda - \lambda_h^t\|_h$	
0	22	8.588035e-02		6.184646e-02		8.310643e-02	
1	176	5.194191e-02	0.73	5.220039e-03	3.57	9.849865e-03	3.08
2	1408	2.538350e-02	1.03	4.361169e-04	3.58	7.810953e-04	3.66
3	11264	1.012701e-02	1.33	4.506948e-05	3.27	6.918887e-05	3.50
4	90112	3.755812e-03	1.43	5.074655e-06	3.15	6.546292e-06	3.40

In all our examples, we observe the optimal asymptotic convergence rates as predicted by the theory. Although we see the same qualitative behavior, some quantitative differences can be observed. However, there is not any essential difference in the discretization errors between different quadratic mortar solutions. Because of the addition of bubble functions at the skeleton Γ, X_h^t has more degree of freedom than X_h^s. However, these bubble functions can locally be eliminated from the algebraic formulation of the saddle point problem leading to a system matrix, which is similar to the algebraic form of the saddle point problem arising from the mortar discretization with a dual Lagrange multiplier space. On the other hand, the growth rate of the number of bubble functions is only a factor of four in each refinement step, and restricted to the skeleton. This is negligible since we can work with the efficient multigrid solver in case of the augmented quadratic serendipity space with the tensor product Lagrange multiplier space. Although we can work with the efficient multigrid solver in case of standard triquadratic finite elements, the approach is not as optimal as the augmented quadratic serendipity approach due to the more degree of freedom and the growth rate of factor eight in each refinement step. It turns out that the most efficient approach is the one given by the augmented quadratic serendipity elements. The discretization errors are as good as in the other cases, and the numerical solution is cheaper.

3.4. Lagrange multiplier spaces for the tetrahedral case

In this section, we discuss the construction of dual Lagrange multiplier spaces for linear and quadratic simplicial finite elements satisfying Assumption 7. Working with tetrahedral finite elements in three dimensions, one arrives at triangular finite elements in a two-dimensional interface. As in the case of serendipity finite elements, the tensor product construction of a dual Lagrange multiplier space cannot be adopted for the simplicial case.

3.4.1. A dual Lagrange multiplier space for linear simplicial elements. To construct a dual Lagrange multiplier space for the lowest order simplicial finite elements, we follow the procedure outlined in [**99, 163**]. In that case, a dual Lagrange multiplier space can be constructed satisfying Assumption 7. Suppose that γ_k is an interface of the decomposition. Assume that l is a vertex of a triangular face $F \in \mathcal{S}_k$ and φ_l the corresponding finite element basis function with $l = 1, 2$ or 3, and $a(l)$ and $b(l)$ are the two opposite vertices. If all three vertices of the triangle lie inside γ_k, then we define the

Lagrange multiplier by

$$\mu_l := 3\varphi_l - \varphi_{a(l)} - \varphi_{b(l)},\ l = 1, \cdots, 3.$$

If two vertices of the triangle F are in γ_k, and hence a vertex l with $l = 1, 2$ or 3 is a crosspoint, we define the Lagrange multiplier by

$$\mu_{a(l)} := \frac{5}{2}\varphi_{a(l)} - \frac{3}{2}\varphi_{b(l)} + \frac{1}{2}\varphi_l, \text{ and } \mu_{b(l)} := \frac{5}{2}\varphi_{b(l)} - \frac{3}{2}\varphi_{a(l)} + \frac{1}{2}\varphi_l.$$

If the triangular face F has only one vertex, say l in γ_k, we simply set $\mu_l := 1$. If all three vertices of the triangle F are crosspoints, we find a neighboring face $\tilde{F} \in \mathcal{S}_k$ with at least one vertex, say l, in γ_k, whose distance from the face F is bounded by a constant multiple of the local meshsize, and we extend the support of the Lagrange multiplier $\tilde{\mu}_l$ corresponding to the l-th vertex of the face $\tilde{F}$ by defining $\tilde{\mu}_l|_F = 1$. It is easy to see that the Lagrange multiplier space thus constructed satisfy the biorthogonality property and the constant function belongs to it, and we obtain the optimal a priori estimates for linear mortar finite elements. Further details can be found in [**99**].

3.4.2. A non-existence result for quadratic simplicial elements. To obtain optimal a priori error estimates for quadratic mortar finite elements, it is sufficient that the linear functions are contained in M_k. In the dual Lagrange multiplier space for quadratic finite elements in two dimensions, even the linear hat functions are elements of M_k, and the bilinear hat functions belong to M_k in case of the dual Lagrange multiplier space for triquadratic finite elements in three dimensions. Unfortunately, this does not hold in three dimensions for simplicial triangulations under Assumption 7. Let us assume that the basis functions of our dual Lagrange multiplier space satisfy $\operatorname{supp}\varphi_i = \operatorname{supp}\mu_i$, where φ_i are the standard nodal quadratic finite element basis functions on the interface γ_k.

LEMMA 3.4. *Under the above assumptions, there exists no dual Lagrange multiplier space M_k such that $W_k^1 \subset M_k$, where W_k^1 is the finite element space of piecewise linear hat functions.*

PROOF. The proof is carried out by contradiction as in Lemma 3.1. Let us assume that

$$\sum_i \alpha_i \mu_i = \phi_p^l, \tag{3.4.1}$$

where ϕ_p^l is the hat function associated with the interior vertex p, see Figure 3.7.

By assumption the functions μ_i are biorthogonal to the finite element basis functions φ_j on the slave side of the interface, see (1.6.2). Hence, after multiplying (3.4.1) by some finite element basis function φ_j and integrating over the interface γ_k, we get

$$\alpha_j = \frac{\int_{\gamma_k} \varphi_j \phi_p^l \, d\sigma}{c_j}.$$

Let j_0 be another interior vertex such that j_0 and p share one edge, see Figure 3.7. Then, we can write

$$\int_{\gamma_k} \varphi_{j_0} \phi_p^l \, d\sigma = \int_{F_1} \varphi_{j_0} \phi_p^l \, d\sigma + \int_{F_2} \varphi_{j_0} \phi_p^l \, d\sigma = -(|F_1| + |F_2|)/60$$

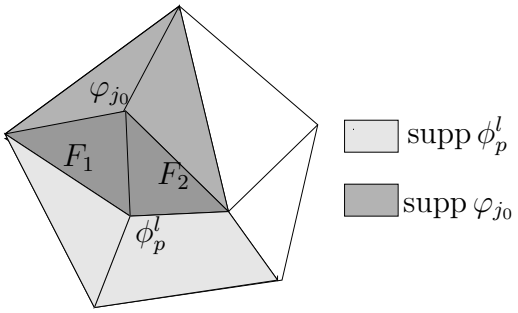

Figure 3.7: 2D interface of 3D simplicial triangulation

and thus $\alpha_{j_0} \neq 0$. Since the basis functions μ_i are locally linearly independent, we obtain that supp $\sum_j \alpha_j \mu_j \supseteq$ supp μ_{j_0}. By construction, we find supp $\mu_{j_0} \not\subset$ supp ϕ_p^l. □

3.5. Dual Lagrange multiplier spaces for quadratic serendipity and simplicial finite elements

In this section, we will show that working with Assumption 2 dual Lagrange multiplier spaces can be constructed for the serendipity and simplicial quadratic finite elements, see also [**103**]. The crucial point is to look for biorthogonality only with finite element basis functions on the interface associated with the vertices and modify the finite element basis functions, see also Section 1.6.

3.5.1. A dual Lagrange multiplier space for quadratic serendipity elements. Assume that $\hat{\varphi}_i^l$, $1 \leq i \leq 4$, and $\hat{\varphi}_i^q$, $1 \leq i \leq 8$, be the bilinear and quadratic serendipity finite element basis functions on the reference square $\hat{F} := (-1,1) \times (-1,1)$, respectively. Here, $\hat{\varphi}_i^q$, $1 \leq i \leq 4$, are the basis functions corresponding to the vertices of the reference face $\hat{F}$, and $\hat{\varphi}_i^q$, $5 \leq i \leq 8$, are the ones corresponding to the edges of $\hat{F}$, see the left picture of Figure 3.8. For some $\alpha \neq 1$, we set

$$\begin{aligned} \hat{\lambda}_1^q &:= \frac{\hat{\varphi}_1^l + \alpha(\hat{\varphi}_3^l - \hat{\varphi}_2^l - \hat{\varphi}_4^l)}{1-\alpha}, \quad \hat{\lambda}_2^q := \frac{\hat{\varphi}_2^l + \alpha(\hat{\varphi}_4^l - \hat{\varphi}_1^l - \hat{\varphi}_3^l)}{1-\alpha}, \\ \hat{\lambda}_3^q &:= \frac{\hat{\varphi}_3^l + \alpha(\hat{\varphi}_1^l - \hat{\varphi}_2^l - \hat{\varphi}_4^l)}{1-\alpha}, \quad \text{and} \quad \hat{\lambda}_4^q := \frac{\hat{\varphi}_4^l + \alpha(\hat{\varphi}_2^l - \hat{\varphi}_1^l - \hat{\varphi}_3^l)}{1-\alpha}. \end{aligned}$$

Note that the global basis functions obtained by mapping the modified local ones $\hat{\lambda}_i^q$, $1 \leq i \leq 4$, with some affine mapping and gluing them together will not be continuous, and they do not span the space of all continuous piecewise bilinear functions with respect to the partition $\mathcal{S}_k$ on γ_k. However, since $\hat{\lambda}_1^q + \hat{\lambda}_2^q = \hat{\varphi}_1^l + \hat{\varphi}_2^l$, $\hat{\lambda}_2^q + \hat{\lambda}_3^q = \hat{\varphi}_2^l + \hat{\varphi}_3^l$, $\hat{\lambda}_3^q + \hat{\lambda}_4^q = \hat{\varphi}_3^l + \hat{\varphi}_4^l$, and $\hat{\lambda}_4^q + \hat{\lambda}_1^q = \hat{\varphi}_4^l + \hat{\varphi}_1^l$, we compute $\hat{\lambda}_1^q + \hat{\lambda}_2^q = \frac{1-y}{2}$, $\hat{\lambda}_2^q + \hat{\lambda}_3^q = \frac{1+x}{2}$, $\hat{\lambda}_3^q + \hat{\lambda}_4^q = \frac{1+y}{2}$, and $\hat{\lambda}_4^q + \hat{\lambda}_1^q = \frac{1-x}{2}$. Denoting the edge joining the corners i and j of the reference element $\hat{F}$ by e_{ij} for four edges (e_{12}, e_{23}, e_{34}, and e_{41}), we see that $\hat{\lambda}_i^q + \hat{\lambda}_j^q = 1$ on e_{ij}, and $\hat{\lambda}_i^q + \hat{\lambda}_j^q = 0$ on the edge opposite to e_{ij}. Thus we can conclude that the global basis functions obtained by mapping the modified local ones with some affine mapping and gluing them together will reproduce any continuous piecewise linear polynomial. Now, defining $\tilde{\varphi}_1^q := \hat{\varphi}_1^q - \theta(\hat{\varphi}_5^q + \hat{\varphi}_8^q)$,

$\tilde{\varphi}_2^q := \hat{\varphi}_2^q - \theta(\hat{\varphi}_5^q + \hat{\varphi}_6^q)$, $\tilde{\varphi}_3^q := \hat{\varphi}_3^q - \theta(\hat{\varphi}_6^q + \hat{\varphi}_7^q)$, and $\tilde{\varphi}_4^q := \hat{\varphi}_4^q - \theta(\hat{\varphi}_7^q + \hat{\varphi}_8^q)$, we find that with $\alpha = \frac{1}{6}$ and $\theta = -\frac{1}{5}$,

$$\left[\langle \tilde{\varphi}_i^q, \hat{\lambda}_j^q \rangle_{0,\hat{F}}\right]_{1\le i,j\le 4} = \frac{1}{5} I_4,$$

where I_4 is the identity matrix of size 4×4. The modified finite element basis functions on vertices $\tilde{\varphi}_i^q,\ 1 \le i \le 4$, vanish on the opposite edges and are symmetric in the barycentric coordinates.

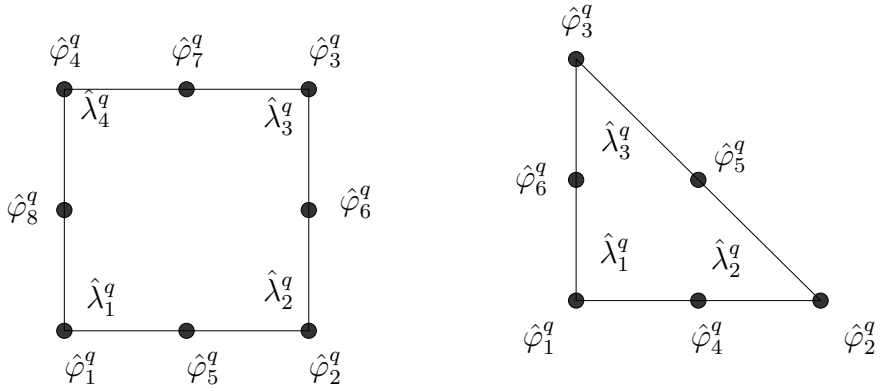

Figure 3.8: Ordering of the local finite element and Lagrange multiplier basis functions, quadratic serendipity (left) and quadratic simplicial (right)

3.5.2. A dual Lagrange multiplier space for simplicial quadratic finite elements. Following similar ideas as in the construction of the dual Lagrange multiplier space for the quadratic serendipity elements as in the previous section, we show that a dual Lagrange multiplier space can be constructed for the simplicial quadratic finite elements, see also [**103**]. Assume that $\hat{\lambda}_i^q,\ 1 \le i \le 3$, and $\hat{\varphi}_i^q,\ 1 \le i \le 6$, be the linear and quadratic finite element basis functions on the reference triangle $\hat{F}$, respectively. Here, $\hat{\varphi}_i^q,\ 1 \le i \le 3$, are the basis functions corresponding to the vertices of the reference triangular face $\hat{F}$ and $\hat{\varphi}_i^q,\ 4 \le i \le 6$, are the ones corresponding to the edges of $\hat{F}$, where $\hat{F} := \{(x,y) |\ 0 \le x, 0 \le y, x + y \le 1\}$, see the left picture of Figure 3.8. With some simple computation, we get

$$\left[\langle \hat{\varphi}_i^q, \hat{\lambda}_j^q \rangle_{0,\hat{F}}\right]_{1\le i,j\le 3} = \begin{bmatrix} \frac{1}{60} & -\frac{1}{120} & -\frac{1}{120} \\ -\frac{1}{120} & \frac{1}{60} & -\frac{1}{120} \\ -\frac{1}{120} & -\frac{1}{120} & \frac{1}{60} \end{bmatrix}.$$

Hence, if we define

$$\tilde{\varphi}_1^q := \hat{\varphi}_1^q + \frac{1}{12}(\hat{\varphi}_4^q + \hat{\varphi}_6^q), \quad \tilde{\varphi}_2^q := \hat{\varphi}_2^q + \frac{1}{12}(\hat{\varphi}_4^q + \hat{\varphi}_5^q), \quad \text{and} \quad \tilde{\varphi}_3^q := \hat{\varphi}_3^q + \frac{1}{12}(\hat{\varphi}_5^q + \hat{\varphi}_6^q),$$

we obtain

$$\left[\langle \tilde{\varphi}_i^q, \hat{\lambda}_j^q \rangle_{0,\hat{F}}\right]_{1\le i,j\le 3} = \frac{1}{36} I_3,$$

where I_3 is the identity matrix of size 3×3. We point out that the modified vertex basis functions $\tilde{\varphi}_i^q$, $1 \leq i \leq 3$, vanish on the opposite edges and are symmetric in the barycentric coordinates. The global Lagrange multipliers are obtained by affinely mapping the local ones and gluing them together. Unfortunately, the dual Lagrange multiplier space cannot be constructed so easily for cubic finite elements on triangles. Construction of a dual Lagrange multiplier space for simplicial cubic finite elements can be found in [**103**].

REMARK 3.5. *Here, for both quadratic serendipity and simplicial elements, the finite element basis functions are modified to obtain a suitable dual Lagrange multiplier space. This modification can be performed either by modifying them only at the slave side of the interface or by modifying the three-dimensional finite element basis functions on the whole domain. Since our multigrid solver is based on the unconstrained product space* [**166**]*, and prolongation and restriction operators should be computed on a reference element, we modify our three-dimensional basis functions.*

3.5.3. Boundary modification. The biorthogonal bases constructed in previous subsections cannot be used in a general mortar situation directly. As in the two-dimensional case we have to remove the degrees of freedom of the Lagrange multipliers associated with the boundary of each interface to obtain a uniform inf-sup condition in a general mortar situation. Furthermore, if Lagrange multipliers associated with the boundary of each interface are not removed, the mass matrix $\mathtt{M}_l$ defined in Section 1.6 does not remain to be a square diagonal matrix. After removing the degrees of freedom of the Lagrange multipliers, the approximation property of the Lagrange multiplier space is lost, that means Assumption 4 does not hold anymore. Referring to [**103**] for a general framework, here we discuss only the quadratic case. Let $\tilde{M}_k$ be the Lagrange multiplier space associated with the interface γ_k before the boundary modification. Recalling the decomposition of interior degrees of freedom of the slave side of an interface γ_k introduced in Section 1.6, we decompose the degrees of freedom corresponding to the nodes in $\mathcal{N}_c$ into two groups with $\mathcal{N}_c = \mathcal{N}_{cv} \cup \mathcal{N}_{ce}$, where $\mathcal{N}_{cv}$ corresponds to the vertex nodes, and $\mathcal{N}_{ce}$ corresponds to the edge nodes on the boundary of the slave side of the interface γ_k. Defining $\mathcal{N}_{\tilde{l}} := \mathcal{N}_l \cup \mathcal{N}_{cv}$, we assume that $\{\tilde{\mu}_i\}_{1 \leq i \leq \tilde{l}_k}$ is the basis of $\tilde{M}_k$ associated with the nodes in $\mathcal{N}_{\tilde{l}}$ of the interface $\bar{\gamma}_k$, where $\tilde{l}_k$ is the number of nodes in $\mathcal{N}_{\tilde{l}}$. The idea is to remove the Lagrange multiplier basis functions associated to the nodes belonging to the group $\mathcal{N}_{cv}$, and add a suitable multiple of them to some of the Lagrange multipliers associated to the inner nodes of the slave side. For each $i \in \mathcal{N}_{cv}$ with the global coordinate x_i we select $i_m \in \mathcal{N}_l$, $1 \leq m \leq 3$, with $\operatorname{dist}(\operatorname{supp} \tilde{\mu}_i, \operatorname{supp} \tilde{\mu}_{i_m}) \leq C \operatorname{diam}(\operatorname{supp} \mu_i)$ having global coordinates x_{i_m}, $1 \leq m \leq 3$, respectively such that the problem of finding scalars α_m, $1 \leq m \leq 3$, with

$$\sum_{m=1}^{3} \alpha_m p(x_{i_m}) = p(x_i), \quad p \in \mathcal{P}_1(\gamma_k) \tag{3.5.1}$$

has a unique solution. Then, we remove $\tilde{\mu}_i$ and redefine $\tilde{\mu}_{i_m}$ with

$$\tilde{\mu}_{i_m} + \alpha_m \tilde{\mu}_i \to \tilde{\mu}_{i_m}, \ 1 \leq m \leq 3.$$

Then the support of the Lagrange multipliers $\tilde{\mu}_{i_m}$, $1 \leq m \leq 3$, will be extended up to the set $\operatorname{supp} \tilde{\mu}_i$. We note that it is sufficient to choose three inner nodes even if the underlying

$(d-1)$-triangulation consists of parallelograms. The reduced and modified collection of basis functions will be called $\{\mu_1, \cdots, \mu_{l_k}\}$. Note that the collection $\{\mu_1, \cdots, \mu_{l_k}\}$ still satisfies the definition of biorthogonality (1.22), and since any linear polynomial $p \in \mathcal{P}_1(\gamma_k)$ was contained in the Lagrange multiplier space $\tilde{M}_k$, and because of (3.5.1) we conclude that this property is retained. In practice, for any $i \in \mathcal{N}_{cv}$, we look for an interior triangle (or parallelogram) $F \in \mathcal{S}_k$ with $\operatorname{dist}(\operatorname{supp}\tilde{\mu}_i, F) \leq C\operatorname{diam}(\operatorname{supp}\mu_i)$, and then the scalars α_m, $1 \leq m \leq 3$ (or 4) can be obtained by computing the barycentric coordinates of x_i with respect to the triangle (or parallelogram) F.

To explain our idea, we take the one-dimensional example considered in [**103**]. In two-dimensional mortar finite elements, the interfaces γ_k are one-dimensional curves or lines, and the boundary of the interface consists only of points. Without loss of generality, we can assume that γ_k is aligned along the x-axis, and so any point on γ_k can be represented by a real number denoting its geometrical coordinates. Furthermore, in the one-dimensional case, we know that the linear basis functions are orthogonal to the quadratic vertex basis functions, see also Lemma 2.7. We assume that $i \in \mathcal{N}_c$ with the geometrical coordinates x_i is on the left corner of γ_k, and let x_{i_1} and x_{i_2} be the two vertices of the first interval e_1 interior to γ_k next to x_i, see Figure 3.9. Then the equation $\sum_{m=1}^{2} \alpha_m p(x_{i_m}) = p(x_i)$ for $p \in \mathcal{P}_1(\gamma_k)$ has only one solution since $\dim \mathcal{P}_1 = 2$: $\alpha_1 = \frac{x_{i_2} - x_i}{x_{i_2} - x_{i_1}}$ and $\alpha_2 = \frac{x_i - x_{i_1}}{x_{i_2} - x_{i_1}}$. We note that the barycentric coordinates of x_i with respect to the one-dimensional element e_1 are given by α_1 and α_2. The modified dual Lagrange multipliers are illustrated in the right picture of Figure 3.9. We observe that the Lagrange multipliers corresponding to x_{i_1} and x_{i_2} are modified and their supports are extended up to the point x_i.

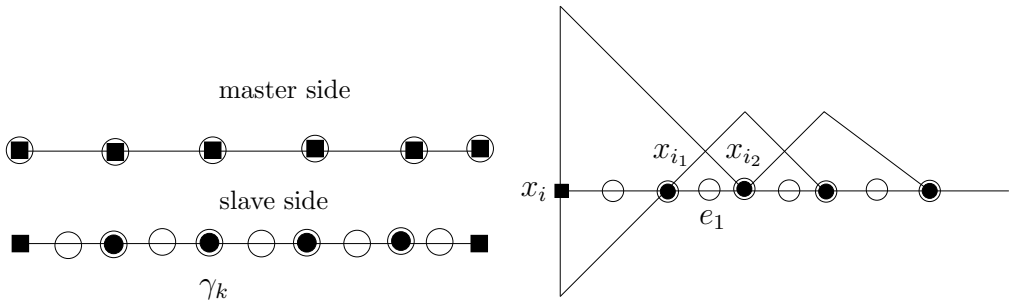

$$\mathcal{N}_s = \{\circledcirc\} \cup \{\bigcirc\},\ \mathcal{N}_l = \{\circledcirc\},\ \mathcal{N}_r = \{\bigcirc\} \cup \{\mathcal{N}_{mc}\}$$

Figure 3.9: Decomposition of interior degrees of freedom at an interface of the master and the slave side and the boundary modification for quadratic mortar finite elements in 2D

REMARK 3.6. *As an alternative to our definition* $M_h = \operatorname{span}\{\mu_i : i \in \mathcal{N}_l\}$, *one can use some auxiliary quadratic functions to define* $M_h = \operatorname{span}\{\mu_i : i \in \mathcal{N}_s\}$, *where the added basis functions* $\{\mu_i : i \in \mathcal{N}_s \backslash \mathcal{N}_l\}$ *are chosen so that the mass matrix* $\mathtt{M}_s$ *restricted to the interface* γ_k *is of the form*

$$\mathtt{M}_s = \begin{bmatrix} \mathtt{D}_1 & 0 \\ \mathtt{R} & \mathtt{D}_2 \end{bmatrix},$$

where $\mathtt{D}_1$ *and* $\mathtt{D}_2$ *are diagonal matrices and* $\mathtt{R}$ *is a rectangular matrix. Then one is in the situation of having quasi-dual Lagrange multipliers as in the definition* (1.20)*, and* $\dim W_k = \dim M_k$*. Although similar static condensation as in the case of dual Lagrange multiplier space can be adopted in this case, the degree of freedom mildly increases in this case, and slightly more complicated coupling between the Lagrange multipliers and the finite element basis functions in* W_k *occur.*

REMARK 3.7. *It is straightforward to verify all Assumptions 2–4 for the Lagrange multiplier spaces constructed above. We note that Assumptions 2 and 4 are satisfied trivially by construction. Letting* $\mu := \sum_{i=1}^{l_k} a_i \mu_i \in M_k$*, and defining* $\varphi := \sum_{i=1}^{l_k} a_i \varphi_i \in W_k$*, we can use the definition of biorthogonality* (1.22)*, and obtain Assumption 3 as in Section 3.2.1.*

3.6. Numerical results

Relaxing Assumption 7 and working with the Lagrange multiplier space with $\dim M_k \leq \dim W_k, 1 \leq k \leq N$, we have constructed dual Lagrange multiplier spaces for quadratic serendipity and simplicial quadratic finite elements in Section 3.2. In this section, we provide numerical results with these Lagrange multiplier spaces. In our examples, we combine tetrahedral and hexahedral elements on different subdomains. We point out that different Lagrange multipliers should be used depending on the hexahedral or tetrahedral partition on the slave side of the interface. The iterative solver is based on the multigrid method introduced in [**166**] as before. We denote by u_h^q the quadratic mortar solution obtained by using the dual Lagrange multipliers introduced in Section 3.5 independent of quadratic simplicial or serendipity finite elements, and similarly the Lagrange multiplier solution will be denoted by λ_h^q. We note that dual Lagrange multiplier spaces for the lowest order case satisfy Assumption 7.

3.6.1. Problems for Poisson and reaction-diffusion equations. In our first two examples, we compare the linear and quadratic serendipity mortar finite elements with dual and quasi-dual Lagrange multiplier spaces. We point out that working with the quasi-dual Lagrange multiplier space, the quadratic serendipity finite element space X_h^s is augmented with bubble functions on the slave side of the interface $\gamma_k, 1 \leq k \leq N$. Therefore, when comparing the numerical results it should be kept in mind that X_h^t has more degrees of freedom that that of X_h^s.

Example 1: Our first problem is given by $-\Delta u = f$ in Ω, with Ω composed of five cubes $\Omega_1 := (0,1)^3$, $\Omega_2 := (1,2) \times (0,1)^2$, $\Omega_3 := (0,1)^2 \times (1,2)$, $\Omega_4 := (-1,0) \times (0,1)^2$ and $\Omega_5 := (0,1)^2 \times (-1,0)$. Here, subdomain Ω_1, which has an initial partition into 27 hexahedra, is the slave subdomain and the others are master subdomains. In each of the master subdomains, the initial partition consists of 6 tetrahedra. The right hand side f and the Dirichlet boundary conditions are computed by using the exact solution is given by

$$u(x,y,z) = e^{-0.25(x^2+y^2+z^2)}(\cos(5x+z) + 3\sin(4y+z)).$$

In Figure 3.10, the decomposition of the domain, the initial finite element partitions, and the isolines of the solution at the interface $z = 1$ are shown. We have presented the discretization errors in the L^2- and H^1-norms in Table 3.13 and Table 3.14, and the error in the weighted Lagrange multiplier norm is shown in Table 3.15.

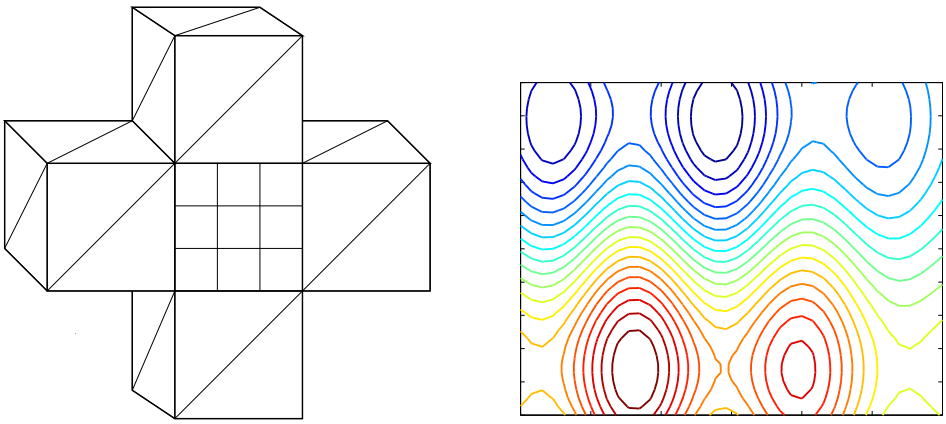

Figure 3.10: Decomposition of the domain and initial partitions (left), isolines of the solution at the plane $z = 1$ (right), Example 1

TABLE 3.13. Discretization errors in the L^2-norm, Example 1

level	# elem.	$\|u - u_h^l\|_0$		$\|u - u_h^q\|_0$		$\|u - u_h^t\|_0$	
0	51	8.421175e-01	0	3.238079e-01	0	3.237593e-01	0
1	408	3.765393e-01	1.16	5.020222e-02	2.69	5.039157e-02	2.68
2	3264	1.089531e-01	1.79	6.788405e-03	2.89	6.801267e-03	2.89
3	26112	2.827887e-02	1.95	8.515666e-04	2.99	8.523621e-04	3

TABLE 3.14. Discretization errors in the H^1-norm, Example 1

level	# elem.	$\|u - u_h^l\|_1$		$\|u - u_h^q\|_1$		$\|u - u_h^t\|_1$	
0	51	9.147052e-01	0	5.754977e-01	0	5.769227e-01	0
1	408	6.301770e-01	0.538	1.702170e-01	1.76	1.712476e-01	1.75
2	3264	3.269237e-01	0.947	4.699663e-02	1.86	4.712672e-02	1.86
3	26112	1.625205e-01	1.01	1.186322e-02	1.99	1.187986e-02	1.99

TABLE 3.15. Discretization errors in the weighted Lagrange multiplier norm, Example 1

level	# elem.	$\|\lambda - \lambda_h^l\|_h$		$\|\lambda - \lambda_h^q\|_h$		$\|\lambda - \lambda_h^t\|_h$	
0	51	5.875210e+00	0	3.198057e+00	0	4.135678e+00	0
1	408	3.210176e+00	0.872	8.440649e-01	1.92	1.306661e+00	1.66
2	3264	1.363125e+00	1.24	1.604852e-01	2.39	2.665296e-01	2.29
3	26112	5.145414e-01	1.41	2.944147e-02	2.45	4.831048e-02	2.46

Example 2: In our second example, we consider a domain and problem used in the last example of Section 3.3. The initial partition is changed to allow the use of hexahedra

and tetrahedra in different subdomains. As before, Ω_2 and Ω_3 are on the slave sides, and Ω_1 and Ω_4 are on the master sides. On both Ω_2 and Ω_3 the initial partition consists of 27 hexahedra, and therefore, the dual Lagrange multipliers for the quadratic serendipity elements are used. The problem for this example is given by a reaction-diffusion equation

$$-\mathrm{div}(a\nabla u) + u = f \quad \text{in} \quad \Omega,$$

where $a = 1$ in Ω_1 and Ω_4, and $a = 10$ in Ω_2 and Ω_3. The right hand side f and the Dirichlet boundary conditions are chosen with the exact solution prescribed in the last example of Section 3.3.

In the left picture of Figure 3.11, the decomposition of the domain together with the initial finite element partitions are shown, and the discretization errors are given in Tables 3.16–3.18.

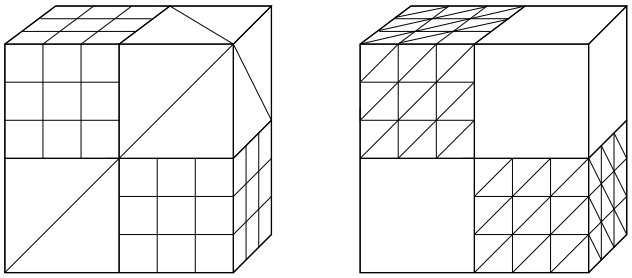

Figure 3.11: Decomposition of the domain and initial partitions, Example 2 (left) and Example 3 (right)

TABLE 3.16. Discretization errors in the L^2-norm, Example 2

level	# elem.	$\|u-u_h^l\|_0$		$\|u-u_h^q\|_0$		$\|u-u_h^t\|_0$	
0	66	2.393378e-01	0	7.943134e-02	0	7.108556e-02	0
1	528	8.882474e-02	1.43	1.692509e-02	2.23	1.686661e-02	2.08
2	4224	3.292171e-02	1.43	2.348709e-03	2.85	2.344396e-03	2.85
3	33792	9.674603e-03	1.77	2.731638e-04	3.1	2.729997e-04	3.1

TABLE 3.17. Discretization errors in the H^1-norm, Example 2

level	# elem.	$\|u-u_h^l\|_1$		$\|u-u_h^q\|_1$		$\|u-u_h^t\|_1$	
0	66	4.267453e-01	0	1.574200e-01	0	1.251658e-01	0
1	528	2.250457e-01	0.923	4.990750e-02	1.66	4.947352e-02	1.34
2	4224	1.186258e-01	0.924	1.478805e-02	1.75	1.476941e-02	1.74
3	33792	6.009470e-02	0.981	3.869100e-03	1.93	3.868980e-03	1.93

TABLE 3.18. Discretization errors in the weighted Lagrange multiplier norm, Example 2

level	# elem.	$\|\lambda - \lambda_h^l\|_h$		$\|\lambda - \lambda_h^q\|_h$		$\|\lambda - \lambda_h^t\|_h$	
0	66	5.874062e-02	0	5.191228e-02	0	2.821116e-02	0
1	528	2.462554e-02	1.25	4.114995e-03	3.66	3.529045e-03	3
2	4224	8.970948e-03	1.46	6.255109e-04	2.72	7.656049e-04	2.2
3	33792	3.138544e-03	1.52	1.042346e-04	2.59	1.473680e-04	2.38

We see that the discretization errors for our first and second examples are optimal. For the error in the H^1-norm, the asymptotic rates of convergence for the linear and quadratic mortar solutions are of order 1 and 2, respectively, whereas we observe the convergence rates of order 2 and 3 for the errors in the L^2-norm. The rate of convergence for the Lagrange multiplier in the weighted L^2-norm is also optimal for both linear and quadratic cases. As we obtain the convergence rate of order 1.5 in the linear case, both quadratic cases yield the convergence rate of order 2.5 in this norm. In these two examples, both dual and quasi-dual Lagrange multiplier spaces give almost the same results in the L^2- and H^1-norms, whereas we can observe some difference in the weighted Lagrange multiplier norm. In this norm, the augmented quadratic serendipity space with the quasi-dual Lagrange multiplier space yields more errors than the quadratic serendipity space with the dual Lagrange multiplier space.

Example 3: In our third example, we present the numerical results for linear and quadratic mortar finite elements with only triangles on the slave side of the interface. Thus the dual Lagrange multiplier space is formed for simplicial finite elements. Here, the domain and the problem is taken from our second example. The decomposition of the domain and the initial triangulation are shown in the right picture of Figure 3.11, and the discretization errors are given in Tables 3.19–3.21. As in previous two examples, we observe correct asymptotic convergence rates for all considered norms.

TABLE 3.19. Discretization errors in the L^2-norm, Example 3

level	# elem.	$\|u - u_h^l\|_0$		$\|u - u_h^q\|_0$	
0	326	4.099152e-01		1.108447e-01	
1	2608	1.457669e-01	1.49	1.169511e-02	3.24
2	20864	3.916084e-02	1.90	1.036543e-03	3.50
3	166912	9.682286e-03	2.02	1.226815e-04	3.08

TABLE 3.20. Discretization errors in the H^1-norm, Example 3

level	# elem.	$\|u - u_h^l\|_1$		$\|u - u_h^q\|_1$	
0	326	7.871914e-01		2.757468e-01	
1	2608	4.413152e-01	0.835	7.078443e-02	1.96
2	20864	2.228219e-01	0.986	1.721378e-02	2.04
3	166912	1.092705e-01	1.03	4.175570e-03	2.04

TABLE 3.21. Discretization errors in the weighted Lagrange multiplier norm, Example 3

level	# elem.	$\|\lambda - \lambda_h^l\|_h$		$\|\lambda - \lambda_h^q\|_h$	
0	326	6.903480e-02		4.312126e-02	
1	2608	2.820101e-02	1.29	5.852327e-03	2.88
2	20864	9.824553e-03	1.52	7.175411e-04	3.03
3	166912	3.514627e-03	1.48	9.258426e-05	2.95

Example 4: Our fourth example is given by $-\Delta u = f$ in Ω, where the non-convex Ω is composed of eight cubes $\Omega_1 := (0,1)^3$, $\Omega_2 := (1,2) \times (0,1)^2$, $\Omega_3 := (2,3) \times (0,1)^2$, $\Omega_4 := (0,1)^2 \times (1,3)$, $\Omega_5 := (2,3) \times (0,1) \times (1,3)$, $\Omega_6 := (0,1)^2 \times (3,4)$, $\Omega_7 := (1,2) \times (0,1) \times (3,4)$ and $\Omega_8 := (2,3) \times (0,1) \times (3,4)$. Here, subdomains Ω_1, Ω_3, Ω_6 and Ω_8 are taken as slave subdomains and the others are master subdomains. The initial partitions consist of tetrahedra for Ω_1 and Ω_3, and of hexahedra for the other subdomains, and they are illustrated in Figure 3.12. The right hand side f and the Dirichlet boundary conditions are chosen such that the exact solution is given by

$$u(x,y,z) = e^{-\frac{1}{4}(x+y+z)}(\sin(5xy) + \cos(5yz))(x + y^2 + z^2).$$

The isolines of this solution at the interface $z = 1$ can also be found in Figure 3.12, and the discretization errors are given in Tables 3.22–3.24. Although, the optimal asymptotic convergence starts later, the asymptotic convergence rates in all considered norms are optimal.

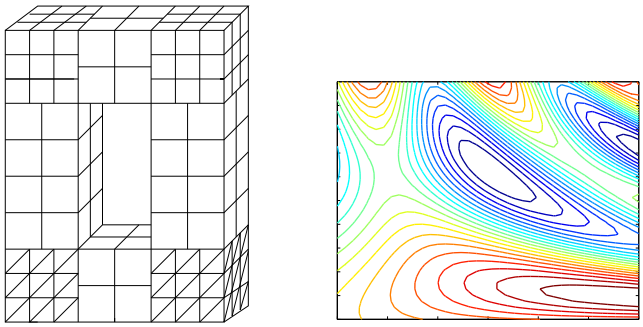

Figure 3.12: Decomposition of the domain and initial partitions (left), isolines of the solution at the plane $z = 1$ (right), Example 4

TABLE 3.22. Discretization errors in the L^2-norm, Example 4

level	# elem.	$\|u - u_h^l\|_0$		$\|u - u_h^q\|_0$	
0	426	1.791973e+00		6.940239e-01	
1	3408	6.330854e-01	1.50	1.433486e-01	2.28
2	27264	1.952988e-01	1.70	1.979148e-02	2.86
3	218112	5.111691e-02	1.93	2.634217e-03	2.91

TABLE 3.23. Discretization errors in the H^1-norm, Example 4

level	# elem.	$\|u-u_h^l\|_1$		$\|u-u_h^q\|_1$	
0	426	1.121512e+00		9.129765e-01	
1	3408	7.578088e-01	0.566	4.181631e-01	1.13
2	27264	4.669157e-01	0.699	1.096319e-01	1.93
3	218112	2.400890e-01	0.96	2.850084e-02	1.94

TABLE 3.24. Discretization errors in the weighted Lagrange multiplier norm, Example 4

level	# elem.	$\|\lambda-\lambda_h^l\|_h$		$\|\lambda-\lambda_h^q\|_h$	
0	426	4.234348e+01		1.070000e+01	
1	3408	3.824327e+01	0.147	5.791507e+00	0.886
2	27264	1.347168e+01	1.51	1.339511e+00	2.11
3	218112	3.009333e+00	2.16	1.707101e-01	2.97

Example 5: In our last example, we consider a problem with a corner singularity at the origin. The exact solution

$$u(x,y,z) := \sqrt[3]{x^2+y^2}\cos(\frac{2\theta_1}{3}) + \sqrt[3]{y^2+z^2}\cos(\frac{2\theta_2}{3}) + \sqrt[3]{z^2+x^2}\cos(\frac{2\theta_3}{3})$$

given in [**132**] has a corner singularity at the origin, and satisfies the Laplace equation, where $\theta_1 = \arctan\frac{y}{x}$, $\theta_2 = \arctan\frac{z}{y}$, and $\theta_3 = \arctan\frac{x}{z}$. To resolve the singularity, we decompose the domain $\Omega := (0,1)^3$ into two subdomains with $\Omega_2 := (0,0.25)^3$, and $\Omega_1 := \Omega\backslash\Omega_2$, and use a comparatively finer mesh in Ω_2. The decomposition of the domain with an initial triangulation is given in the left picture of Figure 3.13, and the isolines of the solution at the plane $z = 0$ can be found in the right picture. We have shown the discretization errors in Tables 3.25–3.27. Theoretically, we expect the convergence rate of order 0.66 in the H^1-norm, which can be seen for linear and quadratic mortar finite element solutions. Furthermore, we observe the convergence rate of order 1.66 in the L^2-norm and of order $0.66 + 0.5$ in the weighted Lagrange multiplier norm.

TABLE 3.25. Discretization errors in the L^2-norm, Example 5

level	# elem.	$\|u-u_h^l\|_0$		$\|u-u_h^q\|_0$	
0	815	3.410175e-03		8.555475e-04	
1	6520	1.058919e-03	1.69	2.640884e-04	1.7
2	52160	3.344432e-04	1.66	8.251362e-05	1.68
3	417280	1.061593e-04	1.66	2.589380e-05	1.67

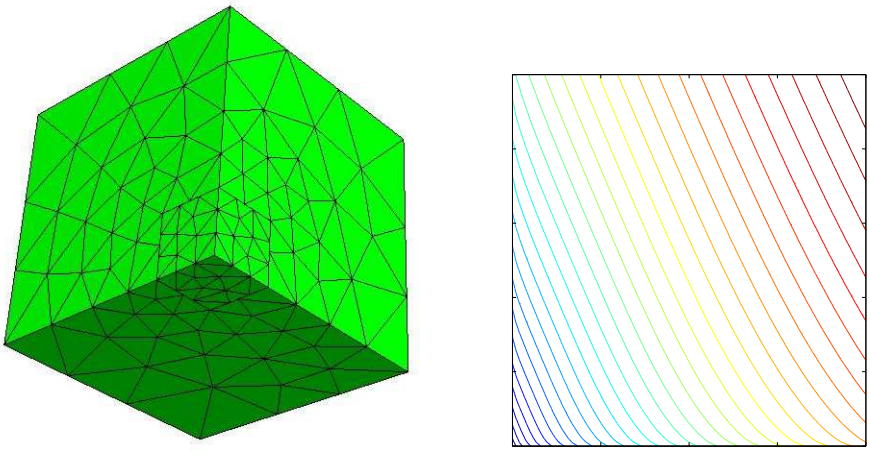

Figure 3.13: Decomposition of the domain and initial partitions (left), isolines of the solution at the plane $z = 0$ (right), Example 5

TABLE 3.26. Discretization errors in the H^1-norm, Example 5

level	# elem.	$\|u - u_h^l\|_1$		$\|u - u_h^q\|_1$	
0	815	1.012748e-01		4.354393e-02	
1	6520	6.388590e-02	0.665	2.695673e-02	0.692
2	52160	4.017100e-02	0.669	1.682146e-02	0.68
3	417280	2.528299e-02	0.668	1.055102e-02	0.673

TABLE 3.27. Discretization errors in the weighted Lagrange multiplier norm, Example 5

level	# elem.	$\|\lambda - \lambda_h^l\|_h$		$\|\lambda - \lambda_h^q\|_h$	
0	815	2.308317e-02		3.864681e-03	
1	6520	1.270988e-02	0.861	2.206944e-03	0.808
2	52160	5.666563e-03	1.17	9.631343e-04	1.2
3	417280	2.410256e-03	1.23	4.297796e-04	1.16

3.6.2. Problems in solid mechanics. In this subsection, we present some numerical results illustrating the performance of our Lagrange multiplier spaces for problems in linear elasticity.

Example 1: In our first example, we consider an example in linear elasticity given in (2.4.1). For this example, we take the domain and the problem from [**99**]. Here, the computational domain Ω, which is a beam, is decomposed into three subdomains Ω_1, Ω_2 and Ω_3 with $\Omega_1 := (0, 50) \times (0, 10) \times (0, 2)$, $\Omega_2 := (0, 50) \times (3, 7) \times (2, 11)$ and $\Omega_3 := (0, 50) \times (0, 10) \times (11, 13)$. The decomposition of the domain is given in the left picture of Figure 3.14 with an initial partition. Here, Ω_2 is the slave subdomain, so that, although the decomposition is geometrically non-conforming, Assumption 1 is satisfied.

The material parameters are set to be $\mu = 8.2$, and $\lambda = 10$. Here, Γ_D is the part of the boundary of Ω with $x = 0$ and $x = 50$ so that the left and the right sides of each subdomain are fixed, and $\Gamma_N := \partial\Omega \backslash \Gamma_D$. The function $\boldsymbol{g}_N = (g_1, g_2, g_3)^T$ on Γ_N is given as $g_1 = g_2 = 0$, and

$$g_3 = \begin{cases} -0.35 & \text{if } 22 \leq x \leq 28 \text{ and } z = 13 \\ 0 & \text{otherwise} \end{cases}$$

so that a constant vertical force is applied from the top boundary ($z = 13$) of Ω. We have computed the solution with quadratic finite elements. The resulting deformation of the beam is given in the right picture of Figure 3.14.

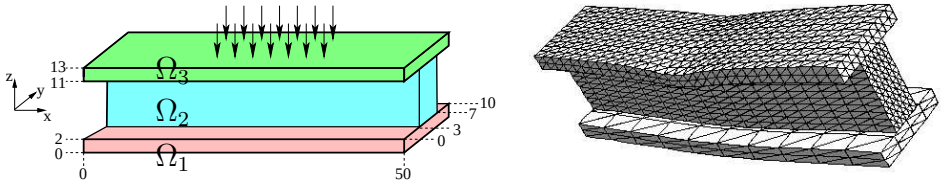

Figure 3.14: Decomposition of the domain with problem setting (left) and the distorted shape (right), Example 1

Example 2: In our second example, we consider the domain of Example 4 of the previous subsection. Taking the problem (2.4.1), the boundary conditions are defined so that Γ_D is the part of the boundary of Ω with $x = 3$ and $y = 4$ so that the right and the top boundary of Ω is fixed, and $\Gamma_N := \partial\Omega \backslash \Gamma_D$. The function $\boldsymbol{g}_N = (g_1, g_2, g_3)^T$ on Γ_N is given as $g_2 = g_3 = 0$, and

$$g_1 = \begin{cases} 40.0 & \text{if } 1 \leq z \leq 3 \text{ and } x = 0 \\ 0 & \text{otherwise} \end{cases}$$

so that a constant horizontal force is applied on the part of the left boundary of Ω. The material parameters E and ν are set to be $E = 4000$ and $\nu = 0.3$. The setting of the problem is shown in the left picture of Figure 3.15, and the deformation of the domain is shown in the right.

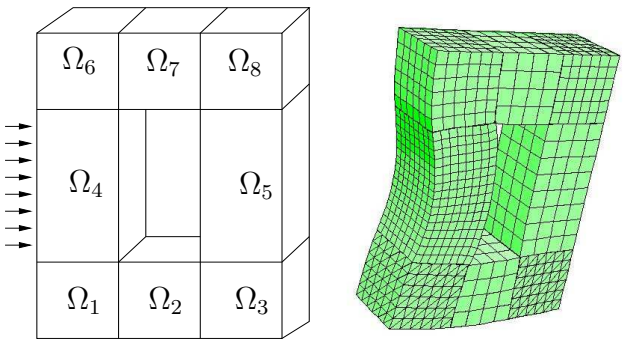

Figure 3.15: Decomposition of the domain with problem setting (left) and the zoomed distorted shape (right), Example 2

CHAPTER 4

Mortar Finite Elements for Interface Problems

4.1. Introduction

We consider interface problems within the framework of mortar finite element methods. Such interface problems arise in different situations, for example, in heat conduction with discontinuous sources or crack propagation in linear elasticity. We start with a saddle point formulation and show that the interface conditions enter into the right-hand side. Using dual Lagrange multipliers, we can work with scaled sparse matrices, and static condensation gives rise to a symmetric and positive definite system on the unconstrained product space. The iterative solver is based on a modified multigrid approach. Using the central idea of mortar methods, we decompose the domain of interest into non-overlapping subdomains and replace the strong point-wise continuity at the interfaces by a weak integral condition. As noted in the first chapter, there are two different equivalent variational formulations. One approach results in a positive definite system on the constrained mortar space [**33, 34**], and a second one gives rise to an indefinite system associated with the unconstrained product space and a Lagrange multiplier space [**22**]. Here, we follow the second approach and rewrite the interface problem as indefinite variational equation.

Conforming finite element methods for elliptic problems with discontinuous coefficients and homogeneous interface conditions are addressed in [**12**]. Finite element methods for non-homogeneous elliptic interface problems are analyzed in [**46**], and it is shown that the discretization error is of optimal order for linear finite elements on quasi-uniform triangulations. A survey on non-overlapping domain decomposition methods for elliptic interface problems can be found in [**171**]. A least-squares finite element method for elliptic interface problems with Dirichlet and Neumann boundary data is proposed and analyzed in [**60**]. In particular, error estimates for non-matching triangulations at the interface are given. Elliptic and parabolic interface problems with a non-zero jump in the flux across a sufficiently smooth interface are considered in [**62, 94**]. In [**62**], nearly optimal error estimates in the energy-norm and in the L^2-norm are established under reasonable regularity assumptions on the original solutions, whereas some new a priori estimates are presented in [**94**]. The immersed interface method is based on using the jumps in the solution and its derivative to modify standard finite difference schemes in the neighborhood of the interface, see [**111**]. The idea to precondition the elliptic equation before using the immersed interface method is proposed in [**113**] resulting in a fast algorithm for elliptic equations with large jumps in the coefficients. An extension of the immersed interface method to boundary value problems on irregular domains with Neumann and Dirichlet boundary conditions can be found in [**157**]. The immersed interface method with a finite element formulation is considered in [**113**]. Nitsche techniques provide flexible domain decomposition techniques and have been successfully used for the numerical approximation of partial differential equations, see, e.g.,

[**18, 89**]. The analysis of the discretization scheme is restricted to homogeneous interface conditions, and optimal a priori estimates are given. A similar approach can be found in [**85**], where a stationary heat conduction problem in two dimensions with a discontinuous conducting coefficient across a smooth interface is considered. Optimal a priori estimates for appropriately modified piecewise linear elements on a quasi-uniform triangulation have been established. Here, we propose an approach based on mortar techniques and dual Lagrange multipliers. We consider non-homogeneous jumps in the flux and in the solution across the interface. Starting with a saddle point formulation of the interface problem, we show the existence and uniqueness of the solution in the continuous and discrete setting. In contrast to the general mortar framework, we decompose the interface into disjoint straight lines and remove the degree of freedom of Lagrange multipliers from its corner nodes. We show that this is essential to prove an optimal a priori estimate for the piecewise linear interface. Compared to standard formulations for the Laplace operator, see [**33**], we have to include two additional terms reflecting the interface conditions. The jump terms enter only in the right-hand side, and the arising stiffness matrix does not depend on the interface conditions. Our approach is quite flexible and can easily be applied to general type of elliptic and parabolic interface problems, where the geometry of and the jump at the interface are a priori known.

This chapter is organized as follows: In the next section, we present our model interface problem and introduce its saddle point formulation in the continuous setting. In Section 4.3, we briefly recall the mortar discretization scheme for our model interface problem and establish a priori estimates for the discretization errors. Moreover, we consider the algebraic formulation of the saddle point problem. Local modifications are carried out to obtain a positive definite system for which we can use multigrid methods. Finally in Section 4.4, we show some numerical results illustrating the performance of our approach. In particular, we give the discretization errors in the L^2- and H^1-norms and in a weighted L^2-norm for the Lagrange multiplier.

4.2. Continuous setting

Let us consider a bounded polygonal domain $\Omega \subset \mathbb{R}^2$, which is decomposed into two non-overlapping subdomains Ω_1 and Ω_2 with the common interior interface Γ, $\bar{\Gamma} := \partial\Omega_1 \cap \partial\Omega_2$, and assume that the interface Γ can be written as union of straight lines, see Figure 4.1. For simplicity, we restrict ourselves to the case of two subdomains. However, the

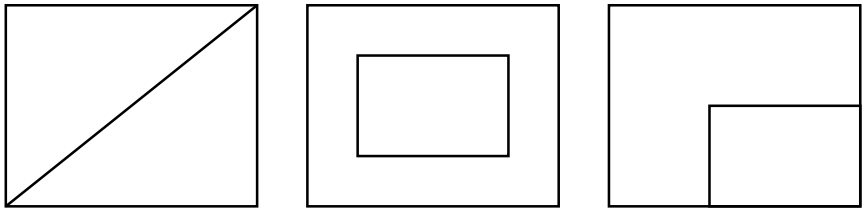

Figure 4.1: Different decompositions of the domain into two subdomains

approach can be generalized to more than two subdomains. We consider the following elliptic interface problem on Ω

$$-\mathrm{div}(\alpha_i \nabla u_i) + b_i u_i = f_i \quad \text{in} \quad \Omega_i, \quad i = 1, 2 \tag{4.2.1}$$

with homogeneous Dirichlet boundary conditions on $\partial\Omega$. Here, α_1 and α_2 are symmetric and locally constant positive-definite second order tensors specifying the diffusion in the two subdomains. Furthermore, we assume that $f_i \in L^2(\Omega_i)$ and $0 \leq b_i \in L^\infty(\Omega_i), i = 1, 2$. The jump conditions at the interface Γ are given by

$$[u] := u_1 - u_2 = g_D \quad \text{on} \quad \Gamma, \tag{4.2.2}$$

$$[u]_{\mathbf{n}} := (\alpha_1 \nabla u_1) \cdot \mathbf{n}_1 + (\alpha_2 \nabla u_2) \cdot \mathbf{n}_2 = g_N \quad \text{on} \quad \Gamma, \tag{4.2.3}$$

where $\mathbf{n}_i$ is the outward normal on $\partial\Omega_i$. We assume that $g_D \in H^{\frac{1}{2}}_{00}(\Gamma)$ and $g_N \in H^{-\frac{1}{2}}(\Gamma) := \left(H^{\frac{1}{2}}_{00}(\Gamma)\right)'$. Defining $H^1_*(\Omega_k)$ as in the first chapter for $k = 1, 2$, we obtain the unconstrained product space $X := H^1_*(\Omega_1) \times H^1_*(\Omega_2)$. In the rest of this section, we consider the variational formulation of the interface problem. The weak formulation of (4.2.1) is obtained by applying Green's formula on Ω_i, for $\phi_i \in H^1_*(\Omega_i)$, $i = 1, 2$

$$\int_{\Omega_i} (\alpha_i \nabla u_i) \cdot \nabla \phi_i \, dx - \int_\Gamma \alpha_i \nabla u_i \cdot \mathbf{n}_i \phi_i \, ds + \int_{\Omega_i} b_i u_i \phi_i \, dx = \int_{\Omega_i} f_i \phi_i \, dx.$$

Taking into account the interface condition for the flux (4.2.3), $\alpha_1 \nabla u_1 \cdot \mathbf{n}_1 = -\alpha_2 \nabla u_2 \cdot \mathbf{n}_2 + g_N$ on Γ, we find for $\phi_1 \in H^1_*(\Omega_1)$

$$\int_{\Omega_1} (\alpha_1 \nabla u_1) \cdot \nabla \phi_1 \, dx + \int_\Gamma \alpha_2 \nabla u_2 \cdot \mathbf{n}_2 \phi_1 \, ds + \int_{\Omega_1} b_1 u_1 \phi_1 \, dx = \int_{\Omega_1} f_1 \phi_1 \, dx + \int_\Gamma g_N \phi_1 \, ds.$$

The weak formulation of the jump of the solution at the interface can be obtained by multiplying the jump condition (4.2.2) with an element of the dual space M so that (4.2.2) and (4.2.3) are replaced by a weak variational equation given by

$$b(u, \mu) := \int_\Gamma [u] \, \mu \, d\sigma = \int_\Gamma g_D \mu \, d\sigma =: g(\mu), \quad \mu \in M. \tag{4.2.4}$$

Utilizing the duality pairing $\langle \cdot, \cdot \rangle_\Gamma$ on the interface, the variational equation (4.2.4) can be written as

$$b(u, \mu) = \langle [v], \mu \rangle_\Gamma, \quad v = (v_1, v_2) \in X, \quad \mu \in M := H^{-\frac{1}{2}}(\Gamma).$$

Introducing the flux $\lambda := \alpha_2 \nabla u_2 \cdot \mathbf{n}_2$ on Γ, we can write the weak form of (4.2.1) as a saddle point problem: find $(u, \lambda) \in X \times M$ such that

$$\begin{array}{rcll} a(u, v) + b(v, \lambda) & = & l(v), & v \in X, \\ b(u, \mu) & = & g(\mu), & \mu \in M, \end{array} \tag{4.2.5}$$

where

$$a(u, v) := \sum_{k=1}^{2} \int_{\Omega_k} (\alpha_k \nabla u) \cdot \nabla v + b_k u v \, dx, \; l(v) := \sum_{k=1}^{2} \int_{\Omega_k} f_k v \, dx + \left\langle v_{|\partial\Omega_1}, g_N \right\rangle_\Gamma.$$

The essential points for the existence and the uniqueness of the solution of a saddle point problem are coercivity, continuity and a suitable inf-sup condition. As usual, we use

the broken H^1-norm on X and the $H^{-\frac{1}{2}}$-norm on M. We start with the continuity of the bilinear form $b(\cdot,\cdot)$. By definition, we find

$$b(v,\mu) = \langle [v], \mu \rangle_\Gamma \leq \|[v]\|_{H_{00}^{\frac{1}{2}}(\Gamma)} \|\mu\|_{-\frac{1}{2},\Gamma}, \quad v \in X,\ \mu \in M.$$

We note that if Γ is a closed curve, see the middle picture of Figure 4.1, we have $H_{00}^{\frac{1}{2}}(\Gamma) = H^{\frac{1}{2}}(\Gamma)$, and thus

$$\|[v]\|_{H_{00}^{\frac{1}{2}}(\Gamma)} = \|[v]\|_{\frac{1}{2},\Gamma} \leq (\|v_{|\Omega_1}\|_{\frac{1}{2},\Gamma} + \|v_{|\Omega_2}\|_{\frac{1}{2},\Gamma}) \leq C\|v\|_1, \quad v \in X.$$

Due to the homogeneous Dirichlet boundary condition imposed on $\partial\Omega$, we find $(v_{|\Omega_i})_{|\Gamma} \in H_{00}^{\frac{1}{2}}(\Gamma)$, $i = 1, 2$, if Γ is not a closed curve. In that case, we can bound

$$\|[v]\|_{H_{00}^{\frac{1}{2}}(\Gamma)} \leq C(\|v_{|\Omega_1}\|_{\frac{1}{2},\partial\Omega_1} + \|v_{|\Omega_2}\|_{\frac{1}{2},\partial\Omega_2}) \leq C\|v\|_1, \quad v \in X.$$

As a consequence, we obtain the continuity of the bilinear form $b(\cdot,\cdot)$ on $X \times M$. The bilinear form $a(\cdot,\cdot)$ is continuous on $X \times X$ and coercive on $B^* \times B^*$, where $B^* = \{v \in X,\ \int_\Gamma [v] ds = 0\}$ as in the first chapter. To see that the inf-sup condition holds, we start with the definition of the dual norm

$$\begin{aligned} \|\mu\|_{-\frac{1}{2},\Gamma} &:= \sup_{v \in H_{00}^{\frac{1}{2}}(\Gamma)\setminus\{0\}} \frac{\langle v, \mu \rangle_\Gamma}{\|v\|_{H_{00}^{\frac{1}{2}}(\Gamma)}} \\ &= \sup_{v \in H_{00}^{\frac{1}{2}}(\Gamma)\setminus\{0\}} \frac{b(\tilde{v}, \mu)}{\|v\|_{H_{00}^{\frac{1}{2}}(\Gamma)}} \leq C \sup_{v \in X\setminus\{0\}} \frac{b(v,\mu)}{\|v\|_1}, \end{aligned}$$

where $\tilde{v}$ denotes the harmonic extension of v to Ω_2 extended by zero on Ω_1. Hence, the variational problem (4.2.5) has a unique solution.

4.3. Mortar discretizations and a priori error estimates

In this section, we briefly recall mortar finite elements for our model interface problem and prove optimal a priori estimates for the discretization errors. Let $\mathcal{T}_1$ and $\mathcal{T}_2$ denote two independent shape regular simplicial triangulations on Ω_1 and Ω_2 with mesh-sizes bounded by h_1 and h_2, respectively. Without loss of generality, the interface Γ inherits its one-dimensional mesh from $\mathcal{T}_2$, and the side of Γ associated with Ω_2 is called slave side and the one associated with Ω_1 master side. We denote by $\mathcal{T}_\Gamma$ the triangulation on Γ with mesh-size bounded by h_2 whose elements are boundary edges of $\mathcal{T}_2$, and assume that the triangulation on Γ is globally quasi-uniform. The unconstrained discrete finite element space is denoted by $X_h := X_1 \times X_2$, where X_k stands for the space of conforming finite elements of order p_k in the subdomain Ω_k associated with the triangulation $\mathcal{T}_k$ and satisfies homogeneous Dirichlet boundary conditions on $\partial\Omega_k \cap \partial\Omega$, $k = 1, 2$. We note that no interface condition is imposed on X_h, and the elements in X_h do not have to satisfy a continuity condition at the interface. Let W_h be the trace space of finite element basis functions from the slave side, i.e., of X_2, restricted to Γ. Due to the homogeneous boundary conditions on $\partial\Omega$, we find $W_h \subset H_{00}^{\frac{1}{2}}(\Gamma)$. To satisfy a suitable discrete inf-sup condition, we use a discrete Lagrange multiplier space such that $\dim M_h \leq \dim W_h$. Under the regularity

assumption $u \in H^{p_2+1}(\Omega_2)$, λ is, in general, not an element in $H^{p_2-\frac{1}{2}}(\Gamma)$. This is due to the fact that the normal has jumps if Γ has corners. Therefore, we decompose Γ into a finite number of disjoint straight segments γ_l, $1 \leq l \leq N$, of maximal length, i.e., $\bar{\Gamma} = \cup_{l=1}^{N} \bar{\gamma}_l$, $\gamma_k \cap \gamma_l = \emptyset$, $l \neq k$ and $\bar{\gamma}_k \cup \bar{\gamma}_l$ is not a straight line, $1 \leq k \neq l \leq N$. In the examples given in Figure 4.1, we find $N = 1$, $N = 4$, and $N = 2$ (from the left to the right). We now work with the Lagrange multiplier spaces defined on γ_l. We remark that we use the decomposition of Γ into straight lines for the definition of the discrete Lagrange multiplier space, but that we work with the $H_{00}^{\frac{1}{2}}$-norm on Γ. Now, we denote by W_l, the trace of X_2 restricted to γ_l satisfying the homogeneous Dirichlet boundary conditions on $\partial\gamma_l$ so that $W_l := \{w|\ w = v_{|\gamma_l},\ v \in X_2\} \cap H_0^1(\gamma_l)$. Our discrete Lagrange multiplier space is defined as the product space $M_h := \prod_{l=1}^{N} M_l$, where $\dim M_l = \dim W_l$. Let us denote the nodal basis functions in W_l, associated with the one-dimensional mesh on the slave side by $\{\varphi_i^l\}_{1 \leq i \leq n_s^l}$, $n_s^l := \dim W_l$. We use dual Lagrange multiplier spaces for linear and quadratic finite elements introduced in [**163**]. We refer to Chapter 2 for the higher order case. Then, the basis functions $\{\mu_i^l\}_{1 \leq i \leq n_s^l}$ of M_l satisfy the following biorthogonality relation (1.6.2)

$$\int_{\gamma_l} \mu_i^l\ \varphi_j^l\, ds = \delta_{ij} \int_{\gamma_l} \varphi_j^l\, ds\ , \quad 1 \leq i, j \leq n_s^l,$$

and we have $\sum_{i=1}^{n_s^l} \mu_i^l = 1$ on γ_l. Furthermore, working with a finite element space of order p, the conforming finite element space of order $p-1$ is contained in the Lagrange multiplier space, and they all satisfy Assumptions 2-4.

To establish a priori estimates for the discretization errors, we consider the saddle point formulation (4.2.5) of the interface problem and apply the theory of mixed finite elements. Replacing the space $X \times M$ by our discrete space $X_h \times M_h$ in (4.2.5), we obtain our discrete variational problem: find $(u_h, \lambda_h) \in X_h \times M_h$ such that

$$\begin{array}{lcll} a(u_h, v) + b(v, \lambda_h) & = & l(v), & v \in X_h, \\ b(u_h, \mu) & = & g(\mu), & \mu \in M_h. \end{array} \tag{4.3.1}$$

Since $X_h \subset X$ and $M_h \subset M$, we get the continuity of the bilinear form $a(\cdot,\cdot)$ on $X_h \times X_h$ and of $b(\cdot,\cdot)$ on $X_h \times M_h$. In addition to the discrete inf-sup condition, we need the coercivity of $a(\cdot,\cdot)$ on the space $\ker B_h := \{v_h \in X_h|\quad b(v_h, \mu) = 0,\ \mu \in M_h\}$. Since $\ker B_h \subset B^*$, we obtain the coercivity of $a(\cdot,\cdot)$ on $\ker B_h \times \ker B_h$. In the following, the set of endpoints of γ_k in Ω, $1 \leq k \leq N$, will be denoted by

$$\mathcal{N}_c := \bigcup_{k \neq l} (\bar{\gamma}_k \cap \bar{\gamma}_l).$$

To establish the discrete inf-sup condition, we introduce $\tilde{W}_h \subset W_h$ with $\dim \tilde{W}_h = \dim M_h$ and assume that $\dim M_k \geq 2$, $1 \leq k \leq N$. We remark that $H^{-\frac{1}{2}}(\Gamma)$ is a stronger norm than the product norm on $\prod_{l=1}^{N} H^{-\frac{1}{2}}(\gamma_l)$, and therefore, we cannot work with $\prod_{l=1}^{N} W_l$ to get a uniform inf-sup condition. The basis functions $\tilde{\varphi}_i$ of $\tilde{W}_h$ are associated with the interior nodes of γ_l. If x_i is a node adjacent to an endpoint $x_j \in \Omega$ of some γ_l, we define $\tilde{\varphi}_i := \varphi_i + 0.5\varphi_j$, where φ_i denotes the standard nodal basis function of W_h, and for all other nodes, we set $\tilde{\varphi}_i := \varphi_i$. We note that only the basis functions associated with a node

adjacent to a corner are modified and that the space $\tilde{W}_h$ has the standard approximation properties. The basis functions of $\tilde{W}_h$ in the linear case are shown in the left picture of Figure 4.2, and the dual Lagrange multiplier basis functions are shown in the right picture.

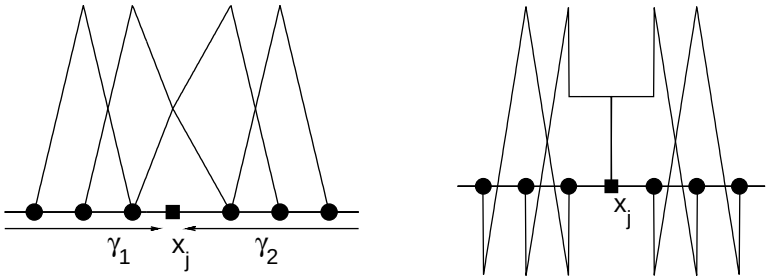

Figure 4.2: Basis functions of $\tilde{W}_h$ (left) and of M_h (right), the basis functions are associated with the filled circles and x_j is a corner

Now, we define a projection operator Q_h by

$$Q_h : L^2(\Gamma) \longrightarrow \tilde{W}_h, \qquad \int_\Gamma Q_h v\, \mu_h\, ds = \int_\Gamma v\, \mu_h\, ds, \qquad \mu_h \in M_h.$$

The biorthogonality of M_l and W_l and the modification of $\tilde{\varphi}_i$ at the nodes adjacent to endpoints of γ_l yield

$$\int_\Gamma \tilde{\varphi}_i \mu_k\, ds = \delta_{ik} \int_\Gamma \varphi_i\, ds + \sum_{x_j \in \mathcal{N}_c} \frac{c_{ij}}{2} \int_\Gamma \varphi_j \mu_k\, ds,$$

where $c_{ij} = 1$ if the node x_i is adjacent to the endpoint x_j and otherwise $c_{ij} = 0$. It can be easily verified that Q_h is well-defined. The structure of the mass matrices guarantees that the action of Q_h can be computed locally. Moreover, it is easy to see that $Q_h v = v$, $v \in \tilde{W}_h$, and $\|Q_h v\|_{0,\Gamma} \leq C\|v\|_{0,\Gamma}$. We denote by P_h the L^2-projection on $\tilde{W}_h$ and note that $\|P_h v\|_{1,\Gamma} \leq \|v\|_{1,\Gamma}$, $v \in H^1(\Gamma)$, see [**40**]. In terms of the L^2-stability of Q_h, the approximation property of P_h and an inverse estimate, the $H^{\frac{1}{2}}_{00}$-stability of Q_h can be shown

$$\begin{aligned}
\|Q_h v\|_{H^{\frac{1}{2}}_{00}(\Gamma)} &\leq \|Q_h v - P_h v\|_{H^{\frac{1}{2}}_{00}(\Gamma)} + \|P_h v\|_{H^{\frac{1}{2}}_{00}(\Gamma)} \\
&\leq C\left(\frac{1}{\sqrt{h_2}}\|Q_h v - P_h v\|_{0,\Gamma} + \|v\|_{H^{\frac{1}{2}}_{00}(\Gamma)}\right) \\
&\leq C\left(\frac{1}{\sqrt{h_2}}\|v - P_h v\|_{0,\Gamma} + \|v\|_{H^{\frac{1}{2}}_{00}(\Gamma)}\right) \leq C\|v\|_{H^{\frac{1}{2}}_{00}(\Gamma)}.
\end{aligned}$$

Using the discrete harmonic extension on X_2, we obtain a uniform discrete inf-sup condition. The $H_{00}^{\frac{1}{2}}$-stability of Q_h guarantees the discrete inf-sup condition

$$\begin{aligned}
\|\mu_h\|_{-\frac{1}{2},\Gamma} &= \sup_{v\in H_{00}^{\frac{1}{2}}(\Gamma)\setminus\{0\}} \frac{\int_\Gamma \mu_h\, Q_h v\, ds}{\|v\|_{H_{00}^{\frac{1}{2}}(\Gamma)}} \le C \sup_{v\in H_{00}^{\frac{1}{2}}(\Gamma)\setminus\{0\}} \frac{\int_\Gamma \mu_h\, Q_h v\, ds}{\|Q_h v\|_{H_{00}^{\frac{1}{2}}(\Gamma)}} \\
&\le C \sup_{w_h\in \tilde{W}_h\setminus\{0\}} \frac{\int_\Gamma \mu_h\, w_h\, ds}{\|w_h\|_{H_{00}^{\frac{1}{2}}(\Gamma)}} \le C \sup_{\tilde{w}_h\in X_2\setminus\{0\}} \frac{\int_\Gamma \mu_h\, \tilde{w}_h\, ds}{\|\tilde{w}_h\|_{1,\Omega_2}} \\
&\le C \sup_{w_h\in X_h\setminus\{0\}} \frac{b(w_h,\mu_h)}{\|w_h\|_1},
\end{aligned}$$

where $\tilde{w}_h$ is the discrete harmonic extension of w_h to Ω_2 extended by zero on Ω_1. In terms of these preliminary considerations, we can apply [**40**, Theorem III, 4.5] and get the following a priori bound for the discretization error

LEMMA 4.1. *The discrete variational problem* (4.3.1) *has a unique solution* (u_h,λ_h), *and there exist two constants* c_1 *and* c_2 *independent of* h *such that*

$$\begin{aligned}
&\|u-u_h\|_1 + \|\lambda-\lambda_h\|_{-\frac{1}{2},\Gamma} \\
&\le c_1 \inf_{v_h\in X_h} \|u-v_h\|_1 + c_2 \inf_{\mu_h\in M_h} \|\lambda-\mu_h\|_{-\frac{1}{2},\Gamma}.
\end{aligned} \tag{4.3.2}$$

In a next step, we define another projection operator Q_h^* by

$$Q_h^* : H^{-\frac{1}{2}}(\Gamma) \longrightarrow M_h, \qquad \int_\Gamma Q_h^*\mu\, w_h\, ds = \int_\Gamma \mu\, w_h\, ds, \qquad w_h\in \tilde{W}_h$$

and note that $Q_h^*\mu = \mu$, $\mu\in M_h$, and $\|Q_h^*\mu\|_{0,\Gamma} \le C\|\mu\|_{0,\Gamma}$ An interpolation argument yields the $H^{\frac{1}{2}-s}$-stability, $0<s<\frac{1}{2}$, of Q_h, and as a result, we find that Q_h^* is $H^{s-\frac{1}{2}}$-stable

$$\begin{aligned}
\|Q_h^*\mu\|_{s-\frac{1}{2},\Gamma} &= \sup_{w\in H^{\frac{1}{2}-s}(\Gamma)\setminus\{0\}} \frac{\langle Q_h^*\mu, w\rangle_\Gamma}{\|w\|_{\frac{1}{2}-s,\Gamma}} = \sup_{w\in H^{\frac{1}{2}-s}(\Gamma)\setminus\{0\}} \frac{\langle Q_h^*\mu, Q_h w\rangle_\Gamma}{\|w\|_{\frac{1}{2}-s,\Gamma}} \\
&= \sup_{w\in H^{\frac{1}{2}-s}(\Gamma)\setminus\{0\}} \frac{\langle \mu, Q_h w\rangle_\Gamma}{\|w\|_{\frac{1}{2}-s,\Gamma}} \le \|\mu\|_{s-\frac{1}{2},\Gamma}.
\end{aligned}$$

Since the operator Q_h is also $H_{00}^{\frac{1}{2}}$-stable, $H^{-\frac{1}{2}}$-stability of Q_h^* can be shown by using the same argument as above.

THEOREM 4.2. *Assume that* $u\in\prod_{k=1}^2 H^{r_k+1}(\Omega_k)$, *and* $\lambda\in\prod_{k=1}^N H^{r_2-\frac{1}{2}}(\gamma_k)$ *with* $r_1>0$ *and* $r_2>\frac{1}{2}$. *Then, we have the following a priori estimate for the discretization error*

$$\|u-u_h\|_1^2 + \|\lambda-\lambda_h\|_{-\frac{1}{2},\Gamma}^2 \le C(h_1^{2t_1}\|u\|_{t_1+1,\Omega_1}^2 + h_2^{2t_2}\|u\|_{t_2+1,\Omega_2}^2),$$

where $t_i := min(r_i,p_i)$, $i=1,2$. *If* $0<r_2\le\frac{1}{2}$, *then we have*

$$\begin{aligned}
&\|u-u_h\|_1^2 + \|\lambda-\lambda_h\|_{-\frac{1}{2},\Gamma}^2 \\
&\le C(h_1^{2t_1}\|u\|_{t_1+1,\Omega_1}^2 + h_2^{2t_2}\|u\|_{t_2+1,\Omega_2}^2 + h_2^{2r_2}\|\lambda\|_{r_2-\frac{1}{2},\Gamma}^2).
\end{aligned}$$

PROOF. The best approximation property of X_h is well known, and we have

$$\inf_{u_h \in X_h} \|u - u_h\|_1^2 \leq C(h_1^{2t_1}\|u\|_{t_1+1,\Omega_1}^2 + h_2^{2t_2}\|u\|_{t_2+1,\Omega_2}^2), \\ u \in H^{r_1+1}(\Omega_1) \times H^{r_2+1}(\Omega_2).$$

To establish the best approximation error of M_h in the $H^{-\frac{1}{2}}$-norm on Γ, we work with Q_h^*. In a first step, we consider the case $r_2 > \frac{1}{2}$. The L^2-stability of Q_h^*, the best approximation property of M_l, see [**163**], and the trace theorem yield for $\lambda \in \prod_{l=1}^N H^{r_2-\frac{1}{2}}(\gamma_l)$,

$$\begin{aligned} \|\lambda - Q_h^*\lambda\|_{-\frac{1}{2},\Gamma}^2 &:= \sup_{v \in H_{00}^{\frac{1}{2}}(\Gamma)\setminus\{0\}} \frac{\langle \lambda - Q_h^*\lambda, v\rangle_\Gamma^2}{\|v\|_{H_{00}^{\frac{1}{2}}(\Gamma)}^2} \\ &\leq \sup_{v \in H_{00}^{\frac{1}{2}}(\Gamma)\setminus\{0\}} \frac{\|\lambda - Q_h^*\lambda\|_{0,\Gamma}^2 \|v - Q_h v\|_{0,\Gamma}^2}{\|v\|_{H_{00}^{\frac{1}{2}}(\Gamma)}^2} \\ &\leq Ch_2 \|\lambda - Q_h^*\lambda\|_{0,\Gamma}^2 \\ &\leq Ch_2^{2t_2} \sum_{l=1}^N |\lambda|_{t_2-\frac{1}{2},\gamma_l}^2 \leq Ch_2^{2t_2}|u|_{t_2+1,\Omega_2}^2. \end{aligned}$$

Now, we consider the case $0 < r_2 \leq \frac{1}{2}$. Using the $H^{r_2-\frac{1}{2}}$-stability of Q_h^*, we have

$$\begin{aligned} \|\lambda - Q_h^*\lambda\|_{-\frac{1}{2},\Gamma}^2 &:= \sup_{v \in H_{00}^{\frac{1}{2}}(\Gamma)\setminus\{0\}} \frac{\langle \lambda - Q_h^*\lambda, v\rangle_\Gamma^2}{\|v\|_{H_{00}^{\frac{1}{2}}(\Gamma)}^2} \\ &\leq \sup_{v \in H_{00}^{\frac{1}{2}}(\Gamma)\setminus\{0\}} \frac{\|\lambda - Q_h^*\lambda\|_{r_2-\frac{1}{2},\Gamma}^2 \|v - Q_h v\|_{H_{00}^{\frac{1}{2}-r_2}(\Gamma)}^2}{\|v\|_{H_{00}^{\frac{1}{2}}(\Gamma)}^2} \\ &\leq Ch_2^{2r_2} \|\lambda - Q_h^*\lambda\|_{r_2-\frac{1}{2},\Gamma}^2 \leq Ch_2^{2r_2}\|\lambda\|_{r_2-\frac{1}{2},\Gamma}^2. \end{aligned}$$

Finally, the proof follows by using (4.3.2). □

We point out that the space $\tilde{W}_h$ and the operators Q_h and Q_h^* are used only for the theoretical analysis. They do not enter into the computation.

REMARK 4.3. *Because of the corners at the interface, the given a priori estimate cannot be established for $r_2 \geq 1$ if we work with a Lagrange multiplier space which is directly defined on Γ. In that case an error term of $\mathcal{O}(h_2^{1-\epsilon})$, $\epsilon > 0$ occurs. This term is crucial in case of a smooth solution and higher order finite elements.*

In the rest of this section, we consider the algebraic formulation of the saddle point problem (4.3.1) and apply a suitable modification to get a positive definite system on the product space. Here and in the following, we use the same notation for the vector representation of the solution and the solution as an element in X_h and M_h. The matrix $\mathtt{A}$ is the stiffness matrix associated with the bilinear form $a(\cdot,\cdot)$ on $X_h \times X_h$, and the matrices $\mathtt{B}$ and $\mathtt{B}^T$ are associated with the bilinear form $b(\cdot,\cdot)$ on $X_h \times M_h$. Then, the

algebraic formulation of the saddle point problem is given by

$$\begin{pmatrix} \mathtt{A} & \mathtt{B}^T \\ \mathtt{B} & 0 \end{pmatrix} \begin{pmatrix} u_h \\ \lambda_h \end{pmatrix} = \begin{pmatrix} f_h \\ g_h \end{pmatrix}, \tag{4.3.3}$$

where f_h and g_h are associated with the linear forms $l(\cdot)$ and $g(\cdot)$. Introducing $W_{0;h} := \prod_{l=1}^{N} W_l$, the algebraic representation of the mortar mapping $\Pi : X_h \longrightarrow W_{0;h} \subset X_h$ with

$$\int_\Gamma \Pi v \, \mu_h \, ds = \int_\Gamma [v] \, \mu_h \, ds, \quad \mu_h \in M_h$$

is denoted by $\mathtt{W}$. We remark that $\mathtt{W}$ applied to an element in $\ker B_h$ is zero. Thus the non-zero blocks of $\mathtt{W}$ are associated with the slave and master nodes on the interface. Moreover in case of dual Lagrange multipliers, the mortar mapping can be locally evaluated and the non-zero blocks of $\mathtt{W}$ are sparse. We denote by $\mathtt{E}$ the matrix associated with the natural embedding of $W_{0;h}$ in X_h and by $\mathtt{D}$ the diagonal matrix with entries $d_{ii} := \int_\Gamma \varphi_i \, ds$, where φ_i are the nodal basis functions of $W_{0;h}$. It is easy to see that $\mathtt{DE}^T\mathtt{W} = \mathtt{B}$ and $\mathtt{ED}^{-1}\mathtt{B} = \mathtt{W}$. Static condensation of the Lagrange multiplier now yields

$$\lambda_h = \mathtt{D}^{-1}\mathtt{E}^T(f_h - \mathtt{A}u_h). \tag{4.3.4}$$

This observation is the starting point for the modification of the algebraic formulation of the discrete saddle point problem (4.3.3). We use the equivalent form $\lambda_h = \mathtt{D}^{-1}\mathtt{E}^T(f_h - \mathtt{A}u_h + \mathtt{AW}u_h) - \mathtt{D}^{-1}\mathtt{E}^T\mathtt{AED}^{-1}g_h$ of (4.3.4) to eliminate λ_h in (4.3.3). Shifting the terms in g_h and f_h to the right side yields

$$\begin{pmatrix} \mathtt{A} & \mathtt{B}^T \\ \mathtt{B} & 0 \end{pmatrix} \begin{pmatrix} \mathtt{Id} \\ \mathtt{D}^{-1}\mathtt{E}^T\mathtt{A}(\mathtt{W} - \mathtt{Id}) \end{pmatrix} u_h = \begin{pmatrix} (\mathtt{Id} - \mathtt{W}^T)f_h + \mathtt{W}^T\mathtt{AED}^{-1}g_h \\ g_h \end{pmatrix}. \tag{4.3.5}$$

We note that the jump in the trace enters now in both block components on the right side. The system (4.3.5) has more equations than unknowns. To obtain a positive definite system for u_h on the product space, we restrict the space of test functions. Assuming that the test function (v_h, μ_h) has the form $(v_h, \mathtt{D}^{-1}\mathtt{E}^T\mathtt{A}(\mathtt{W} - \mathtt{Id})v_h)$, we get

$$\tilde{\mathtt{A}}u_h = \tilde{f}_h := (\mathtt{Id} - \mathtt{W}^T)f_h + (2\mathtt{W}^T - \mathtt{Id})\mathtt{AED}^{-1}g_h, \tag{4.3.6}$$

where $\tilde{\mathtt{A}} := (\mathtt{Id} - \mathtt{W}^T)\mathtt{A}(\mathtt{Id} - \mathtt{W}) + \mathtt{W}^T\mathtt{AW}$. The matrix $\tilde{\mathtt{A}}$ is symmetric and positive definite, see [**163**].

LEMMA 4.4. *The saddle point problem* (4.3.1) *for* (u_h, λ_h) *and the positive definite system* (4.3.6) *for* u_h *together with the post-processing step* (4.3.4) *are equivalent.*

The proof follows by construction. We note that the matrix $\tilde{\mathtt{A}}$ has exactly the same form as in a standard mortar problem with dual Lagrange multipliers, see [**166**]. The interface conditions enter only into the right side $\tilde{f}_h$ and do not influence the iterative solver. To solve the symmetric positive definite problem (4.3.6), we apply the modified multigrid approach proposed in [**166**] in combination with one local post-processing step of lower complexity. It is based on the decomposition of u_h in $u_h = (u_h - \mathtt{ED}^{-1}g_h) + \mathtt{ED}^{-1}g_h$.

REMARK 4.5. *Applying a Gauß–Seidel smoother, we do not have to carry out the post-process. The structure of the smoother guarantees that the weak discrete form of* (4.2.2) *is automatically satisfied within the multigrid approach.*

4.4. Numerical results

Here, we present some numerical examples illustrating the flexibility and efficiency of the mortar finite element method with dual Lagrange multipliers to treat interface problems. We present the numerical results for various types of interface problems using linear and quadratic mortar finite elements. We denote by M_h^q and M_h^l the discontinuous dual Lagrange multiplier spaces for quadratic and linear finite elements, respectively, see [**163**]. In case of M_h^q, the basis functions are piecewise quadratic, whereas the basis functions of M_h^l are piecewise linear. The mortar finite element solutions associated with the different Lagrange multiplier spaces M_h^q and M_h^l are denoted by u_h^q and u_h^l, respectively. For all our numerical examples, we use uniform refinement. We measure the error in the Lagrange multipliers in the mesh-dependent L^2-norm given by (1.6.3).

Example 1: For our first example, we decompose $\Omega := (0,2) \times (0,1)$ into $\Omega_2 := (0.5, 1.5) \times (0.25, 0.75)$, and $\Omega_1 := \Omega \backslash \bar{\Omega}_2$, see the left picture of Figure 4.3. We note that Γ can be decomposed into four straight segments, γ_l, $1 \leq l \leq 4$. The corner nodes of Ω_2 do not carry a degree of freedom for the Lagrange multiplier space. Here, we consider the problem (4.2.1)–(4.2.3) with

$$\alpha_1 := \begin{pmatrix} 2.5 & 0 \\ 0 & 1 \end{pmatrix}, \; \alpha_2 := \begin{pmatrix} 1 & 0 \\ 0 & 2.5 \end{pmatrix},$$

and $b_1(x,y) := x^2 + y^2 + xy$, $b_2(x,y) := 0$. The right-hand side, the interface conditions and Dirichlet boundary conditions are set such that one obtains the exact solution given by $u_1(x,y) = \sin(x^2 + y)\exp(-(x-y)^2)$, and $u_2(x,y) = 1.5\exp(-(x-1)^2 - (y-0.5)^2)$.

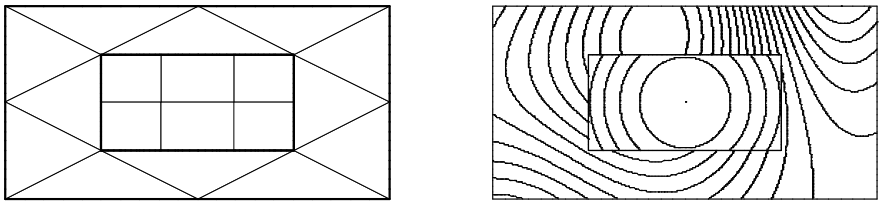

Figure 4.3: Decomposition of the domain and initial triangulation (left) and isolines of the solution (right), Example 1

The isolines of the solution are given in the right picture of Figure 4.3, and the discretization errors are shown in Figure 4.4. The numerical results confirm the asymptotic rates as predicted by the theory. Having a decomposition where Γ is not a straight line does not influence the convergence rates. In contrast to mortar techniques with many subdomains and crosspoints, we do not have to reduce the dimension of the Lagrange multiplier space at the corners because of the inf-sup condition. The inf-sup condition is also satisfied for the higher dimensional space $\tilde{M}_h^l$ (or $\tilde{M}_h^q$), where $\tilde{M}_h^l$ (or $\tilde{M}_h^q$) is spanned by the biorthogonal basis functions (linear or quadratic) associated with all nodes including the corner nodes on the slave side. However, replacing the Lagrange multiplier space M_h^q by $\tilde{M}_h^q$ yields considerably worse numerical results for the discretization errors in the Lagrange multiplier. This is due to the fact that λ is not in $H^{\frac{1}{2}}(\Gamma)$, and this is crucial for quadratic finite elements, see Remark 4.3. In the right picture of Figure 4.4, we have given the errors

in the weighted Lagrange multiplier norm using the space $\tilde{M}_h^q$ (not modified) and the space M_h^q (modified). Here, we see that if we work with the space $\tilde{M}_h^q$, the error in the weighted Lagrange multiplier norm is only of order $O(h)$.

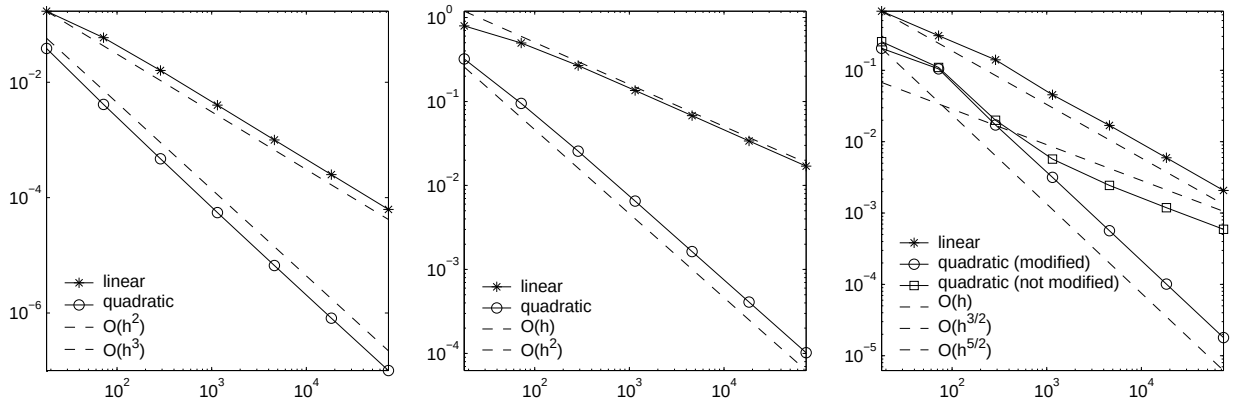

Figure 4.4: Error plot versus number of elements, L^2-norm (left), H^1-norm (middle) and weighted Lagrange multiplier norm (right), Example 1

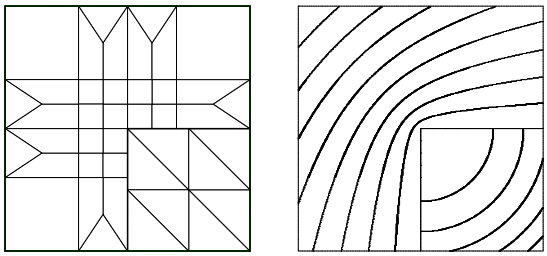

Figure 4.5: Decomposition into two subdomains and initial triangulation (left) and isolines of the solution (right), Example 2

Example 2: In our second example, we consider a problem with a corner singularity. Here, we decompose the unit square into two subdomains Ω_1 and Ω_2. The subdomain Ω_1 is a L-shape domain and $\Omega_2 := (0.5, 1) \times (0, 0.5)$, see the left picture of Figure 4.5. The initial triangulation does not match at the interface. The problem for this example is given by $-\Delta u = f$, and the exact solution is chosen as $u_1(r, \phi) = r^{2/3} \sin(\frac{2\phi}{3})$, and $u_2(r, \phi) = r^2$, where (r, ϕ) are the polar coordinates with origin shifted to $(0.5, 0.5)$. The isolines of the solution are shown in the right picture of Figure 4.5. Here, the solution is not piecewise H^2-regular, and asymptotically we cannot expect the same order of convergence as in the first example. The errors in the L^2-, H^1- and the weighted Lagrange multiplier norms are given in Table 4.1. Here we use lowest order finite elements. Asymptotically, we expect an order $h^{2/3}$ for the H^1-norm which can be observed. We note that the convergence rates are considerably better in the beginning. In contrast to the first example, the Lagrange multiplier does not show a better asymptotic convergence rate. Asymptotically, we obtain the same convergence rate as in the H^1-norm. This is due to the concentration of the error at the point $(0.5, 0.5)$ which is located on the interface. Better convergence rates in the

Lagrange multiplier norm can only be observed if the solution has no singularity at the interface.

TABLE 4.1. Discretization errors in the L^2-, H^1- and weighted Lagrange multiplier norm, Example 2

level	# elem.	$\|u-u_h^l\|_0$	ratio	$\|u-u_h^l\|_1$	ratio	$\|\lambda-\lambda_h^l\|_h$	ratio
0	41	3.325808e-02		1.370511e-01		1.667159e-02	
1	164	8.446641e-03	3.94	7.408534e-02	1.85	4.399131e-03	3.79
2	656	2.122112e-03	3.98	4.111530e-02	1.80	1.584474e-03	2.78
3	2624	5.335827e-04	3.98	2.343380e-02	1.75	7.218470e-04	2.19
4	10496	1.348615e-04	3.96	1.369342e-02	1.71	3.889129e-04	1.86
5	41984	3.434135e-05	3.93	8.173967e-03	1.68	2.289971e-04	1.70
6	167936	8.837528e-06	3.89	4.961475e-03	1.65	1.403140e-04	1.63
7	671744	2.307613e-06	3.83	3.048681e-03	1.63	8.741203e-05	1.61

Example 3: In our third example, the domain, the problem and the exact solution are taken from [**2**]. For this example, the domain $\Omega := (-1,1)\times(-1,1)$ is decomposed into two subdomains Ω_1 and Ω_2, where Ω_2 is a circle with radius 0.5 centered at the origin, and $\Omega_1 := \Omega\backslash\bar{\Omega}_2$, see the left picture of Figure 4.6. We remark that, in this example, the interface cannot be decomposed into straight lines. In addition to the analysis given in Section 4.3, the polygonal approximation of Γ has to be taken into account. Mortar finite elements with curved interface are anaylzed in [**75**]. Here, $b_1(x,y) := 0$, $b_2(x,y) := 0$, $\alpha_1 := 0.1\, I_2$, and $\alpha_2 := (x^2+y^2+1)\, I_2$ in (4.2.1)–(4.2.3), where I_2 is the 2×2 identity matrix. The exact solution is given as $u_1(x,y) = -\frac{41}{16} + 5\,(x^2+y^2)^2 + 10\,x^2 + 10\,y^2 + 10\,C\ln\left(2\sqrt{x^2+y^2}\right)$, and $u_2(x,y) = x^2+y^2$. The jump of the trace and of the flux across the interface Γ are computed as $[u]=0$, and $[u]_n = -2C$, and we have set $C := 10$. The right-hand side and the Dirichlet boundary condition on $\partial\Omega$ are computed by using the given exact solution. Here too, we use only the lowest order finite elements. The discretization errors in the L^2-, H^1- and the weighted Lagrange multiplier norm (weighted L^2-norm) for the linear finite elements are given in the right picture of Figure 4.6. As before, we observe numerically the predicted convergence rates.

Example 4: In our fourth example, we consider a problem of linear elasticity. We remark that the theoretical results can easily be generalized to this case. For this example, we take the domain $\Omega := (-1,1)\times(-1,1)$ decomposed into an upper and a lower triangle, Ω_1 and Ω_2, respectively, with the common interface $\Gamma := \{(x,x) : -1 \le x \le 1\}$, see the left picture of Figure 4.7.

We have used homogeneous Dirichlet boundary condition on $\partial\Omega$, and the jump of the flux and the jump of the trace are given by $g_N := (0,0)^T$ and $g_D := (g(x),0)^T$, respectively. Here, $g(x)$ is defined by

$$g(x) := \begin{cases} 0 & \text{if } x \in [-1,-0.6]\cup[0.6,1] \\ 0.5(x+0.6)(x-0.6) & \text{if } x \in (-0.6,0.6). \end{cases}$$

This leads to a crack on the interface Γ, which is shown in the middle picture of Figure 4.7. Young's modulus E and Poisson ratio ν are chosen to be $71GPa$ and 0.35 for the lower

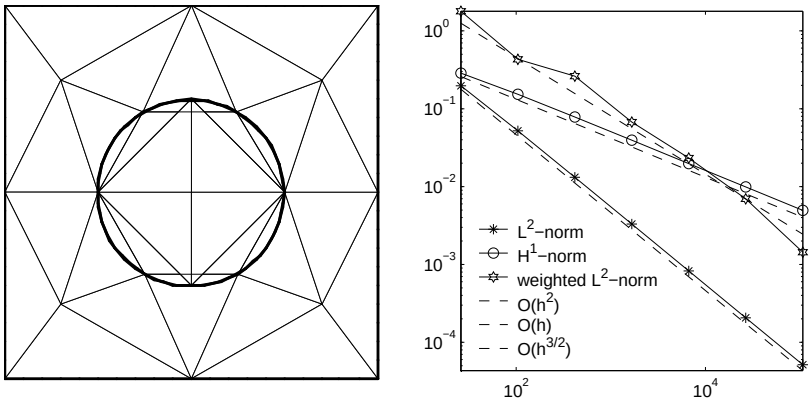

Figure 4.6: Decomposition into two subdomains and initial triangulation (left) and error plot versus number of elements (right), Example 3

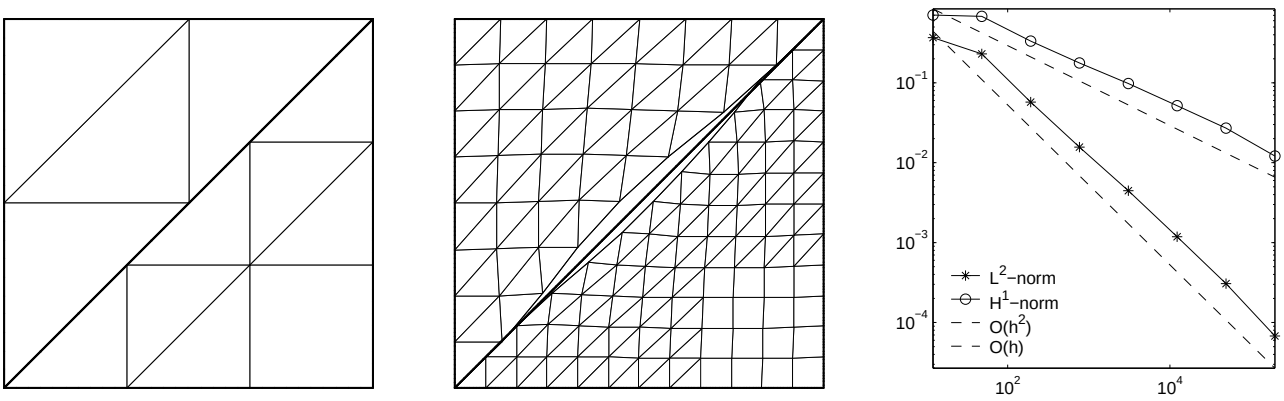

Figure 4.7: Decomposition into two subdomains and initial triangulation (left), distorted grid on level 2 (middle) and error plot versus number of elements (right), Example 4

triangle, and $35GPa$ and 0.17 for the upper triangle, respectively. We apply the body force of $4MN$ on Ω along both directions. We do not have an analytical solution for this problem. To obtain the discretization error, we compute a reference solution on a very fine triangulation with mesh-size h_{ref}, and compute an approximation of the error by comparing u_{ref} with u_h. We use the same u_{ref} for all refinement levels. On level 7 (starting from level 0), we have $h = 2h_{\text{ref}}$. As a result, we observe numerically better convergence rate in the last refinement step. There is a weak singularity in the stress at the opening of the crack. Thus, we apply only linear finite elements. The discretization errors are given in the right picture of Figure 4.7. This shows that we get an almost optimal order of convergence even in this case.

CHAPTER 5

Mortar Finite Elements for Coupled Problems

5.1. Introduction

When different physical models should be used in different simulation regions, a suitable discretization scheme has to be used in each region. Mortar finite elements can be efficiently used to couple these different discretization schemes or different physical models without losing the optimality of the approach. In particular, we apply mortar methods to couple different physical models in different simulation regions. In all our examples, we work with dual Lagrange multiplier spaces so that the Lagrange multipliers can locally be eliminated, and optimal multigrid methods can be applied to the resulting positive definite system for such coupled problems. Similar coupled problems are also considered in [**77, 106**]. This chapter is organized as follows. In the next section, we present an application to an elasto-acoustic problem, and we consider the coupling of different material laws in Section 5.4. In Section 5.5, we consider mortar finite elements for time-dependent problems. Finally, in the last section, we apply mortar finite elements for heat transfer problems with sliding meshes.

5.2. An application to an elasto-acoustic problem

In this section, we show the application of mortar finite element methods for an elasto-acoustic problem. We consider the situation that the fluid is completely surrounded by the structure. The problem is described by a linear elastic structure occupying a subdomain $\Omega_S \subset \mathbb{R}^2$ coupled with an irrotational fluid in $\Omega_F \subset \mathbb{R}^2$. The interface $\Gamma(= \partial\Omega_S \cap \partial\Omega_F)$ separates the fluid and solid regions. Given the fluid-density ρ_F, the solid-density ρ_S, and the acoustic speed c, we seek the frequency ω, the velocity-field $\mathbf{u}$, and the pressure p such that

$$\begin{aligned}
\nabla p - \omega^2 \rho_F \mathbf{u}_F &= \mathbf{0} \quad \text{in} \quad \Omega_F, \\
p + c^2 \rho_F \nabla \cdot \mathbf{u}_F &= 0 \quad \text{in} \quad \Omega_F, \\
\nabla \cdot \boldsymbol{\sigma}(\mathbf{u}_S) + \omega^2 \rho_S \mathbf{u}_S &= \mathbf{0} \quad \text{in} \quad \Omega_S, \\
\mathbf{u}_S &= \mathbf{0} \quad \text{on} \quad \Gamma_D, \\
\boldsymbol{\sigma}(\mathbf{u}_S) \cdot \mathbf{n}_S &= \mathbf{0} \quad \text{on} \quad \Gamma_N, \\
\boldsymbol{\sigma}_n(\mathbf{u}_S) + p = 0, \quad \boldsymbol{\sigma}_t(\mathbf{u}_S) &= \mathbf{0}, \quad \text{and} \quad (\mathbf{u}_F - \mathbf{u}_S) \cdot \mathbf{n} = 0 \quad \text{on} \quad \Gamma.
\end{aligned}$$

Here, $\boldsymbol{\sigma}$ is the usual Cauchy stress tensor from linear elasticity, $\boldsymbol{\sigma}_n = \mathbf{n} \cdot (\boldsymbol{\sigma} \cdot \mathbf{n})$ is the normal stress on Γ, and $\boldsymbol{\sigma}_t = \boldsymbol{\sigma} \cdot \mathbf{n} - \boldsymbol{\sigma}_n \mathbf{n}$ is the tangential traction vector on Γ, where $\mathbf{n}$ is the outward normal to Ω_F on Γ. This problem has become a subject of different papers, see, e.g., [**86, 29, 5**]. We introduce the following function spaces to formulate our problem

in the weak form

$$\begin{aligned} X &:= \mathbf{H}(\mathrm{div}, \Omega_F) \times \mathbf{H}^1_{\Gamma_D}(\Omega_S), \text{ and} \\ \mathbf{V} &:= \{(\mathbf{u}_F, \mathbf{u}_S) \in X, \ [\mathbf{u}] \cdot \mathbf{n} = 0 \text{ on } \Gamma\}, \end{aligned}$$

where

$$\begin{aligned} \mathbf{H}(\mathrm{div}, \Omega_F) &:= \{\mathbf{v} \in L^2(\Omega_F)^2, \ \|\nabla \cdot \mathbf{v}\|_{L^2(\Omega_F)} < \infty\}, \\ \mathbf{H}^1_{\Gamma_D}(\Omega_S) &:= \{\mathbf{v} \in H^1(\Omega_S)^2, \ \mathbf{v}_{|\Gamma_D} = 0\}, \quad \text{and} \quad [\mathbf{u}] := (\mathbf{u}_F - \mathbf{u}_S). \end{aligned}$$

The weak form of the continuous problem is: find $\mathbf{u} \in \mathbf{V}$ and $\omega \in \mathbb{R}$ such that

$$a(\mathbf{u}, \mathbf{v}) = \omega^2 m(\mathbf{u}, \mathbf{v}), \quad \mathbf{v} \in \mathbf{V},$$

where

$$\begin{aligned} a(\mathbf{u}, \mathbf{v}) &:= (\rho_F c^2 \nabla \cdot \mathbf{u}_F, \nabla \cdot \mathbf{v}_F)_{\Omega_F} + (\boldsymbol{\sigma}(\mathbf{u}_S), \epsilon(\mathbf{v}_S))_{\Omega_S}, \quad \text{and} \\ m(\mathbf{u}, \mathbf{v}) &:= (\omega^2 \rho_F \mathbf{u}_F, \mathbf{v}_F)_{\Omega_F} + (\omega^2 \rho_S \mathbf{u}_S, \mathbf{v}_S)_{\Omega_S}. \end{aligned}$$

Here, $\epsilon(\mathbf{v}_S)$ is the linear strain tensor and is related to the stress tensor by Hooke's law, i.e., $\boldsymbol{\sigma}_{ij}(\mathbf{v}_S) = 2\mu\epsilon_{ij}(\mathbf{v}_S) + \lambda \sum_{k=1}^{2} \epsilon_{kk}(\mathbf{v}_S)\delta_{ij}$, $i, j = 1, 2$. Let $\mathcal{T}_{h_s}$ and $\mathcal{T}_{h_f}$ be shape regular simplicial triangulations on Ω_S and Ω_F, respectively, and Γ inherits its triangulation $\mathcal{T}_\Gamma$ from the side of Ω_F. It is a well-known fact that if standard Lagrangian finite elements are used to discretize the fluid, it will give rise to spurious eigensolutions with positive eigenvalues interspersed among the 'real' ones, and a possible remedy of this problem is to use Raviart-Thomas elements in the fluid domain, see [**28**]. Therefore, we discretize the fluid domain with Raviart-Thomas elements of lowest order:

$$RT_0 := \{\mathbf{u} \in \mathbf{H}(\mathrm{div}, \Omega_F) : \mathbf{u}_{|_K} = (a + bx, c + by), \ K \in \mathcal{T}_{h_f}, \ \ a, b, c \in \mathbb{R}\},$$

and the solid domain with Lagrangian finite elements of lowest order:

$$W_h^D := S_D(\Omega_S, \mathcal{T}_{h_s}) \times S_D(\Omega_S, \mathcal{T}_{h_s}),$$

where $S_D(\Omega_S, \mathcal{T}_{h_s})$ is the finite element space on Ω_S satisfying the Dirichlet boundary condition on Γ_D. The kinematic constraint can be efficiently imposed by piecewise constant Lagrange multipliers yielding a uniform inf-sup condition. Suppose $X_h := RT_0 \times W_h^D$, and $M_h := \{\mu_h \in L^2(\Gamma) : \mu_h|_e \in \mathcal{P}_0(e), e \in \mathcal{T}_\Gamma\}$. Now the finite element space can be written as

$$\mathbf{V}_h := \{(\mathbf{u}_{hF}, \mathbf{u}_{hS}) \in X_h, \ \int_\Gamma [\mathbf{u}_h] \cdot \mathbf{n} \, \mu_h \, d\sigma = 0, \ \mu_h \in M_h\}.$$

The discrete problem reads: find $\mathbf{u}_h \in \mathbf{V}_h$, and $\omega_h \in \mathbb{R}$ such that

$$a(\mathbf{u}_h, \mathbf{v}_h) = \omega_h^2 m(\mathbf{u}_h, \mathbf{v}_h), \quad \mathbf{v}_h \in \mathbf{V}_h.$$

REMARK 5.1. *We remark that the Lagrange multiplier λ_h approximates the pressure on the interface Γ. The Lagrange multipliers are associated with the one-dimensional mesh inherited from the triangulation on the fluid domain. Due to the special structure of the support of the nodal basis functions of RT_0 and M_h, the degree of freedom corresponding to the Lagrange multiplier can locally be eliminated by inverting a diagonal mass matrix.*

In [**5**], an adaptive finite element scheme is analyzed to solve the fluid-structure vibration problem, where the kinematic constraint is imposed by means of piecewise constant Lagrange multiplier. Following this technique, we arrive at the same mortar setting as we discuss here. Now, we consider the domain $\Omega := \{(x, y) \in \mathbb{R}^2,\, x^2 + y^2 < 1\}$ decomposed into two subdomains Ω_S and Ω_F with $\Omega_F := \{(x, y) \in \mathbb{R}^2,\, x^2+y^2 < 0.6\}$, and $\Omega_S := \Omega \backslash \bar{\Omega}_F$. Here, $\Gamma_D = \{(\cos\theta, \sin\theta),\, \frac{5\pi}{4} \leq \theta \leq \frac{7\pi}{4}\}$. The decomposition of the domain and initial triangulation is given in the left picture of Figure 5.1.

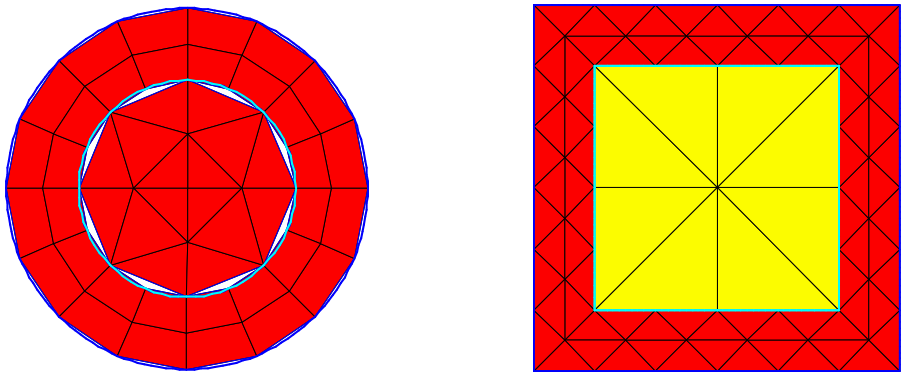

Figure 5.1: The decomposition of domain and initial triangulation, first example (left) and second example (right)

We have used the following parameters in our numerical example: $\rho_F = 1000kg/m^3$, $c = 1430m/s$, $\rho_S = 7700kg/m^3$, $E = 144GPa$, and $\nu = 0.35$ (fluid: water and solid: steel). We have given the three consecutive eigenmodes along with the pressure in the fluid domain and the distorted grids in the solid domain in Figure 5.2. We have presented the five consecutive eigenfrequencies (rad/s) in Table 5.1. The eigenfrequencies presented in Table 5.1 are computed after uniformly refining the initial grid given in the left picture of Figure 5.1 five times.

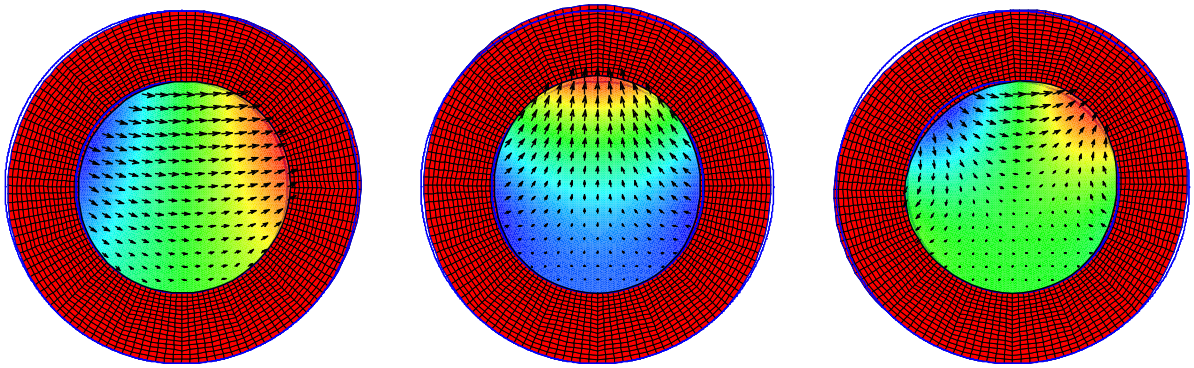

Figure 5.2: The first, second and the third eigenmodes corresponding to the eigenvalues 809.1481, 1980.7519 and 3606.3907 (rad/s), first example

The second numerical example is taken from [**29**]. The domain $\Omega := (0, 1.5) \times (0, 1.5)$ is decomposed into two subdomains Ω_S and Ω_F with $\Omega_F := (0.25, 1.25) \times (0.25, 1.25)$,

TABLE 5.1. The computed eigenfrequencies for the first example

Eigenmodes	Computed Eigenfrequencies
1	809.1481
2	1980.7519
3	3606.3907
4	4883.7319
5	5582.4929

$\Omega_S := \Omega \backslash \bar{\Omega}_F$, and $\Gamma_D = \{(x, 0) \in \mathbb{R}^2,\ 0 \leq x \leq 1.5\}$. We have shown the decomposition of domain and initial triangulation in the right picture of Figure 5.1, and three consecutive eigenmodes together with distorted grids in the structure and pressure in the fluid are given in Figure 5.3.

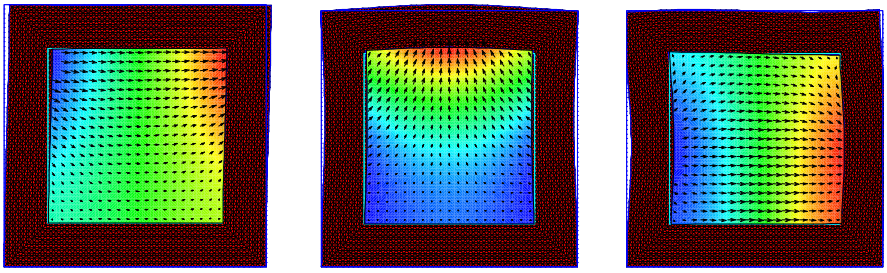

Figure 5.3: The first, second and the third eigenmodes, second example

We have used the same physical parameters as in the previous example. The computed eigenfrequencies (in rad/s) along with the extrapolated ones referred to as 'Exact' in [**29**] are given in Table 5.2. The eigenvalues presented in Table 5.2 are computed after uniformly refining the initial grid four times shown in the right picture of Figure 5.1. We point out that the solid domain has reentrant corners and varying boundary conditions on $\Gamma_D \cup \Gamma_N$, and that is the motivation to use a finer grid on the solid domain.

TABLE 5.2. The computed eigenfrequencies using mortar techniques compared with the extrapolated eigenfrequencies ('Exact') in [**29**], second example

Eigenmodes	Computed Eigenfrequencies	'Exact'
1	648.1847	641.837
2	2147.3593	2116.398
3	3419.5020	3201.475
4	3885.9022	3804.124
5	4214.0865	4211.620
6	4699.6782	4687.927

5.3. Coupling linear and quadratic finite elements

In this section, we apply the mortar approach to couple linear and quadratic finite elements. We consider the problem of linear elasticity given in [**4**] with the exact solution $\boldsymbol{u} := (u_1, u_2)$ defined as

$$\begin{aligned} u_1(r,\theta) &:= \frac{1}{2\mu} r^{\alpha}[-(\alpha+1)\cos((\alpha+1)\theta) + (C_2 - (\alpha+1))C_1\cos((\alpha-1)\theta)], \\ u_2(r,\theta) &:= \frac{1}{2\mu} r^{\alpha}[(\alpha+1)\sin((\alpha+1)\theta) + (C_2 + \alpha - 1)C_1\sin((\alpha-1)\theta)] \end{aligned}$$

in polar coordinates, where $C_1 := -\frac{\cos((\alpha+1)\omega)}{\cos((\alpha-1)\omega)}, C_2 := \frac{2(\lambda+2\mu)}{\lambda+\mu}$. Setting $\alpha = 0.544483737$, and $\omega = 3\pi/4$, the given exact solution solves the linear elasticity equation with the right hand side $\boldsymbol{f} = \boldsymbol{0}$. The Dirichlet boundary condition on Ω is computed from the exact solution. The domain Ω considered in [**4**] is a sort of L-shape polygon formed by joining the points $(-1,-1), (0,-2), (2,0), (0,2), (-1,1)$ and $(0,0)$. This example models a re-entrant corner with a typical singularity in the stress at $(0,0)$. Here, we decompose the domain Ω into two subdomains Ω_1 and Ω_2, where Ω_2 is on the slave side of the interface and again a L-shape polygon formed by joining the points $(-0.25,-0.25), (0,-0.5), (0.5,0), (0,0.5), (-0.25,0.25)$ and $(0,0)$, and $\Omega_1 := \Omega \backslash \Omega_2$. To resolve the singularity at the origin, we use bilinear elements in subdomain Ω_2 with a very fine grid, and work with quadratic finite elements in Ω_1 with a relatively coarser grid, see the left picture of Figure 5.4. The material parameters are

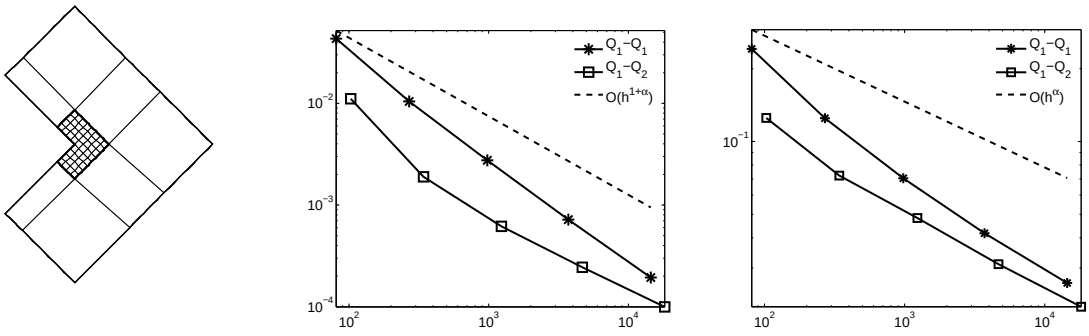

Figure 5.4: Decomposition of the domain and initial triangulation (left), error plot versus number of degrees of freedom in L^2-norm (middle) and error plot versus number of degrees of freedom in H^1-norm (right)

specified as $E = 100000$ and $\nu = 0.3$ for bronze. We solve the problem with two different approaches. In the first approach, we use bilinear elements in both subdomains (Q_1-Q_1), and in the second one we use bilinear and quadratic serendipity elements in subdomains Ω_2 and Ω_1, respectively (Q_1-Q_2). We have shown the errors in the L^2 and H^1-norms in the middle and the right pictures of Figure 5.4. Although the asymptotic rate of convergence is the same in both approaches, we can observe that the accuracy of the coupled approach is better in the beginning.

5.4. Coupling different material laws

In this section, we briefly outline how different material laws can be coupled using mortar techniques. For simplicity, we restrict ourselves to the case of two subdomains, but allow that the material laws can be nonlinear in one subdomain, and linear in another subdomain. We consider a bounded polygonal or polyhedral domain $\Omega \subset \mathbb{R}^d$, $d = \{2, 3\}$, which is decomposed into two non-overlapping subdomains Ω_1 and Ω_2 with the common interior interface Γ, $\bar{\Gamma} := \partial\Omega_1 \cap \partial\Omega_2$, and assume that we have two independent variational forms $a_1(u, v)$, and $a_2(u, v)$ in Ω_1 and Ω_2 respectively. Defining a global variational form $a(u, v) := \sum_{k=1}^{2} a_k(u, v)$, and using the weak form of the matching condition at the interface Γ, the global variational problem can be written exactly as the saddle point problem (4.2.5). Assuming the jump of the solution across the interface is zero, we can write the weak discrete formulation of the problem as: find $(u_h, \lambda_h) \in X_h \times M_h$ such that

$$\begin{array}{rcll} a(u_h, v) + b(v, \lambda_h) & = & l(v), & v \in X_h, \\ b(u_h, \mu) & = & 0, & \mu \in M_h, \end{array} \tag{5.4.1}$$

where $b(v, \mu)$ and $l(v)$ are as defined in the last chapter. Assume that $\{\phi_1, \phi_2, \cdots, \phi_{n_f}\}$ and $\{\lambda_1, \lambda_2, \cdots, \lambda_{n_l}\}$ be bases of X_h and M_h, respectively, where $n_f = \dim X_h$, and $n_l = \dim M_h$. Then for functions $u_h \in X_h$ and $\lambda_h \in M_h$, we can write $u_h = \sum_{k=1}^{n_f} u_k\phi_k$ and $\lambda_h = \sum_{k=1}^{n_l} \lambda_k\mu_k$. Taking $w = (u_1, \cdots, u_{n_f}, \lambda_1, \cdots, \lambda_{n_l}) \in X_h \times M_h$, we define $F(w) := (F_1(w), F_2(w))^T$ with

$$F_1(w) := \begin{pmatrix} a(u_h, \phi_1) + b(\phi_1, \lambda_h) - l(\phi_1) \\ \vdots \\ a(u_h, \phi_{n_f}) + b(\phi_{n_f}, \lambda_h) - l(\phi_{n_f}) \end{pmatrix}, \quad F_2(w) := \begin{pmatrix} b(u_h, \mu_1) \\ \vdots \\ b(u_h, \mu_{n_l}) \end{pmatrix}.$$

In general, the system $F(w) = 0$ is nonlinear if a nonlinear material law is used at least in one subdomain, and so we apply the Newton method to solve this system. First, we initialize the solution vector w_0 satisfying the given Dirichlet boundary conditions. Then, we iterate until convergence with

$$J_k \Delta w_k = F(w_k),$$

where $\Delta w_k := w_k - w_{k+1}$, and J_k is the Jacobian of F evaluated at w_k. Working with a dual Lagrange multiplier space has the advantage that the Jacobian matrix J_k has exactly the same form as the saddle point matrix arising from the mortar finite elements with a dual Lagrange multiplier space for the Laplace operator, see [**166**]. Hence, the modification of the algebraic system can be performed, and the multigrid approach introduced in [**166**] can be applied to solve the linear system on each level.

Example 1: Coupling Laplace and p-Laplace operator. In this example, we consider the coupling of a linear and a non-linear model described by a Poisson equation and by the p-Laplace equation, respectively. Here, we decompose the domain $\Omega := (-1, 1) \times (-1, 1)$ into four non-overlapping subdomains defined by $\Omega_1 := (-1, 0) \times (-1, 0)$, $\Omega_2 := (0, 1) \times (-1, 0)$, $\Omega_3 := (-1, 0) \times (0, 1)$ and $\Omega_4 := (0, 1) \times (0, 1)$. We have given the decomposition of the domain and the initial triangulation in the left picture of Figure 5.5. We consider the Poisson equation $-\nabla \cdot (\alpha\nabla)u = f$ in Ω_1 and Ω_4 and the p-Laplacian $-\nabla \cdot (\alpha|\nabla u|^{p-2}\nabla u) = f$ in Ω_2 and Ω_3. The p-Laplace equation occurs in the theory of

two-dimensional plasticity under longitudinal shear or in the diffusion problem with nonlinear diffusivity, see [**11**], and we are considering here different material models in different subdomains. For the regularity of the solutions and error estimates of the p-Laplacian, we refer to [**116**] and [**117**]. The interface $\Gamma := \{(0,y), -1 < y < 1\} \cup \{(x,0), -1 < x < 1\}$ inherits its one-dimensional triangulation $\mathcal{T}_\Gamma$ from the mesh on Ω_2 and Ω_3. We recall that $(0,0)$ is a crosspoint, and M_h does not have any degree of freedom at this point. Now, the Lagrange multiplier space M_h is defined on Γ and is associated with the triangulation $\mathcal{T}_\Gamma$. Assuming $q_1 := 2$, $q_2 := p$, $q_3 := p$, and $q_4 := 2$, we can write the global variational form

$$a(u,v) := \sum_{i=1}^{4} \int_{\Omega_i} \alpha |\nabla u|^{q_i - 2} \nabla u \cdot \nabla v \, dx$$

so that we have to solve the nonlinear saddle point problem (4.2.5). If $\alpha > 0$, and the right hand side function f is sufficiently smooth, we can show by monotonicity techniques that the problem (5.4.1) has a unique solution, see [**115**]. However, the regularity of the solution is not known.

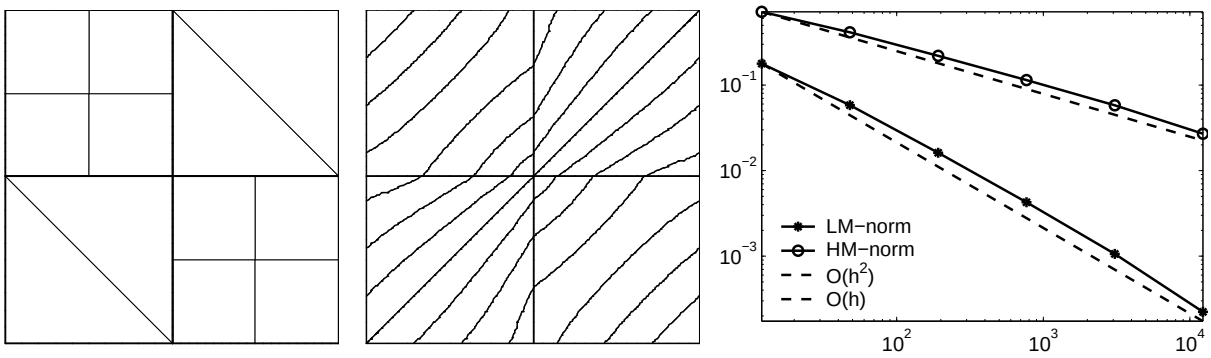

Figure 5.5: Decomposition of the domain and initial triangulation (left), isolines of the solution (middle) and discretization errors versus number of elements (right)

Suppose that $\tilde{\Omega}_l := \Omega_1 \cup \Omega_4$, and $\tilde{\Omega}_p := \Omega_2 \cup \Omega_3$. In our numerical example, we choose $\alpha = 0.5$ in $\tilde{\Omega}_l$, and $\alpha = 1$ in $\tilde{\Omega}_p$, $p = 1.5$, and $f = 0$. Hence, the system $F(w) = 0$ is a nonlinear system since $p \neq 2$. For boundary conditions, we set $u(-1,-1) = u(1,1) = 0$, $u(-1,1) = 1$ and $u(1,-1) = -1$, and the Dirichlet boundary condition on $\partial\Omega$ is imposed by taking the linear combination of them in between. Here, we do not have the exact solution. To get the approximation of the discretization errors, we compute a reference solution u_{ref} at a fine level and compare it with the solution u_h at each level until $h_{ref} \leq 2h$. We have given the discretization errors in the LM- and HM- norms defined by

$$\|v\|_{LM} := \|v\|_{L^2(\tilde{\Omega}_l)} + \|v\|_{L^p(\tilde{\Omega}_p)}, \quad \text{and} \quad \|v\|_{HM} := |v|_{W^{1,2}(\tilde{\Omega}_l)} + |v|_{W^{1,p}(\tilde{\Omega}_p)}$$

in the right picture of Figure 5.5, and the isolines of the solution are given in the middle. Although the regularity of the solution is not known, we get convergence of order h^2 in the LM-norm and of order h in the HM-norm.

Example 2: Coupling different material laws in elasticity. In this example, we consider Cook's membrane problem decomposed into two subdomains, and apply mortar techniques to couple different material models in different subdomains. In particular, we consider linear, neo-Hookean and Mooney-Rivlin material laws. For more information on linear and nonlinear elasticity, we refer to Chapter 6 or to the standard references [**64, 21**]. The left picture of Figure 2.16 shows the decomposition of the domain Ω and initial triangulation. As in the standard Cook's membrane problem, the left boundary of Ω is fixed and an in-plane shearing load of 100N is applied along the positive y-direction on the right boundary.

In Tables 5.3 and 5.4, we have shown the vertical tip displacement at the top right corner of the membrane for different levels of refinement using different material laws in different subdomains, where NH, MR or LN denotes that neo-Hookean, Mooney-Rivlin or linear material law is applied in the whole domain Ω, whereas NH-MR denotes that neo-Hookean law is applied in subdomain Ω_1, and Mooney-Rivlin law is applied in the subdomain Ω_2; and MR-NH denotes vice-versa. LN-NH and NH-LN also have a similar meaning. We consider the following material parameters $E_1 = 250, \nu_1 = 0.25$ and $E_2 = 350, \nu_2 = 0.35$, where suffices indicate the corresponding subdomains, and the material parameter c_m is set to be 0.25 in case of Mooney-Rivlin law. We can see that the Mooney-Rivlin and linear model yield larger deformation in this example than the neo-Hookean model. Although the choice between Mooney-Rivlin and neo-Hookean material laws depends on the material property, the nonlinear material models should be normally used if the deformation is large. Since the deformation is not so large in the inner subdomain, it is reasonable to use linear material law for the inner subdomain and nonlinear material law for the outer subdomain.

TABLE 5.3. Vertical tip displacement at the right top corner of the membrane

level	NH	MR	NH-MR	MR-NH
0	6.1311	7.0004	6.3284	6.7758
1	6.8940	7.9442	7.1276	7.6785
2	7.1970	8.3337	7.4387	8.0603
3	7.2919	8.4596	7.5357	8.1849

TABLE 5.4. Vertical tip displacement at the right top corner of the membrane

level	LN	NH	LN-NH	NH-LN
0	7.1321	6.1311	6.7774	6.3007
1	8.2729	6.8940	7.7906	7.0645
2	8.7665	7.1970	8.2152	7.3838
3	8.9343	7.2919	8.3627	7.4848

Example 3: Coupling different material laws in elasticity. This example is also concerned with the coupling between different material laws in elasticity. Here, we consider a three-dimensional domain Ω composed of three subdomains $\Omega_1 := (2, 10)^2 \times (0, 6)$, $\Omega_2 :=$

$(0,12)^2 \times (6,16)$ and $\Omega_3 := (4,8)^2 \times (16,20)$, see the left picture of Figure 5.6. The right and left sides of the middle cube Ω_2 are clamped so that Γ_D is the part of the boundary of Ω with $x = 0$, $x = 12$, and $\Gamma_N := \partial\Omega \backslash \Gamma_D$. The upper and lower cubes are pressed from the top and bottom boundaries, respectively, so that the function $\boldsymbol{g} = (g_1, g_2, g_3)^T$ on Γ_N is given as $g_1 = g_2 = 0$, and

$$g_3 = \begin{cases} 100.0 & \text{if } z = 0 \\ -100.0 & \text{if } z = 20 \\ 0 & \text{otherwise.} \end{cases}$$

The material parameters are set to be $E_1 = 4500, \nu_1 = 0.32, E_2 = 400, \nu_2 = 0.4$ and $E_3 = 4500, \nu_3 = 0.35$ for different subdomains. Since the forces are applied from the bottom and the top of subdomains Ω_1 and Ω_3, respectively, and these subdomains are occupied with hard materials, we infer that the deformation is large only in subdomain Ω_2. Therefore, we assume that it is enough to work with the model of linear elasticity in subdomains Ω_1 and Ω_3, and with neo-Hookean law in subdomain Ω_2 (LN-NH). In the left and right pictures of Figure 5.7, we have plotted the vertical displacement computed with different approaches along the lines $x = 6, z = 6$ and $x = 6, z = 16$, respectively. As can be seen from these pictures, the linear elastic law in all subdomains (LN) result in a large unrealistic solution, whereas the nonlinear neo-Hookean law in all subdomains (NH) and the coupled approach (LN-NH) as described above yield the same numerical results.

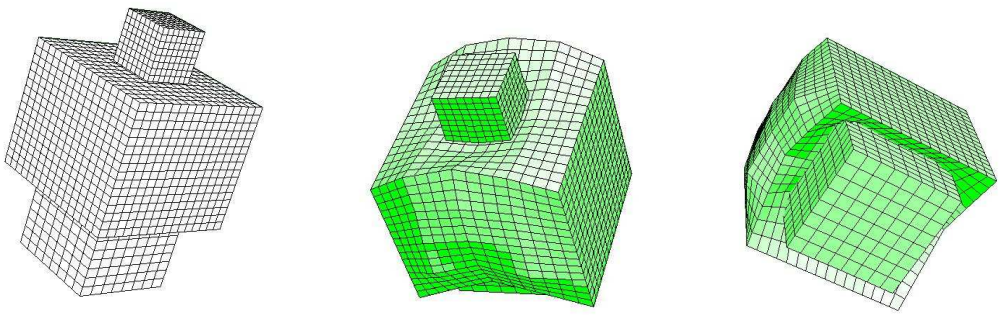

Figure 5.6: Decomposition of the domain (left), deformation of the domain looked from the top (middle) and deformation of the domain looked from the bottom (right), zoomed with factor 5

5.5. Applications to time-dependent problems

In this section, we consider some applications of mortar finite elements for time-dependent interface problems. We consider a bounded polygonal domain $\Omega \subset \mathbb{R}^2$, which is decomposed into two non-overlapping subdomains Ω_1 and Ω_2 with the common interior interface Γ, $\bar{\Gamma} := \partial\Omega_1 \cap \partial\Omega_2$. We are interested in solving the following scalar time-dependent partial differential equation in Ω:

$$\frac{\partial u(t)}{\partial t} - \nabla \cdot (a \nabla u(t)) + \mathbf{b} \cdot \nabla u(t) + c u(t) = f(t), \text{ and } u(0) = u_0 \text{ in } \Omega \tag{5.5.1}$$

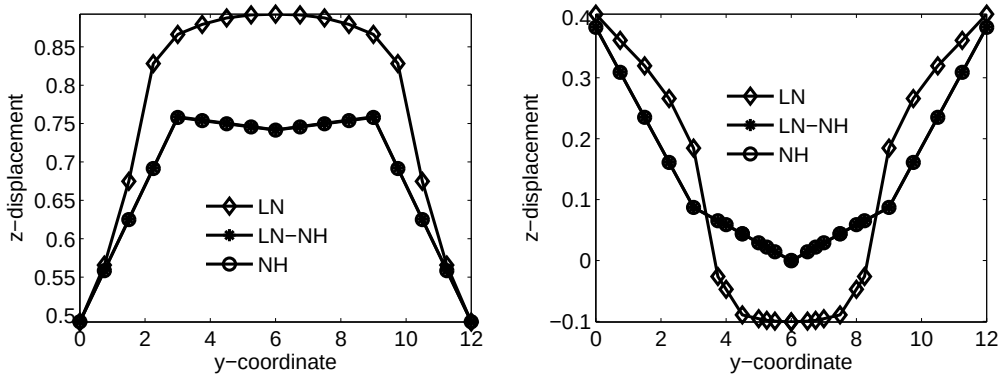

Figure 5.7: Vertical displacements along the line $x = 6, z = 6$ (left) and along the line $x = 6, z = 16$ (right)

with homogeneous Dirichlet boundary condition on $\partial\Omega$, where $u(t)$, $f(t)$ and u_0 are functions defined on Ω.

Proceeding as in the last chapter, the mortar discretization of the partial differential equation (5.5.1) yields the saddle point formulation: find $(u_h(t), \lambda_h(t)) \in X_h \times M_h$ so that

$$\begin{array}{lcll} a(u_h(t), v_h) + b(v_h, \lambda_h(t)) & = & l(v_h), & v_h \in X_h, \\ b(u_h(t), \mu_h) & = & 0, & \mu_h \in M_h, \end{array} \tag{5.5.2}$$

where the forms $b(\cdot,\cdot)$ and $l(\cdot)$ are as defined in the last chapter, and

$$a(u_h(t), v_h) := \sum_{k=1}^{2} \int_{\Omega_k} (a\nabla u_h(t)) \cdot \nabla v_h + (cu_h(t) + \frac{\partial u_h(t)}{\partial t}) v_h + \mathbf{b} \cdot \nabla u_h(t) v_h \, dx,$$

and X_h and M_h are defined as in the previous chapters. Under suitable assumptions on the piecewise defined tensor a, the vector function $\mathbf{b}$ and the constant c, we can show the existence and the uniqueness of the solution.

Using u_h and λ_h for the vector representation of the solutions $u_h(t)$ and $\lambda_h(t)$ and denoting the time derivative of u_h by $\dot{u}_h$, we write an algebraic formulation of the variational equation (5.5.2)

$$\begin{pmatrix} \mathtt{M} & 0 \\ 0 & 0 \end{pmatrix} \begin{pmatrix} \dot{u}_h \\ 0 \end{pmatrix} + \begin{pmatrix} \mathtt{A} & \mathtt{B}^T \\ \mathtt{B} & 0 \end{pmatrix} \begin{pmatrix} u_h \\ \lambda_h \end{pmatrix} = \begin{pmatrix} f_h \\ 0 \end{pmatrix}, \tag{5.5.3}$$

where the matrix $\mathtt{A}$ comes from the time-independent part of the bilinear form $a(\cdot,\cdot)$, and $\mathtt{M}$ is the usual mass matrix. Here, we use the same notations for the finite element solution in $X_h \times M_h$ and the vector representation of the solution. Performing the time-discretization with the so-called θ-scheme [**130**] for the semi-discrete saddle point system (5.5.3), we obtain

$$\begin{pmatrix} \frac{\mathtt{M}}{\delta t} + \theta\mathtt{A} & \mathtt{B}^T \\ \theta\mathtt{B} & 0 \end{pmatrix} \begin{pmatrix} u_h^{n+1} \\ \lambda_h^{n+1} \end{pmatrix} = \begin{pmatrix} \theta f_h^{n+1} + (1-\theta) f_h^n + (\frac{\mathtt{M}}{\delta t} - (1-\theta)\mathtt{A}) u_h^n - (1-\theta)\mathtt{B}^T \lambda_h^n \\ (\theta - 1)\mathtt{B} u_h^n \end{pmatrix},$$

where $0 \leq \theta \leq 1$. We recall that the θ-scheme includes: forward Euler ($\theta = 0$), backward Euler ($\theta = 1$), and Crank-Nicolson ($\theta = 1/2$).

Thus we see that the algebraic saddle point system arising from the mortar discretization of a time-dependent problem with the θ-scheme is exactly the same as the algebraic saddle point system coming from a time-independent problem. Hence we can apply the modification and multigrid solver as proposed in [**166**].

Example 1: In this example, we consider the heat equation in Ω with constant Dirichlet boundary condition on $\partial\Omega$, where the domain $\Omega := (0,1) \times (0,1)$ is decomposed into four squares $\Omega_{ij} = ((i-1)/2,\, i/2) \times ((j-1)/2,\, j/2)$, $i, j = 1, 2$. The diffusion coefficient a is set to 2.0 on Ω_{11}, 0.6 on Ω_{12}, 1.0 on Ω_{21}, and 1.4 on Ω_{22}. We have given the decomposition of the domain and the initial triangulation in the left picture of Figure 5.5. Four snapshots of the heat distribution in Ω are give in Figure 5.8, where we can see the influence of the diffusion coefficient a.

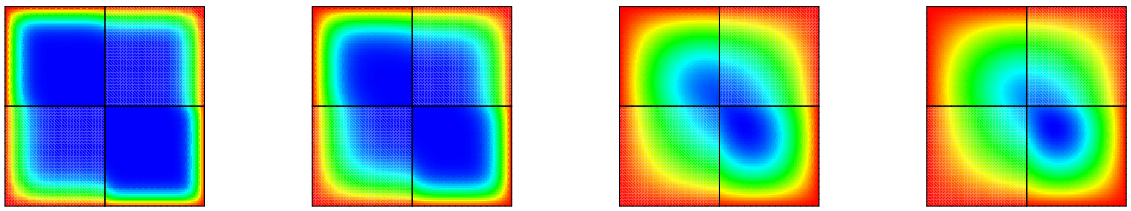

Figure 5.8: Snapshots of the heat distribution on Ω at times $t = 0.008, t = 0.02, t = 0.1$ and $t = 0.5$

Example 2: Here, we solve the equation (5.5.1) with $c = 0$ in the global domain $\Omega := (0,4) \times (0,3)$ composed of three subdomains $\Omega_1 := (0,4) \times (0,1)$, $\Omega_2 := (0,4) \times (1,2)$, and $\Omega_3 := (0,4) \times (2,3)$, see the left picture of Figure 5.9. The diffusion coefficient a is set to be 1.0 on Ω_2, and 10.0 on Ω_1 and Ω_3. A parabolic heat flux $g(x) = 0.4x(4-x)$ is applied from the top and the bottom boundary of Ω and a constant temperature is applied on the left boundary of Ω_2. The advective velocity is prescribed as $\mathbf{b} = (10, 0)$ so that we have an advection diffusion equation with jump in the diffusivity coefficients and advection velocity. Using $\delta t = 0.002$, we compute the solution with implicit Euler scheme for different time steps. We have shown three snapshots of the heat distribution in Ω in Figure 5.9.

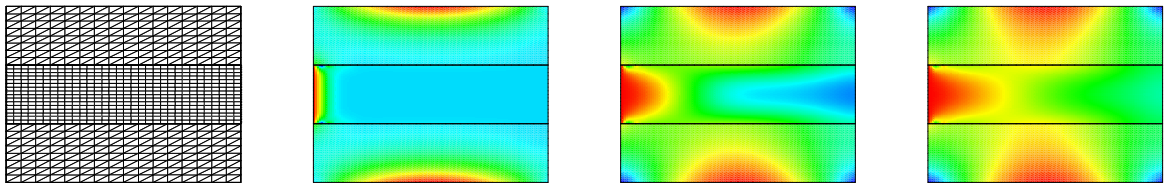

Figure 5.9: Decomposition of the domain and triangulation (left), and three snapshots of the heat distribution at times $t = 0.008, t = 0.12, t = 0.2$

In the left and right pictures of Figure 5.10, we have plotted the heat along the line $y = 1.5$ at times $t = 0.12$ and $t = 0.2$ for advected ($\mathbf{b} = (10, 0)$) and non-advected heat

flow ($\mathbf{b} = (0, 0)$), where we can see that the heat is advected forward with the advection velocity.

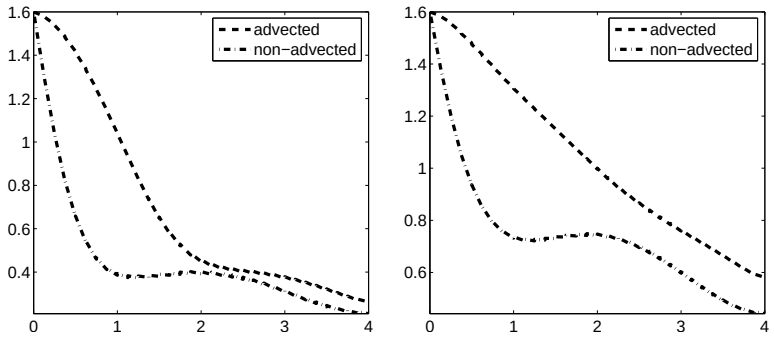

Figure 5.10: The heat distribution along the line $y = 1.5$ for advected and non-advected case, $t = 0.12$ (left) and $t = 0.2$ (right)

5.6. Applications to heat transfer problems in sliding meshes

In this section, we consider a time-dependent heat transfer problem when a body is sliding against another body causing heat generation on the interface due to friction, see also [**122, 119, 127, 169, 109**]. Neglecting the mechanical part, we assume that the pressure on the contact interface is a known function. A complete thermo-mechanical model can be found in [**169, 109**]. As before, we consider a bounded polygonal or polyhedral domain $\Omega \subset \mathbb{R}^d$, $d = \{2, 3\}$, decomposed into two non-overlapping subdomains Ω_1 and Ω_2 with the common interior interface Γ, $\bar{\Gamma} := \partial\Omega_1 \cap \partial\Omega_2$. The heat conduction equation for both bodies can be written as

$$\rho_i c_i \frac{\partial u_i(t)}{\partial t} - \nabla \cdot (\alpha_i \nabla u_i(t)) = f_i(t) \text{ in } \Omega_i, \ i = 1, 2, \tag{5.6.1}$$

where ρ_i is the density, c_i is the specific heat, α_i is the thermal conductivity, and f_i is the heat source within Ω_i, $i = 1, 2$. The initial temperature is prescribed as $u_i(0, x) = u_i^0(x)$, $i = 1, 2$. Denoting the outer normal on Γ from Ω_i by $\mathbf{n}_i$, and the jump of the solution u across the interface $u_1 - u_2$ by $[u]$, the transmission conditions on the interface are given in terms of the heat fluxes $\alpha_1 \nabla u_1(t, x) \cdot \mathbf{n}_1$ and $\alpha_2 \nabla u_2(t, x) \cdot \mathbf{n}_2$ across Γ from the first and the second body, respectively with

$$\alpha_1 \nabla u_1(t, x) \cdot \mathbf{n}_1 = c_D \beta v p - \hat{a}[u], \text{ and } \alpha_2 \nabla u_2(t, x) \cdot \mathbf{n}_2 = c_D(1 - \beta) v p + \hat{a}[u],$$

where c_D is the frictional constant, $\hat{a}$ is the heat transfer parameter, and $\beta = \frac{\alpha_1}{\alpha_1 + \alpha_2}$. The functions $v(t, x)$ and $p(t, x)$ are the relative velocity and the pressure at the real contact interface at the point x and at time t, respectively. We assume that the heat transfer parameter $\hat{a}$ is directly proportional to the contact pressure p on the contact interface so that $\hat{a} = \bar{\gamma}_c p$, where $\bar{\gamma}_c$ is the heat transfer coefficient, see [**119, 109**]. The heat transfer parameter has the unit $W/m^{2\circ}$C, whereas the unit of $\bar{\gamma}_c$ is W/N°C. A different model in which the heat transfer parameter $\hat{a}$ depends on the contact pressure p with the relation $\hat{a} = h_{s_0}(\frac{p}{H_c})^\epsilon$ can be found in [**169**], where h_{s_0} is the contact resistance coefficient, H_c the Vickers hardness and ϵ a fixed exponent. We consider the boundary conditions of Robin

type on $\Gamma_i := \partial\Omega_i \backslash \Gamma$ for $i = 1, 2$ with $\alpha_i \nabla u_i(t,x) \cdot \mathbf{n}_i = -\tilde{a}_i(u_i(t,x) - u_\infty)$, where $\tilde{a}_i$ is the coefficient of convective heat transfer for Ω_i, and u_∞ is the ambient temperature of the surrounding medium, which is assumed to be zero for simplicity. The ideal thermally isolated boundary condition can be recovered with $\tilde{a}_i = 0$. The mortar discretization is achieved by using the same notation and the method as in the previous chapter. We point out that here the Neumann jump of the solution g_N is given by $g_N = c_D vp$, and the jump of the solution is coupled with the heat flux on the interface Γ. Introducing the heat flux on Γ from the second body $\lambda = \alpha_2 \nabla u_2(t,x) \cdot \mathbf{n}_2$ as the Lagrange multiplier, the mortar formulation is attained by writing the weak form of

$$\lambda = c_D(1-\beta)vp + \bar{\gamma}_c p\,[u]. \tag{5.6.2}$$

In contrast to the approach in the previous chapter, the weak formulation cannot be achieved by multiplying the equation (5.6.2) by a dual test function. Since $\lambda \in (H^{1/2}(\Gamma))'$, we have to multiply the equation (5.6.2) with a more regular test function $\phi \in H^{1/2}(\Gamma)$ to get the weak form. This leads to a Petrov-Galerkin mortar formulation. Defining $g_D := -c_D(1-\beta)vp$, this formulation in the discrete setting can be written as: find $(u_h(t), \lambda_h(t)) \in X_h \times M_h$ so that

$$\begin{array}{rcrcll} a(u_h(t), v_h) & + & b_1(v_h, \lambda_h(t)) & = & l(v_h), & v_h \in X_h, \\ b_2(u_h(t), \phi_h) & - & c(\lambda_h(t), \phi_h) & = & g(\phi_h), & \phi_h \in W_h, \end{array} \tag{5.6.3}$$

where the forms $l(\cdot)$ and $g(\cdot)$, and sets X_h and M_h are as defined in the last chapter, whereas

$$\begin{aligned} a(u_h(t), v_h) &:= \sum_{k=1}^{2} \int_{\Omega_k} \alpha_k \nabla u_h(t) \cdot \nabla v_h + \rho_k c_k \frac{\partial u_h(t)}{\partial t} v_h \, dx + \tilde{a}_k \int_{\Gamma_k} u_h(t) v_h \, d\sigma, \\ b_1(v_h, \lambda_h(t)) &:= \int_\Gamma \lambda_h(t)\,[v_h]\, d\sigma, \quad b_2(u_h(t), \phi_h) := \int_\Gamma \bar{\gamma}_c p\,[u_h(t)]\,\phi_h \, d\sigma, \text{ and} \\ c(\lambda_h(t), \phi_h) &:= \int_\Gamma \lambda_h(t)\,\phi_h \, d\sigma. \end{aligned}$$

Here, W_h is the trace of the finite element space from the slave side of the interface Γ and is the so-called standard Lagrange multiplier space, see [**34**]. In contrast to the general mortar situation, we have assumed Robin boundary conditions on Γ_i, $i = 1, 2$, and so we do not need to remove the degrees of freedom of M_h and W_h from $\partial\Gamma$. Using the same notation for the vector representation of the solutions as in the previous section, we can write the algebraic formulation of the variational equation (5.6.3) as

$$\begin{pmatrix} \mathtt{M} & 0 \\ 0 & 0 \end{pmatrix} \begin{pmatrix} \dot{u}_h \\ 0 \end{pmatrix} + \begin{pmatrix} \mathtt{A} & \mathtt{B}_1^T \\ \mathtt{B}_2 & \mathtt{C} \end{pmatrix} \begin{pmatrix} u_h \\ \lambda_h \end{pmatrix} = \begin{pmatrix} f_h \\ g_h \end{pmatrix}, \tag{5.6.4}$$

where we have a non-zero matrix $\mathtt{C}$ in the saddle point system. If M_h is a dual Lagrange multiplier space, the matrix $\mathtt{C}$ is diagonal, and the static condensation of the Lagrange multiplier can be done easily.

REMARK 5.2. *Under the assumption that* $\dim W_h = \dim M_h$, *an isomorphism* $I_h : M_h \longrightarrow W_h$ *can be defined. Then, we can introduce an approach alternative to the Petrov-Galerkin approach writing the discrete variational problem as: find* $(u_h(t), \lambda_h(t)) \in X_h \times M_h$

so that

$$\begin{array}{rcrcll} a(u_h(t), v_h) & + & b_1(v_h, \lambda_h(t)) & = & l(v_h), & v_h \in X_h, \\ b_2(u_h(t), \mu_h) & - & c(\lambda_h(t), I_h\mu_h) & = & g(\mu_h), & \mu_h \in M_h. \end{array}$$

As we have tested both approaches, they yield almost the same numerical results.

Example 1: In the first example, we test our numerical scheme for a heat transfer problem through the contact interface introduced in [**119, 109**]. Here, we solve the steady state heat transfer problem between two bodies $\Omega_1 := (0, 1.5)^2$, and $\Omega_2 := (0, 1.5) \times (1.5, 3)$, which are in contact along the line $y = 1.5$, see the left picture of Figure 5.11. The material parameters for this problem are given by $\alpha = \alpha_1 = \alpha_2 = 55W/m°\text{C}$, and $\bar{\gamma}_c = 1W/N°\text{C}$. The temperature at the lower boundary of Ω_1 and the upper boundary of Ω_2 is fixed to be $\theta_1 = 100°\text{C}$ and $\theta_2 = 200°\text{C}$, respectively, and the other boundaries are thermally isolated. This problem can be solved analytically, and the exact solutions at the contact interface are given by $u_1 = \frac{(1+\eta)\theta_1+\eta\theta_2}{1+2\eta}$, and $u_2 = \frac{(1+\eta)\theta_2+\eta\theta_1}{1+2\eta}$ for Ω_1 and Ω_2, respectively, where $\eta = \frac{\bar{\gamma}_c p}{\alpha}$. Since the exact solution is piecewise linear, the numerical solution of the problem is exactly the same as the analytical solution. The temperature at the contact interface for both bodies versus the total contact pressure can be found in the right picture of Figure 5.11. In this picture, the upper part shows the temperature at the contact interface from Ω_2, whereas the lower part shows the temperature at the contact interface from Ω_1. In case of the perfect conductance, we obtain the temperature 150°C from both sides.

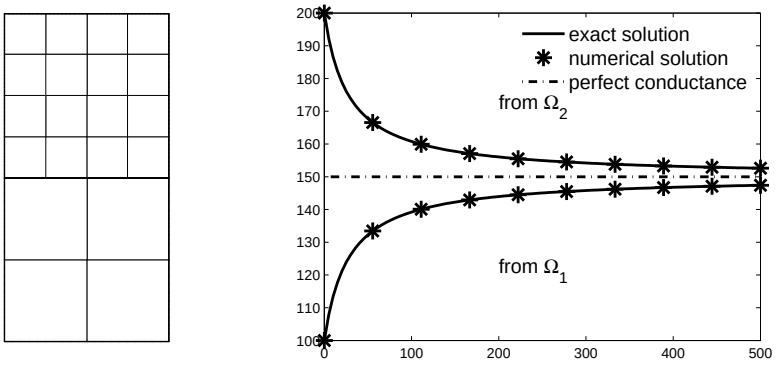

Figure 5.11: Two bodies with triangulation (left) and contact temperature in °C versus total contact pressure in N (right)

Example 2: In this example, we consider a problem where the contact pressure is known, see the first numerical example in [**119**]. Using the same material parameters as in the first example, we solve the steady state heat conduction problem with the heat flux on the contact interface linearly depending on the contact pressure. The global domain consists of two subdomains $\Omega_1 := (0, 40) \times (0, 20)$, and $\Omega_2 := (12, 28) \times (20, 30)$, see the left picture of Figure 5.12. As in the first example, the temperature at the lower boundary of Ω_1 and the upper boundary of Ω_2 is fixed to be $\theta_1 = 100°\text{C}$, and $\theta_2 = 200°\text{C}$, respectively. The other boundaries are thermally isolated. Applying the uniformly distributed load q on the free upper surface of Ω_1 and Ω_2, the contact pressure should be equal to q independent of any material parameters, see [**119, 109**]. In the right two pictures of Figure 5.12, we

have given the temperature for different levels of applied pressure at the contact interface from Ω_1 and Ω_2, respectively.

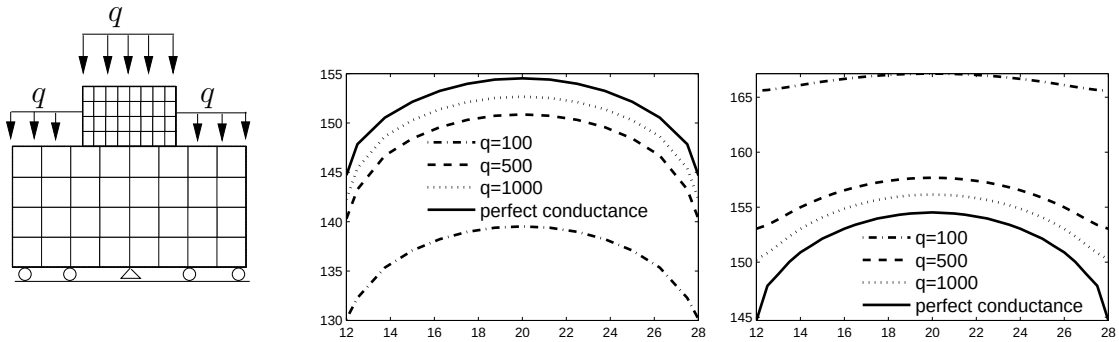

Figure 5.12: Mechanical problem definition with initial grid (left) and contact temperature in °C from Ω_1 (middle) and from Ω_2 (right) for different pressure levels

Example 3: In our third example, we consider a time-dependent problem where the heat is generated through sliding friction. In this problem, the global domain Ω is initially composed of two subdomains with

$$\Omega_1 := (0,5) \times (0,1.25) \text{ and } \Omega_2 := (0,1.25) \times (1.25,2.5)$$

with unit of length in centimeters. The material parameters for Ω_1 and Ω_2 are chosen for copper and iron, respectively, where $\rho_1 = 8960kg/m^3$, $c_1 = 385J/kg°\text{C}$, $\alpha_1 = 386W/m°\text{C}$, and $\rho_2 = 7860kg/m^3$, $c_2 = 444J/kg°\text{C}$, $\alpha_2 = 80.2W/m°\text{C}$. We assume that the body Ω is thermally isolated. The upper subdomain Ω_2 begins to slide over the lower subdomain with the velocity $1.875cm/s$ so that it reaches the right end of the subdomain Ω_2 in 2 seconds. The coefficient of friction and the heat transfer coefficient are chosen as $c_D = 0.2$, and $\bar{\gamma}_c = 1W/N°\text{C}$, respectively. Applying the load of $1MPa$ on the interface Γ at each time step, we compute the solution with implicit Euler scheme using $\delta t = 0.01$ and zero initial temperature. In the left picture of Figure 5.13, we have given the decomposition of the domain and the triangulation, and two snapshots of the heat distribution in Ω are given in the right. We can see that as time increases, the heat increases in the area which is exposed to the contact for longer time, and the conduction is more rapid in copper than in iron.

Example 4: In the last example, we consider an iron cube sliding between two copper bodies $\Omega_1 := (0,5) \times (0,1)^2$ and $\Omega_3 := (0,5) \times (0,1) \times (2,3)$ with the unit of length in centimeters. The iron cube Ω_2 initially occupies the region $(2,3) \times (0,1) \times (1,2)$, and begins to slide with the velocity $2cm/s$ to the right, and when it reaches the right end returns back to the left with the same velocity. In this way, the cube oscillates between two left and right end points of Ω_1 and Ω_3. The material parameters considered are the same as in the previous example. We apply $1MPa$ pressure on the interface Γ at each time step and Robin boundary condition is applied on the upper and lower boundaries of Ω_1 and Ω_3 with Robin parameter $\tilde{a}_1 = \tilde{a}_3 = 25000W/m^{2\circ}\text{C}$, whereas the other boundaries are thermally isolated. The initial temperature is set to be zero. The domain $\Omega := \cup_{i=1}^{3} \Omega_i$ at time $t = 0$ with the triangulation is shown in the left picture of Figure 5.14, and the solutions at two

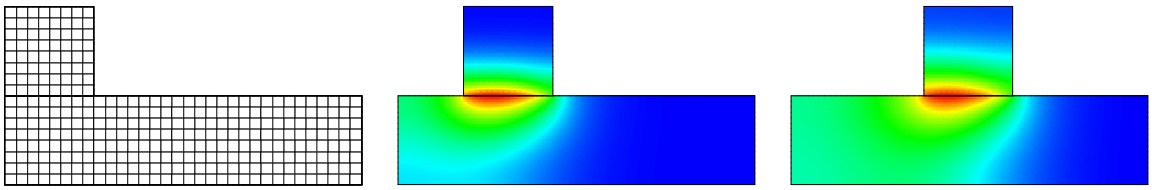

Figure 5.13: Decomposition of the domain and triangulation (left), and two snapshots of the heat distribution at times $t = 0.5s$ and $t = 1s$ (right)

different times computed using $\delta t = 0.01$ are shown in the right. In the right picture of Figure 5.14, we can see the effect of convective boundary condition on the lower surface of Ω_1 and the upper surface of Ω_3, where the cooling process does not allow this area to be heated quickly.

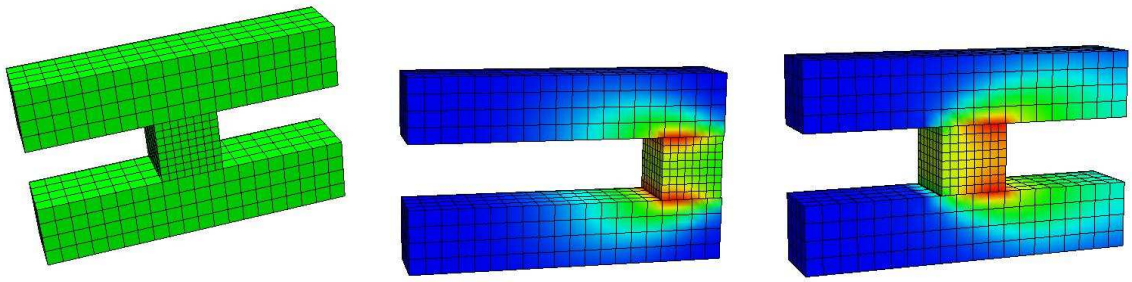

Figure 5.14: Decomposition of the domain and triangulation (left), and two snapshots of the heat distribution at times $t = 1$ and $t = 2$ (right)

CHAPTER 6

Locking-Free Finite Element Methods Based on the Hu-Washizu and Related Formulations

6.1. Introduction

It is well known that low order finite elements based on four-noded quadrilaterals or eight-noded hexahedra have two drawbacks in finite element computation of solid mechanics. The first one is the locking effect in the nearly incompressible case; in other words, they do not converge uniformly with respect to the Lamé parameter λ. The second one is that these standard elements lead to poor accuracy in bending-dominated problems when coarse meshes are used. There are many approaches to overcome these difficulties. One obvious remedy for these problems is to work with higher order finite elements. For example, in [**138**], it is shown that working with the h-version finite elements of order higher than three on a class of triangular meshes locking in linear elasticity can completely be avoided. On the other hand, in [**14**], it has been shown that the h-version can never be fully free of locking in rectangular meshes no matter how higher-order finite elements are used in the sense that suboptimal convergence rates are observed. For the mathematical analysis of the locking effect, we refer to [**14, 15**]. An another approach is related to mixed methods. The linear elasticity problem can be formulated as a mixed formulation in many different ways, see [**52, 40, 38, 158, 10, 8**]. The general approach in these mixed formulations is to introduce extra variables leading to a saddle point problem. The essential point is to prove that the method is robust for the limiting problem, which is the Stokes problem. Treating displacements and the 'mean pressure' as two independent field variables, one of the mixed formulations is given by Herrmann [**90**], which is also known as the reduced form of the Hellinger-Reissner principle. The Herrmann principle has also been extended to nonlinear hyperelastic problems in [**135, 153, 71, 129**]. As in the linear case [**96, 52, 40**], the approaches based on the bilinear or trilinear displacement and piecewise constant pressure are often used to overcome the volumetric locking in the nearly incompressible nonlinear elasticity. Separation of volumetric and deviatoric response leads to the so-called B-bar method for linear and nonlinear elasticity, see [**96, 121, 144**]. However, these elements suffer from so-called shear locking in the thin structure and show poor coarse mesh accuracy in bending dominated problems. These elements also exhibit a sort of numerical instability, the so-called hourglass effect when applied to certain nonlinear problems [**141**]. The approach based on mixed formulations has a close link with reduced integration schemes, see [**20, 51**]. Nonconforming finite element methods have also been analyzed for linear elastic problems leading to the uniform convergence in the nearly incompressible case, see [**74, 51, 110, 47, 48**].

Most popular methods with low order finite elements are the methods associated with the enhancement of the strain or stress field. The method of enhanced assumed strain,

first proposed by Simo and Rifai [**143**], has become a popular approach in overcoming these difficulties of standard elements in linear and nonlinear elasticity [**141, 142**]. The a priori error estimate for the enhanced assumed strain method for linear elastic problems has been studied by Reddy and Simo in [**133**]. They showed that for affine-equivalent meshes the displacement converges with the standard rate. Later Braess [**39**] re-examined the sufficient conditions for convergence clarifying the influence of the Lamé parameter λ. The detailed mathematical analysis of enhanced assumed strain has been done by Braess, Carstensen and Reddy [**41**], where a robust asymptotic convergence of the displacement has been proved for a class of meshes. However, these elements when applied to nonlinear elasticity also show the same numerical instability in compressive deformation later shown by Wriggers and Reese [**170**]. This observation leads to the development of different alternative enhancement strategies, see [**100, 81, 7**]. The assumed stress approach proposed in [**128**] has a very similar feature to that based on enhanced strains, and in fact the two are equivalent under certain conditions [**6, 41**]. Simo and Rifai have started from the Hu-Washizu principle [**93, 156**] to derive the method based on the enhancement of the strains, and similar path has been followed to extend this approach to the nonlinear regime. Another approach based on the Hu-Washizu formulation of linear elasticity is the mixed enhanced strain approach introduced by Kasper and Taylor [**97**]. These authors take the Hu-Washizu functional as a starting point and subsequently eliminate stresses and strains from the Hu-Washizu formulation to arrive at the displacement based formulation. The method of mixed enhanced strain is also applied to nonlinear hyperelasticity [**98**]. Another relevant method having a close link with the Hu-Washizu formulation is the strain gap method due to Romano, Marotti, and Diaco [**137**]. However, the analysis presented in [**137**] does not cover the uniform convergence of the finite element solution in the nearly incompressible case.

All these methods, variationally based on the Hu-Washizu principle, show a promising approach to overcome the difficulties referred to earlier. However, a full mathematical analysis of the Hu-Washizu formulation is still an open question so that under what conditions this formulation is uniformly convergent in the nearly incompressible case. Here, we want to fill this gap by analyzing the Hu-Washizu formulation in linear elasticity in the nearly incompressible limit. We show the uniform convergence of the finite element solution in the nearly incompressible case through the modification of the Hu-Washizu formulation that is equivalent to the standard Hu-Washizu formulation in the continuous setting. However, the modified Hu-Washizu formulation might be different in the discrete setting. We refer to [**102**] for the similar analysis in case of plane elasticity. We exploit the invertibility of the Saint-Venant Kirchhoff constitutive law to arrive at the modified Hu-Washizu formulation, which depends on a parameter α. Following the same idea, we obtain an α-dependent three-field formulation for the geometrically nonlinear elasticity with Saint-Venant Kirchhoff law.

However, in case of general hyperelasticity, the constitutive equation cannot be easily inverted, and therefore, we follow a different route to obtain an α-dependent formulation. To obtain a three-field formulation for the general hyperelastic material law, we use two crucial observations from the linear analysis. First we observe that the modified Hu-Washizu formulation can be reduced to a modified Hellinger-Reissner formulation, where

we have stress and displacement as two unknowns. This motivates us to use only the stress and the displacement as two unknowns. The second point is that to get a robust numerical scheme in the nearly incompressible limit with low order finite elements, we have to project the part of the stress involving the determinant of the deformation gradient onto piecewise constant functions. Using these two ingredients, we develop a three-field formulation for general hyperelastic problems. This new formulation can also be viewed as a combination of the Herrmann and the Hellinger-Reissner principle.

The structure of the rest of this chapter is organized as follows. In the rest of this section, we briefly recall the standard displacement formulation of linear elasticity. The next section is devoted to the introduction and analysis of the standard and modified Hu-Washizu formulations of linear elasticity in the continuous setting. Starting with a mixed formulation of the linear elastic problem based on the displacement and pressure, we present the standard Hu-Washizu formulation, which also provides a motivation to introduce our parameter-dependent three-field formulation. Sections 6.3–6.4 are devoted to the analysis of the modified Hu-Washizu formulation in the discrete setting. In Section 6.5, we arrive at an equivalent displacement-based formulation using static condensation and show that the displacement converges uniformly with respect to the Lamé parameter λ. The robust convergence of the stress obtained by a post-processing and a filtering is shown in Section 6.6. Then we present the extension of our α-dependent three-field formulation of linear elasticity to the geometrically nonlinear elastic case with Saint-Venant Kirchhoff law in Section 6.7. In Section 6.8, starting from a suitable three-field formulation, we derive a three-field formulation for general hyperelasticity. Finally, numerical results are presented in Section 6.9.

We start with an introduction of the boundary value problem of linear elasticity. We consider a homogeneous isotropic linear elastic material body occupying a bounded domain Ω in $\mathbb{R}^d$, $d = \{2, 3\}$ with Lipschitz boundary Γ. For a prescribed body force $\boldsymbol{f} \in L^2(\Omega)^d$, the governing equilibrium equation in Ω reads

$$-\operatorname{div} \boldsymbol{\sigma} = \boldsymbol{f}, \tag{6.1.1}$$

where $\boldsymbol{\sigma}$ is the symmetric Cauchy stress tensor. The infinitesimal strain tensor $\boldsymbol{d}$ is defined as a function of the displacement $\boldsymbol{u}$ by

$$\boldsymbol{d} = \boldsymbol{\varepsilon}(\boldsymbol{u}) := \tfrac{1}{2}(\nabla \boldsymbol{u} + [\nabla \boldsymbol{u}]^t). \tag{6.1.2}$$

The displacement is assumed to satisfy the homogeneous Dirichlet boundary condition

$$\boldsymbol{u} = \boldsymbol{0} \quad \text{on} \quad \Gamma. \tag{6.1.3}$$

With the fourth-order elasticity tensor denoted by $\mathcal{C}$, the Saint-Venant Kirchhoff constitutive law reads

$$\boldsymbol{\sigma} = \mathcal{C}\boldsymbol{d} := \lambda(\operatorname{tr} \boldsymbol{d})\mathbf{1} + 2\mu\, \boldsymbol{d}. \tag{6.1.4}$$

Here, $\mathbf{1}$ is the identity tensor, and λ and μ are Lamé parameters, which are constant in view of the assumption of a homogeneous body, and which are assumed positive. Of particular interest is the incompressible limit, which corresponds to $\lambda \to \infty$.

The inverse $\mathcal{C}^{-1}$ of $\mathcal{C}$ is given by

$$\boldsymbol{d} = \mathcal{C}^{-1}\boldsymbol{\sigma} = \frac{1}{2\mu}\left(\boldsymbol{\sigma} - \frac{\gamma}{2 + d\,\gamma}(\operatorname{tr}\boldsymbol{\sigma})\mathbf{1}\right), \quad \gamma := \frac{\lambda}{\mu}.$$

As usual, the scalar product of two vectors $\boldsymbol{u}$ and $\boldsymbol{v}$ will be denoted by $\boldsymbol{u}\cdot\boldsymbol{v}$, whereas $\boldsymbol{\sigma} : \boldsymbol{\tau}$ will denote the scalar product of two tensors $\boldsymbol{\sigma}$ and $\boldsymbol{\tau}$.

Standard weak formulation. To write the weak or variational formulations of the boundary value problem of linear elasticity, we will use the vector-valued Sobolev space $\mathbf{V} := [H_0^1(\Omega)]^d$ with the standard inner product, and norm induced by this inner product. We will use the same notation for norms and inner product on $\mathbf{V}$ and $H^1(\Omega)$, however, the vector and tensor-valued functions will be denoted by bold symbols, and the components of the vector and tensor-valued functions will be denoted by indexed letters. For example, the letter d stands for the dimension of the domain, whereas the bold symbol $\boldsymbol{d}$ is used for the strain tensor, and its components are denoted by d_{ij}.

The space of stresses is denoted by $\boldsymbol{S}$, while the space of strains is denoted by $\boldsymbol{D}$, and both stress and strain are symmetric. For the continuous case these spaces are equal, and $\boldsymbol{D} := \{\boldsymbol{e} \mid e_{ji} = e_{ij},\ e_{ij} \in L^2(\Omega),\ 1 \le i, j \le d\} =: \boldsymbol{S}$, with the norm $\|\cdot\|_{0,\Omega}$ generated in the standard way by the L^2-norm. We also introduce the space $\boldsymbol{S}_0$ defined by

$$\boldsymbol{S}_0 := \{\boldsymbol{\tau} \in \boldsymbol{S} \mid (\boldsymbol{\tau}, \mathbf{1})_{0,\Omega} = 0\};$$

this is a closed subspace of $\boldsymbol{S}$. We define the bilinear form $A(\cdot,\cdot)$ and the linear functional $\ell(\cdot)$ by

$$\begin{array}{lll} A : \mathbf{V}\times\mathbf{V} \to \mathbb{R}, & A(\boldsymbol{u},\boldsymbol{v}) & := \int_\Omega \mathcal{C}\boldsymbol{\varepsilon}(\boldsymbol{u}) : \boldsymbol{\varepsilon}(\boldsymbol{v})\, dx, \\ \ell : \mathbf{V} \to \mathbb{R}, & \ell(\boldsymbol{v}) & := \int_\Omega \boldsymbol{f}\cdot\boldsymbol{v}\, dx. \end{array}$$

Then, the standard weak form of linear elasticity problem is as follows: given $\ell \in \mathbf{V}'$, find $\boldsymbol{u} \in \mathbf{V}$ that satisfies

$$A(\boldsymbol{u},\boldsymbol{v}) = \ell(\boldsymbol{v}), \quad \boldsymbol{v} \in \mathbf{V}. \tag{6.1.5}$$

The assumptions on $\mathcal{C}$ guarantee that $A(\cdot,\cdot)$ is symmetric, continuous, and $\mathbf{V}$-elliptic. Hence by using the standard arguments it can be shown that (6.1.5) has a unique solution $\boldsymbol{u} \in \mathbf{V}$. Furthermore, we assume that the domain Ω is convex and smooth enough so that $\boldsymbol{u} \in [H^2(\Omega)]^d \cap \mathbf{V}$, and there exists a constant C, independent of λ, such that

$$\|\boldsymbol{u}\|_{2,\Omega} + \lambda\|\operatorname{div}\boldsymbol{u}\|_{1,\Omega} \le C\,\|\boldsymbol{f}\|_{0,\Omega}. \tag{6.1.6}$$

The a priori estimate (6.1.6) has been proved in [**51**] for the two-dimensional linear elasticity problem posed in a convex domain with a polygonal boundary, see also [**154**].

6.2. The standard and modified Hu-Washizu formulations of linear elasticity

As pointed out in the introduction of this chapter, the linear elasticity problem can be recast into different mixed formulations. The easiest mixed formulation is given by introducing the pressure as an extra variable, which leads to a penalized Stokes system. Defining $p := \lambda \operatorname{div}\boldsymbol{u}$, a mixed variational formulation of linear elastic problem (6.1.5) is given by: find $(\boldsymbol{u}, p) \in \mathbf{V}\times L_0^2(\Omega) := \{q \in L^2(\Omega) | \int_\Omega q\, dx = 0\}$ such that

$$\begin{array}{lllllll} 2\mu\int_\Omega \boldsymbol{\varepsilon}(\boldsymbol{u}) : \boldsymbol{\varepsilon}(\boldsymbol{v})\, dx & + & \int_\Omega p\, \operatorname{div}\boldsymbol{v}\, dx & = & \ell(\boldsymbol{v}), & \boldsymbol{v} & \in \mathbf{V}, \\ \int_\Omega \operatorname{div}\boldsymbol{u}\, q\, dx & - & \frac{1}{\lambda}\int_\Omega p\, q\, dx & = & 0, & q & \in L_0^2(\Omega). \end{array}$$

If one discretizes the displacement with bilinear or trilinear finite elements and the pressure with piecewise constant functions, one arrives at the so-called $\mathrm{Q}_1\mathrm{P}_0$ formulation. We will see that this mixed formulation can also be derived from a suitable three-field formulation. Therefore, we focus on the three-field Hu-Washizu formulation, in which the displacement, strain, and stress are unknown variables. We consider both standard and modified formulations.

The standard Hu-Washizu formulation is obtained by considering the constitutive equation, the strain-displacement equation and the equation of equilibrium in a weak form. This corresponds to the weak problem of finding $(\boldsymbol{u}, \boldsymbol{d}, \boldsymbol{\sigma}) \in \mathbf{V} \times \boldsymbol{D} \times \boldsymbol{S}_0$ that satisfy

$$
\begin{array}{rcll}
\int_\Omega (\mathcal{C}\boldsymbol{d} - \boldsymbol{\sigma}) : \boldsymbol{e}\; dx &=& 0, & \boldsymbol{e} \in \boldsymbol{D}, \\
\int_\Omega (\boldsymbol{\varepsilon}(\boldsymbol{u}) - \boldsymbol{d}) : \boldsymbol{\tau}\; dx &=& 0, & \boldsymbol{\tau} \in \boldsymbol{S}_0, \\
\int_\Omega \boldsymbol{\sigma} : \boldsymbol{\varepsilon}(\boldsymbol{v})\; dx &=& \ell(\boldsymbol{v}), & \boldsymbol{v} \in \mathbf{V},
\end{array}
\tag{6.2.1}
$$

which can be recast into an equivalent saddle point form: find $(\boldsymbol{u}, \boldsymbol{d}, \boldsymbol{\sigma}) \in \mathbf{V} \times \boldsymbol{D} \times \boldsymbol{S}_0$ that satisfy

$$
\begin{array}{rcll}
a_\gamma((\boldsymbol{u}, \boldsymbol{d}), (\boldsymbol{v}, \boldsymbol{e})) + b_\gamma((\boldsymbol{v}, \boldsymbol{e}), \boldsymbol{\sigma}) &=& \ell(\boldsymbol{v}), & (\boldsymbol{v}, \boldsymbol{e}) \in \mathbf{V} \times \boldsymbol{D}, \\
b_\gamma((\boldsymbol{u}, \boldsymbol{d}), \boldsymbol{\tau}) &=& 0, & \boldsymbol{\tau} \in \boldsymbol{S}_0,
\end{array}
\tag{6.2.2}
$$

where

$$
\begin{array}{rcl}
a_\gamma((\boldsymbol{u}, \boldsymbol{d}), (\boldsymbol{v}, \boldsymbol{e})) &:=& (\mathcal{C}\boldsymbol{d}, \boldsymbol{e})_{0,\Omega}, \\
b_\gamma(\boldsymbol{v}, \boldsymbol{e}, \boldsymbol{\tau}) &:=& (\boldsymbol{\varepsilon}(\boldsymbol{v}) - \boldsymbol{e}, \boldsymbol{\tau})_{0,\Omega}.
\end{array}
\tag{6.2.3}
$$

By using the Babuška-Brezzi theory [**52, 80**], it is easy to show that there exists a unique solution. However in this case, the continuity constant of the bilinear form $a_\gamma(\cdot,\cdot)$ tends to infinity as λ does. Thus, our analysis is not directly based on the standard Hu-Washizu formulation. Therefore, we will consider a modification of Hu-Washizu formulation depending on a parameter $\alpha \in \mathbb{R}$: find $(\boldsymbol{u}, \boldsymbol{d}, \boldsymbol{\sigma}) \in \mathbf{V} \times \boldsymbol{D} \times \boldsymbol{S}_0$ such that

$$
\begin{array}{rcrcrcl}
a_\alpha((\boldsymbol{u}, \boldsymbol{d}), (\boldsymbol{v}, \boldsymbol{e})) &+& b_\alpha((\boldsymbol{v}, \boldsymbol{e}), \boldsymbol{\sigma}) &=& \ell(\boldsymbol{v}), & (\boldsymbol{v}, \boldsymbol{e}) \in \mathbf{V} \times \boldsymbol{D}, \\
b_\alpha((\boldsymbol{u}, \boldsymbol{d}), \boldsymbol{\tau}) &-& \tfrac{(\lambda - \alpha\mu)}{\kappa^2}\, c(\boldsymbol{\sigma}, \boldsymbol{\tau}) &=& 0, & \boldsymbol{\tau} \in \boldsymbol{S}_0,
\end{array}
\tag{6.2.4}
$$

where the bilinear forms are defined by

$$
\begin{array}{rcl}
a_\alpha((\boldsymbol{u}, \boldsymbol{d}), (\boldsymbol{v}, \boldsymbol{e})) &:=& 2\mu(\boldsymbol{d}, \boldsymbol{e})_{0,\Omega} + \alpha\mu(\operatorname{tr}\boldsymbol{d}, \operatorname{tr}\boldsymbol{e})_{0,\Omega}, \\
b_\alpha((\boldsymbol{v}, \boldsymbol{e}), \boldsymbol{\sigma}) &:=& (\boldsymbol{\varepsilon}(\boldsymbol{v}) - 2\mu\, \mathcal{C}^{-1}\boldsymbol{e}, \boldsymbol{\sigma})_{0,\Omega} - \tfrac{\alpha\mu}{\kappa}(\operatorname{tr}\boldsymbol{\sigma}, \operatorname{tr}\boldsymbol{e})_{0,\Omega}, \\
c(\boldsymbol{\sigma}, \boldsymbol{\tau}) &:=& (\operatorname{tr}\boldsymbol{\sigma}, \operatorname{tr}\boldsymbol{\tau})_{0,\Omega},
\end{array}
$$

and κ is defined as $\kappa := 2\mu + d\,\lambda$. The standard Hu-Washizu formulation is given by $\alpha = \gamma$.

The spherical part of the stresses is crucial for the analysis in the incompressible limit, see also [**41**]. Therefore, in the following, we will make frequent use of the L^2-orthogonal decomposition of $\boldsymbol{S}$ into its deviatoric and spherical parts. We define the L^2-orthogonal projections sph and dev on $\boldsymbol{S}$ by $\operatorname{sph}\boldsymbol{\tau} := (1/d)\,(\operatorname{tr}\boldsymbol{\tau})\mathbf{1}$, and $\operatorname{dev}\boldsymbol{\tau} := \boldsymbol{\tau} - \operatorname{sph}\boldsymbol{\tau}$. We note that $\operatorname{dev}\boldsymbol{S}$ is a proper subset of $\boldsymbol{S}_0$.

Lemma 6.1. *For $\alpha \neq -1$, there exists a unique solution $(\boldsymbol{u}, \boldsymbol{d}, \boldsymbol{\sigma}) \in \mathbf{V} \times \boldsymbol{D} \times \boldsymbol{S}_0$ of the modified Hu-Washizu formulation (6.2.4). Moreover, the solution does not depend on α and satisfies the bound*

$$
\|\boldsymbol{u}\|_{1,\Omega} + \|\boldsymbol{d}\|_{0,\Omega} + \|\boldsymbol{\sigma}\|_{0,\Omega} \leq C\|\ell\|_{\mathbf{V}'},
$$

in which the constant C is independent of λ.

PROOF. In a first step, we show that the solution of (6.2.4) does not depend on α. The first equation in (6.2.4) with $\boldsymbol{v} = 0$ yields

$$0 = \left(\mathcal{C}\boldsymbol{d} - \boldsymbol{\sigma}, \boldsymbol{e} + \frac{\alpha\mu - \lambda}{\kappa} (\operatorname{tr} \boldsymbol{e})\, \mathbf{1} \right)_{0,\Omega} =: (\mathcal{C}\boldsymbol{d} - \boldsymbol{\sigma}, \mathcal{B}_\alpha \boldsymbol{e})_{0,\Omega}, \quad \boldsymbol{e} \in \boldsymbol{D}. \tag{6.2.5}$$

The inverse of $\mathcal{B}_\alpha$ exists for $\alpha \neq -1$ and satisfies $\mathcal{B}_\alpha^{-1}\boldsymbol{e} = \boldsymbol{e} - \frac{\alpha\mu - \lambda}{2\mu(1+\alpha)} (\operatorname{tr} \boldsymbol{e})\, \mathbf{1}$. As a consequence, we find $\boldsymbol{\sigma} = \mathcal{C}\boldsymbol{d}$, and thus $\operatorname{tr} \boldsymbol{\sigma} = \kappa \operatorname{tr} \boldsymbol{d}$. The bilinear forms $a_\alpha(\cdot,\cdot)$ and $b_\alpha(\cdot,\cdot)$ can be equivalently written as

$$\begin{aligned} a_\alpha((\boldsymbol{w},\boldsymbol{g}),(\boldsymbol{v},\boldsymbol{e})) &= a_\gamma((\boldsymbol{w},\boldsymbol{g}),(\boldsymbol{v},\boldsymbol{e})) + (\alpha\mu - \lambda) c(\boldsymbol{g},\boldsymbol{e}), \\ b_\alpha((\boldsymbol{v},\boldsymbol{e}),\boldsymbol{\tau}) &= b_\gamma((\boldsymbol{v},\boldsymbol{e}),\boldsymbol{\tau}) - \tfrac{\alpha\mu - \lambda}{\kappa} c(\boldsymbol{\tau},\boldsymbol{e}). \end{aligned} \tag{6.2.6}$$

Using $\kappa c(\boldsymbol{d},\boldsymbol{e}) = c(\boldsymbol{\sigma},\boldsymbol{e})$ and (6.2.6), it is trivial to see that the solution does not depend on α.

The proof of uniform stability is carried out by showing that the bilinear forms for $\alpha = 0$ satisfy the conditions for well-posedness for the extended case in which $c(\cdot,\cdot) \neq 0$ (see [**52**, Section II.1.2] and [**38**]). First, we note that $c(\cdot,\cdot)$ is symmetric and positive semi-definite, and that $\ker B^t := \{\boldsymbol{\tau} \in \boldsymbol{S}_0 \mid b_0((\boldsymbol{v},\boldsymbol{e}),\boldsymbol{\tau}) = 0, \quad (\boldsymbol{v},\boldsymbol{e}) \in \mathbf{V} \times \boldsymbol{D}\} = \{0\}$, so that $c(\cdot,\cdot)$ plays no further role in determining the well-posedness of the problem.

Next, it is easy to see that all bilinear forms for $\alpha = 0$ are continuous, and that the continuity constants do not depend on λ. It remains therefore to verify that the coercivity and inf-sup conditions are satisfied. We establish the coercivity of the bilinear form $a_0(\cdot,\cdot)$ on the kernel Z of $b_0(\cdot,\cdot)$, which is given by

$$\begin{aligned} Z &= \{(\boldsymbol{v},\boldsymbol{e}) \in \mathbf{V} \times \boldsymbol{D} \mid b_0((\boldsymbol{v},\boldsymbol{e}),\boldsymbol{\tau}) = 0,\ \boldsymbol{\tau} \in \boldsymbol{S}_0\} \\ &= \{(\boldsymbol{v},\boldsymbol{e})\ \in \mathbf{V} \times \boldsymbol{D} \mid \boldsymbol{\varepsilon}(\boldsymbol{v}) - 2\mu\, \mathcal{C}^{-1}\boldsymbol{e} \in \boldsymbol{S}_0^\perp\}. \end{aligned}$$

Let $(\boldsymbol{v},\boldsymbol{e})$ be in Z; using Korn's inequality and the uniform continuity of $\mathcal{C}^{-1}$, and noting that $(\boldsymbol{\varepsilon}(\boldsymbol{v}), \mathbf{1})_{0,\Omega} = 0$, we find

$$a_0((\boldsymbol{v},\boldsymbol{e}),(\boldsymbol{v},\boldsymbol{e})) = 2\mu \|\boldsymbol{e}\|_{0,\Omega}^2 \geq c(\|\boldsymbol{e}\|_{0,\Omega}^2 + \|\boldsymbol{\varepsilon}(\boldsymbol{v})\|_{0,\Omega}^2) \geq c(\|\boldsymbol{e}\|_{0,\Omega}^2 + \|\boldsymbol{v}\|_{1,\Omega}^2).$$

We note that the coercivity constant depends on μ but not on λ.

Next, to establish the inf-sup condition we note that there exists a constant $C < \infty$ such that for each $q \in L_0^2(\Omega)$, there exists $\boldsymbol{v}_q \in \mathbf{V}$ satisfying

$$\operatorname{div} \boldsymbol{v}_q = q, \quad \|\boldsymbol{v}_q\|_{1,\Omega} \leq C \|q\|_{0,\Omega}, \tag{6.2.7}$$

(see, for example, [**80, 79**]). For $\boldsymbol{\tau} \in \boldsymbol{S}_0$, we have $\operatorname{tr} \boldsymbol{\tau} \in L_0^2(\Omega)$, and we define $\boldsymbol{e}_{\boldsymbol{\tau}} := \operatorname{dev}(\boldsymbol{\varepsilon}(\boldsymbol{v}_{\operatorname{tr}\boldsymbol{\tau}}) - \boldsymbol{\tau}) \in \boldsymbol{D}$. Then, using (6.2.7), the norm of $(\boldsymbol{v}_{\operatorname{tr}\boldsymbol{\tau}}, \boldsymbol{e}_{\boldsymbol{\tau}})$ is bounded by

$$\|\boldsymbol{v}_{\operatorname{tr}\boldsymbol{\tau}}\|_{1,\Omega}^2 + \|\boldsymbol{e}_{\boldsymbol{\tau}}\|_{0,\Omega}^2 \leq C(\|\operatorname{tr}\boldsymbol{\tau}\|_{0,\Omega}^2 + \|\operatorname{dev}\boldsymbol{\tau}\|_{0,\Omega}^2) \leq C\|\boldsymbol{\tau}\|_{0,\Omega}^2.$$

The inf-sup condition now results from the orthogonality of the decomposition of $\boldsymbol{\tau}$ into its spherical and deviatoric parts; using also (6.2.7), we find that

$$\begin{aligned} b_0((\boldsymbol{v}_{\operatorname{tr}\boldsymbol{\tau}}, \boldsymbol{e}_{\boldsymbol{\tau}}), \boldsymbol{\tau}) &= (\operatorname{sph} \boldsymbol{\varepsilon}(\boldsymbol{v}_{\operatorname{tr}\boldsymbol{\tau}}), \operatorname{sph}\boldsymbol{\tau})_{0,\Omega} + (\operatorname{dev}\boldsymbol{\tau}, \operatorname{dev}\boldsymbol{\tau})_{0,\Omega} \\ &= (1/d)(\operatorname{div} \boldsymbol{v}_{\operatorname{tr}\boldsymbol{\tau}}, \operatorname{tr}\boldsymbol{\tau})_{0,\Omega} + (\operatorname{dev}\boldsymbol{\tau}, \operatorname{dev}\boldsymbol{\tau})_{0,\Omega} \\ &= (1/d)\|\operatorname{tr}\boldsymbol{\tau}\|_{0,\Omega}^2 + \|\operatorname{dev}\boldsymbol{\tau}\|_{0,\Omega}^2 = \|\boldsymbol{\tau}\|_{0,\Omega}^2. \end{aligned}$$

□

REMARK 6.2. *The result of Lemma 6.1 can be generalized to the case $\alpha = -1$ for which the operator $\mathcal{B}_\alpha$ is singular. The kernel of $\mathcal{B}_\alpha$ is then given by $\{\boldsymbol{e} \in \boldsymbol{D} \mid \operatorname{dev} \boldsymbol{e} = 0\}$. To obtain a unique solution of (6.2.4), we therefore have to seek a solution in the subspace $\{(\boldsymbol{v}, \boldsymbol{e}, \boldsymbol{\tau}) \in \mathbf{V} \times \boldsymbol{D} \times \boldsymbol{S}_0 \mid tr\,\boldsymbol{\tau} = \kappa tr\,\boldsymbol{e}\}$.*

6.3. Finite element formulations

Let $\mathcal{T}_h$ be a quasi-uniform, shape-regular quadrilateral or hexahedral triangulation of the polygonal or polyhedral domain Ω. The diameter of an element K in $\mathcal{T}_h$ is denoted by h_K. Finite element spaces are defined by maps from a reference square $\hat{K} = (-1, 1)^d$. As before, for a non-negative integer k, the space of polynomials in d variables of total degree less than or equal to k is denoted by $\mathcal{P}_k(\cdot)$ and $\mathcal{Q}_k(\cdot)$ denotes the space of polynomials in d variables of total degree less than or equal to k in each variable. A typical element $K \in \mathcal{T}_h$ is generated by an isoparametric map F_K from the reference element $\hat{K}$. We recall that if $\hat{v} \in \mathcal{Q}_1(\hat{K})$, then $\hat{v} \circ F_K^{-1}$ is in general not a polynomial on the quadrilateral or hexahedron K. However, for the simplicity of exposition, we restrict our analysis to the case of meshes for which F_K is an affine mapping for each element $K \in \mathcal{T}_h$. Numerical results will also be given for the more general case of meshes of arbitrary quadrilaterals and hexahedra. The finite element space for the displacement is taken to be the space of continuous functions whose restrictions to an element K are obtained by maps of bilinear or trilinear functions from the reference element; that is,

$$\mathbf{V}_h := \left\{ \boldsymbol{v}_h \in \mathbf{V},\ \boldsymbol{v}_h|_K = \hat{\boldsymbol{v}}_h \circ F_K^{-1}, \hat{\boldsymbol{v}}_h \in \mathcal{Q}_1(\hat{K})^d \text{ for all } K \in \mathcal{T}_h \right\}.$$

The spaces of stresses and strains are discretized by defining the finite-dimensional spaces

$$\begin{aligned} \boldsymbol{S}_h : &= \left\{ \boldsymbol{\tau}_h \in \boldsymbol{S}_0 \mid (\boldsymbol{\tau}_h|_K)_{ij} = (\hat{\boldsymbol{\tau}}_h)_{ij} \circ F_K^{-1},\ \ \hat{\boldsymbol{\tau}}_h \in \boldsymbol{S}_\square \text{ for all } K \in \mathcal{T}_h \right\}, \\ \boldsymbol{D}_h : &= \left\{ \boldsymbol{e}_h \in \boldsymbol{S}_0 \mid (\boldsymbol{e}_h|_K)_{ij} = (\hat{\boldsymbol{e}}_h)_{ij} \circ F_K^{-1},\ \ \hat{\boldsymbol{e}}_h \in \boldsymbol{D}_\square \text{ for all } K \in \mathcal{T}_h \right\}, \end{aligned}$$

where $\boldsymbol{D}_\square$ and $\boldsymbol{S}_\square$ are the reference bases of strains and stresses, defined on $\hat{K}$. These two variables are defined locally on each element and no continuity conditions apply at the element boundaries. Moreover, we define the space R_h by

$$R_h := \operatorname{tr} \boldsymbol{S}_h.$$

We recall the Voigt representation of the tensorial quantities stress and strain in vectorial form in two and three dimensions

$$\begin{aligned} \boldsymbol{\sigma} &= [\sigma_{11}, \sigma_{22}, \sigma_{13}]^T, \quad \boldsymbol{d} = [d_{11}, d_{22}, 2d_{13}]^T \quad \text{for } d = 2, \text{ and} \\ \boldsymbol{\sigma} &= [\sigma_{11}, \sigma_{22}, \sigma_{33}, \sigma_{12}, \sigma_{23}, \sigma_{13}]^T, \quad \boldsymbol{d} = [d_{11}, d_{22}, d_{33}, 2d_{12}, 2d_{23}, 2d_{13}]^T \quad \text{for } d = 3, \end{aligned}$$

so that, in vectorial form, $\boldsymbol{\sigma}^T\boldsymbol{d} = \sum_{i,j}\sigma_{ij}d_{ij}$. The spaces $\boldsymbol{S}_h$ and $\boldsymbol{D}_h$ will be generated from bases defined on $\hat{K}$, and we will make use of the following bases on $\hat{K}$:

$$A_2 := \operatorname{span}\begin{bmatrix}\hat{y} & 0\\ 0 & \hat{x}\\ 0 & 0\end{bmatrix},\ A_3 := \operatorname{span}\begin{bmatrix}\hat{y} & \hat{z} & \hat{y}\hat{z} & 0 & 0 & 0 & 0 & 0 & 0 & 0 & 0 & 0\\ 0 & 0 & 0 & \hat{x} & \hat{z} & \hat{x}\hat{z} & 0 & 0 & 0 & 0 & 0 & 0\\ 0 & 0 & 0 & 0 & 0 & 0 & \hat{x} & \hat{y} & \hat{x}\hat{y} & 0 & 0 & 0\\ 0 & 0 & 0 & 0 & 0 & 0 & 0 & 0 & 0 & \hat{z} & 0 & 0\\ 0 & 0 & 0 & 0 & 0 & 0 & 0 & 0 & 0 & 0 & \hat{x} & 0\\ 0 & 0 & 0 & 0 & 0 & 0 & 0 & 0 & 0 & 0 & 0 & \hat{y}\end{bmatrix},$$

$$B_2 := \operatorname{span}\begin{bmatrix}\hat{x} & 0\\ 0 & \hat{y}\\ 0 & 0\end{bmatrix},\ B_3 := \operatorname{span}\begin{bmatrix}\hat{x} & \hat{x}\hat{y} & \hat{x}\hat{z} & 0 & 0 & 0 & 0 & 0 & 0\\ 0 & 0 & 0 & \hat{y} & \hat{y}\hat{z} & \hat{x}\hat{y} & 0 & 0 & 0\\ 0 & 0 & 0 & 0 & 0 & 0 & \hat{z} & \hat{y}\hat{z} & \hat{x}\hat{z}\\ 0 & 0 & 0 & 0 & 0 & 0 & 0 & 0 & 0\\ 0 & 0 & 0 & 0 & 0 & 0 & 0 & 0 & 0\\ 0 & 0 & 0 & 0 & 0 & 0 & 0 & 0 & 0\end{bmatrix},$$

$$C_2 := \operatorname{span}\begin{bmatrix}0 & 0\\ 0 & 0\\ \hat{x} & \hat{y}\end{bmatrix},\ C_3 := \operatorname{span}\begin{bmatrix}0 & 0 & 0 & 0 & 0 & 0 & 0 & 0 & 0\\ 0 & 0 & 0 & 0 & 0 & 0 & 0 & 0 & 0\\ 0 & 0 & 0 & 0 & 0 & 0 & 0 & 0 & 0\\ \hat{x} & \hat{y} & \hat{z} & 0 & 0 & 0 & 0 & 0 & 0\\ 0 & 0 & 0 & \hat{x} & \hat{y} & \hat{z} & 0 & 0 & 0\\ 0 & 0 & 0 & 0 & 0 & 0 & \hat{x} & \hat{y} & \hat{z}\end{bmatrix},$$

$$D_2 := \operatorname{span}\begin{bmatrix}0 & 0\\ 0 & 0\\ \hat{x} & \hat{y}\end{bmatrix},\ D_3 := \operatorname{span}\begin{bmatrix}0 & 0 & 0 & 0 & 0 & 0 & 0 & 0 & 0 & 0 & 0 & 0\\ 0 & 0 & 0 & 0 & 0 & 0 & 0 & 0 & 0 & 0 & 0 & 0\\ 0 & 0 & 0 & 0 & 0 & 0 & 0 & 0 & 0 & 0 & 0 & 0\\ \hat{x} & \hat{y} & \hat{y}\hat{z} & \hat{x}\hat{z} & 0 & 0 & 0 & 0 & 0 & 0 & 0 & 0\\ 0 & 0 & 0 & 0 & \hat{y} & \hat{z} & \hat{x}\hat{z} & \hat{x}\hat{y} & 0 & 0 & 0 & 0\\ 0 & 0 & 0 & 0 & 0 & 0 & 0 & 0 & \hat{z} & \hat{x} & \hat{x}\hat{y} & \hat{y}\hat{z}\end{bmatrix}. \tag{6.3.1}$$

Of special interest will be the following choices $(\boldsymbol{S}_h^i, \boldsymbol{D}_h^i)$, $1 \le i \le 5$:

TABLE 6.1. Different cases for the discrete spaces, $d = 2, 3$

Case	I	II	III	IV	V
$\boldsymbol{S}_\square$	$\mathfrak{I}_d + A_d$	$\mathfrak{I}_d + A_d$	$\mathfrak{I}_d + C_d$	$\mathfrak{I}_d + A_d + D_d$	$\mathfrak{I}_d + A_d + D_d$
$\boldsymbol{D}_\square$	$\mathfrak{I}_d + A_d$	$\mathfrak{I}_d + A_d + B_d$	$\mathfrak{I}_d + C_d$	$\mathfrak{I}_d + A_d + D_d$	$\mathfrak{I}_d + A_d + B_d + D_d$
	$\boldsymbol{S}_h^1 = \boldsymbol{D}_h^1$	$\boldsymbol{S}_h^2 \subset \boldsymbol{D}_h^2$	$\boldsymbol{S}_h^3 = \boldsymbol{D}_h^3$	$\boldsymbol{S}_h^4 = \boldsymbol{D}_h^4$	$\boldsymbol{S}_h^5 \subset \boldsymbol{D}_h^5$

Here, $\mathfrak{I}_d$ stands for the span of the identity matrix of size $\frac{d(d+1)}{2} \times \frac{d(d+1)}{2}$. We note that we have five different spaces of stresses and strains for the two and the three-dimensional case. Case II corresponds to the method of mixed enhanced strains [**97, 98**] while Case V corresponds to the method of enhanced assumed strains [**143**].

The discrete modified Hu-Washizu formulation is as follows: find $(\boldsymbol{u}_h^\alpha, \boldsymbol{d}_h^\alpha, \boldsymbol{\sigma}_h^\alpha) \in \mathbf{V}_h \times \boldsymbol{D}_h \times \boldsymbol{S}_h$ such that

$$\begin{array}{lcllll} a_\alpha((\boldsymbol{u}_h^\alpha, \boldsymbol{d}_h^\alpha), (\boldsymbol{v}_h, \boldsymbol{e}_h)) & + & b_\alpha((\boldsymbol{v}_h, \boldsymbol{e}_h), \boldsymbol{\sigma}_h^\alpha) & = & \ell(\boldsymbol{v}_h), & (\boldsymbol{v}_h, \boldsymbol{e}_h) \in \mathbf{V}_h \times \boldsymbol{D}_h,\\ b_\alpha((\boldsymbol{u}_h^\alpha, \boldsymbol{d}_h^\alpha), \boldsymbol{\tau}_h) & - & \frac{(\lambda-\alpha\mu)}{\kappa^2}\, c(\boldsymbol{\sigma}_h^\alpha, \boldsymbol{\tau}_h) & = & 0, & \boldsymbol{\tau}_h \in \boldsymbol{S}_h. \end{array} \tag{6.3.2}$$

In contrast to the continuous setting (6.2.4), the discrete solution can depend on α. However for simplicity of notation, we suppress from now on the additional index α in the solution and replace $(\boldsymbol{u}_h^\alpha, \boldsymbol{d}_h^\alpha, \boldsymbol{\sigma}_h^\alpha)$ by $(\boldsymbol{u}_h, \boldsymbol{d}_h, \boldsymbol{\sigma}_h)$. In the following, we assume that $\boldsymbol{S}_h \subset \boldsymbol{D}_h$.

LEMMA 6.3. *Under the assumption that* $\mathrm{tr}\,\boldsymbol{D}_h\mathbf{1} \subset \boldsymbol{D}_h$ *the solution of* (6.3.2) *does not depend on* $\alpha \neq -1$.

PROOF. Let $(\boldsymbol{u}_h, \boldsymbol{d}_h, \boldsymbol{\sigma}_h) \in \mathbf{V}_h \times \boldsymbol{D}_h \times \boldsymbol{S}_h$ be the solution of (6.3.2). Using (6.2.5) and $\mathrm{tr}\,\boldsymbol{D}_h\mathbf{1} \subset \boldsymbol{D}_h$, we find that $\mathcal{B}_\alpha \boldsymbol{e}_h$, $\mathcal{C}\boldsymbol{d}_h$, $\boldsymbol{\sigma}_h$ all belong to $\boldsymbol{D}_h$ and thus $\boldsymbol{\sigma}_h = \mathcal{C}\boldsymbol{d}_h$. The rest of the proof follows the same lines as in the continuous setting. □

We see that if $\mathrm{tr}\,\boldsymbol{D}_h\mathbf{1} \subset \boldsymbol{D}_h$ the solution does not depend on α. Therefore, we restrict ourselves to two types of discretization.

- Type 1: $\boldsymbol{S}_h \subset \boldsymbol{D}_h$ and $\mathrm{tr}\,\boldsymbol{D}_h\mathbf{1} \subset \boldsymbol{D}_h$.
- Type 2: $\boldsymbol{S}_h = \boldsymbol{D}_h$ and $\mathrm{tr}\,\boldsymbol{D}_h\mathbf{1} \not\subset \boldsymbol{D}_h$.

We note that if $\mathrm{tr}\,\boldsymbol{D}_h\mathbf{1} \not\subset \boldsymbol{D}_h$, the numerical solution depends on α, see also the numerical results. Here, Cases II, III and V in Table 6.1 correspond to the discretization of Type 1, and Cases I and IV correspond to that of Type 2. Furthermore, Case IV in combination with the classical Hu-Washizu formulation ($\alpha = \gamma$) leads to the standard Q_1-approach. We recall a result concerning the equivalence between the Hu-Washizu and the Hellinger-Reissner formulation in the linear case. STOLARSKI AND BELYTSCHKO [**148**] have shown that, if the spaces of stresses and strains satisfy the inclusion

$$\boldsymbol{S}_h \subset \mathcal{C}\boldsymbol{D}_h$$

then the classical Hu-Washizu formulation is equivalent to the Hellinger-Reissner problem of finding $(\boldsymbol{u}_h, \boldsymbol{\sigma}_h) \in \mathbf{V}_h \times \boldsymbol{S}_h$ such that

$$\begin{array}{llcll} \int_\Omega \mathcal{C}^{-1}\boldsymbol{\sigma}_h : \boldsymbol{\tau}_h \, dx & - \int_\Omega \boldsymbol{\varepsilon}(\boldsymbol{u}_h) : \boldsymbol{\tau}_h \, dx & = & 0, & \boldsymbol{\tau}_h \in \boldsymbol{S}_h, \\ \int_\Omega \boldsymbol{\varepsilon}(\boldsymbol{v}_h) : \boldsymbol{\sigma}_h \, dx & & = & \ell(\boldsymbol{v}_h), & \boldsymbol{v}_h \in \mathbf{V}_h. \end{array} \tag{6.3.3}$$

Under the assumption $\mathrm{tr}\,\boldsymbol{D}_h\mathbf{1} \subset \boldsymbol{D}_h$, the modified Hu-Washizu formulation (6.3.2) can be shown to be equivalent to the Hellinger-Reissner formulation (6.3.3). The connection between the modified Hu-Washizu formulation (6.3.2), the Hellinger-Reissner, Mixed Enhanced Strain, Enhanced Assumed Strain and the classical $\mathrm{Q}_1\mathrm{P}_0$ formulation has been discussed in [**73**].

6.4. Analysis of the modified Hu-Washizu formulation

In this section, we turn to the task of establishing conditions under which the discrete saddle point problem (6.3.2) is uniformly stable in the limit case. For the inf-sup condition, we need some preliminary results. First we note that $\mathrm{dev}\,\boldsymbol{S}_h$ and $\mathrm{sph}\,\boldsymbol{S}_h$ are in general not subspaces of $\boldsymbol{S}_h$. This is remedied by introducing the discrete deviatoric operator $\mathrm{dev_h}$ defined by $\mathrm{dev_h}\,\boldsymbol{S}_h := P_{\boldsymbol{S}_h}\,\mathrm{dev}\,\boldsymbol{S}_h$, where $P_{\boldsymbol{S}_h}$ is the orthogonal projection onto $\boldsymbol{S}_h$, and by decomposing $\boldsymbol{S}_h$ according to

$$\boldsymbol{S}_h = \mathrm{dev_h}\,\boldsymbol{S}_h \oplus \mathrm{sph_h}\,\boldsymbol{S}_h. \tag{6.4.1}$$

Here the discrete spherical operator $\mathrm{sph_h}$ is defined in such a way that $\mathrm{sph_h}\,\boldsymbol{S}_h$ is the orthogonal complement of $\mathrm{dev_h}\,\boldsymbol{S}_h$. Next, we define $\widetilde{R}_h := \mathrm{tr}\,\mathrm{sph_h}\,\boldsymbol{S}_h$, and remark that $\dim R_h \geq \dim \widetilde{R}_h$, where $R_h = \mathrm{tr}\,\boldsymbol{S}_h$.

LEMMA 6.4. *The orthogonal complement* $\operatorname{sph_h} \boldsymbol{S}_h$ *can be written as*

$$\operatorname{sph_h} \boldsymbol{S}_h = \{\boldsymbol{\tau}_h \in \boldsymbol{S}_h \mid \boldsymbol{\tau}_h = \frac{1}{d}(tr\,\boldsymbol{\tau}_h)\mathbf{1}\} = \widetilde{R}_h\mathbf{1}.$$

PROOF. We start by establishing that the spaces $\operatorname{sph_h} \boldsymbol{S}_h$ and $\widetilde{R}_h\mathbf{1}$ are equal. Using the decomposition of $\operatorname{sph_h} \boldsymbol{\tau}_h$ into its deviatoric and spherical parts and the definition of $\operatorname{dev_h} \boldsymbol{S}_h$, we see that

$$0 = (\operatorname{sph_h} \boldsymbol{\tau}_h, P_{\boldsymbol{S}_h} \operatorname{dev} \operatorname{sph_h} \boldsymbol{\tau}_h)_{0,\Omega} = (\operatorname{sph_h} \boldsymbol{\tau}_h, \operatorname{dev} \operatorname{sph_h} \boldsymbol{\tau}_h)_{0,\Omega} = \| \operatorname{dev} \operatorname{sph_h} \boldsymbol{\tau}_h\|^2_{0,\Omega},$$

and thus $\operatorname{sph_h} \boldsymbol{\tau}_h = \frac{1}{d}\operatorname{tr} \operatorname{sph_h} \boldsymbol{\tau}_h\mathbf{1} \in \widetilde{R}_h\mathbf{1}$. Conversely, for $\widetilde{\boldsymbol{\tau}}_h \in \widetilde{R}_h\mathbf{1}$, there exists $\boldsymbol{\sigma}_h \in \boldsymbol{S}_h$ such that

$$\widetilde{\boldsymbol{\tau}}_h = \operatorname{tr}(\operatorname{sph_h} \boldsymbol{\sigma}_h)\mathbf{1} = d \operatorname{sph_h} \boldsymbol{\sigma}_h \in \operatorname{sph_h} \boldsymbol{S}_h.$$

Now, it is trivial to see that

$$\widetilde{R}_h\mathbf{1} = \widetilde{R}_h\mathbf{1} \cap \boldsymbol{S}_h \subset \{\boldsymbol{\tau}_h \in \boldsymbol{S}_h,\ \boldsymbol{\tau}_h = \frac{1}{d}\operatorname{tr} \boldsymbol{\tau}_h\mathbf{1}\}.$$

Using the definition of $\operatorname{dev_h} \boldsymbol{S}_h$, we can write any element $\hat{\boldsymbol{\tau}}_h \in \operatorname{dev_h} \boldsymbol{S}_h$ as $\hat{\boldsymbol{\tau}}_h = P_{\boldsymbol{S}_h} \operatorname{dev} \boldsymbol{\sigma}_h$, $\boldsymbol{\sigma}_h \in \boldsymbol{S}_h$. Let $\boldsymbol{\tau}_h = \frac{1}{d}\operatorname{tr} \boldsymbol{\tau}_h\mathbf{1} \in \boldsymbol{S}_h$; then we find that

$$(\boldsymbol{\tau}_h, \hat{\boldsymbol{\tau}}_h)_{0,\Omega} = (\boldsymbol{\tau}_h, P_{\boldsymbol{S}_h} \operatorname{dev} \boldsymbol{\sigma}_h)_{0,\Omega} = (\frac{1}{d}\operatorname{tr} \boldsymbol{\tau}_h\mathbf{1}, \operatorname{dev} \boldsymbol{\sigma}_h)_{0,\Omega} = 0, \quad \hat{\boldsymbol{\tau}}_h \in \operatorname{dev_h} \boldsymbol{S}_h,$$

yielding $\{\boldsymbol{\tau}_h \in \boldsymbol{S}_h \mid \boldsymbol{\tau}_h = \frac{1}{d}\operatorname{tr} \boldsymbol{\tau}_h\mathbf{1}\} \subset \operatorname{sph_h} \boldsymbol{S}_h$. □

As a result of Lemma 6.4, we find that not only the elements $\boldsymbol{\tau}_h \in \operatorname{sph_h} \boldsymbol{S}_h$ and $\hat{\boldsymbol{\tau}}_h \in \operatorname{dev_h} \boldsymbol{S}_h$ are orthogonal with respect to the L^2-inner product, but also their traces: that is,

$$d(\operatorname{tr} \boldsymbol{\tau}_h, \operatorname{tr} \hat{\boldsymbol{\tau}}_h)_{0,\Omega} = (\operatorname{tr} \boldsymbol{\tau}_h\mathbf{1}, \operatorname{tr} \hat{\boldsymbol{\tau}}_h\mathbf{1})_{0,\Omega} = d(\boldsymbol{\tau}_h, \hat{\boldsymbol{\tau}}_h)_{0,\Omega} = 0. \tag{6.4.2}$$

To get a better feeling for the discrete spherical and deviatoric parts, we consider Case I with $d = 2$ in more detail. We have

$$\operatorname{dev}(\mathcal{I}_2 + A_2) = \operatorname{span}\begin{bmatrix} 1 & 0 & \hat{x} & \hat{y} \\ -1 & 0 & -\hat{x} & -\hat{y} \\ 0 & 1 & 0 & 0 \end{bmatrix}, \quad \operatorname{sph}(\mathcal{I}_2 + A_2) = \operatorname{span}\begin{bmatrix} 1 & \hat{x} & \hat{y} \\ 1 & \hat{x} & \hat{y} \\ 0 & 0 & 0 \end{bmatrix},$$

and we find that $\dim(\mathcal{I}_2 + A_2) = 5$, $\dim \operatorname{dev}(\mathcal{I}_2 + A_2) = 4$, and $\dim \operatorname{sph}(\mathcal{I}_2 + A_2) = 3$. We point out that in general $\operatorname{sph_h} \boldsymbol{S}_h \neq P_{\boldsymbol{S}_h} \operatorname{sph} \boldsymbol{S}_h$; for example

$$\operatorname{dev_h}(\mathcal{I}_2 + A_2) = \operatorname{span}\begin{bmatrix} 1 & 0 & \hat{y} & 0 \\ -1 & 0 & 0 & \hat{x} \\ 0 & 1 & 0 & 0 \end{bmatrix}, \quad P_{\boldsymbol{S}_h} \operatorname{sph}(\mathcal{I}_2 + A_2) = \operatorname{span}\begin{bmatrix} 1 & \hat{y} & 0 \\ 1 & 0 & \hat{x} \\ 0 & 0 & 0 \end{bmatrix},$$

whereas $\operatorname{sph_h}(\mathcal{I}_2 + A_2) = [1, 1, 0]^T$. In the continuous setting, the definition of the deviatoric part yields that the trace of the deviatoric part is equal to zero. This is not the case for an element in $\operatorname{dev_h} \boldsymbol{S}_h$.

For $\boldsymbol{\tau} \in \boldsymbol{S}$, the norm of the trace is bounded by $\|\operatorname{tr} \boldsymbol{\tau}\|^2_{0,\Omega} \leq d\|\boldsymbol{\tau}\|^2_{0,\Omega}$. The following lemma shows that a stronger bound holds for the norm of the trace of an element in $\operatorname{dev_h} \boldsymbol{S}_h$.

LEMMA 6.5. *There exists a $\omega < 1$ such that*

$$\|tr\,\boldsymbol{\tau}_h\|_{0,\Omega}^2 \leq d\,\omega\|\boldsymbol{\tau}_h\|_{0,\Omega}^2, \quad \boldsymbol{\tau}_h \in \mathrm{dev_h}\,\boldsymbol{S}_h,$$

and thus $(\mathcal{C}^{-1}\boldsymbol{\tau}_h, \boldsymbol{\tau}_h)_{0,\Omega} \geq \frac{1-\omega}{2\mu}\|\boldsymbol{\tau}_h\|_{0,\Omega}^2$, $\boldsymbol{\tau}_h \in \mathrm{dev_h}\,\boldsymbol{S}_h$.

PROOF. The proof is based on a discrete norm equivalence on the reference element. To start, we define $\|\boldsymbol{\tau}\|_{*,\hat{K}} := \|\operatorname{dev}\boldsymbol{\tau}\|_{0,\hat{K}}$. It is trivial to see that $\|\cdot\|_*$ defines a semi-norm on $(L^2(\hat{K}))^{d\times d}$ and that it is zero if and only if $\operatorname{dev}\boldsymbol{\tau}$ is zero. Given $\boldsymbol{\tau}_h \in \mathrm{dev_h}\,\boldsymbol{S}_\square$ and $\operatorname{dev}\boldsymbol{\tau}_h = 0$, we find by means of (6.4.1) and Lemma 6.4 that $\boldsymbol{\tau}_h \in \mathrm{dev_h}\,\boldsymbol{S}_\square \cap \mathrm{sph_h}\,\boldsymbol{S}_\square = \{0\}$. Thus the semi-norm $\|\cdot\|_{*,K}$ restricted to $\mathrm{dev_h}\,\boldsymbol{S}_\square$ is a norm. The dimension of the space $\mathrm{dev_h}\,\boldsymbol{S}_\square$ is finite and thus $\|\cdot\|_{*,\hat{K}}$ is equivalent to $\|\cdot\|_{0,\hat{K}}$. Using the definition of $\boldsymbol{S}_h$ and the special structure of the isoparametric element map F_K, the equivalence of $\|\cdot\|_*^2 := \sum_{K\in\mathcal{T}_h}\|\cdot\|_{*,K}^2$ and $\|\cdot\|_{0,\Omega}^2$ on $\mathrm{dev_h}\,\boldsymbol{S}_h$ is established. Now let $0 < \beta < 1$ be such that $\|\boldsymbol{\tau}_h\|_*^2 \geq \beta\|\boldsymbol{\tau}_h\|_{0,\Omega}^2$, $\boldsymbol{\tau}_h \in \mathrm{dev_h}\,\boldsymbol{S}_h$; then a straightforward computation reveals that

$$d(1-\beta)\|\boldsymbol{\tau}_h\|_{0,\Omega}^2 \geq \|\operatorname{tr}\boldsymbol{\tau}_h\|_{0,\Omega}^2, \quad (\mathcal{C}^{-1}\boldsymbol{\tau}_h, \boldsymbol{\tau}_h)_{0,\Omega} \geq \frac{1}{2\mu}(\|\boldsymbol{\tau}_h\|_{0,\Omega}^2 - d\frac{\lambda}{\kappa}(1-\beta)\|\boldsymbol{\tau}_h\|_{0,\Omega}^2).$$

□

ASSUMPTION 8. *The following assumptions are essential for uniform stability in the discrete case:*

- 8(i) $\|P_{\boldsymbol{S}_h}\boldsymbol{\varepsilon}(\boldsymbol{v}_h)\|_{0,\Omega} \geq c\|\boldsymbol{\varepsilon}(\boldsymbol{v}_h)\|_{0,\Omega}$,
- 8(ii) $\max(-\frac{2c_l}{d}, \gamma(1-\frac{c_l}{\omega})) \leq \alpha \leq \min(c_u, \gamma)$, $0 < c_l < 1$, $0 < c_u < \infty$,
- 8(iii) $(\mathbf{V}_h, \widetilde{R}_h)$ *forms a stable Stokes pairing,*

where ω is the bound from Lemma 6.5.

In the following the generic constants depend on c_l and c_u. Therefore, care has to be exercised to choose these constants. It is easy to verify that $\alpha = 0$ or when $\mu \leq \lambda$, $\alpha = 1$ are possible choices that satisfy Assumption 8 (ii) with some suitable c_l and c_u. As we will see later, of special interest for Cases I and IV will be a negative value of α. However, the choice of a negative α can lead to the loss of coercivity.

Roughly speaking, Assumption 8 (i) says that $\boldsymbol{S}_h$ has to be large enough and Assumption 8 (iii), that $\boldsymbol{S}_h$ has to be small enough. We point out that Assumption 8 (iii) is weaker than the assumption that $(\mathbf{V}_h, R_h)$ forms a stable Stokes pairing. For example, in Case I we find that $\operatorname{tr}(\mathfrak{I}_2 + A_2) = P_1(\hat{K})$, whereas $\operatorname{tr}\mathrm{sph_h}(\mathfrak{I}_2 + A_2) = \mathrm{P}_0(\hat{K})$.

The discrete kernel associated with the bilinear form $b_\alpha(\cdot,\cdot)$ is given by

$$Z_h := \{(\boldsymbol{v}_h, \boldsymbol{e}_h) \in \mathbf{V}_h \times \boldsymbol{D}_h \mid P_{\boldsymbol{S}_h}\boldsymbol{\varepsilon}(\boldsymbol{v}_h) = P_{\boldsymbol{S}_h}(2\mu\,\mathcal{C}^{-1}\boldsymbol{e}_h + \frac{\alpha\mu}{\kappa}\operatorname{tr}\boldsymbol{e}_h\mathbf{1})\}.$$

LEMMA 6.6. *Under Assumptions 8 (i) and 8 (ii), the bilinear form $a_\alpha(\cdot,\cdot)$ is uniformly coercive on $Z_h \times Z_h$ and uniformly continuous on $(\mathbf{V}_h \times \boldsymbol{D}_h) \times (\mathbf{V}_h \times \boldsymbol{D}_h)$.*

PROOF. Let $(\boldsymbol{v}_h, \boldsymbol{e}_h) \in Z_h$. Assuming 8 (i) and 8 (ii), we find that

$$\begin{aligned}\|\boldsymbol{v}_h\|_{1,\Omega}^2 \leq C\|\boldsymbol{\varepsilon}(\boldsymbol{v}_h)\|_{0,\Omega}^2 &\leq C\|P_{\boldsymbol{S}_h}\boldsymbol{\varepsilon}(\boldsymbol{v}_h)\|_{0,\Omega}^2 = C\|P_{\boldsymbol{S}_h}(2\mu\,\mathcal{C}^{-1}\boldsymbol{e}_h + \frac{\alpha\mu}{\kappa}(\operatorname{tr}\boldsymbol{e}_h)\mathbf{1})\|_{0,\Omega}^2 \\ &\leq C\|\boldsymbol{e}_h\|_{0,\Omega}^2 \leq Ca_\alpha((\boldsymbol{v}_h,\boldsymbol{e}_h),(\boldsymbol{v}_h,\boldsymbol{e}_h)).\end{aligned}$$

□

LEMMA 6.7. *Under Assumptions 8 (ii) and 8 (iii), the bilinear form $b_\alpha(\cdot,\cdot)$ satisfies a uniform inf-sup condition.*

PROOF. The proof is based on the decomposition of $\boldsymbol{\tau}_h$ into its discrete deviatoric and spherical parts, that is,

$$\boldsymbol{\tau}_h = \operatorname{dev_h} \boldsymbol{\tau}_h + \operatorname{sph_h} \boldsymbol{\tau}_h = \operatorname{dev_h} \boldsymbol{\tau}_h + q_h \mathbf{1},$$

where $\operatorname{dev_h} \boldsymbol{\tau}_h \in \operatorname{dev_h} \boldsymbol{S}_h$, $\operatorname{sph_h} \boldsymbol{\tau}_h \in \operatorname{sph_h} \boldsymbol{S}_h$ and $q_h \in \widetilde{R}_h$. Under Assumption 8 (iii) we can find, for each $q_h \in \widetilde{R}_h$, a displacement $\boldsymbol{v}_{q_h} \in \mathbf{V}_h$ such that

$$(\operatorname{div} \boldsymbol{v}_{q_h}, q_h)_{0,\Omega} = \|q_h\|^2_{0,\Omega}, \quad \|\boldsymbol{v}_{q_h}\|_{1,\Omega} \le C\|q_h\|_{0,\Omega}. \tag{6.4.3}$$

Using the unique decomposition of $P_{\boldsymbol{S}_h}\boldsymbol{\varepsilon}(\boldsymbol{v}_{q_h})$ into its discrete spherical and deviatoric parts, so that $P_{\boldsymbol{S}_h}\boldsymbol{\varepsilon}(\boldsymbol{v}_{q_h}) = \operatorname{sph_h} P_{\boldsymbol{S}_h}\boldsymbol{\varepsilon}(\boldsymbol{v}_{q_h}) + \operatorname{dev_h} P_{\boldsymbol{S}_h}\boldsymbol{\varepsilon}(\boldsymbol{v}_{q_h})$, we define $\boldsymbol{e}_{\boldsymbol{\tau}_h} \in \boldsymbol{D}_h$ by

$$\boldsymbol{e}_{\boldsymbol{\tau}_h} := \operatorname{dev_h} P_{\boldsymbol{S}_h}\boldsymbol{\varepsilon}(\boldsymbol{v}_{q_h}) - \beta \operatorname{dev_h} \boldsymbol{\tau}_h, \quad \beta > 0.$$

By means of (6.4.3) and the fact that $\|\operatorname{dev_h} P_{\boldsymbol{S}_h}\boldsymbol{\varepsilon}(\boldsymbol{v}_{q_h})\|_{0,\Omega} \le \|\boldsymbol{\varepsilon}(\boldsymbol{v}_{q_h})\|_{0,\Omega} \le C\|\boldsymbol{v}_{q_h}\|_{1,\Omega}$, we can bound the norm of $(\boldsymbol{v}_{q_h}, \boldsymbol{e}_{\boldsymbol{\tau}_h})$ by

$$\|\boldsymbol{v}_{q_h}\|^2_{1,\Omega} + \|\boldsymbol{e}_{\boldsymbol{\tau}_h}\|^2_{0,\Omega} \le C(\|q_h\|^2_{0,\Omega} + \beta^2\|\operatorname{dev_h} \boldsymbol{\tau}_h\|^2_{0,\Omega}) \le C(1+\beta^2)\|\boldsymbol{\tau}_h\|^2_{0,\Omega}.$$

To obtain the inf-sup condition, we use the equivalence (6.2.6) and consider the two terms of $b_\alpha(\cdot,\cdot)$ separately. We start by obtaining a lower bound for $b_\gamma((\boldsymbol{v}_{q_h}, \boldsymbol{e}_{\boldsymbol{\tau}_h}), \boldsymbol{\tau}_h)$:

$$\begin{aligned} b_\gamma((\boldsymbol{v}_{q_h}, \boldsymbol{e}_{\boldsymbol{\tau}_h}), \boldsymbol{\tau}_h) &= (P_{\boldsymbol{S}_h}\boldsymbol{\varepsilon}(\boldsymbol{v}_{q_h}) - \boldsymbol{e}_{\boldsymbol{\tau}_h}, \boldsymbol{\tau}_h)_{0,\Omega} = (\operatorname{sph_h} P_{\boldsymbol{S}_h}\boldsymbol{\varepsilon}(\boldsymbol{v}_{q_h}) + \beta \operatorname{dev_h} \boldsymbol{\tau}_h, \boldsymbol{\tau}_h)_{0,\Omega} \\ &= (\operatorname{sph_h} P_{\boldsymbol{S}_h}\boldsymbol{\varepsilon}(\boldsymbol{v}_{q_h}), q_h\mathbf{1})_{0,\Omega} + \beta\|\operatorname{dev_h} \boldsymbol{\tau}_h\|^2_{0,\Omega} \\ &= (\boldsymbol{\varepsilon}(\boldsymbol{v}_{q_h}), q_h\mathbf{1})_{0,\Omega} + \beta\|\operatorname{dev_h} \boldsymbol{\tau}_h\|^2_{0,\Omega} \\ &= (\operatorname{div} \boldsymbol{v}_{q_h}, q_h)_{0,\Omega} + \beta\|\operatorname{dev_h} \boldsymbol{\tau}_h\|^2_{0,\Omega} = \|q_h\|^2_{0,\Omega} + \beta\|\operatorname{dev_h} \boldsymbol{\tau}_h\|^2_{0,\Omega}. \end{aligned}$$

Next, we bound $c(\boldsymbol{e}_{\boldsymbol{\tau}_h}, \boldsymbol{\tau}_h)$ by applying Lemma 6.5, (6.4.2) and (6.4.3):

$$\begin{aligned} c(\boldsymbol{e}_{\boldsymbol{\tau}_h}, \boldsymbol{\tau}_h) &= (\operatorname{tr} \boldsymbol{e}_{\boldsymbol{\tau}_h}, \operatorname{tr} \boldsymbol{\tau}_h)_{0,\Omega} = (\operatorname{tr}(\operatorname{dev_h} P_{\boldsymbol{S}_h}\boldsymbol{\varepsilon}(\boldsymbol{v}_{q_h})) - \beta \operatorname{tr} \operatorname{dev_h} \boldsymbol{\tau}_h, \operatorname{tr} \operatorname{dev_h} \boldsymbol{\tau}_h)_{0,\Omega} \\ &= (\operatorname{tr} P_{\boldsymbol{S}_h}\boldsymbol{\varepsilon}(\boldsymbol{v}_{q_h}), \operatorname{tr} \operatorname{dev_h} \boldsymbol{\tau}_h)_{0,\Omega} - \beta\|\operatorname{tr} \operatorname{dev_h} \boldsymbol{\tau}_h\|^2_{0,\Omega} \\ &\ge -C\|q_h\|_{0,\Omega}\|\operatorname{dev_h} \boldsymbol{\tau}_h\|_{0,\Omega} - d\,\beta\omega\|\operatorname{dev_h} \boldsymbol{\tau}_h\|^2_{0,\Omega}. \end{aligned}$$

Combining the lower bounds for $b_\gamma((\boldsymbol{v}_{q_h}, \boldsymbol{e}_{\boldsymbol{\tau}_h}), \boldsymbol{\tau}_h)$ and $c(\boldsymbol{e}_{\boldsymbol{\tau}_h}, \boldsymbol{\tau}_h)$ we find that

$$\begin{aligned} b_\alpha((\boldsymbol{v}_{q_h}, \boldsymbol{e}_{\boldsymbol{\tau}_h}), \boldsymbol{\tau}_h) &\ge \|q_h\|^2_{0,\Omega} + \beta\|\operatorname{dev_h} \boldsymbol{\tau}_h\|^2_{0,\Omega} - \\ &\quad \frac{\lambda - \alpha\mu}{\kappa}\left(C\|q_h\|_{0,\Omega}\|\operatorname{dev_h} \boldsymbol{\tau}_h\|_{0,\Omega} + d\,\beta\omega\|\operatorname{dev_h} \boldsymbol{\tau}_h\|^2_{0,\Omega}\right) \\ &\ge \|q_h\|^2_{0,\Omega} - \frac{\lambda - \alpha\mu}{\kappa}C\|q_h\|_{0,\Omega}\|\operatorname{dev_h} \boldsymbol{\tau}_h\|_{0,\Omega} + \\ &\quad \beta(1 - d\,\omega\frac{\lambda - \alpha\mu}{\kappa})\|\operatorname{dev_h} \boldsymbol{\tau}_h\|^2_{0,\Omega}. \end{aligned}$$

From Assumption 8 (ii), we have $\lambda - \alpha\mu \ge 0$, and $\omega(\lambda - \alpha\mu) \le \lambda c_l$. Therefore, using $\frac{d\,\omega(\lambda-\alpha\mu)}{\kappa} \le \frac{d\,\lambda}{\kappa}c_l \le c_l$, we find that

$$b_\alpha((\boldsymbol{v}_{q_h}, \boldsymbol{e}_{\boldsymbol{\tau}_h}), \boldsymbol{\tau}_h) \ge \|q_h\|^2_{0,\Omega} - 2C\|q_h\|_{0,\Omega}\|\operatorname{dev_h} \boldsymbol{\tau}_h\|_{0,\Omega} + \beta(1 - c_l)\|\operatorname{dev_h} \boldsymbol{\tau}_h\|^2_{0,\Omega}.$$

We can apply Young's inequality to find

$$b_\alpha((\boldsymbol{v}_{q_h}, \boldsymbol{e}_{\boldsymbol{\tau}_h}), \boldsymbol{\tau}_h) \ge (1 - C\epsilon)\|q_h\|^2_{0,\Omega} + (\beta(1 - c_l) - C\epsilon^{-1})\|\operatorname{dev_h} \boldsymbol{\tau}_h\|^2_{0,\Omega}.$$

For $0 < \epsilon$ small enough and $\beta < \infty$ large enough, we obtain $b_\alpha((\boldsymbol{v}_{q_h}, \boldsymbol{e}_{\boldsymbol{\tau}_h}), \boldsymbol{\tau}_h) \geq c(\|q_h\|^2_{0,\Omega} + \|\operatorname{dev}_{\mathrm{h}} \boldsymbol{\tau}_h\|^2_{0,\Omega}) \geq c\|\boldsymbol{\tau}_h\|^2_{0,\Omega}$. □

We now formulate our main result. The following theorem provides optimal a priori estimates for the displacement, strain and stress.

THEOREM 6.8. *Under Assumptions 8 (i)–8 (iii), the discretization error* $\eta_h^2 := \|\boldsymbol{u} - \boldsymbol{u}_h\|^2_{1,\Omega} + \|\boldsymbol{d} - \boldsymbol{d}_h\|^2_{0,\Omega} + \|\boldsymbol{\sigma} - \boldsymbol{\sigma}_h\|^2_{0,\Omega}$, *where* $(\boldsymbol{u}_h, \boldsymbol{d}_h, \boldsymbol{\sigma}_h)$ *is the solution of (6.3.2), is bounded by the best approximation error*

$$\eta_h^2 \leq C \left(\inf_{\boldsymbol{v}_h \in \mathbf{V}_h} \|\boldsymbol{u} - \boldsymbol{v}_h\|^2_{1,\Omega} + \inf_{\boldsymbol{e}_h \in \boldsymbol{D}_h} \|\boldsymbol{d} - \boldsymbol{e}_h\|^2_{0,\Omega} + \inf_{\boldsymbol{\tau}_h \in \boldsymbol{S}_h} \|\boldsymbol{\sigma} - \boldsymbol{\tau}_h\|^2_{0,\Omega} \right).$$

PROOF. The a priori estimate results from the continuity of the bilinear forms and Lemmas 6.1, 6.6 and 6.7; see, for example, [**52**]. In particular, it is seen that $\ker B_h^T = \{\mathbf{0}\}$, as in the continuous case, and $c(\cdot, \cdot)$ is uniformly continuous. These conditions suffice to establish the uniqueness of $\boldsymbol{\sigma}_h$ and the uniform error estimate (see [**52**, Section II] and [**38**]). □

Finally, we consider Assumption 8 (iii) in more detail. We recall that Assumption 8 (iii) is on $\widetilde{R}_h$, which must be such that it forms with $\mathbf{V}_h$ a stable Stokes pair. Now for all our five choices of pairings from Table 6.1, $(\boldsymbol{D}_h^i, \boldsymbol{S}_h^i)$, $1 \leq i \leq 5$, we find that $\widetilde{R}_h^i$ is given by

$$\widetilde{R}_h^i = \{q \in L_0^2(\Omega) \mid \ q|_K \in \mathrm{P}_0(K), \ K \in \mathfrak{T}_h\}, \quad 1 \leq i \leq 5.$$

Using bilinear or trilinear elements for the displacement, it is well known that the pairing $(\mathbf{V}_h, \widetilde{R}_h^i)$ does not satisfy the Assumption 8 (iii), and that one can observe some spurious modes for the elements in $\widetilde{R}_h^i$. Such spurious modes are well known to be checkerboard modes, see [**80**]. In the two-dimensional case, the restrictions of functions in $\widetilde{R}_h^i$ to a macro-element are shown in Figure 6.1, and the functions having signs indicated in Figure 6.1(d) are the local checkerboard modes. In contrast to the two-dimensional case, things are more complicated in the three-dimensional case, and many spurious modes can occur. Some of them are truly three-dimensional checkerboard modes and some of them are coming from an assembly of two-dimensional modes. For a more detailed discussion on this topic we refer to [**52**, page 244]. There are different ways to overcome this difficulty coming from

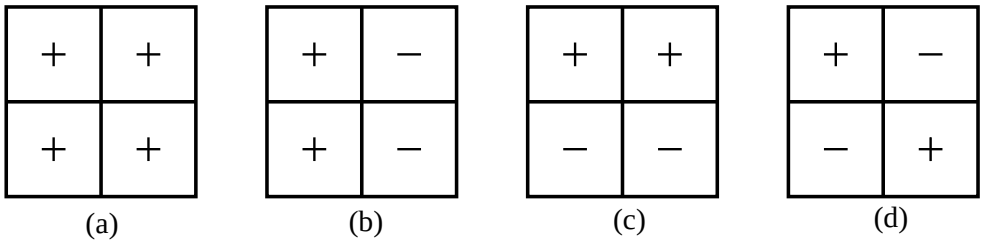

Figure 6.1: Restrictions of the basis functions of $\widetilde{R}_h^i$ to a macro-element with ± indicating the sign inside the elements

the spurious modes. Assume that $\widetilde{R}_h^u$ be the space spanned by all these spurious modes so that $\widetilde{R}_h = \widetilde{R}_h^u \oplus \widetilde{R}_h^s$. Then, the one way is to project each element of $\widetilde{R}_h$ onto $\widetilde{R}_h^s$, see

also [**53**]. However, in the following section, we demonstrate that if the primary variable of interest is the displacement, there is no effect of the spurious modes, and we obtain an optimal a priori estimate for the displacement.

6.5. An optimal and robust a priori estimate for the displacement

In this section, we provide an a priori estimate for the displacement. Since the stress and strain are defined element-wise and no continuity requirement is imposed on inter-element boundaries, they can be statically condensed out from the saddle point system (6.3.2) to obtain another system based only on the displacement

$$A_h(\boldsymbol{u}_h, \boldsymbol{v}_h) = \ell(\boldsymbol{v}_h), \qquad \boldsymbol{v}_h \in \mathbf{V}_h. \tag{6.5.1}$$

Here, we point out that with the orthogonal decomposition of the space $\widetilde{R}_h = \widetilde{R}_h^u \oplus \widetilde{R}_h^s$, we have a uniform inf-sup condition

$$\inf_{q_h \in \widetilde{R}_h^s} \sup_{\boldsymbol{v}_h \in \mathbf{V}_h^s} \frac{\int_\Omega \operatorname{div} \boldsymbol{v}_h q_h}{\|\boldsymbol{v}_h\|_{1,\Omega} \|q_h\|_{0,\Omega}} = \tilde{\beta}_h > 0$$

for $\mathbf{V}_h^s := \{\boldsymbol{v}_h \in \mathbf{V}_h : (\operatorname{div} \boldsymbol{v}_h, q_h)_{0,\Omega} = 0,\ q_h \in \widetilde{R}_h^u\}$. We assume that the triangulation has a macro-structure so that $\widetilde{R}_{2h} \subset \widetilde{R}_h$, then $\widetilde{R}_{2h} \subset \widetilde{R}_h^s$, where $\widetilde{R}_{2h} := \{q \in L_0^2(\Omega) |\ q_{|_K} \in \mathrm{P}_0(K),\ K \in \mathcal{T}_{2h}\}$. Hence the spaces $\mathbf{V}_h^s$ and $\widetilde{R}_h^s$ satisfy suitable approximation properties, [**80, 52**]. To get an optimal λ-independent estimate, we need the following assumption.

Assumption 9. $\operatorname{sph}_h \boldsymbol{S}_{h|_K} \subset \mathcal{I}_d \subset \boldsymbol{S}_{h|_K}$, $K \in \mathcal{T}_h$.

By construction all our cases satisfy $\mathcal{I}_d \subset \boldsymbol{S}_{h|_K}$ and $\operatorname{sph}_h \boldsymbol{S}_{h|_K} = \mathrm{P}_0(K)\mathbf{1} \subset \mathcal{I}_d$. Thus Assumption 9 is satisfied for all our cases.

To obtain the explicit expression for the discrete bilinear form $A_h(\boldsymbol{u}_h, \boldsymbol{v}_h)$, we decompose $\boldsymbol{S}_h$ orthogonally $\boldsymbol{S}_h = \boldsymbol{S}_h^c \oplus \boldsymbol{S}_h^t$ with $\boldsymbol{S}_h^c := \{\boldsymbol{\tau} \in \boldsymbol{S}_h \mid \mathcal{C}\boldsymbol{\tau} \in \boldsymbol{S}_h\}$. We note that $\boldsymbol{S}_h^t \subset \operatorname{dev}_h \boldsymbol{S}_h$, $\operatorname{sph}_h \boldsymbol{S}_h \subset \boldsymbol{S}_h^c$ and $\operatorname{tr}(\operatorname{sph}_h \boldsymbol{S}_h) = \operatorname{tr} \boldsymbol{S}_h^c$. Furthermore, Assumption 9 guarantees that the best approximation error in the L^2-norm of the space $\boldsymbol{S}_h^c \subset \boldsymbol{S}_h$ is of linear order.

The following lemma gives a simple property of the elements in $\boldsymbol{S}_h^t$.

Lemma 6.9. *If for $\boldsymbol{\sigma}_h \in \boldsymbol{S}_h$, $(\sigma_h)_{ij}$ is either bilinear or trilinear, $1 \le i, j \le d$, and Assumption 9 is satisfied, then $(\boldsymbol{\tau}_h^t, \boldsymbol{\omega}_h^t)_{0,\Omega} = (tr\,\boldsymbol{\tau}_h^t, tr\,\boldsymbol{\omega}_h^t)_{0,\Omega}$, $\boldsymbol{\tau}_h^t, \boldsymbol{\omega}_h^t \in \boldsymbol{S}_h^t$.*

Proof. The proof is carried out by computing the relevant quantities in the reference element $\hat{K}$. The general case follows by using the affine equivalence. Assuming, in general, the trilinear form of $\hat{\boldsymbol{\tau}}_h \in \boldsymbol{S}_\square$ with Assumption 9, $\hat{\boldsymbol{\tau}}_{h_{ij}}^t \in \boldsymbol{S}_\square^t$ on $\hat{K} = (-1,1)^3$ can be written as $\hat{\boldsymbol{\tau}}_{h_{ii}}^t = a_{ii}\hat{x} + b_{ii}\hat{y} + c_{ii}\hat{z} + d_{ii}\hat{x}\hat{y} + e_{ii}\hat{y}\hat{z} + f_{ii}\hat{z}\hat{x} + g_{ii}\hat{x}\hat{y}\hat{z}$ for $1 \le i \le 3$, and $\hat{\boldsymbol{\tau}}_{h_{ij}}^t = 0$ else. Similarly for $\hat{\boldsymbol{\omega}}_h \in \boldsymbol{S}_\square$, assuming $\hat{\boldsymbol{\omega}}_{h_{ii}}^t = \tilde{a}_{ii}\hat{x} + \tilde{b}_{ii}\hat{y} + \tilde{c}_{ii}\hat{z} + \tilde{d}_{ii}\hat{x}\hat{y} + \tilde{e}_{ii}\hat{y}\hat{z} + \tilde{f}_{ii}\hat{z}\hat{x} + \tilde{g}_{ii}\hat{x}\hat{y}\hat{z}$

on $\hat{K}$, we have

$$\begin{aligned}(\hat{\boldsymbol{\tau}}_h^t, \hat{\boldsymbol{\omega}}_h^t)_{0,\hat{K}} &= \sum_{i=1}^{3} \int_{\hat{K}} \hat{\boldsymbol{\tau}}_{h_{ii}}^t \hat{\boldsymbol{\omega}}_{h_{ii}}^t \, dx\, dy\, dz = \sum_{i=1}^{3} \int_{\hat{K}} a_{ii}\tilde{a}_{ii}\hat{x}^2 + b_{ii}\tilde{b}_{ii}\hat{y}^2 + c_{ii}\tilde{c}_{ii}\hat{z}^2 \\ &+ d_{ii}\tilde{d}_{ii}(\hat{x}\hat{y})^2 + d_{ii}\tilde{e}_{ii}(\hat{y}\hat{z})^2 + f_{ii}\tilde{f}_{ii}(\hat{z}\hat{x})^2 + g_{ii}\tilde{g}_{ii}(\hat{x}\hat{y}\hat{z})^2 \, dx\, dy\, dz \\ &= \int_{\hat{K}} \sum_{i=1}^{3} \hat{\boldsymbol{\tau}}_{h_{ii}}^t \sum_{i=1}^{3} \hat{\boldsymbol{\omega}}_{h_{ii}}^t \, dx\, dy\, dz = (\operatorname{tr} \hat{\boldsymbol{\tau}}_h^t, \operatorname{tr} \hat{\boldsymbol{\omega}}_h^t)_{0,\hat{K}}.\end{aligned}$$

□

It is straightforward to verify the assertion of this lemma for all our Cases I–V. For Case III, we find $\boldsymbol{S}_h^t = \{\mathbf{0}\}$, and for all other cases, $\boldsymbol{S}_h^t$ is spanned locally by the basis

$$\begin{bmatrix} \hat{y} & \hat{z} & \hat{y}\hat{z} & 0 & 0 & 0 & 0 & 0 & 0 \\ 0 & 0 & 0 & \hat{x} & \hat{z} & \hat{x}\hat{z} & 0 & 0 & 0 \\ 0 & 0 & 0 & 0 & 0 & 0 & \hat{x} & \hat{y} & \hat{x}\hat{y} \\ 0 & 0 & 0 & 0 & 0 & 0 & 0 & 0 & 0 \\ 0 & 0 & 0 & 0 & 0 & 0 & 0 & 0 & 0 \\ 0 & 0 & 0 & 0 & 0 & 0 & 0 & 0 & 0 \end{bmatrix}$$

for $d = 3$ and by A_2 for $d = 2$. The following lemma will give the explicit representation of the statically condensed system (6.5.1).

LEMMA 6.10. *We define*

$\theta(\mu, \lambda, \alpha) := \frac{2\mu(2\mu+d\,\lambda)}{2\mu+\lambda(d-1)}$, $\alpha \neq -1$, *for the discretization of Type 1, and*
$\theta(\mu, \lambda, \alpha) := \frac{(2\mu+d\,\lambda)^2\mu(2+\alpha)}{\mu(2+\alpha)(2\mu+2d\,\lambda-\lambda)+(d-1)^2\lambda^2}$, $\alpha \notin \{-1, -2\}$, *for the discretization of Type 2.*

Then, under Assumption 9, we have

$$A_h(\boldsymbol{u}_h, \boldsymbol{v}_h) = (Q_h\boldsymbol{\varepsilon}(\boldsymbol{u}_h), \boldsymbol{\varepsilon}(\boldsymbol{v}_h))_{0,\Omega},$$

where $Q_h\boldsymbol{\varepsilon}(\boldsymbol{u}_h) := \mathcal{C}P_{\boldsymbol{S}_h^c}\boldsymbol{\varepsilon}(\boldsymbol{u}_h) + \theta(\mu, \lambda, \alpha)P_{\boldsymbol{S}_h^t}\boldsymbol{\varepsilon}(\boldsymbol{u}_h)$, *and* $P_{\boldsymbol{S}_h^c}$ *and* $P_{\boldsymbol{S}_h^t}$ *are orthogonal projections onto the spaces* $\boldsymbol{S}_h^c$ *and* $\boldsymbol{S}_h^t$, *respectively. Furthermore, under Assumption 8 (i), and* $0 < c \leq \mu(2+\alpha) \leq C < \infty$, *the bilinear form* $A_h(\cdot,\cdot)$ *is* $\mathbf{V}_h$*-elliptic, and there exists a* λ*-independent constant* C *with*

$$\|(Q_h\boldsymbol{\varepsilon}(\boldsymbol{v}_h) - \boldsymbol{\Pi}_h\mathcal{C}\boldsymbol{\varepsilon}(\boldsymbol{v}_h)\|_{0,\Omega} \leq C\|(\mathbf{Id} - \boldsymbol{\Pi}_{\mathrm{h}})\boldsymbol{\varepsilon}(\boldsymbol{v}_{\mathrm{h}})\|_{0,\Omega}, \tag{6.5.2}$$

where $\boldsymbol{\Pi}_h$ *is the element-wise* L^2*-projector with respect to* $\mathcal{T}_h$.

PROOF. The main idea of the proof is to use the orthogonal decomposition of $\boldsymbol{S}_h$ as given above and to apply static condensation. In the first case, we have $\boldsymbol{\sigma}_h = \mathcal{C}\boldsymbol{d}_h$, and so in terms of the decomposition given above, we can write $\boldsymbol{\sigma}_h = \boldsymbol{\sigma}_h^c + \boldsymbol{\sigma}_h^t$, $\boldsymbol{\sigma}_h^c \in \boldsymbol{S}_h^c$, $\boldsymbol{\sigma}_h^t \in \boldsymbol{S}_h^t$. Using $\boldsymbol{d}_h = \mathcal{C}^{-1}\boldsymbol{\sigma}_h$, Lemma 6.9, and the orthogonal decomposition of $\boldsymbol{S}_h$ in the second equation of (6.3.2), we get

$$\boldsymbol{\sigma}_h^c = \mathcal{C}P_{\boldsymbol{S}_h^c}\boldsymbol{\varepsilon}(\boldsymbol{u}_h), \text{ and } \boldsymbol{\sigma}_h^t = \frac{2\mu(2\mu + d\,\lambda)}{2\mu + \lambda(d-1)}P_{\boldsymbol{S}_h^t}\boldsymbol{\varepsilon}(\boldsymbol{u}_h). \tag{6.5.3}$$

If $\boldsymbol{S}_h = \boldsymbol{D}_h$, the first equation in (6.3.2) yields $P_{\boldsymbol{S}_h}(\mathcal{B}_\alpha(\mathcal{C}\boldsymbol{d}_h - \boldsymbol{\sigma}_h)) = 0$. Using the decomposition for $\boldsymbol{d}_h$, we find that $\boldsymbol{d}_h = \boldsymbol{d}_h^c + \boldsymbol{d}_h^t$, $\boldsymbol{d}_h^c \in \boldsymbol{S}_h^c$, $\boldsymbol{d}_h^t \in \boldsymbol{S}_h^t$, and

$$\boldsymbol{d}_h^c = \mathcal{C}^{-1}\boldsymbol{\sigma}_h^c\,, \quad P_{\boldsymbol{S}_h^t}(\mathcal{B}_\alpha(\mathcal{C}\boldsymbol{d}_h^t - \boldsymbol{\sigma}_h^t)) = \boldsymbol{0}. \tag{6.5.4}$$

Lemma 6.9 in $P_{\boldsymbol{S}_h^t}(\mathcal{B}_\alpha(\mathcal{C}\boldsymbol{d}_h^t - \boldsymbol{\sigma}_h^t)) = \boldsymbol{0}$ yields

$$\boldsymbol{d}_h^t = \frac{(d-1)\lambda + (2+\alpha)\mu}{\mu(2+\alpha)(2\mu + d\,\lambda)}\boldsymbol{\sigma}_h^t. \tag{6.5.5}$$

In terms of (6.5.4) and (6.5.5), we can eliminate $\boldsymbol{d}_h^c$ and $\boldsymbol{d}_h^t$ from the second equation of (6.3.2). The elimination of $\boldsymbol{d}_h^c$ gives $\boldsymbol{\sigma}_h^c = \mathcal{C}P_{\boldsymbol{S}_h^c}\boldsymbol{\varepsilon}(\boldsymbol{u}_h)$, and using (6.5.5), we obtain

$$\boldsymbol{\sigma}_h^t = \frac{(2\mu + d\,\lambda)^2\mu(2+\alpha)}{\mu(2+\alpha)(2\mu + 2d\,\lambda - \lambda) + (d-1)^2\lambda^2}P_{\boldsymbol{S}_h^t}\boldsymbol{\varepsilon}(\boldsymbol{u}_h). \tag{6.5.6}$$

Now, we turn to the second part of the lemma. By using this representation of the bilinear form $A_h(\cdot,\cdot)$ and noting that $\theta(\mu,\lambda,\alpha)$ is positive and bounded independently of λ from below, Assumption 8 (i) in combination with Korn's inequality guarantees the ellipticity. To show (6.5.2), we start with Assumption 9, which yields $\operatorname{tr}(P_{\boldsymbol{S}_h^c} - \boldsymbol{\Pi}_{\mathrm{h}})\boldsymbol{\varepsilon}(\boldsymbol{v}_h) = 0$, and thus

$$\begin{aligned}(Q_h - \mathcal{C}\boldsymbol{\Pi}_h)\boldsymbol{\varepsilon}(\boldsymbol{v}_h) &= \mathcal{C}P_{\boldsymbol{S}_h^c}\boldsymbol{\varepsilon}(\boldsymbol{v}_h) + \theta(\mu,\lambda,\alpha)P_{\boldsymbol{S}_h^t}\boldsymbol{\varepsilon}(\boldsymbol{v}_h) - \mathcal{C}\boldsymbol{\Pi}_h\boldsymbol{\varepsilon}(\boldsymbol{v}_h)\\ &= 2\mu(P_{\boldsymbol{S}_h^c}\boldsymbol{\varepsilon}(\boldsymbol{v}_h) - \boldsymbol{\Pi}_h\boldsymbol{\varepsilon}(\boldsymbol{v}_h)) + \theta(\mu,\lambda,\alpha)P_{\boldsymbol{S}_h^t}\boldsymbol{\varepsilon}(\boldsymbol{v}_h).\end{aligned}$$

Since $\theta(\mu,\lambda,\alpha)$ is bounded independently of λ from above, to prove

$$\|(Q_h\boldsymbol{\varepsilon}(\boldsymbol{v}_h) - \boldsymbol{\Pi}_h\mathcal{C}\boldsymbol{\varepsilon}(\boldsymbol{v}_h)\|_{0,\Omega} \le C\|(\mathbf{Id} - \boldsymbol{\Pi}_{\mathrm{h}})\boldsymbol{\varepsilon}(\boldsymbol{v}_{\mathrm{h}})\|_{0,\Omega},$$

it is sufficient to show

$$\begin{aligned}\|(P_{\boldsymbol{S}_h^c} - \boldsymbol{\Pi}_h)\boldsymbol{\varepsilon}(\boldsymbol{v}_h)\|_{0,\Omega} &\le C\|(\mathbf{Id} - \boldsymbol{\Pi}_{\mathrm{h}})\boldsymbol{\varepsilon}(\boldsymbol{v}_{\mathrm{h}})\|_{0,\Omega},\\ \|P_{\boldsymbol{S}_h^t}\boldsymbol{\varepsilon}(\boldsymbol{v}_h)\|_{0,\Omega} &\le C\|(\mathbf{Id} - \boldsymbol{\Pi}_{\mathrm{h}})\boldsymbol{\varepsilon}(\boldsymbol{v}_{\mathrm{h}})\|_{0,\Omega}.\end{aligned} \tag{6.5.7}$$

To prove the first inequality in (6.5.7), we start with the identity

$$\|(P_{\boldsymbol{S}_h^c} - \mathbf{Id})\boldsymbol{\varepsilon}(\boldsymbol{v}_h)\|_{0,\Omega}^2 = ((P_{\boldsymbol{S}_h^c} - \mathbf{Id})\boldsymbol{\varepsilon}(\boldsymbol{v}_h), (P_{\boldsymbol{S}_h^c} - \boldsymbol{\Pi}_h + \boldsymbol{\Pi}_h - \mathbf{Id})\boldsymbol{\varepsilon}(\boldsymbol{v}_h))_{0,\Omega}.$$

By definition of $P_{\boldsymbol{S}_h^c}$ and Assumption 9, we find that $(P_{\boldsymbol{S}_h^c} - \boldsymbol{\Pi}_h)\boldsymbol{\varepsilon}(\boldsymbol{v}_h) \in \boldsymbol{S}_h^c$, and so

$$\|(P_{\boldsymbol{S}_h^c} - \mathbf{Id})\boldsymbol{\varepsilon}(\boldsymbol{v}_h)\|_{0,\Omega} \le \|(\boldsymbol{\Pi}_h - \mathbf{Id})\boldsymbol{\varepsilon}(\boldsymbol{v}_h)\|_{0,\Omega}.$$

Hence the first inequality in (6.5.7) results from the triangle inequality. Using $\boldsymbol{\Pi}_h\boldsymbol{\varepsilon}(\boldsymbol{v}_h) \in \boldsymbol{S}_h^c$, and the orthogonality of $\boldsymbol{S}_h^c$ and $\boldsymbol{S}_h^t$, we obtain the following upper bound

$$\begin{aligned}\|P_{\boldsymbol{S}_h^t}\boldsymbol{\varepsilon}(\boldsymbol{v}_h)\|_{0,\Omega}^2 &= (-P_{\boldsymbol{S}_h^t}\boldsymbol{\varepsilon}(\boldsymbol{v}_h), (\mathbf{Id} - P_{\boldsymbol{S}_h^t} - \mathbf{Id} + \boldsymbol{\Pi}_h)\boldsymbol{\varepsilon}(\boldsymbol{v}_h))_{0,\Omega}\\ &\le \|P_{\boldsymbol{S}_h^t}\boldsymbol{\varepsilon}(\boldsymbol{v}_h)\|_{0,\Omega}\|(\mathbf{Id} - \boldsymbol{\Pi}_{\mathrm{h}})\boldsymbol{\varepsilon}(\boldsymbol{v}_{\mathrm{h}})\|_{0,\Omega},\end{aligned}$$

which proves the second inequality in (6.5.7). □

For the uniform convergence of the finite element solutions of the statically condensed formulation (6.5.1) in the incompressible limit, we need the following lemma.

LEMMA 6.11. *Assume that* $\boldsymbol{u}$ *and* $\boldsymbol{u}_h$ *be the solutions of* (6.1.5) *and* (6.5.1)*, respectively. Then under the assumptions of Lemma 6.10 and the regularity estimate* (6.1.6)*, there exists a* $\boldsymbol{v}_h \in \mathbf{V}_h^s$ *so that*

$$|A(\boldsymbol{u}_h - \boldsymbol{v}_h, \boldsymbol{u}) - A_h(\boldsymbol{u}_h - \boldsymbol{v}_h, \boldsymbol{v}_h)| \leq C\|\boldsymbol{u}_h - \boldsymbol{v}_h\|_{1,\Omega} h \|\boldsymbol{f}\|_{0,\Omega}.$$

PROOF. The crucial point is to use the approximation property of Fortin interpolation operator in combination with the regularity estimate (6.1.6). Setting $W := [H^2(\Omega) \cap H_0^1(\Omega)]^2$, we recall that Fortin's interpolation operator $\boldsymbol{I}_h^F : W \longrightarrow \mathbf{V}_h^s$ for the stable Stokes pairing $(\mathbf{V}_h^s, \widetilde{R}_h^s)$ is then given by the problem of finding $(\boldsymbol{I}_h^F \boldsymbol{w}, p_h) \in \mathbf{V}_h^s \times \widetilde{R}_h^s$ such that

$$\begin{array}{rcll} (\nabla \boldsymbol{I}_h^F \boldsymbol{w}, \nabla \boldsymbol{z}_h)_{0,\Omega} + (\operatorname{div} \boldsymbol{z}_h, p_h)_{0,\Omega} & = & (\nabla \boldsymbol{w}, \nabla \boldsymbol{z}_h)_{0,\Omega}, & \boldsymbol{z}_h \in \mathbf{V}_h^s, \\ (\operatorname{div} \boldsymbol{I}_h^F \boldsymbol{w}, q_h)_{0,\Omega} & = & (\operatorname{div} \boldsymbol{w}, q_h)_{0,\Omega}, & q_h \in \widetilde{R}_h^s. \end{array} \tag{6.5.8}$$

Under the regularity assumption (6.1.6), the following approximation property of this operator can be proved as in [**41**].

$$\|\boldsymbol{u} - \boldsymbol{I}_h^F \boldsymbol{u}\|_{1,\Omega} + \lambda \|\operatorname{div} \boldsymbol{u} - \Pi_h(\operatorname{div} \boldsymbol{I}_h^F \boldsymbol{u})\|_{0,\Omega} \leq Ch\|\boldsymbol{f}\|_{0,\Omega},$$

where Π_h is the L^2-projection onto $\widetilde{R}_h^s$. Using the explicit representation of the bilinear form $A_h(\cdot,\cdot)$ from Lemma 6.10, the triangle inequality yields

$$|A(\boldsymbol{u}_h - \boldsymbol{v}_h, \boldsymbol{u}) - A_h(\boldsymbol{u}_h - \boldsymbol{v}_h, \boldsymbol{v}_h)| = |(\mathcal{C}\boldsymbol{\varepsilon}(\boldsymbol{u}_h - \boldsymbol{v}_h), \boldsymbol{\varepsilon}(\boldsymbol{u}))_{0,\Omega} - (Q_h \boldsymbol{\varepsilon}(\boldsymbol{u}_h - \boldsymbol{v}_h), \boldsymbol{\varepsilon}(\boldsymbol{v}_h))_{0,\Omega}|.$$

Now, we use the symmetricity of the tensor $\mathcal{C}$ and the operator Q_h to obtain

$$|A(\boldsymbol{u}_h - \boldsymbol{v}_h, \boldsymbol{u}) - A_h(\boldsymbol{u}_h - \boldsymbol{v}_h, \boldsymbol{v}_h)| = |(\boldsymbol{\varepsilon}(\boldsymbol{u}_h - \boldsymbol{v}_h), \mathcal{C}\boldsymbol{\varepsilon}(\boldsymbol{u}) - Q_h \boldsymbol{\varepsilon}(\boldsymbol{v}_h))_{0,\Omega}|.$$

In terms of the inequality $\|\boldsymbol{\varepsilon}(\boldsymbol{u}_h - \boldsymbol{v}_h)\|_{0,\Omega} \leq C\|\boldsymbol{u}_h - \boldsymbol{v}_h\|_{1,\Omega}$, we have

$$\begin{array}{rl} & |A(\boldsymbol{u}_h - \boldsymbol{v}_h, \boldsymbol{u}) - A_h(\boldsymbol{u}_h - \boldsymbol{v}_h, \boldsymbol{v}_h)| \\ \leq & \|\boldsymbol{u}_h - \boldsymbol{v}_h\|_{1,\Omega} \|\mathcal{C}\boldsymbol{\varepsilon}(\boldsymbol{u}) - Q_h \boldsymbol{\varepsilon}(\boldsymbol{v}_h)\|_{0,\Omega} \\ \leq & \|\boldsymbol{u}_h - \boldsymbol{v}_h\|_{1,\Omega} \left(\|\mathcal{C}\boldsymbol{\varepsilon}(\boldsymbol{u}) - \mathcal{C}\boldsymbol{\Pi}_h \boldsymbol{\varepsilon}(\boldsymbol{v}_h)\|_{0,\Omega} + \|\mathcal{C}\boldsymbol{\Pi}_h \boldsymbol{\varepsilon}(\boldsymbol{v}_h) - Q_h \boldsymbol{\varepsilon}(\boldsymbol{v}_h)\|_{0,\Omega} \right), \end{array}$$

where in the last step, we have used the triangle inequality. Since

$$\|\mathcal{C}\boldsymbol{\varepsilon}(\boldsymbol{u}) - \mathcal{C}\boldsymbol{\Pi}_h \boldsymbol{\varepsilon}(\boldsymbol{v}_h)\|_{0,\Omega} \leq C(\|\boldsymbol{u} - \boldsymbol{v}_h\|_{1,\Omega} + \lambda \|\operatorname{div} \boldsymbol{u} - \Pi_h \operatorname{div} \boldsymbol{v}_h\|_{0,\Omega}),$$

the proof follows by using $\boldsymbol{v}_h := I_h^F \boldsymbol{u}$ and the second result of Lemma 6.10. □

Now, we formulate the main result of this section.

THEOREM 6.12. *Suppose that Assumptions 8 (i), 9 and* $0 < c \leq \mu(2+\alpha) \leq C < \infty$ *hold. Then, under the regularity estimate* (6.1.6)*, we obtain an optimal a priori estimate for the discretization error in the displacement*

$$\|\boldsymbol{u} - \boldsymbol{u}_h\|_{1,\Omega} \leq Ch\|\boldsymbol{f}\|_{0,\Omega},$$

where $C < \infty$ *is independent of* λ *and* h*.*

PROOF. The essential idea of the proof is to adapt the first lemma of Strang, see [**40**], in our setting. Using the coercivity of $A_h(\cdot,\cdot)$, Lemma 6.11 and (6.1.5), we find that for $\boldsymbol{v}_h := I_h^F \boldsymbol{u}$

$$\begin{aligned}\|\boldsymbol{u}_h - \boldsymbol{v}_h\|_{1,\Omega}^2 &\leq C|A_h(\boldsymbol{u}_h - \boldsymbol{v}_h, \boldsymbol{u}_h - \boldsymbol{v}_h)| = C|A_h(\boldsymbol{u}_h - \boldsymbol{v}_h, \boldsymbol{u}_h) - A_h(\boldsymbol{u}_h - \boldsymbol{v}_h, \boldsymbol{v}_h)| \\ &= C|A(\boldsymbol{u}_h - \boldsymbol{v}_h, \boldsymbol{u}) - A_h(\boldsymbol{u}_h - \boldsymbol{v}_h, \boldsymbol{v}_h)| \leq C\|\boldsymbol{u}_h - \boldsymbol{v}_h\|_{1,\Omega} h \|\boldsymbol{f}\|_{0,\Omega}.\end{aligned}$$

In terms of the triangle inequality, we obtain

$$\|\boldsymbol{u} - \boldsymbol{u}_h\|_{1,\Omega} \leq C(\|\boldsymbol{u} - \boldsymbol{v}_h\|_{1,\Omega} + \|\boldsymbol{v}_h - \boldsymbol{u}_h\|_{1,\Omega}) \leq Ch\|\boldsymbol{f}\|_{0,\Omega}.$$

□

REMARK 6.13. *Theorem 6.12 provides sufficient conditions such that the displacement based formulation* (6.5.1) *is well defined and yields λ-independent optimal a priori estimates for both types of discretization. We recall that for Cases I and IV, the choice of α is crucial. Setting $\alpha = \frac{\lambda}{\mu}$ will result in volumetric locking whereas the case $\alpha = 0$, for example, will give good numerical results. For the λ-independent estimate, the assumption $0 < c \leq (2+\alpha) \leq C < \infty$ is essential. We remark that this condition on α is weaker than Assumption 8 (ii).*

In the rest of this section, we show that the well known $\mathrm{Q}_1\mathrm{P}_0$ saddlepoint problem can be analyzed as a special situation of our modified Hu-Washizu formulation.

LEMMA 6.14. *Case IV with $\alpha = -2\frac{2d\,\lambda-\lambda+2\mu}{d^2\lambda+2\mu}$ is equivalent to the penalized Q_1P_0 saddlepoint problem (Stokes)*

$$\begin{array}{lcllll} 2\mu(\boldsymbol{\varepsilon}(\boldsymbol{v}_h), \boldsymbol{\varepsilon}(\boldsymbol{u}_h))_{0,\Omega} & + & (\operatorname{div} \boldsymbol{v}_h, p_h)_{0,\Omega} & = & \ell(\boldsymbol{v}_h), & \boldsymbol{v}_h \in \mathbf{V}_h, \\ (\operatorname{div} \boldsymbol{u}_h, q_h)_{0,\Omega} & - & \frac{1}{\lambda}(p_h, q_h)_{0,\Omega} & = & 0, & q_h \in \widetilde{R}_h. \end{array}$$

PROOF. By static condensation, we can eliminate the pressure from the saddle point problem and arrive at

$$2\mu(\boldsymbol{\varepsilon}(\boldsymbol{v}_h), \boldsymbol{\varepsilon}(\boldsymbol{u}_h))_{0,\Omega} + \lambda(\Pi_h \operatorname{div} \boldsymbol{v}_h, \Pi_h \operatorname{div} \boldsymbol{u}_h)_{0,\Omega} = \ell(\boldsymbol{v}_h), \qquad \boldsymbol{v}_h \in \mathbf{V}_h. \tag{6.5.9}$$

Using the given α, we show that (6.5.1) is equivalent to (6.5.9). With the given α, we get $Q_h \boldsymbol{e}_h = \mathcal{C} P_{\boldsymbol{S}_h^c} \boldsymbol{e}_h + 2\mu P_{\boldsymbol{S}_h^t} \boldsymbol{e}_h$. Hence

$$\begin{aligned}(Q_h\boldsymbol{\varepsilon}(\boldsymbol{v}_h), \boldsymbol{\varepsilon}(\boldsymbol{u}_h))_{0,\Omega} &= (P_{\boldsymbol{S}_h^c}\boldsymbol{\varepsilon}(\boldsymbol{v}_h), \mathcal{C} P_{\boldsymbol{S}_h^c}\boldsymbol{\varepsilon}(\boldsymbol{u}_h))_{0,\Omega} + (P_{\boldsymbol{S}_h^t}\boldsymbol{\varepsilon}(\boldsymbol{v}_h), 2\mu P_{\boldsymbol{S}_h^t}\boldsymbol{\varepsilon}(\boldsymbol{u}_h))_{0,\Omega} \\ &= 2\mu(P_{\boldsymbol{S}_h}\boldsymbol{\varepsilon}(\boldsymbol{v}_h), P_{\boldsymbol{S}_h}\boldsymbol{\varepsilon}(\boldsymbol{u}_h))_{0,\Omega} + \lambda(\operatorname{tr} P_{\boldsymbol{S}_h^c}\boldsymbol{\varepsilon}(\boldsymbol{v}_h), \operatorname{tr} P_{\boldsymbol{S}_h^c}\boldsymbol{\varepsilon}(\boldsymbol{u}_h))_{0,\Omega} \\ &= 2\mu(P_{\boldsymbol{S}_h}\boldsymbol{\varepsilon}(\boldsymbol{v}_h), P_{\boldsymbol{S}_h}\boldsymbol{\varepsilon}(\boldsymbol{u}_h))_{0,\Omega} + \lambda(\Pi_h \operatorname{div} \boldsymbol{v}_h, \Pi_h \operatorname{div} \boldsymbol{u}_h)_{0,\Omega}.\end{aligned}$$

Finally, the result follows by using the fact that $P_{\boldsymbol{S}_h}\boldsymbol{\varepsilon}(\boldsymbol{v}_h) = \boldsymbol{\varepsilon}(\boldsymbol{v}_h)$ for Case IV. □

REMARK 6.15. *The choice $\alpha = -2\frac{2d\,\lambda-\lambda+2\mu}{d^2\lambda+2\mu}$ does not satisfy Assumption 8 (ii) but $0 < c \leq (2+\alpha) \leq C < \infty$.*

6.6. A priori results for the stress

The results of the previous sections show that the lack of stability resulting from the presence of a checkerboard mode is confined to the stress, and does not affect the displacement. In this section, we establish an optimal a priori result for a post-processed stress. Let $(\boldsymbol{u}_h, \boldsymbol{d}_h, \boldsymbol{\sigma}_h)$ be the unique solution of the modified Hu-Washizu formulation (6.3.2), and $\boldsymbol{\sigma}_h^s$ be the post-processed stress given by

$$\begin{array}{lcll} \boldsymbol{\sigma}_h & = & \operatorname{dev_h} \boldsymbol{\sigma}_h + \operatorname{sph_h} \boldsymbol{\sigma}_h = \operatorname{dev_h} \boldsymbol{\sigma}_h + p_h \mathbf{1}, & p_h \in \widetilde{R}_h, \\ \boldsymbol{\sigma}_h^s & := & \operatorname{dev_h} \boldsymbol{\sigma}_h + p_h^s \mathbf{1}, & p_h^s := \Pi_h^s p_h, \end{array}$$

where Π_h^s is the L^2-projection onto the checkerboard-free subspace $\widetilde{R}_h^s$.

THEOREM 6.16. *Under the assumptions of Theorem 6.12, the following λ-independent upper bound for the discretization error for the stress holds*

$$\|\boldsymbol{\sigma} - \boldsymbol{\sigma}_h^s\|_{0,\Omega} \leq Ch \|\boldsymbol{f}\|_{0,\Omega}.$$

PROOF. We start by eliminating the strain from the saddlepoint problem (6.3.2), to obtain a modified Hellinger-Reissner two-field formulation. Using (6.5.3), (6.5.6) and the definition of $\theta(\mu, \lambda, \alpha)$, we find that

$$\begin{array}{lcll} \hat{a}(\boldsymbol{\sigma}_h, \boldsymbol{\tau}_h) - (\boldsymbol{\varepsilon}(\boldsymbol{u}_h), \boldsymbol{\tau}_h)_{0,\Omega} & = & 0, & \boldsymbol{\tau}_h \in \boldsymbol{S}_h, \\ (\boldsymbol{\varepsilon}(\boldsymbol{v}_h), \boldsymbol{\sigma}_h)_{0,\Omega} & = & \ell(\boldsymbol{v}_h), & \boldsymbol{v}_h \in \mathbf{V}_h, \end{array}$$

where $\hat{a}(\boldsymbol{\sigma}_h, \boldsymbol{\tau}_h) := (\mathcal{C}_h^{-1} \boldsymbol{\sigma}_h, \boldsymbol{\tau}_h)_{0,\Omega}$ with $\mathcal{C}_h^{-1} \boldsymbol{\tau}_h = \mathcal{C}^{-1} P_{\boldsymbol{S}_h^c} \boldsymbol{\tau}_h + 1/\theta(\mu, \lambda, \alpha) P_{\boldsymbol{S}_h^t} \boldsymbol{\tau}_h$. We define $\boldsymbol{S}_h^s$ and $\mathbf{V}_h^\perp$ such that the orthogonal decomposition of $\boldsymbol{S}_h = \boldsymbol{S}_h^s \oplus \widetilde{R}_h^u \mathbf{1}$, and $\mathbf{V}_h = \mathbf{V}_h^s \oplus \mathbf{V}_h^\perp$ holds, respectively. Then, we have

$$(\boldsymbol{\varepsilon}(\boldsymbol{v}_h^s), q_h^u \mathbf{1})_{0,\Omega} = (\operatorname{div} \boldsymbol{v}_h^s, q_h^u)_{0,\Omega} = 0, \ \boldsymbol{v}_h^s \in \mathbf{V}_h^s, \ q_h^u \in \widetilde{R}_h^u.$$

Using the orthogonality between $\boldsymbol{S}_h^s$ and $\widetilde{R}_h^u \mathbf{1}$ and observing $(\boldsymbol{\varepsilon}(\boldsymbol{v}_h^s), p_h \mathbf{1})_{0,\Omega} = (\boldsymbol{\varepsilon}(\boldsymbol{v}_h^s), p_h^s \mathbf{1})_{0,\Omega}$, we find that $(\boldsymbol{\sigma}_h^s, \boldsymbol{u}_h) \in \boldsymbol{S}_h^s \times \mathbf{V}_h$ satisfies

$$\begin{array}{lcll} \hat{a}(\boldsymbol{\sigma}_h^s, \boldsymbol{\tau}_h^s) - (\boldsymbol{\varepsilon}(\boldsymbol{u}_h), \boldsymbol{\tau}_h^s)_{0,\Omega} & = & 0, & \boldsymbol{\tau}_h^s \in \boldsymbol{S}_h^s, \\ (\boldsymbol{\varepsilon}(\boldsymbol{v}_h^s), \boldsymbol{\sigma}_h^s)_{0,\Omega} & = & \ell(\boldsymbol{v}_h^s), & \boldsymbol{v}_h^s \in \mathbf{V}_h^s. \end{array} \tag{6.6.1}$$

The bilinear form $\hat{a}(\cdot, \cdot)$ is not coercive on $\boldsymbol{S}_h^s \times \boldsymbol{S}_h^s$ uniformly in λ. We recall that $\boldsymbol{S}_h^t \subset \operatorname{dev}_h \boldsymbol{S}_h$, and decompose $\boldsymbol{\tau}_h^s$ according to $\boldsymbol{\tau}_h^s = \boldsymbol{\tau}_h^c + \boldsymbol{\tau}_h^t$, $\boldsymbol{\tau}_h^c \in \boldsymbol{S}_h^c$, $\boldsymbol{\tau}_h^t \in \boldsymbol{S}_h^t$, and $\boldsymbol{\tau}_h^c$ according to $\boldsymbol{\tau}_h^c = \operatorname{dev}_h \boldsymbol{\tau}_h^c + \operatorname{sph}_h \boldsymbol{\tau}_h^c$. Using this decomposition, we have

$$\begin{aligned} \hat{a}(\boldsymbol{\tau}_h^s, \boldsymbol{\tau}_h^s) &= (\mathcal{C}^{-1} \boldsymbol{\tau}_h^c, \boldsymbol{\tau}_h^c)_{0,\Omega} + \frac{1}{\theta(\mu, \lambda, \alpha)} (\boldsymbol{\tau}_h^t, \boldsymbol{\tau}_h^t)_{0,\Omega} \\ &= (\mathcal{C}^{-1} \operatorname{dev_h} \boldsymbol{\tau}_h^c, \operatorname{dev_h} \boldsymbol{\tau}_h^c)_{0,\Omega} + (\mathcal{C}^{-1} \operatorname{sph_h} \boldsymbol{\tau}_h^c, \operatorname{sph_h} \boldsymbol{\tau}_h^c)_{0,\Omega} + \frac{1}{\theta(\mu, \lambda, \alpha)} (\boldsymbol{\tau}_h^t, \boldsymbol{\tau}_h^t)_{0,\Omega}. \end{aligned}$$

Using Lemma 6.5 and the fact that $\theta(\mu, \lambda, \alpha)$ is uniformly bounded from above, we obtain

$$\hat{a}(\boldsymbol{\tau}_h^s, \boldsymbol{\tau}_h^s) \geq c(\|\operatorname{dev_h} \boldsymbol{\tau}_h^c\|_{0,\Omega}^2 + \|\boldsymbol{\tau}_h^t\|_{0,\Omega}^2) \geq c \|\operatorname{dev_h}(\boldsymbol{\tau}_h^c + \boldsymbol{\tau}_h^t)\|_{0,\Omega}^2 = c \|\operatorname{dev_h} \boldsymbol{\tau}_h^s\|_{0,\Omega}^2.$$

To establish an upper bound for the norm of $\boldsymbol{\tau}_h^s$, we have to consider $\operatorname{sph_h} \boldsymbol{\tau}_h^s$ in more detail. Lemma 6.4 and the definition of $\boldsymbol{S}_h^s$ yield that $\operatorname{sph_h} \boldsymbol{\tau}_h^s = q_h^s \mathbf{1}$, $d\, q_h^s = \operatorname{tr} \operatorname{sph_h} \boldsymbol{\tau}_h^s \in \widetilde{R}_h^s$. Since $(\mathbf{V}_h^s, \widetilde{R}_h^s)$ forms a stable Stokes pairing, we can find $\boldsymbol{v}_{q_h^s}^s \in \mathbf{V}_h^s$ such that

$$(q_h^s, \operatorname{div} \boldsymbol{v}_{q_h^s}^s)_{0,\Omega} = d\|q_h^s\|_{0,\Omega}^2, \quad \|\boldsymbol{v}_{q_h^s}^s\|_{1,\Omega} \leq C\|q_h^s\|_{0,\Omega}.$$

and the discrete spherical part of $\boldsymbol{\tau}_h^s$ can be bounded by

$$\begin{aligned} \|\operatorname{sph_h} \boldsymbol{\tau}_h^s\|_{0,\Omega}^2 &= d\|q_h^s\|_{0,\Omega}^2 = (q_h^s, \operatorname{div} \boldsymbol{v}_{q_h^s}^s)_{0,\Omega} = (q_h^s \mathbf{1}, \boldsymbol{\varepsilon}(\boldsymbol{v}_{q_h^s}^s))_{0,\Omega} = (\operatorname{sph_h} \boldsymbol{\tau}_h^s, \boldsymbol{\varepsilon}(\boldsymbol{v}_{q_h^s}^s))_{0,\Omega} \\ &= (\boldsymbol{\tau}_h^s, \boldsymbol{\varepsilon}(\boldsymbol{v}_{q_h^s}^s))_{0,\Omega} - (\operatorname{dev_h} \boldsymbol{\tau}_h^s, \boldsymbol{\varepsilon}(\boldsymbol{v}_{q_h^s}^s))_{0,\Omega} \\ &\leq (\boldsymbol{\tau}_h^s, \boldsymbol{\varepsilon}(\boldsymbol{v}_{q_h^s}^s))_{0,\Omega} + C\|\operatorname{dev_h} \boldsymbol{\tau}_h^s\|_{0,\Omega}\|\operatorname{sph_h} \boldsymbol{\tau}_h^s\|_{0,\Omega}. \end{aligned}$$

Applying Young's inequality, we obtain

$$\|\boldsymbol{\tau}_h^s\|_{0,\Omega}^2 = \|\operatorname{sph_h} \boldsymbol{\tau}_h^s\|_{0,\Omega}^2 + \|\operatorname{dev_h} \boldsymbol{\tau}_h^s\|_{0,\Omega}^2 \leq C\left((\boldsymbol{\tau}_h^s, \boldsymbol{\varepsilon}(\boldsymbol{v}_{q_h^s}^s))_{0,\Omega} + \hat{a}(\boldsymbol{\tau}_h^s, \boldsymbol{\tau}_h^s)\right). \tag{6.6.2}$$

Replacing $\boldsymbol{\tau}_h^s$ by $\boldsymbol{\tau}_h^s - \boldsymbol{\sigma}_h^s$ and using the second equation in (6.6.1), the first term in the upper bound of (6.6.2) can be estimated by

$$\begin{aligned} (\boldsymbol{\tau}_h^s - \boldsymbol{\sigma}_h^s, \boldsymbol{\varepsilon}(\boldsymbol{v}_{q_h^s - p_h^s}^s))_{0,\Omega} &= (\boldsymbol{\tau}_h^s - \boldsymbol{\sigma}, \boldsymbol{\varepsilon}(\boldsymbol{v}_{q_h^s - p_h^s}^s))_{0,\Omega} + (\boldsymbol{\sigma} - \boldsymbol{\sigma}_h^s, \boldsymbol{\varepsilon}(\boldsymbol{v}_{q_h^s - p_h^s}^s))_{0,\Omega} \\ &\leq \|\boldsymbol{\tau}_h^s - \boldsymbol{\sigma}\|_{0,\Omega}\|\boldsymbol{\tau}_h^s - \boldsymbol{\sigma}_h^s\|_{0,\Omega}. \end{aligned}$$

To bound $\hat{a}(\boldsymbol{\tau}_h^s - \boldsymbol{\sigma}_h^s, \boldsymbol{\tau}_h^s - \boldsymbol{\sigma}_h^s)$, we have to use the first equation in (6.6.1). This gives

$$\begin{aligned} \hat{a}(\boldsymbol{\tau}_h^s - \boldsymbol{\sigma}_h^s, \boldsymbol{\tau}_h^s - \boldsymbol{\sigma}_h^s) &= (\mathcal{C}_h^{-1}\boldsymbol{\tau}_h^s, \boldsymbol{\tau}_h^s - \boldsymbol{\sigma}_h^s)_{0,\Omega} - (\boldsymbol{\varepsilon}(\boldsymbol{u}_h), \boldsymbol{\tau}_h^s - \boldsymbol{\sigma}_h^s)_{0,\Omega} \\ &= (\mathcal{C}_h^{-1}\boldsymbol{\tau}_h^s - \mathcal{C}^{-1}\boldsymbol{\sigma}, \boldsymbol{\tau}_h^s - \boldsymbol{\sigma}_h^s)_{0,\Omega} + (\boldsymbol{\varepsilon}(\boldsymbol{u}) - \boldsymbol{\varepsilon}(\boldsymbol{u}_h), \boldsymbol{\tau}_h^s - \boldsymbol{\sigma}_h^s)_{0,\Omega} \\ &\leq \|\boldsymbol{\tau}_h^s - \boldsymbol{\sigma}_h^s\|_{0,\Omega}(\|\mathcal{C}_h^{-1}\boldsymbol{\tau}_h^s - \mathcal{C}^{-1}\boldsymbol{\sigma}\|_{0,\Omega} + \|\boldsymbol{\varepsilon}(\boldsymbol{u} - \boldsymbol{u}_h)\|_{0,\Omega}). \end{aligned}$$

Combining the last two estimates with (6.6.2), we find that

$$\|\boldsymbol{\tau}_h^s - \boldsymbol{\sigma}_h^s\|_{0,\Omega} \leq C(\|\mathcal{C}^{-1}\boldsymbol{\sigma} - \mathcal{C}_h^{-1}\boldsymbol{\tau}_h^s\|_{0,\Omega} + \|\boldsymbol{\sigma} - \boldsymbol{\tau}_h^s\|_{0,\Omega} + \|\boldsymbol{\varepsilon}(\boldsymbol{u}) - \boldsymbol{\varepsilon}(\boldsymbol{u}_h)\|_{0,\Omega}). \tag{6.6.3}$$

Since $\boldsymbol{S}_{2h}^c \subset \boldsymbol{S}_{2h} \subset \boldsymbol{S}_h^s$, Assumption 9 guarantees that the best approximation error in the subspace $\boldsymbol{S}_h^c \cap \boldsymbol{S}_h^s$ satisfies $\inf_{\boldsymbol{\tau}_h^s \in \boldsymbol{S}_h^c \cap \boldsymbol{S}_h^s} \|\boldsymbol{\tau}_h^s - \boldsymbol{\sigma}\|_{0,\Omega} \leq Ch\|\boldsymbol{f}\|_{0,\Omega}$. In terms of Theorem 6.12, the triangle inequality in combination with (6.6.3) yields

$$\|\boldsymbol{\sigma} - \boldsymbol{\sigma}_h^s\|_{0,\Omega} \leq C(\inf_{\boldsymbol{\tau}_h^s \in \boldsymbol{S}_h^c \cap \boldsymbol{S}_h^s}(\|\boldsymbol{\sigma} - \boldsymbol{\tau}_h^s\|_{0,\Omega} + \|\boldsymbol{\varepsilon}(\boldsymbol{u}) - \boldsymbol{\varepsilon}(\boldsymbol{u}_h)\|_{0,\Omega}) \leq Ch\|\boldsymbol{f}\|_{0,\Omega}.$$

□

6.7. Extension to nonlinear elasticity with Saint-Venant Kirchhoff law

In this subsection, starting from a suitable three-field formulation, we give an α-dependent three-field mixed formulation for geometrically nonlinear elasticity with Saint-Venant Kirchhoff law. First, we recall the standard boundary value problem of nonlinear elasticity with Saint-Venant Kirchhoff law. For a prescribed body force $\boldsymbol{f} \in L^2(\Omega)^d$, the standard variational formulation of nonlinear elasticity in Ω with Saint-Venant Kirchhoff law with homogeneous Dirichlet boundary condition on $\partial\Omega$ can be written as: given $\ell \in \mathbf{V}'$ find $\boldsymbol{u} \in \mathbf{V}$ such that

$$A_{gn}(\boldsymbol{u}, \boldsymbol{v}) = \ell(\boldsymbol{v}), \quad \boldsymbol{v} \in \mathbf{V}, \tag{6.7.1}$$

where now $\mathbf{V} := W_0^{1,4}(\Omega)^d$ is a Banach space, and the form $A_{gn}(\cdot,\cdot)$ is defined by

$$A_{gn} : \mathbf{V} \times \mathbf{V} \to \mathbb{R}, \qquad A_{gn}(\boldsymbol{u},\boldsymbol{v}) \;:=\; \int_\Omega (\mathbf{1}+\nabla \boldsymbol{u})\mathcal{C}\boldsymbol{E}(\boldsymbol{u}) : \nabla \boldsymbol{v}\; dx$$

in terms of the Green-Lagrange strain tensor $\boldsymbol{E}(\boldsymbol{u}) := \frac{1}{2}[(\mathbf{1}+\nabla \boldsymbol{u})^T(\mathbf{1}+\nabla \boldsymbol{u}) - \mathbf{1}]$. Here $W_0^{1,4}(\Omega) := \{u \in W^{1,4}(\Omega) |\; u = 0 \text{ on } \partial\Omega\}$. The mathematical analysis of the standard boundary value problem (6.7.1) can be found in [**112**]. The three-field formulation for geometrically nonlinear elasticity with Saint-Venant Kirchhoff law is obtained by taking the second Piola-Kirchhoff stress $\boldsymbol{s}$, the Green-Lagrange strain $\boldsymbol{d}$ and the displacement $\boldsymbol{u}$ as unknowns. In a discrete variational form, this consists of finding $(\boldsymbol{u}_h, \boldsymbol{d}_h, \boldsymbol{s}_h) \in \mathbf{V}_h \times \boldsymbol{D}_h \times \boldsymbol{S}_h$ that satisfy

$$\begin{array}{lcll} \int_\Omega (\mathcal{C}\boldsymbol{d}_h - \boldsymbol{s}_h) : \boldsymbol{e}_h\; dx &=& 0, & \boldsymbol{e}_h \in \boldsymbol{D}_h, \\ \int_\Omega (\boldsymbol{E}(\boldsymbol{u}_h) - \boldsymbol{d}_h) : \boldsymbol{t}_h\; dx &=& 0, & \boldsymbol{t}_h \in \boldsymbol{S}_h, \\ \int_\Omega (\mathbf{1}+\nabla \boldsymbol{u}_h)\boldsymbol{s}_h : \nabla \boldsymbol{v}_h\; dx &=& \ell(\boldsymbol{v}_h), & \boldsymbol{v}_h \in \mathbf{V}_h, \end{array} \tag{6.7.2}$$

where $\boldsymbol{D}_h$ and $\boldsymbol{S}_h$ are as defined before, and $\mathbf{V}_h \subset W_0^{1,4}(\Omega)^d$.

Working with this natural three-field formulation, we cannot expect that we obtain a uniform convergence of the numerical solution with respect to the Lamé parameter λ. As in the linear case, we can infer that the continuity constant of the form $(\mathcal{C}\boldsymbol{d}_h - \boldsymbol{s}_h, \boldsymbol{e}_h)_{0,\Omega}$ is not bounded independently of λ. Therefore, we introduce an α-dependent three-field formulation

$$\begin{array}{lcll} \mu(2\boldsymbol{d}_h + \alpha \operatorname{tr} \boldsymbol{d}_h \mathbf{1}, \boldsymbol{e}_h)_{0,\Omega} + (\delta \operatorname{tr} \boldsymbol{s}_h \mathbf{1} - \boldsymbol{s}_h, \boldsymbol{e}_h)_{0,\Omega} &=& 0, & \boldsymbol{e}_h \in \boldsymbol{D}_h, \\ (\boldsymbol{E}(\boldsymbol{u}_h) - \boldsymbol{d}_h, \boldsymbol{t}_h)_{0,\Omega} + \delta(\operatorname{tr} \boldsymbol{d}_h, \operatorname{tr} \boldsymbol{t}_h)_{0,\Omega} - \frac{\delta}{\kappa}(\operatorname{tr} \boldsymbol{s}_h, \operatorname{tr} \boldsymbol{t}_h)_{0,\Omega} &=& 0, & \boldsymbol{t}_h \in \boldsymbol{S}_h, \\ ((\mathbf{1}+\nabla \boldsymbol{u}_h)\boldsymbol{s}_h, \nabla \boldsymbol{v}_h)_{0,\Omega} &=& \ell(\boldsymbol{v}_h) & \boldsymbol{v}_h \in \mathbf{V}_h, \end{array}$$

where $\delta := \frac{\lambda - \alpha\mu}{\kappa}$. This α-dependent three-field formulation can also be written as a nonlinear saddle point problem: find $(\boldsymbol{u}_h, \boldsymbol{d}_h, \boldsymbol{s}_h) \in \mathbf{V}_h \times \boldsymbol{D}_h \times \boldsymbol{S}_h$ such that

$$\begin{array}{rcrcll} a_\alpha((\boldsymbol{u}_h, \boldsymbol{d}_h), (\boldsymbol{v}_h, \boldsymbol{e}_h)) &+& b_\alpha^1(\boldsymbol{u}_h, (\boldsymbol{v}_h, \boldsymbol{e}_h), \boldsymbol{s}_h) &=& \ell(\boldsymbol{v}_h), & (\boldsymbol{v}_h, \boldsymbol{e}_h) \in \mathbf{V}_h \times \boldsymbol{D}_h, \\ b_\alpha^2((\boldsymbol{u}_h, \boldsymbol{d}_h), \boldsymbol{t}_h) &-& \frac{\delta}{\kappa}\, c(\boldsymbol{s}_h, \boldsymbol{t}_h) &=& 0, & \boldsymbol{t}_h \in \boldsymbol{S}_h, \end{array} \tag{6.7.3}$$

where the bilinear forms $a_\alpha(\cdot,\cdot)$ and $c(\cdot,\cdot)$, are defined as before, and

$$\begin{aligned} b_\alpha^1(\boldsymbol{u}, (\boldsymbol{v}, \boldsymbol{e}), \boldsymbol{s}) &:= (\delta \operatorname{tr} \boldsymbol{s}\mathbf{1} - \boldsymbol{s}, \boldsymbol{e})_{0,\Omega} + ((\mathbf{1}+\nabla \boldsymbol{u})\boldsymbol{s}, \nabla \boldsymbol{v})_{0,\Omega} \\ b_\alpha^2((\boldsymbol{u}, \boldsymbol{d}), \boldsymbol{t}) &:= (\boldsymbol{E}(\boldsymbol{u}) - \boldsymbol{d}, \boldsymbol{t})_{0,\Omega} + \delta(\operatorname{tr} \boldsymbol{d}, \operatorname{tr} \boldsymbol{t})_{0,\Omega}. \end{aligned}$$

As in the case of linear elasticity, the solution of (6.7.3) does not depend on α under the assumption $\operatorname{tr} \boldsymbol{D}_h \mathbf{1} \subset \boldsymbol{D}_h$.

As in the linear case, under the assumption $\operatorname{tr} \boldsymbol{D}_h \mathbf{1} \subset \boldsymbol{D}_h$ the geometrically nonlinear Hu-Washizu formulation (6.7.2) can be reduced to a two-field variational problem of the Hellinger-Reissner type so that the weak discrete form can be written as: find $(\boldsymbol{u}_h, \boldsymbol{s}_h) \in \mathbf{V}_h \times \boldsymbol{S}_h$ such that

$$\begin{array}{lcll} \int_\Omega \mathcal{C}^{-1}\boldsymbol{s}_h : \boldsymbol{t}_h\; dx - \int_\Omega \boldsymbol{E}(\boldsymbol{u}_h) : \boldsymbol{t}_h\; dx &=& 0, & \boldsymbol{t}_h \in \boldsymbol{S}_h \\ \int_\Omega (\mathbf{1}+\nabla \boldsymbol{u}_h)\boldsymbol{s}_h : \nabla \boldsymbol{v}_h\; dx &=& \ell(\boldsymbol{v}_h), & \boldsymbol{v}_h \in \mathbf{V}_h. \end{array} \tag{6.7.4}$$

Following exactly as in Lemma 6.10, the stress and strain can be statically condensed out from the system to obtain the following displacement-based formulation.

LEMMA 6.17. *Under the assumption of Lemma 6.9, defining function $\theta(\cdot,\cdot,\cdot)$ and operator Q_h as in Lemma 6.10, the displacement-based formulation of* (6.7.3) *is given by*

$$((\mathbf{1}+\nabla \boldsymbol{u}_h)Q_h\boldsymbol{E}(\boldsymbol{u}_h),\nabla \boldsymbol{v}_h)_{0,\Omega}=\ell(\boldsymbol{v}_h).$$

6.8. Extension to general hyperelasticity

Exploiting the invertibility of the constitutive equation, we derived α-dependent three-field formulations for linear and geometrically nonlinear elasticity with Saint-Venant Kirchhoff law in the previous sections. The general hyperelastic constitutive equation cannot be inverted easily, and therefore, we have to follow an another route to obtain an α-dependent three-field formulation. However, as pointed out in the introduction, using two crucial points from the linear analysis, we obtain a three-field formulation for the general hyperelastic material law. As before we start with the standard displacement-based formulation of finite elasticity. The boundary value problem of a nonlinear elastic body clamped on Γ_D consists in finding a displacement field $\boldsymbol{u}:\Omega\to\mathbb{R}^d$ with $\boldsymbol{u}|_{\Gamma_D}=\mathbf{0}$ so that

$$-\nabla\cdot \boldsymbol{F}\boldsymbol{s} \;=\; \mathbf{f}, \tag{6.8.1}$$

where $\mathbf{f}:\Omega\to\mathbb{R}^d$ denotes the body force, $\boldsymbol{s}:\Omega\to\mathbb{R}^{d\times d}$ is the second Piola-Kirchhoff tensor and $\boldsymbol{F}:\Omega\to\mathbb{R}^{d\times d}$ is the deformation gradient. The deformation gradient $\boldsymbol{F}$ is related to the displacement field $\boldsymbol{u}$ by $\boldsymbol{F}=\mathbf{1}+\nabla\boldsymbol{u}$. On the remaining part $\Gamma_N:=\partial\Omega\backslash\Gamma_D$ of the boundary $\partial\Omega$, the traction boundary condition is applied $\boldsymbol{F}\boldsymbol{s}\cdot\mathbf{n}=\boldsymbol{g}_N$. The second Piola-Kirchhoff tensor $\boldsymbol{s}$ is symmetric and is related to the deformation gradient by some constitutive relation. We assume that the material is hyperelastic and isotropic so that a stored energy function W exists with $\boldsymbol{s}=2\frac{\partial W(\boldsymbol{C})}{\partial \boldsymbol{C}}$, where $\boldsymbol{C}$ is the right Cauchy-Green strain tensor and is given by $\boldsymbol{C}=\boldsymbol{F}^T\boldsymbol{F}$. The energy function W depends on the right Cauchy-Green strain tensor and hence from it on the deformation gradient. The first Piola-Kirchhoff tensor $\boldsymbol{p}$ is related to the second Piola-Kirchhoff tensor $\boldsymbol{s}$ with the relation $\boldsymbol{p}=\boldsymbol{F}\boldsymbol{s}$, and hence defining $\tilde{W}(\boldsymbol{F}):=W(\boldsymbol{C})$, we can write $\boldsymbol{p}=\frac{\partial\tilde{W}(\boldsymbol{F})}{\partial\boldsymbol{F}}$ under the assumption of hyperelasticity. For the isotropic material the energy function W depends only on the three principal invariants I_C, II_C and III_C of $\boldsymbol{C}$, where $I_C=\mathrm{tr}\,(\boldsymbol{C}), II_C=\frac{1}{2}(\mathrm{tr}^{\,2}(\boldsymbol{C})-\mathrm{tr}\,(\boldsymbol{C}^2))$, and $III_C=\det(\boldsymbol{C})=J^2$ with $J:=\det(\boldsymbol{F})$. Further details on hyperelastic material laws can be found in [**168, 123, 21**]. If the material law satisfies the Saint-Venant Kirchhoff law, we have

$$W(\boldsymbol{C})=\frac{\lambda}{2}(\mathrm{tr}\,\boldsymbol{E})^2+\mu\mathrm{tr}\,(\boldsymbol{E}^2),\;\; \boldsymbol{s}=2\mu\boldsymbol{E}+\lambda\mathrm{tr}\,(\boldsymbol{E})\mathbf{1},$$

where $\boldsymbol{E}$ is the Green-Lagrange strain tensor and is defined as $\boldsymbol{E}=\frac{1}{2}(\boldsymbol{C}-\mathbf{1})$. For the material satisfying two-term Mooney-Rivlin law [**146**], we have

$$\begin{aligned} W(\boldsymbol{C})&=\lambda U(J)-\mu\ln(J)+c_1(I_C-3)+c_2(II_C-3), \text{ and}\\ \boldsymbol{s}&=\lambda U'(J)J\boldsymbol{C}^{-1}+2c_1\mathbf{1}+2c_2(\mathrm{tr}\,\boldsymbol{C}\mathbf{1}-\boldsymbol{C})-\mu\boldsymbol{C}^{-1}, \end{aligned} \tag{6.8.2}$$

where c_1 and c_2 are material constants such that $2(c_1+c_2)=\mu$. We recall that the standard neo-Hookean law is recovered with $c_2=0$, and $c_1=\frac{\mu}{2}$. In an equivalent form, the energy

function W and the second Piola-Kirchhoff stress $\boldsymbol{s}$ can be written as

$$W(\boldsymbol{C}) = \lambda\, U\,(J) + \frac{\mu}{2}\left[(1-c_m)\,(I_C - 3 - 2\ln(J)) + c_m\,(II_C - 3 - 2\ln(J))\right], \text{ and}$$
$$\boldsymbol{s} = \lambda U'(J) J \boldsymbol{C}^{-1} + \mu\left[(1-c_m)\left(\mathbf{1} - \boldsymbol{C}^{-1}\right) + c_m\left(\operatorname{tr}\boldsymbol{C}\mathbf{1} - \boldsymbol{C} - \boldsymbol{C}^{-1}\right)\right],$$

where $c_m = 0$ gives the standard neo-Hookean law. Comparing with (6.8.2), we obtain $c_1 = \frac{\mu}{2}(1-c_m)$, and $c_2 = \frac{\mu}{2}c_m$. The real-valued function U can be chosen at least in three ways:

$$U(J) = \tfrac{1}{4}(J^2 - 1 - 2\ln J),\ U(J) = \tfrac{1}{4}(J-1)^2 \text{ or } U(J) = \tfrac{1}{2}\ln^2 J.$$

Unless otherwise stated we use $U(J) = \frac{1}{4}(J^2-1-2\ln J)$ in our numerical results. Although $\boldsymbol{C}$, $\boldsymbol{E}$, $\boldsymbol{F}$, $\boldsymbol{s}$ and J are functions of $\boldsymbol{u}$, we will write them without the argument $\boldsymbol{u}$ for simplicity of notation.

In order to recast the problem (6.8.1) into a weak formulation, we define a Banach space $\mathbf{V} := \{\boldsymbol{u} \in W^{1,p}(\Omega)^d |\ \boldsymbol{u}|_{\Gamma_D} = \mathbf{0}\}$ with $p \geq 4$. The displacement-based formulation of boundary value problem of finite elastostatics with homogeneous Dirichlet boundary condition on Γ_D is to find a displacement field $\boldsymbol{u} \in \mathbf{V}$ with $\boldsymbol{u}_{|_{\Gamma_D}} = 0$ so that

$$A_{ne}(\boldsymbol{u}, \boldsymbol{v}) = \ell(\boldsymbol{v}), \quad \boldsymbol{v} \in \mathbf{V}, \tag{6.8.3}$$

where $A_{ne}(\boldsymbol{u}, \boldsymbol{v}) := \int_\Omega (\mathbf{1} + \nabla \boldsymbol{u})\boldsymbol{s} : \nabla \boldsymbol{v}\, dx$, and $\ell(\boldsymbol{v}) := \int_\Omega \mathbf{f}\cdot\boldsymbol{v}\, dx + \int_{\Gamma_N} \boldsymbol{g}_N \cdot \boldsymbol{v}\, d\sigma$. The existence of the solution of the problem (6.8.3) is studied in [**16**] under the assumption of poly-convex energy functions, see also [**64**]. Although depending on the relation of the energy function W with displacement field $\boldsymbol{u}$, different materials can be treated, we focus mainly on neo-Hookean and Mooney-Rivlin material laws.

6.8.1. Mixed formulations. As we discussed in the introduction of this chapter, there now exist many mixed formulations to treat linear and nonlinear elasticity in the nearly incompressible range. For an overview of some mixed formulations for the finite elasticity, we refer to [**56**]. We recall that the standard Hu-Washizu formulation for linear elastic problems is obtained by considering the constitutive equation, the strain-displacement equation and the equation of equilibrium in the weak form. In the nonlinear Hu-Washizu formulation considered in [**143, 97, 98**], the displacement, the first Piola-Kirchhoff stress tensor and the deformation gradient are regarded as independent variables. Different Hu-Washizu functionals are considered in [**121, 144**]. Here, we consider a three-field formulation with the displacement $\boldsymbol{u}$, the Kirchhoff stress $\boldsymbol{\tau}$ and the pressure p as independent variables. We note that the Kirchhoff stress $\boldsymbol{\tau}$ is related to the second Piola-Kirchhoff stress $\boldsymbol{s}$ with the relation $\boldsymbol{\tau} = \boldsymbol{F}\boldsymbol{s}\boldsymbol{F}^T$. We start with the three-field formulation where the displacement $\boldsymbol{u}$, the Kirchhoff stress $\boldsymbol{\tau}$ and the deformation gradient $\boldsymbol{F}$ are unknowns. Denoting the inverse of $\boldsymbol{F}^T$ by $\tilde{\boldsymbol{F}}$, this formulation in its strong form can be written as: given a body force $\mathbf{f} : \Omega \to \mathbb{R}^d$ and suitable boundary conditions on $\partial\Omega$, find $(\boldsymbol{u}, \boldsymbol{\tau}, \boldsymbol{F})$ so that

$$\begin{aligned} -\nabla\cdot(\boldsymbol{\tau}\tilde{\boldsymbol{F}}) &= \mathbf{f}, \\ \boldsymbol{\tau} &= \tfrac{\partial \tilde{W}(\boldsymbol{F})}{\partial \boldsymbol{F}}\boldsymbol{F}^T, \\ \boldsymbol{F} &= \mathbf{1} + \nabla \boldsymbol{u}. \end{aligned} \tag{6.8.4}$$

We point out that the first equation of (6.8.4) refers to the balance law, the second equation is the constitutive relation and the third one signifies the relation between the deformation gradient and the displacement field. We assume that the relation between the deformation gradient and the displacement is satisfied in the strong form and introduce the notation

$$G(\boldsymbol{u}) := \frac{\partial \tilde{W}(\boldsymbol{F})}{\partial \boldsymbol{F}} \boldsymbol{F}^T \big|_{\boldsymbol{F}=\mathbf{1}+\nabla \boldsymbol{u}}$$

so that the three-field formulation can be reduced to a two-field formulation. In this case, the weak form of the formulation (6.8.4) can be written as: find $(\boldsymbol{u}, \boldsymbol{\tau}) \in \mathbf{V} \times \boldsymbol{S}$ such that

$$\begin{array}{rcll} \int_\Omega \boldsymbol{\tau} : \nabla \boldsymbol{v} (\mathbf{1} + \nabla \boldsymbol{u})^{-1} \, dx & = & \ell(\boldsymbol{v}), & \boldsymbol{v} \in V, \\ \int_\Omega (\boldsymbol{\tau} - G(\boldsymbol{u})) : \boldsymbol{\zeta} \, dx & = & 0, & \boldsymbol{\zeta} \in \boldsymbol{S}. \end{array}$$

We also assume that the function G can be written as $G(\boldsymbol{u}) = G_1(\boldsymbol{u}) + \lambda G_2(J)\mathbf{1}$. Recalling the Mooney-Rivlin material law, the functions G_1 and G_2 are given by

$$G_1(\boldsymbol{u}) = 2c_1 \boldsymbol{B}(\boldsymbol{u}) + 2c_2(\operatorname{tr} \boldsymbol{B}(\boldsymbol{u}) \boldsymbol{B}(\boldsymbol{u}) - \boldsymbol{B}^2(\boldsymbol{u})) - \mu \mathbf{1}, \; G_2(J) = U'(J) J,$$

where $\boldsymbol{B}(\boldsymbol{u})$ is the left Cauchy-Green tensor and is defined by $\boldsymbol{B}(\boldsymbol{u}) := (\mathbf{1} + \nabla \boldsymbol{u})(\mathbf{1} + \nabla \boldsymbol{u})^T$. Using $c_1 = \frac{\mu}{2}(1 - c_m)$, and $c_2 = \frac{\mu}{2} c_m$, we get $G_1(\boldsymbol{u}) = \mu(1 - c_m)\boldsymbol{B}(\boldsymbol{u}) + \mu c_m(\operatorname{tr} \boldsymbol{B}(\boldsymbol{u}) \boldsymbol{B}(\boldsymbol{u}) - \boldsymbol{B}^2(\boldsymbol{u})) - \mu \mathbf{1}$. Since $J \to 1$ and $\lambda \to \infty$ for the nearly incompressible material, $G_2(J) \to \mathbf{0}$. This assumption is crucial for developing a robust numerical scheme for a nearly incompressible material. To treat the nearly incompressible material, we introduce a pressure-like variable $p \in L^2(\Omega)$ and write an another variational equation

$$\int_\Omega (p - \lambda G_2(J)) q \, dx = 0, \; q \in L^2(\Omega).$$

A similar pressure-like variable is introduced in [**45**] to study the convergence of finite element approximations of the nonlinear elasticity problems in the incompressible limit. Making use of the variable p, we define an α-dependent function $\tilde{G}(\boldsymbol{u}, p, \alpha) = G_1(\boldsymbol{u}) + \mu \alpha G_2(J)\mathbf{1} + (1 - \frac{\mu\alpha}{\lambda}) p \mathbf{1}$ to arrive at an α-dependent three-field formulation involving the displacement $\boldsymbol{u}$, the Kirchhoff stress $\boldsymbol{\tau}$ and the pressure p. Combining all these three variational equations, our problem is: given a body force $\boldsymbol{f}$ and suitable boundary conditions on $\partial\Omega$ find $(\boldsymbol{u}, \boldsymbol{\tau}, p) \in \mathbf{V} \times \boldsymbol{S} \times L^2(\Omega)$ so that

$$\begin{array}{rcll} \int_\Omega \boldsymbol{\tau} : \nabla \boldsymbol{v} (\mathbf{1} + \nabla \boldsymbol{u})^{-1} \, dx & = & \ell(\boldsymbol{v}), & \boldsymbol{v} \in V, \\ \int_\Omega (\boldsymbol{\tau} - \tilde{G}(\boldsymbol{u}, p, \alpha)) : \boldsymbol{\zeta} \, dx & = & 0, & \boldsymbol{\zeta} \in \boldsymbol{S}, \\ \int_\Omega (p - \lambda G_2(J)) q \, dx & = & 0, & q \in L^2(\Omega). \end{array} \tag{6.8.5}$$

In the following, we concentrate on the three-field formulation (6.8.5). In contrast to the Hu-Washizu type formulation given in [**98, 141**], we consider the symmetric Kirchhoff stress as an independent variable. Working with a symmetric tensor as an unknown leads to a symmetric formulation and a reduction of the number of unknowns. Furthermore, we point out that the first and second Piola-Kirchhoff stress tensors are the rational functions of the displacement and the displacement gradient, whereas the Kirchhoff stress depends polynomially on the displacement and displacement gradient. Since the stress will be discretized by using some piecewise polynomial space $\boldsymbol{S}_h$, it is more reasonable to work with the Kirchhoff stress rather than first or second Piola-Kirchhoff stresses.

6.8.2. Discretizations. From the linear analysis, see also [**102, 41**], it is crucial to project $G_2(J)$ onto piecewise constant functions to obtain a robust numerical scheme for the nearly incompressible case based on bilinear or trilinear finite element interpolations for displacements. Therefore, the pressure is discretized by using piecewise constant functions denoted by R_h, and the space of stress is discretized by defining a finite-dimensional space $\boldsymbol{S}_\square$ on a reference element $\hat{K}$ as before. Both stress and pressure variables are defined locally on each element and no continuity conditions apply at the element boundaries. Defining $\tilde{A}_d$ for $d = 2$ and $d = 3$ with

$$\tilde{A}_2 := \operatorname{span}\begin{bmatrix} \hat{x} & \hat{y} & 0 & 0 \\ 0 & 0 & \hat{x} & \hat{y} \\ 0 & 0 & 0 & 0 \end{bmatrix},\ \tilde{A}_3 := \operatorname{span}\begin{bmatrix} \hat{x} & \hat{y} & \hat{z} & 0 & 0 & 0 & 0 & 0 & 0 & 0 & 0 & 0 \\ 0 & 0 & 0 & \hat{x} & \hat{y} & \hat{z} & 0 & 0 & 0 & 0 & 0 & 0 \\ 0 & 0 & 0 & 0 & 0 & 0 & \hat{x} & \hat{y} & \hat{z} & 0 & 0 & 0 \\ 0 & 0 & 0 & 0 & 0 & 0 & 0 & 0 & 0 & \hat{z} & 0 & 0 \\ 0 & 0 & 0 & 0 & 0 & 0 & 0 & 0 & 0 & 0 & \hat{x} & 0 \\ 0 & 0 & 0 & 0 & 0 & 0 & 0 & 0 & 0 & 0 & 0 & \hat{y} \end{bmatrix},$$

respectively and using the definitions of A_d, B_d, C_d and D_d from (6.3.1), we are interested in the following choices of $\boldsymbol{S}_h^i$, $1 \le i \le 5$:

TABLE 6.2. Different cases for the discrete spaces, $d = 2, 3$

Case	I	II	III	IV	V
$\boldsymbol{S}_\square$	$\mathfrak{I}_d + A_d$	$\mathfrak{I}_d + \tilde{A}_d$	$\mathfrak{I}_d + C_d$	$\mathfrak{I}_d + A_d + D_d$	$\mathfrak{I}_d + A_d + B_d + D_d$

As before, $\mathfrak{I}_d$ stands for the span of the identity matrix of size $\frac{d(d+1)}{2} \times \frac{d(d+1)}{2}$.

Defining the discrete determinant $J_h := \det(\mathbf{1} + \nabla \boldsymbol{u}_h)$ and utilizing the discrete spaces introduced above, we can write our discrete three-field variational formulation as: find $(\boldsymbol{u}_h, \boldsymbol{\tau}_h, p_h) \in \mathbf{V}_h \times \boldsymbol{S}_h \times R_h$ so that

$$\begin{array}{lcll} \int_\Omega \boldsymbol{\tau}_h : \nabla \boldsymbol{v}_h (\mathbf{1} + \nabla \boldsymbol{u}_h)^{-1}\, dx & = & \ell(\boldsymbol{v}_h), & \boldsymbol{v}_h \in \mathbf{V}_h, \\ \int_\Omega (\boldsymbol{\tau}_h - \tilde{G}(\boldsymbol{u}_h, p_h, \alpha)) : \boldsymbol{\zeta}_h\, dx & = & 0, & \boldsymbol{\zeta}_h \in \boldsymbol{S}_h, \\ \int_\Omega (p_h - \lambda G_2(J_h))) q_h\, dx & = & 0, & q_h \in R_h. \end{array} \tag{6.8.6}$$

We denote the projection onto the space of piecewise constant functions with respect to the mesh $\mathcal{T}_h$ by Π_h so that the pressure p_h can be written as $p_h = \lambda \Pi_h G_2(J_h)$. Furthermore, static condensation of the stress from (6.8.6) yields the following displacement-based formulation.

LEMMA 6.18. *The displacement-based formulation of* (6.8.6) *is given by*

$$\int_\Omega P_{S_h} \tilde{G}(\boldsymbol{u}_h, p_h, \alpha) : \nabla \boldsymbol{v}_h (\mathbf{1} + \nabla \boldsymbol{u}_h)^{-1}\, dx = \ell(\boldsymbol{v}_h),$$

where $p_h = \lambda \Pi_h G_2(J_h)$.

LEMMA 6.19. *If for* $\boldsymbol{\tau}_h \in S_h$, $(\boldsymbol{\tau}_h)_{ii}, 1 \le i \le N$, *are piecewise constant functions with respect to* $\mathcal{T}_h$, *the numerical solution is independent of* α.

PROOF. In this case, $P_{\boldsymbol{S}_h}(G_2(J_h)\mathbf{1}) = \Pi_h G_2(J_h)\mathbf{1}$, and we have $P_{\boldsymbol{S}_h}\tilde{G}(\boldsymbol{u}_h, p_h, \alpha) = P_{\boldsymbol{S}_h} G(\boldsymbol{u}_h)$. The proof now follows by using the displacement-based formulation from Lemma 6.18. □

Lemma 6.19 tells that the numerical solution is independent of α for Case III. We remind that we have an α-independent numerical solution for Cases II, III and V for the linear and geometrically nonlinear elasticity with Saint-Venant Kirchhoff law. We recall that Assumption 9 is crucial to get a robust and optimal numerical scheme in the linear case. In case of our nonlinear mixed formulation (6.8.6), the approximation property of the stress is still essential, however, it is not necessary that $\mathrm{sph}_h \boldsymbol{S}_{h|_K} \subset \mathcal{I}_d$. The reason behind this is that we have decomposed the Kirchhoff stress into two parts, and the part involving the determinant of the deformation gradient is already projected onto the space of piecewise constant functions. Therefore, in addition to these five cases, more cases can also be considered.

6.9. Numerical results

In this section, we illustrate the performance of the formulation discussed in the preceding sections in some numerical tests. In particular, we show the locking free response in the incompressible limit of the proposed formulation by comparing the results with the analytical solution and the results obtained from the standard displacement approach. Our examples in two and three dimensions are based on four-noded quadrilateral and eight-noded hexahedral elements with standard bilinear and trilinear interpolation, respectively, of the displacement field. Furthermore, plane strain is assumed in two-dimensional examples.

6.9.1. Numerical results in small strain elasticity. In this subsection, numerical examples are presented illustrating some applications of the modified Hu-Washizu formulation in linear and nonlinear elasticity with Saint-Venant Kirchhoff law. One example with a typical shear locking situation is also considered.

Example 1: Cook's membrane problem. In this popular benchmark problem [**143, 97, 101**], we set $\Omega := \mathrm{conv}\{(0,0),(48,44),(48,60),(0,44)\}$, where $\mathrm{conv}\xi$ is the convex hull of the set ξ. The left boundary of the tapered panel Ω is clamped, and the right one is subjected to an in-plane shearing load of $100N$ along the y-direction, as shown in Figure 6.2(a). The material properties are taken to be $E = 250$ and $\nu = 0.4999$, so that a nearly incompressible response is obtained. The relation between Lamé parameters λ and μ, and Young's modulus E and Poisson ratio ν is given by the equation(2.4.3). In this example and in the forthcoming examples, if the units of measurement are not specified, the measurement units should be scaled consistently. The vertical tip displacement at point T is computed for different cases and different refinement levels. The initial triangulation is shown in Figure 6.2 (a). The numerical results using the linear and geometrically nonlinear model with Saint-Venant Kirchhoff law are given in Tables 6.3 and 6.4, respectively. As can be seen from these tables the standard displacement approach and the standard Hu-Washizu formulation ($\alpha = \gamma$) with stress and strain spaces given in Cases I and IV exhibit locking whereas all other cases show rapid convergence. We also observe the coarse mesh accuracy of Cases II and III. We recall that $\alpha = \gamma$ corresponds to the standard Hu-Washizu formulation.

Example 2: Square beam. In the second example, we consider a linear elastic square beam $\Omega := (0,2) \times (0,2)$, which is fixed in the x-direction at the point $(0,2)$ and fixed

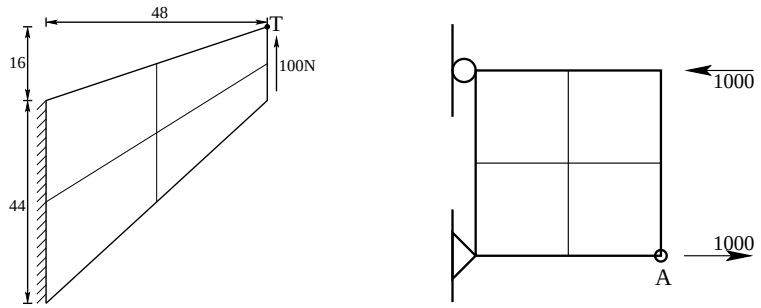

Figure 6.2: (a) Cook's membrane problem with initial triangulation; (b) the square beam problem with a mesh of four squares

TABLE 6.3. Vertical tip displacement at point T with linear elasticity, Example 1

	$\alpha=\gamma$		α independent			$\alpha=\frac{1}{4}$		$\alpha=-\frac{1}{4}$		$\alpha=0$		Q_1P_0
lev	$Q_1\equiv$ IV	I	II	III	V	I	IV	I	IV	I	IV	
0	2.07	2.08	5.40	5.64	4.42	4.18	3.76	4.53	3.97	4.34	3.86	4.31
1	2.10	2.12	6.73	7.02	6.24	5.93	5.60	6.20	5.83	6.06	5.71	6.28
2	2.15	2.22	7.59	7.52	7.17	7.00	6.85	7.13	6.97	7.06	6.91	7.21
3	2.32	2.54	7.59	7.68	7.53	7.45	7.40	7.50	7.45	7.48	7.42	7.55
4	2.84	3.39	7.69	7.73	7.67	7.63	7.62	7.66	7.64	7.64	7.63	7.68
5	4.03	4.94	7.74	7.75	7.73	7.71	7.70	7.72	7.71	7.71	7.71	7.73

TABLE 6.4. Vertical tip displacement at point T with geometrically nonlinear elasticity, Example 1

	$\alpha=\gamma$		α independent			$\alpha=\frac{1}{4}$		$\alpha=-\frac{1}{4}$		$\alpha=0$		Q_1P_0
lev	Q_1	I	II	III	V	I	IV	I	IV	I	IV	
0	2.07	2.08	4.83	5.10	4.08	3.96	3.62	4.25	3.79	4.02	3.63	4.07
1	2.10	2.12	5.74	6.00	5.44	5.25	5.03	5.44	5.19	5.29	5.06	5.52
2	2.15	2.21	6.16	6.32	6.06	5.96	5.87	6.04	5.95	5.97	5.89	6.12
3	2.31	2.52	6.33	6.41	6.30	6.25	6.23	6.29	6.26	6.26	6.23	6.33
4	2.80	3.29	6.40	6.44	6.39	6.37	6.36	6.39	6.38	6.37	6.36	6.40
5	3.85	4.53	6.43	6.45	6.43	6.42	6.42	6.43	6.42	6.42	6.42	6.44

in both directions at the origin. A linearly varying horizontal force is applied in the x-direction along the boundary $x=2$, with resultant point forces 1000 at $(2,0)$ and -1000 at $(2,2)$ (Figure 6.2 (b)), see also [**172**]. In Table 6.5, we present the vertical tip displacement at the point $A:=(2,0)$ for $E=1500$ and for different values of Poisson's ratio ν, where ν_1,ν_2,ν_3 and ν_4 are given by $0.4, 0.49, 0.499$ and 0.4999, respectively. The exact vertical displacement at A is $4(1-\nu^2)$.

As in the previous example, the standard displacement approach and the standard Hu-Washizu formulation with Cases I and IV show the locking effect whereas all other cases exhibit stable behavior. In particular, Cases II, V and Q_1P_0 give better numerical results. Furthermore, the numerical results from Case II are almost exact.

TABLE 6.5. Vertical tip displacement at point A with linear elasticity, Example 2

	$\alpha=\gamma$		α independent			$\alpha=\frac{1}{4}$		$\alpha=-\frac{1}{4}$		$\alpha=0$		Q_1P_0
ν	Q_1	I	II	III	V	I	IV	I	IV	I	IV	
ν_1	2.64	2.80	3.36	4.07	3.13	3.04	2.85	3.13	2.92	3.08	2.88	3.45
ν_2	0.75	0.76	3.04	3.74	2.86	2.39	2.27	2.60	2.47	2.49	2.36	3.23
ν_3	0.09	0.09	3.00	3.70	2.83	2.30	2.19	2.53	2.41	2.41	2.29	3.20
ν_4	0.01	0.01	3.00	3.69	2.82	2.29	2.18	2.53	2.40	2.40	2.29	3.20

Example 3: Rectangular beam. In this third example, we consider a linear elastic beam of rectangular size subjected to a couple at one end, as shown in the left picture of Figure 6.3. Along the edge $x=0$, the horizontal displacement and vertical surface traction are zero. At the point $(0,0)$, the vertical displacement is also zero. The exact solution is given by $\boldsymbol{u} := (u_1, u_2)$ with

$$u_1(x,y) = \frac{2f(1-\nu^2)}{El} x\left(\frac{l}{2} - y\right), \text{ and } \quad u_2(x,y) = \frac{f(1-\nu^2)}{El}\left[x^2 + \frac{\nu}{1-\nu} y(y-l)\right].$$

We set $L=10$, $l=2$, $E=1500$, $\nu=0.4999$, and $f=3000$. We have shown the setting of the problem in the left picture of Figure 6.3. We further investigate the behavior of the solution with respect to α for Cases I and IV with two different meshes illustrated in Figure 6.3. The variation with $\frac{\alpha}{2}$ of the absolute error of the vertical and horizontal tip displacements at the top right-hand corner (that is, at the point (10,2) in the left picture of Figure 6.3), is shown in Figure 6.4 for Cases I and IV, for the 2×1 mesh, and in Figure 6.5 for the 10×2 mesh. To avoid the singularity at $\alpha=-1$, we use the projection-based formulation derived in Lemma 6.10. For $\alpha=-2$, the Case IV reduces to the Case III. As

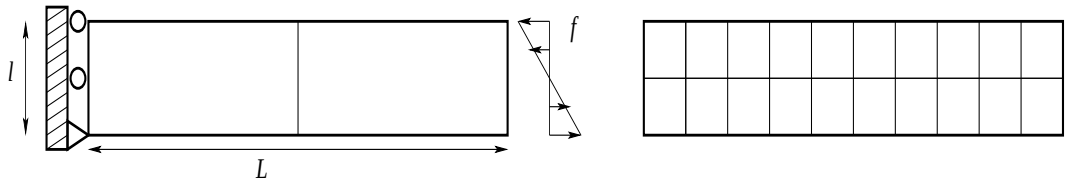

Figure 6.3: The Cantilever beam with coarse mesh (and problem setting), (left) and fine mesh (right)

can be seen from Figures 6.4 and 6.5, the locking effect increases for larger α, and there is a singularity at $\alpha=-2$ for Case I with the coarse mesh. In the left and right pictures of Figure 6.6, we show the discretization errors in the L^2- and H^1-norms for the different cases of the modified Hu-Washizu formulation. To obtain the discretization errors, we start with the initial triangulation shown in the right picture of Figure 6.3 and refine uniformly. We can see that Case II shows an excellent behavior in comparison to all other cases.

Example 4: Bending of a clamped plate. In this example [**150**], we consider a clamped plate subjected to bending. We test the performance of our formulation for a bending dominated condition of a thin plate of dimension $2.0mm \times 2.0mm \times 0.01mm$.

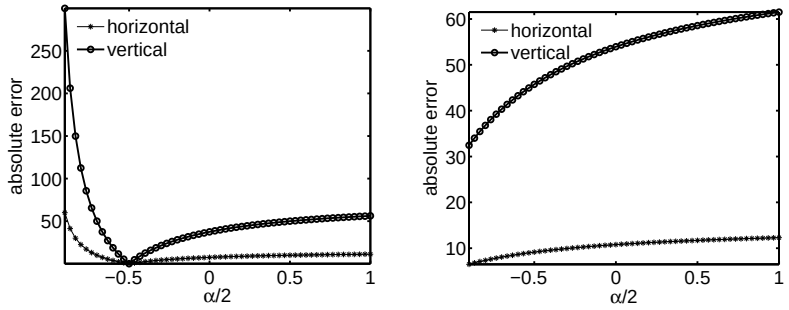

Figure 6.4: Tip displacement error versus $\frac{\alpha}{2} \in (-1, 1]$ for the coarse mesh, Cases I (left) and Case IV (right)

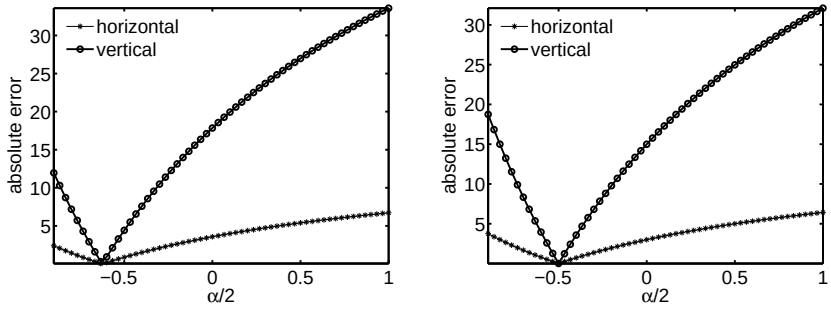

Figure 6.5: Tip displacement error versus $\frac{\alpha}{2} \in (-1, 1]$ for the fine mesh, Case I (left) and Case IV (right)

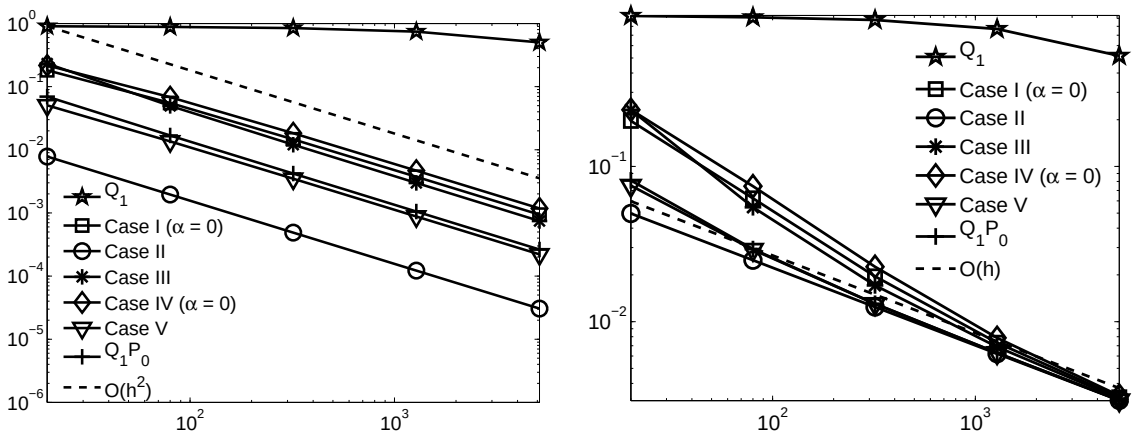

Figure 6.6: Error plot versus number of elements, L^2-norm (left) and H^1-norm (right), rectangular beam

The plate is clamped along the complete boundary, and it is subjected to a uniformly distributed pressure $-100.0\, N/mm^2$ on the top surface [**120**]. A linear elastic material is

considered with Young's modulus $E = 1.7472 \cdot 10^7 N/mm^2$ and Poisson's ratio $\nu = 0.3$. Taking advantage of the symmetry of the problem, only one fourth of the plate is discretized

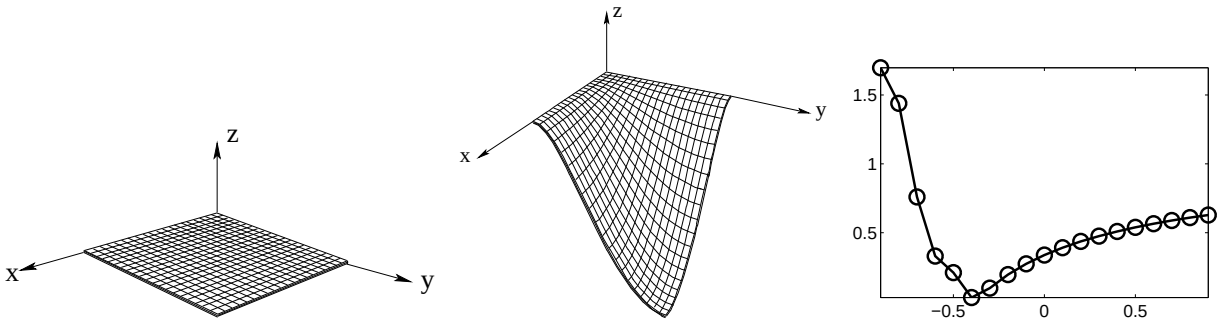

Figure 6.7: Problem setting (left), deformed mesh (middle) and relative error versus $\frac{\alpha}{2}$ with Case I (right), Example 4

as shown in Figure 6.7, with 2 elements in thickness direction. The results obtained using the proposed mixed formulation are compared with the results obtained using the standard Q_1 and Q_1P_0 formulation. In Table 6.6, the vertical displacement of the top central point of the plate is shown, whereas the variation of the deflection with respect to the thickness of the plate is shown in Table 6.7. As can be seen from both tables Case I with $\alpha = 0$ and Case II show an excellent behavior in this example, whereas all other formulations show extreme locking effects. The exact solution of the problem is calculated using the classical plate theory, see [**150**].

TABLE 6.6. Vertical displacement at the center of the plate, the exact solution is -1.264

elements	I ($\alpha = 0$)	II	III	Q_1P_0	Q_1
8	-1.1047	-1.153	-2.232e-03	-2.117e-03	-2.117e-03
50	-1.1788	-1.227	-1.217e-02	-1.203e-02	-1.202e-02
72	-1.1850	-1.233	-1.731e-02	-1.716e-02	-1.713e-02
200	-1.1974	-1.246	-4.655e-02	-4.619e-02	-4.597e-02
450	-1.2038	-1.252	-1.006e-01	-9.942e-02	-9.839e-02
800	-1.2071	-1.256	-1.703e-01	-1.671e-01	-1.642e-01
1250	-1.2090	-1.258	-2.507e-01	-2.440e-01	-2.379e-01

In a second step, we consider a nearly incompressible plate keeping Young's modulus the same and thickness $0.01mm$. The numerical solution at the center of the plate for Poisson's ratio $\nu = 0.4999$ is tabulated in Table 6.8. Case II and Case I ($\alpha = 0$) work well whereas all other cases show locking.

In the right picture of Figure 6.7, the relative error of the solution for the nearly incompressible plate using Case I (mesh $10 \times 10 \times 2$) is plotted with respect to the parameter $\alpha/2$. The error is calculated with respect to the reference solution with Case II using a very fine mesh. We find the minimum of the error when $\alpha \approx -0.8$, and increasing locking effect can be observed when α becomes larger.

TABLE 6.7. Vertical displacement at the center of the plate with respect to the thickness

thickness	exact	I ($\alpha = 0$)	II	III	Q_1P_0	Q_1
3e-01	-4.681e-05	-6.119e-05	-6.126e-05	-7.153e-05	-6.313e-05	-5.736e-05
2e-01	-1.580e-04	-1.757e-04	-1.793e-04	-2.063e-04	-1.801e-04	-1.617e-04
1e-01	-1.264e-03	-1.251e-03	-1.299e-03	-1.237e-03	-1.094e-03	-9.931e-04
9e-02	-1.734e-03	-1.702e-03	-1.768e-03	-1.594e-03	-1.418e-03	-1.291e-03
8e-02	-2.468e-03	-2.405e-03	-2.500e-03	-2.095e-03	-1.877e-03	-1.718e-03
7e-02	-3.684e-03	-3.567e-03	-3.708e-03	-2.818e-03	-2.548e-03	-2.346e-03
6e-02	-5.851e-03	-5.631e-03	-5.856e-03	-3.887e-03	-3.556e-03	-3.303e-03
5e-02	-1.011e-02	-9.684e-03	-1.007e-02	-5.524e-03	-5.126e-03	-4.815e-03
4e-02	-1.975e-02	-1.884e-02	-1.960e-02	-8.139e-03	-7.682e-03	-7.315e-03
3e-02	-4.681e-02	-4.451e-02	-4.631e-02	-1.262e-02	-1.213e-02	-1.174e-02
2e-02	-1.580e-01	-1.499e-01	-1.559e-01	-2.143e-02	-2.097e-02	-2.062e-02
1e-02	-1.264	-1.197	-1.246	-4.655e-02	-4.619e-02	-4.597e-02

TABLE 6.8. Vertical displacement at the center of the nearly incompressible clamped plate

Number of Elements	Case I ($\alpha = 0$)	Case II	Case III	Q_1	Q_1P_0
$25 \times 25 \times 2$	-0.7197	-1.0024	-0.2729	-0.0036	-0.2629
$20 \times 20 \times 2$	-0.7101	-0.9923	-0.1888	-0.0036	-0.1831
$15 \times 15 \times 2$	-0.6943	-0.9756	-0.1134	-0.0035	-0.1106
$10 \times 10 \times 2$	-0.6637	-0.9428	-0.0531	-0.0032	-0.0521
$6 \times 6 \times 2$	-0.6061	-0.8791	-0.0200	-0.0028	-0.0196
$5 \times 5 \times 2$	-0.5789	-0.8490	-0.0140	-0.0026	-0.0138
$2 \times 2 \times 2$	-0.2589	-0.4894	-0.0026	-0.0014	-0.0024

Example 5: Thick walled sphere under internal pressure. In this numerical example, a thick walled sphere having inner radius $r_i = 7.5mm$ and outer radius $r_e = 10mm$ subjected to a uniform internal pressure $P = 1N/mm^2$ is considered [**150, 97**]. The linear elastic material is assumed with modulus of elasticity $E = 250N/mm^2$, and different Poisson's ratios ν as shown in Table 6.9. Only one octant of the sphere is discretized as shown in Figure 6.8 with symmetrical boundary conditions. The normalized radial displacement (with respect to the analytical solution [**150**]) at point A is compared using different discretizations in Table 6.9. As expected, standard trilinear elements show locking in the incompressible range of ν, while all other formulations show a good behavior.

Example 6: Arch subjected to bending load. In this numerical example, the formulation is tested for bending condition with linear and geometrically nonlinear elasticity. The fixed circular arch beam with $\theta_r = 60\,^\circ$, $t = 0.1m$ and $r = 1m$ is considered as shown in Figure 6.9. The beam is subjected to a uniformly distributed load $P = -25N/m$ in radial direction on the upper boundary in a range $|x| \leq 0.09151$. For the geometrically nonlinear case, quasi-static finite element computation is performed where the load is applied in 20 equal increment steps. The deflected finite element mesh obtained for $\nu = 0.4999$ using

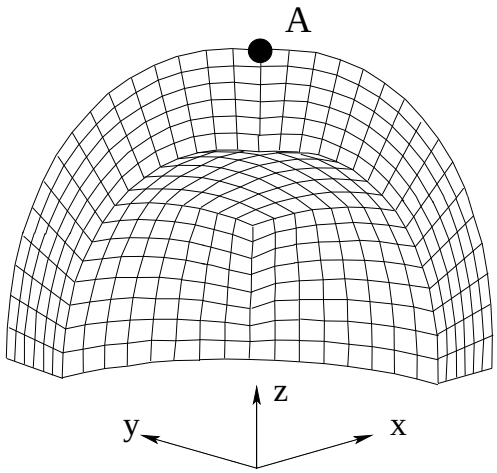

Figure 6.8: Problem setting for Example 5

TABLE 6.9. The normalized radial displacements for thick walled sphere

Poisson's ratio	Case I $\alpha = 0$	Case II	Case III	Q_1	Q_1P_0
0.490000	0.9927	0.9915	0.9943	0.9921	0.9963
0.499000	0.9921	0.9914	0.9942	0.6918	0.9963
0.499900	0.9921	0.9913	0.9942	0.1834	0.9962
0.499990	0.9921	0.9913	0.9942	0.0200	0.9962
0.499999	0.9921	0.9913	0.9942	0.0002	0.9962

Case II of the mixed formulation is shown in the right picture of Figure 6.9. We show the load-deflection curves for linear and geometrically nonlinear elasticity with Saint-Venant Kirchhoff law with $E = 250N/m^2$ and $\nu = 0.4999$ in Figure 6.10. We can see that the geometrically nonlinear case yields larger deformation than the linear elastic case in this example.

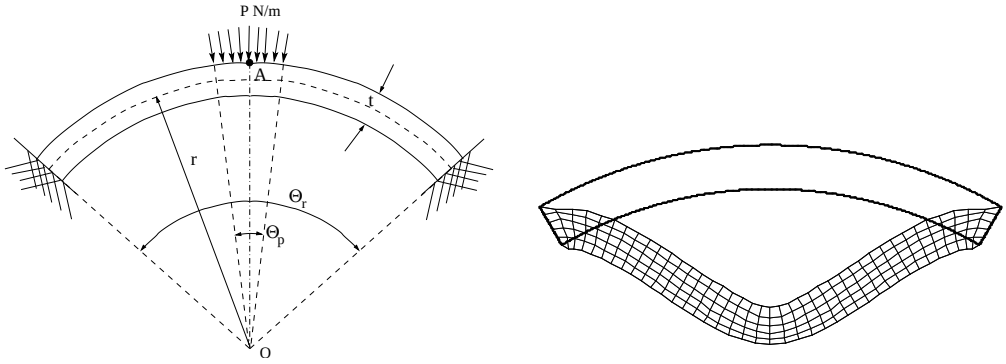

Figure 6.9: Problem setting and deformed mesh, circular arch

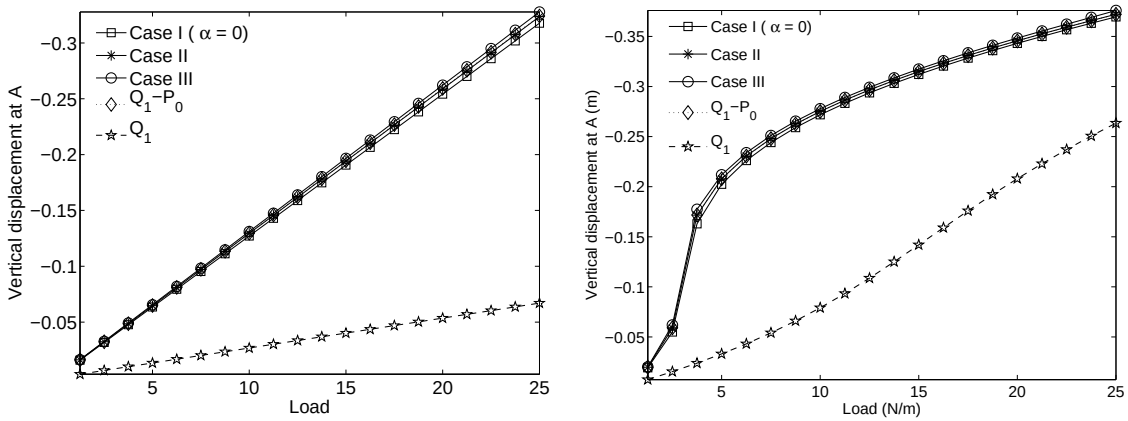

Figure 6.10: Load-deflection curve for circular arch, linear case (left) and geometrically nonlinear case (right)

In Tables 6.10 and 6.11, the vertical deflection at the central point A is compared for different formulations with linear and geometrically nonlinear elasticity, respectively. All cases of our mixed formulations show good behavior while the standard Q_1 formulation shows locking as ν tends to 0.5.

TABLE 6.10. Numerical results for circular arch, linear case

ν	Case I ($\alpha = 0$)	Case II	Case III	Q_1	Q_1P_0
0.49000	-0.324	-0.329	-0.333	-0.272	-0.329
0.49900	-0.318	-0.324	-0.328	-0.143	-0.325
0.49990	-0.318	-0.324	-0.328	-0.067	-0.324
0.49999	-0.318	-0.324	-0.328	-0.032	-0.324

TABLE 6.11. Numerical results for circular arch, geometrically nonlinear case

ν	Case I ($\alpha = 0$)	Case II	Case III	Q_1	Q_1P_0
0.49000	-0.371	-0.373	-0.377	-0.352	-0.373
0.49900	-0.370	-0.372	-0.376	-0.263	-0.372
0.49990	-0.369	-0.372	-0.377	-0.101	-0.372
0.49999	-0.369	-0.372	-0.376	-0.056	-0.372

6.9.2. Numerical results in large strain elasticity. In this subsection, we present some numerical results in finite elasticity using the proposed mixed formulation. In particular, all numerical examples are computed applying the formulation (6.8.6) for neo-Hookean and Mooney-Rivlin laws.

Example 1: Cook's membrane problem. We apply our new nonlinear mixed formulation to the Cook's membrane problem considered in the last section. Keeping the problem setting and material parameters exactly the same, we compute the vertical tip

displacement at the top right corner of the membrane by using different cases with neo-Hookean and Mooney-Rivlin constitutive laws. In case of Mooney-Rivlin material law, we set $c_m = 0.25$. The computed vertical tip displacement using different cases of our mixed formulation with neo-Hookean and Mooney-Rivlin laws are provided in Tables 6.12 and 6.13, respectively. These tables show that the standard formulation completely locks, whereas all cases of our mixed formulation converge rapidly. In particular, Case I and III show extremely good behavior from the beginning.

TABLE 6.12. Vertical tip displacement at the top right corner of Cook's membrane, neo-Hookean

level	Q_1	Case I	Case II	Case III	Case IV	Case V	Q_1P_0
		$\alpha = 0$	$\alpha = 0$		$\alpha = 0$	$\alpha = 0$	
0	2.0337	5.8166	4.6998	5.2442	4.5828	4.0429	4.0385
1	2.0818	6.2960	5.9552	6.2106	5.9041	5.6435	5.6421
2	2.1355	6.5445	6.4476	6.5381	6.4146	6.3300	6.3296
3	2.2917	6.6375	6.6092	6.6405	6.5913	6.5665	6.5665
4	2.7522	6.6769	6.6680	6.6790	6.6591	6.6516	6.6516
5	3.7658	6.6946	6.6914	6.6957	6.6871	6.6846	6.6846

TABLE 6.13. Vertical tip displacement at the top right corner of Cook's membrane, Mooney-Rivlin

level	Q_1	Case I	Case II	Case III	Case IV	Case V
		$\alpha = 0$	$\alpha = 0$		$\alpha = 0$	$\alpha = 0$
0	2.7105	6.8317	5.4527	6.8603	5.7123	4.9284
1	2.7706	7.8366	7.3247	7.9541	7.4433	7.0226
2	2.8271	8.2558	8.0998	8.3231	8.1220	7.9799
3	2.9849	8.4059	8.3602	8.4359	8.3586	8.3166
4	3.4646	8.4661	8.4520	8.4789	8.4481	8.4353
5	4.5907	8.4921	8.4873	8.4979	8.4847	8.4804

In Figure 6.11, we show the relative error of the vertical displacement at T with respect to α using the Case I of our mixed formulation for both neo-Hookean and Mooney-Rivlin laws after refining the initial mesh two times. The error is calculated using a reference solution from Case I ($\alpha = 0$) with a very fine mesh. We observe that the locking increases with the increase in α.

Example 2: Nearly incompressible block under compression. In this example, we analyze the performance of our mixed formulation when applied to a problem with strong compression, see [**134, 120**]. A nearly incompressible block $\Omega := (-1mm, 1mm)^3$ is under the compression force applied on the middle part of the top surface. Due to symmetry only an octant of the structure is discretized as shown in the left picture of Figure 6.12 so that symmetric boundary conditions are considered except on the top surface, where the nodes are constrained along the x- and y-directions. We compute the final solution

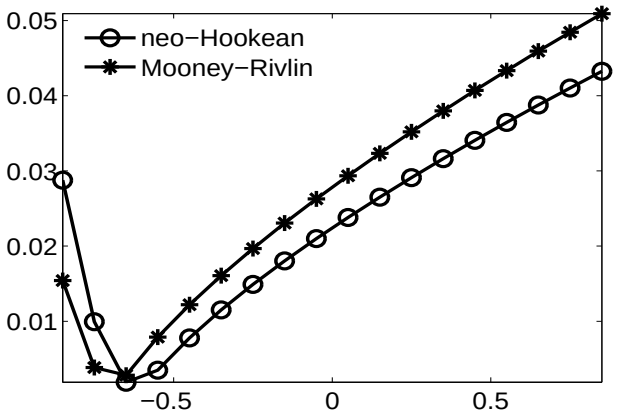

Figure 6.11: The relative error in the vertical tip displacement versus $\frac{\alpha}{2}$ with neo-Hookean and Mooney-Rivlin laws, Example 1

in 80 quasi-static steps by applying compression force $p = 4N/mm^2$ on the grey area in each step. The material model used is the compressible neo-Hookean material model with material parameters $\mu = 80.194N/mm^2$ and $\lambda = 400889.806N/mm^2$. We have shown the deformations of the grid in the middle and right pictures of Figure 6.12, where the solutions are computed using Case I ($\alpha = 0$) of the mixed formulation and the standard displacement formulation, respectively. As can be seen from these pictures, the standard displacement formulation shows extreme locking whereas the proposed mixed formulation yields good numerical results.

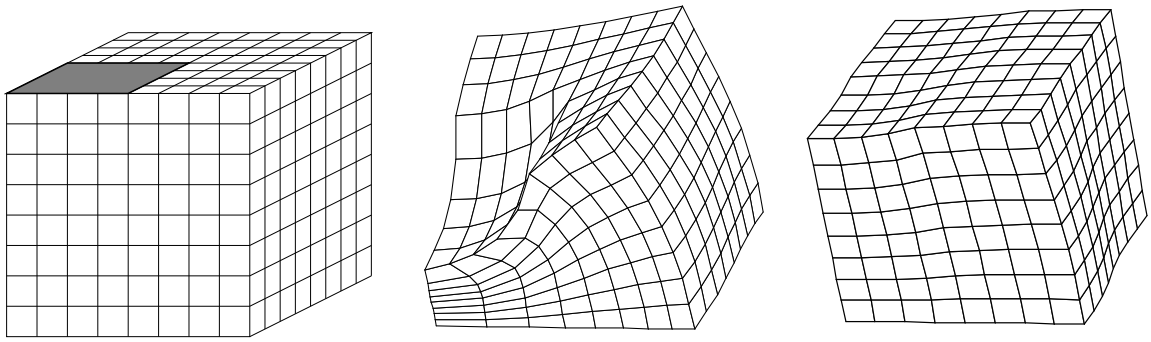

Figure 6.12: Problem setting (left), deformed shape with Case I ($\alpha = 0$) of the mixed formulation (middle) and deformed shape with the standard displacement formulation (right), nearly incompressible block

We have given the vertical tip displacement at the point $(0, 0, 1)$ at different load steps with respect to different levels of refinement in Table 6.14, where we can see a good convergence behavior of the numerical approximation with our mixed formulation.

Example 3: Bending of a cylindrical shell. In this example, the proposed three-dimensional finite element formulation is used to compute the deformation of a cylindrical shell under bending. Taking advantage of the symmetry of the problem, only one quarter of the cylinder is modeled. In addition to the symmetric boundary conditions, the cylinder

TABLE 6.14. Convergence of numerical results with Case I (with $\alpha = 0$ and neo-Hookean material law), Example 2

Number of Elements Load step	8	16	64	256
10	-0.1326	-0.1107	-0.1102	-0.1101
20	-0.2663	-0.2221	-0.2207	-0.2203
30	-0.3961	-0.3315	-0.3281	-0.3272
40	-0.5171	-0.4365	-0.4286	-0.4265
50	-0.6256	-0.5343	-0.5188	-0.5145
60	-0.7194	-0.6220	-0.5973	-0.5894
70	-0.7981	-0.6976	-0.6644	-0.6511
80	-0.8626	-0.7605	-0.7214	-0.7012

is pinched by a radial load along the outer edge, and the external lower edge of the cylinder is fixed in the y-direction. The load is applied as a uniformly distributed force on the upper longitudinal section. The geometrical dimensions and material data used are given in Table 6.15.

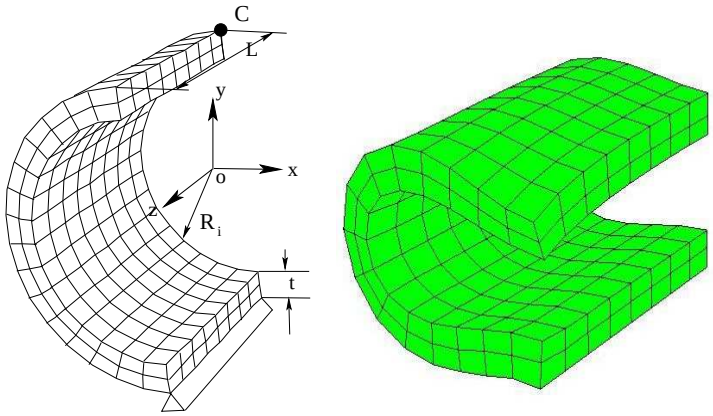

Figure 6.13: Problem setting (left) and deformed configuration (right), cylindrical shell

TABLE 6.15. Geometrical and material data (bending of cylindrical shell)

E	17853.6585 N/mm^2
ν	0.488
t	$2mm$
R_i	$9mm - t/2$
L	$15mm$
c_m	0.2

Finite element analysis is performed using 24 quasi-static steps with an equal load increment in each step resulting in a total load of $P_0 = 450N/mm^2$. The study of convergence has been performed with shell thickness $2mm$.

The numerical solution at C along the y-direction using neo-Hookean material law are given in Tables 6.16, 6.17 and 6.18 for Cases I, II and III, respectively, of the proposed mixed formulation, whereas numerical results with Cases I, II and III of the proposed mixed formulation with Mooney-Rivlin material model ($c_m = 0.2$) using different finite element meshes are presented in Tables 6.19, 6.20 and 6.21, respectively. We have set $\alpha = 0$ for all numerical results. The load factor γ_p is defined as $\gamma_p = P/P_0$ with the applied load P. As in previous examples, we can observe a good convergence behavior for all considered cases.

TABLE 6.16. Convergence of numerical results with Case I (neo-Hookean material law)

Mesh Load factor γ_p	8×4 $\times 2$	12×6 $\times 2$	16×8 $\times 2$	20×10 $\times 2$	24×12 $\times 2$
0.1667	-1.2193	-1.402	-1.470	-1.502	-1.521
0.3333	-2.6437	-3.066	-3.230	-3.311	-3.357
0.5000	-4.2480	-4.974	-5.272	-5.423	-5.510
0.6667	-5.9512	-7.046	-7.519	-7.765	-7.909
0.8333	-7.6452	-9.167	-9.852	-10.218	-10.435
1.0000	-9.2555	-11.252	-12.188	-12.698	-13.004

TABLE 6.17. Convergence of numerical results with Case II (neo-Hookean material law)

Mesh Load factor γ_p	8×4 $\times 2$	12×6 $\times 2$	16×8 $\times 2$	20×10 $\times 2$	24×12 $\times 2$
0.1667	-1.0491	-1.270	-1.354	-1.396	-1.419
0.3333	-2.2573	-2.763	-2.964	-3.063	-3.120
0.5000	-3.6225	-4.470	-4.827	-5.008	-5.112
0.6667	-5.1140	-6.338	-6.891	-7.179	-7.347
0.8333	-6.6658	-8.276	-9.059	-9.478	-9.727
1.0000	-8.1959	-10.203	-11.242	-11.817	-12.164

In all our numerical results, we get the locking-free response in the nearly incompressible limit from all cases of our mixed formulations. In particular, the space of stress from Case I shows better behavior in almost all considered examples. However, more numerical experiments are necessary to test the performance of our α-dependent mixed formulation for general hyperelasticity. In particular, benchmark numerical tests and comparison among different cases with different nonlinear material laws should be performed.

TABLE 6.18. Convergence of numerical results with Case III (neo-Hookean material law)

Mesh Load factor γ_p	8×4 $\times 2$	12×6 $\times 2$	16×8 $\times 2$	20×10 $\times 2$	24×12 $\times 2$
0.1667	-0.8396	-1.158	-1.342	-1.450	-1.517
0.3333	-1.7649	-2.497	-2.933	-3.193	-3.356
0.5000	-2.7872	-4.026	-4.782	-5.238	-5.523
0.6667	-3.9204	-5.732	-6.859	-7.534	-7.952
0.8333	-5.1755	-7.584	-9.091	-9.977	-10.521
1.0000	-6.5520	-9.535	-11.392	-12.474	-13.141

TABLE 6.19. Convergence of numerical results with Case I (Mooney-Rivlin material law)

Mesh Load factor γ_p	8×4 $\times 2$	12×6 $\times 2$	16×8 $\times 2$	20×10 $\times 2$	24×12 $\times 2$
0.1667	-1.2318	-1.409	-1.476	-1.509	-1.527
0.3333	-2.6285	-3.040	-3.201	-3.281	-3.327
0.5000	-4.1948	-4.906	-5.197	-5.345	-5.431
0.6667	-5.8555	-6.931	-7.392	-7.634	-7.776
0.8333	-7.5121	-9.005	-9.673	-10.031	-10.243
1.0000	-9.0944	-11.044	-11.952	-12.450	-12.749

TABLE 6.20. Convergence of numerical results with Case II (Mooney-Rivlin material law)

Mesh Load factor γ_p	8×4 $\times 2$	12×6 $\times 2$	16×8 $\times 2$	20×10 $\times 2$	24×12 $\times 2$
0.1667	-1.2670	-1.267	-1.349	-1.389	-1.412
0.3333	-2.7033	-2.714	-2.908	-3.005	-3.059
0.5000	-4.3408	-4.364	-4.708	-4.882	-4.982
0.6667	-6.1335	-6.171	-6.703	-6.979	-7.140
0.8333	-7.9992	-8.050	-8.801	-9.203	-9.440
1.0000	-9.8577	-9.921	-10.917	-11.466	-11.795

TABLE 6.21. Convergence of numerical results with Case III (Mooney-Rivlin material law)

Mesh Load factor γ_p	8×4 $\times 2$	12×6 $\times 2$	16×8 $\times 2$	20×10 $\times 2$	24×12 $\times 2$
0.1667	-0.8710	-1.189	-1.374	-1.482	-1.549
0.3333	-1.7959	-2.529	-2.965	-3.225	-3.388
0.5000	-2.8172	-4.056	-4.813	-5.269	-5.555
0.6667	-3.9484	-5.760	-6.889	-7.565	-7.985
0.8333	-5.2002	-7.609	-9.118	-10.006	-10.553
1.0000	-6.5717	-9.555	-11.413	-12.498	-13.164

CHAPTER 7

Mortar Finite Elements for Coupling Compressible and Nearly Incompressible Materials

7.1. Introduction

Often coupled problems with completely different material properties occur in solid mechanics. For example, one material can be nearly incompressible, whereas the other can be a compressible material. To get optimal a priori estimates, a proper discretization scheme should be used in each subdomain. In this chapter, we consider coupling of compressible and nearly incompressible linear elastic materials with mortar techniques. As noted in the last chapter, the standard low order discretization schemes based on quadrilaterals or hexahedra applied to nearly incompressible materials suffer from the so-called locking effect yielding a poor convergence. We refer to Chapter 6 for an overview of several approaches to overcome the locking effect in nearly incompressible elasticity. Taking into account the locking effect, we consider suitable discretization schemes for nearly incompressible materials. Introducing the pressure as an additional unknown for the nearly incompressible case, we arrive at the problem of coupling a saddle point problem with a positive definite one. Working exclusively with non-matching triangulations, we use mortar techniques to realize the coupling of different discretization schemes.

This chapter is organized as follows. In the next section, we describe the boundary value problem of linear elasticity and introduce a new formulation of the boundary value problem in the continuous setting suitable for coupling a nearly incompressible material with a compressible material. In Section 7.3, we show the stability of the scheme and prove optimal a priori estimates. Finally in Section 7.4, we present some numerical results illustrating the performance of our approach.

7.2. The problem of linear elasticity in the mortar framework

We consider a bounded polygonal or polyhedral domain $\Omega \subset \mathbb{R}^d$, $d = \{2, 3\}$, which is decomposed into two non-overlapping subdomains Ω_1 and Ω_2 with the common interior interface Γ, $\bar{\Gamma} = \partial\Omega_1 \cap \partial\Omega_2$. For simplicity, we restrict ourselves to the case of two subdomains. However, the approach can easily be generalized to more than two subdomains.

We assume that the subdomains Ω_1 and Ω_2 are occupied with different isotropic linear elastic materials. Furthermore, the material in Ω_1 is supposed to be nearly incompressible, whereas Ω_2 is occupied with a compressible material. We consider the following linear elasticity problem of finding the displacement field $\boldsymbol{u}$ in Ω such that

$$
\begin{aligned}
-\operatorname{div}(\mathcal{C}_1\boldsymbol{\varepsilon}(\boldsymbol{u})) &= \boldsymbol{f}_1 \quad \text{in} \quad \Omega_1, \\
-\operatorname{div}(\mathcal{C}_2\boldsymbol{\varepsilon}(\boldsymbol{u})) &= \boldsymbol{f}_2 \quad \text{in} \quad \Omega_2
\end{aligned}
\tag{7.2.1}
$$

with homogeneous Dirichlet boundary conditions on $\partial\Omega$. Here, $\mathcal{C}_1$ and $\mathcal{C}_2$ are constant and symmetric fourth-order elasticity tensors corresponding to the different materials in Ω_1 and Ω_2, respectively, and the plane strain is assumed in the two-dimensional case. We define the global Hooke tensor $\mathcal{C}$ which takes the value $\mathcal{C}_1$ on Ω_1 and $\mathcal{C}_2$ on Ω_2, and set $\boldsymbol{u}_1 := \boldsymbol{u}_{|\Omega_1}$ and $\boldsymbol{u}_2 := \boldsymbol{u}_{|\Omega_2}$. We assume that $\boldsymbol{f}_i \in (L^2(\Omega_i))^d, i = 1, 2$. The interface conditions on Γ are given by

$$
\begin{aligned}
[\boldsymbol{u}] &:= \boldsymbol{u}_1 - \boldsymbol{u}_2 = 0 \quad \text{on} \quad \Gamma, \\
[\boldsymbol{u}]_n &:= (\mathcal{C}_1\boldsymbol{\varepsilon}(\boldsymbol{u}_1))\mathbf{n} - (\mathcal{C}_2\boldsymbol{\varepsilon}(\boldsymbol{u}_2))\mathbf{n} = 0 \quad \text{on} \quad \Gamma,
\end{aligned} \tag{7.2.2}
$$

where $\mathbf{n}$ is the outer normal to Γ from Ω_1. For more details on linear elasticity, we refer to Chapter 6.

In order to write the variational formulation of the linear elasticity problem (7.2.1), we introduce $\mathbf{H}^1(\Omega_k) := (H^1(\Omega_k))^d$ for $k = 1, 2$ and define the unconstrained product space

$$
\mathbf{X} := \prod_{k=1}^{2} \{\boldsymbol{v} \in \mathbf{H}^1(\Omega_k) |\ \boldsymbol{v}_{|\partial\Omega\cap\partial\Omega_k} = 0\}.
$$

The interpolation space $\mathbf{H}_{00}^{1/2}(\Gamma)$ is defined by $\mathbf{H}_{00}^{1/2}(\Gamma) := (H_{00}^1(\Gamma))^d$, and its dual space will be denoted by $\mathbf{H}^{-1/2}(\Gamma)$. The weak matching condition on the interface is imposed by introducing the vector-valued Lagrange multiplier space $\mathbf{M} := \mathbf{H}^{-1/2}(\Gamma)$ on the interface Γ. Here, we consider the positive definite variational problem on the constrained finite element space which is given by means of the global Lagrange multiplier space $\mathbf{M}$

$$
\mathbf{V} := \{\boldsymbol{v} \in \mathbf{X} \,|\, \int_\Gamma [\boldsymbol{v}] \cdot \boldsymbol{\psi}\, d\boldsymbol{\sigma} = 0,\ \boldsymbol{\psi} \in \mathbf{M}\}. \tag{7.2.3}
$$

Then, the variational problem of linear elasticity in the mortar formulation can be written as: given $l \in \mathbf{V}'$ find $\boldsymbol{u} \in \mathbf{V}$ such that

$$
a(\boldsymbol{u}, \boldsymbol{v}) = l(\boldsymbol{v}), \quad \boldsymbol{v} \in \mathbf{V}, \tag{7.2.4}
$$

where the bilinear form $a(\cdot, \cdot)$ and the linear form $l(\cdot)$ are defined by

$$
\begin{aligned}
a(\boldsymbol{u}, \boldsymbol{v}) : &= \int_{\Omega_1} \mathcal{C}_1\boldsymbol{\varepsilon}(\boldsymbol{u}) : \boldsymbol{\varepsilon}(\boldsymbol{v})\, dx + \int_{\Omega_2} \mathcal{C}_2\boldsymbol{\varepsilon}(\boldsymbol{u}) : \boldsymbol{\varepsilon}(\boldsymbol{v})\, dx, \quad \text{and} \\
l(\boldsymbol{v}) : &= \int_{\Omega_1} \boldsymbol{f}_1 \cdot \boldsymbol{v}\, dx + \int_{\Omega_2} \boldsymbol{f}_2 \cdot \boldsymbol{v}\, dx,
\end{aligned}
$$

respectively. Taking into account the definition of $\mathcal{C}\boldsymbol{\varepsilon}(\boldsymbol{u})$, we can write the variational formulation (7.2.4) as

$$
\sum_{i=1}^{2} 2\mu_i \int_{\Omega_i} \boldsymbol{\varepsilon}(\boldsymbol{u}) : \boldsymbol{\varepsilon}(\boldsymbol{v})\, dx + \lambda_i \int_{\Omega_i} \operatorname{div} \boldsymbol{u}\, \operatorname{div} \boldsymbol{v}\, dx = \sum_{i=1}^{2} \int_{\Omega_i} \boldsymbol{f}_i \cdot \boldsymbol{v}\, dx. \tag{7.2.5}
$$

As before, we will use the same notation for norms on $\mathbf{H}^s(\Omega)$ and $H^s(\Omega)$. From the assumption on $\mathcal{C}$, we find that $a(\cdot, \cdot)$ is symmetric, continuous and $\mathbf{V}$-elliptic, and hence the problem (7.2.5) has a unique solution $\boldsymbol{u} \in \mathbf{V}$. Since the material occupying Ω_1 is supposed to be nearly incompressible λ_1 is very large, and hence the divergence of the exact solution $\operatorname{div} \boldsymbol{u}_1$ is very small. This constraint for the low order approximation based

on displacement approach leads to the locking. In the next paragraph, we will relax this constraint by introducing an additional variable for the pressure.

Alternative formulation. There are many efficient numerical approaches to handle a nearly incompressible material, see also Chapter 6. In general, they are more complex than the standard displacement formulation. Our goal is to combine the standard formulation with a suitable scheme for a nearly incompressible material without losing the simplicity and optimality of the approach. For that purpose, we want to get a variational formulation which is uniformly well-posed in terms of λ_1. Now we introduce an additional unknown variable $p := \lambda_1 \operatorname{div} \boldsymbol{u}$ in Ω_1 leading to a mixed formulation. Then the variational problem (7.2.5) is given by: find $(\boldsymbol{u}, p) \in \mathbf{V} \times L^2(\Omega_1)$ such that

$$\begin{array}{rcrcll} \tilde{a}(\boldsymbol{u},\boldsymbol{v}) & + & \tilde{b}(\boldsymbol{v},p) & = & l(\boldsymbol{v}), & \boldsymbol{v} \in \mathbf{V}, \\ \tilde{b}(\boldsymbol{u},q) & - & \frac{1}{\lambda_1}\tilde{c}(p,q) & = & 0, & q \in L^2(\Omega_1), \end{array} \tag{7.2.6}$$

where

$$\begin{aligned} \tilde{a}(\boldsymbol{u},\boldsymbol{v}) &:= \sum_{i=1}^{2} 2\mu_i \int_{\Omega_i} \boldsymbol{\varepsilon}(\boldsymbol{u}) : \boldsymbol{\varepsilon}(\boldsymbol{v})\, dx + \lambda_2 \int_{\Omega_2} \operatorname{div} \boldsymbol{u}\, \operatorname{div} \boldsymbol{v}\, dx, \\ \tilde{b}(\boldsymbol{v},q) &:= \int_{\Omega_1} \operatorname{div} \boldsymbol{v}\, q\, dx \quad \text{and} \quad \tilde{c}(p,q) := \int_{\Omega_1} p\, q\, dx. \end{aligned}$$

We remark that in contrast to the setting of the Stokes problem with homogeneous boundary condition, where $p \in L^2_0(\Omega_1)$, here, the pressure $p \in L^2(\Omega_1)$. The essential points for the existence and the uniqueness of the solution of a saddle point problem are ellipticity, continuity and a suitable inf-sup condition. Furthermore, for the saddle point problem with penalty, it is necessary that the bilinear form $\tilde{c}(\,,\cdot,\,)$ should be positive semi-definite and bounded, see [**38**]. The bilinear form $\tilde{a}(\cdot,\cdot)$ is symmetric, continuous and $\mathbf{V}$-elliptic uniformly with respect to λ_1. It is also clear that the bilinear form $\tilde{c}(\cdot,\cdot)$ is continuous, symmetric and positive definite. The continuity of $\tilde{b}(\cdot,\cdot)$ follows from its definition.

LEMMA 7.1. *The bilinear form $\tilde{b}(\cdot,\cdot)$ on $\mathbf{V} \times L^2(\Omega_1)$ satisfies an inf-sup condition uniformly with respect to λ_1.*

PROOF. The proof is based on applying the argument due to Boland and Nicolaides [**35**]. Given $q \in L^2(\Omega_1)$, we split $q = q_0 + q_c$, where $\int_{\Omega_1} q_0\, dx = 0$ and q_c is a constant such that $\int_{\Omega_1} q\, dx = \int_{\Omega_1} q_c\, dx = |\Omega_1| q_c$. Thus $\|q\|^2_{0,\Omega_1} = \|q_0\|^2_{0,\Omega_1} + \|q_c\|^2_{0,\Omega_1}$. Since $q_0 \in L^2_0(\Omega_1)$, there exists a $\boldsymbol{v}_0 \in \mathbf{H}^1_0(\Omega_1)$ with $\|\boldsymbol{v}_0\|_{1,\Omega_1} \le C\|q_0\|_{0,\Omega_1}$ such that

$$\|q_0\|^2_{0,\Omega_1} = \tilde{b}(\boldsymbol{v}_0, q_0), \quad \text{see [**80**, Corollary 2.4].}$$

Hence $\|q\|^2_{0,\Omega_1} = \tilde{b}(\boldsymbol{v}_0, q_0) + q_c^2|\Omega_1|$. Now, we define a piecewise constant function $\tilde{f}$ in Ω with

$$\tilde{f}(x) := \begin{cases} q_c & \text{if } x \in \Omega_1, \\ -\frac{q_c|\Omega_1|}{|\Omega_2|} & \text{if } x \in \Omega_2 \end{cases}$$

so that $\tilde{f} \in L^2_0(\Omega)$, and hence the divergence equation

$$\nabla \cdot \boldsymbol{w} = \tilde{f} \quad \text{in} \quad \Omega \tag{7.2.7}$$

has a solution $\boldsymbol{v}_c \in \mathbf{H}_0^1(\Omega)$ with $\|\boldsymbol{v}_c\|_1 \leq C\|\tilde{f}\|_0$, see [**9, 79**]. Thus

$$\|q\|_{0,\Omega_1}^2 \;=\; \tilde{b}(\boldsymbol{v}_0, q_0) + q_c^2|\Omega_1| = \tilde{b}(\boldsymbol{v}_0, q_0) + \int_{\Omega_1} \nabla \cdot \boldsymbol{v}_c q_c \, dx = \tilde{b}(\boldsymbol{v}_0, q_0) + \tilde{b}(\boldsymbol{v}_c, q_c).$$

Since $\boldsymbol{v}_0 \in \mathbf{H}_0^1(\Omega_1)$, we can extend $\boldsymbol{v}_0$ trivially on Ω by defining $\tilde{\boldsymbol{v}}_0 := \boldsymbol{v}_0$ in Ω_1 and $\tilde{\boldsymbol{v}}_0 := 0$ in Ω_2, and find that $\tilde{\boldsymbol{v}}_0 \in \mathbf{H}_0^1(\Omega)$. Hence $\tilde{b}(\boldsymbol{v}_0, q_0) = \tilde{b}(\tilde{\boldsymbol{v}}_0, q_0)$. On the other hand,

$$\tilde{b}(\tilde{\boldsymbol{v}}_0 + \boldsymbol{v}_c, q_0 + q_c) = \tilde{b}(\tilde{\boldsymbol{v}}_0, q_0) + \tilde{b}(\boldsymbol{v}_c, q_c) + \tilde{b}(\tilde{\boldsymbol{v}}_0, q_c) + \tilde{b}(\boldsymbol{v}_c, q_0).$$

Noting that $\tilde{b}(\tilde{\boldsymbol{v}}_0, q_c) = 0,$ and $\tilde{b}(\boldsymbol{v}_c, q_0) = 0$, we get

$$\|q\|_{0,\Omega_1}^2 \;=\; \tilde{b}(\tilde{\boldsymbol{v}}_0 + \boldsymbol{v}_c, q_0 + q_c).$$

Finally, taking into account that $\tilde{\boldsymbol{v}}_0 \in \mathbf{H}_0^1(\Omega)$ we get $\boldsymbol{v}_c + \tilde{\boldsymbol{v}}_0 =: \boldsymbol{v} \in \mathbf{H}_0^1(\Omega)$ with $\|\boldsymbol{v}\|_1 \leq \|\boldsymbol{v}_c + \tilde{\boldsymbol{v}}_0\|_1 \leq C(\|\tilde{f}\|_0 + \|q_0\|_{0,\Omega_1})$, which completes the proof. □

An immediate consequence of the previous Lemma is the following:

THEOREM 7.2. *The problem 7.2.6 has a unique solution and there exists a constant C independent of λ_1 such that*

$$\|\boldsymbol{u}\|_1 + \|p\|_{0,\Omega_1} \leq C\|l\|_0.$$

7.3. Mortar discretizations and a priori estimates

Using the notation of Section 4.3 of Chapter 4, we define the unconstrained discrete finite element space for the displacement $\mathbf{X}_h := \mathbf{X}_1 \times \mathbf{X}_2$, where $\mathbf{X}_k := X_k^d$, X_k being the conforming finite element space of order p_k in Ω_k. We recall that no interface condition is imposed on $\mathbf{X}_h$, and the elements in $\mathbf{X}_h$ do not have to satisfy a continuity condition at the interface. The pressure space $L^2(\Omega_1)$ is discretized by some finite elements and will be denoted by $R_h \subset L^2(\Omega_1)$. The efficiency and optimality of the mortar method depends on the choice of a discrete Lagrange multiplier space, which should satisfy Assumptions 2–4 stated in the first chapter. Without loss of generality, the Lagrange multiplier space is based on a one-dimensional mesh $\mathcal{T}_{\Gamma_2}$ inherited from $\mathcal{T}_2$, and its basis functions are defined locally having the same support as finite element basis functions associated with the interior nodes of the slave side.

As in Chapter 4, we observe that since the normal has jumps if Γ has corners although $\boldsymbol{u} \in \mathbf{H}^{s+1}(\Omega_1)$, $\boldsymbol{\varepsilon}(\boldsymbol{u})\mathbf{n}$ is, in general, not an element in $\mathbf{H}^{s-1/2}(\Gamma)$. Therefore, we decompose Γ into a finite number of subsets γ_i, $1 \leq i \leq N$, such that each γ_i entirely lies in a $(d-1)$-dimensional hyperplane, and

$$\bar{\Gamma} = \bigcup_{i=1}^{N} \bar{\gamma}_i,$$

where $\gamma_k \cap \gamma_l = \emptyset$, and $\bar{\gamma}_k \cup \bar{\gamma}_l$ does not entirely lie in a $(d-1)$-dimensional hyperplane, $1 \leq k \neq l \leq N$. Denoting the discrete Lagrange multiplier spaces on γ_i by M_i, $1 \leq i \leq N$, we define $\mathbf{M}_i := M_i^d$, and our global discrete Lagrange multiplier space is then given as the product space

$$\mathbf{M}_h := \prod_{i=1}^{N} \mathbf{M}_i.$$

The finite element nodes in $\partial\gamma_i$ on the slave side, $1 \le i \le N$, are the crosspoints and they do not carry any degree of freedom for the Lagrange multipliers. We assume that $\mathbf{W}_i^m$ and $\mathbf{W}_i^s$ are the trace spaces of $\mathbf{X}_1$ and $\mathbf{X}_2$ restricted to γ_i, respectively, satisfying homogeneous boundary conditions on $\partial\gamma_i$, and we set

$$\mathbf{W}_h^m := \prod_{i=1}^N \mathbf{W}_i^m,\ \mathbf{W}_h^s := \prod_{i=1}^N \mathbf{W}_i^s.$$

As in the continuous setting, we consider the positive-definite variational problem on the constrained finite element space $\mathbf{V}_h$ which is given by means of the discrete global Lagrange multiplier space $\mathbf{M}_h$

$$\mathbf{V}_h := \{\boldsymbol{v}_h \in \mathbf{X}_h \mid b(\boldsymbol{v}_h, \boldsymbol{\psi}_h) = 0,\ \boldsymbol{\psi}_h \in \mathbf{M}_h\}, \tag{7.3.1}$$

where $b(\boldsymbol{v}_h, \boldsymbol{\psi}_h) := \sum_{i=1}^N \int_{\gamma_i} [\boldsymbol{v}_h] \cdot \boldsymbol{\psi}_h \, d\boldsymbol{\sigma}$. We remark that the elements of the space $\mathbf{V}_h$ satisfy a weak continuity condition on the skeleton Γ in terms of the discrete Lagrange multiplier space $\mathbf{M}_h$. However, $\mathbf{V}_h$ is, in general, not a subspace of $\mathbf{H}_0^1(\Omega)$. Replacing the space $\mathbf{V} \times L^2(\Omega_1)$ by our discrete space $\mathbf{V}_h \times R_h$ in (7.2.6), we obtain our discrete variational problem: find $(\boldsymbol{u}_h, p_h) \in \mathbf{V}_h \times R_h$ such that

$$\begin{array}{rcll} \tilde{a}(\boldsymbol{u}_h, \boldsymbol{v}) + \tilde{b}(\boldsymbol{v}, p_h) & = & l(\boldsymbol{v}), & \boldsymbol{v} \in \mathbf{V}_h, \\ \tilde{b}(\boldsymbol{u}_h, q) - \frac{1}{\lambda_1}\tilde{c}(p_h, q) & = & 0, & q \in R_h. \end{array} \tag{7.3.2}$$

To establish a priori estimates for the discretization errors, we consider the saddle point formulation (7.3.2) of the elasticity problem and apply the theory of mixed finite elements. The continuity of the bilinear form $\tilde{a}(\cdot,\cdot)$ on $\mathbf{V}_h \times \mathbf{V}_h$, of $\tilde{b}(\cdot,\cdot)$ on $\mathbf{V}_h \times R_h$ and of $\tilde{c}(\cdot,\cdot)$ on $R_h \times R_h$ is straightforward. Moreover, the continuity constants are independent of λ_1. Furthermore, we need the ellipticity of the bilinear form $\tilde{a}(\cdot,\cdot)$ on $\mathbf{V}_h \times \mathbf{V}_h$, and a uniform inf-sup condition for the bilinear form $\tilde{b}(\cdot,\cdot)$ on $\mathbf{V}_h \times R_h$.

7.3.1. Uniform inf-sup condition and ellipticity.

ASSUMPTION 10. *The following two assumptions will be crucial to prove the inf-sup condition in the discrete setting and are supposed to hold in the following:*

10(i) *For a constant $q_c \in \mathbb{R}$, there exist functions $\boldsymbol{v}_h^s \in \mathbf{W}_i^s, \boldsymbol{v}_h^m \in \mathbf{W}_i^m$ for some $i \in \{1, \cdots, N\}$ with $\|\boldsymbol{v}_h^s\|_{\mathbf{H}_{00}^{1/2}(\gamma_i)} \le C|q_c|, \|\boldsymbol{v}_h^m\|_{\mathbf{H}_{00}^{1/2}(\gamma_i)} \le C|q_c|$ so that*

$$\int_{\gamma_i} \boldsymbol{v}_h^s \cdot \mathbf{n} \, d\boldsymbol{\sigma} = q_c, \text{ and } \int_{\gamma_i} (\boldsymbol{v}_h^s - \boldsymbol{v}_h^m) \cdot \boldsymbol{\psi} \, d\boldsymbol{\sigma} = 0,\ \boldsymbol{\psi} \in \mathbf{M}_i.$$

10(ii) *For any $q \in R_h \cap L_0^2(\Omega_1)$, there exists a constant $C > 0$ independent of the meshsize such that*

$$\sup_{\boldsymbol{v}_h \in \mathbf{X}_1 \cap \mathbf{H}_0^1(\Omega_1)} \frac{\tilde{b}(\boldsymbol{v}_h, q)}{\|\boldsymbol{v}_h\|_{1,\Omega_1}} \ge C\|q\|_{0,\Omega_1}.$$

Assumption 10 (i) is readily met if the triangulation is fine enough under Assumption 3, and Assumption 10 (ii) tells that the spaces $\mathbf{X}_1$ and R_h should be chosen carefully so that they form a stable pair for the Stokes problem. The following lemma provides a necessary tool to prove inf-sup condition.

LEMMA 7.3. *For a constant $q_c \in \mathbb{R}$, there exists a $\boldsymbol{v}_h \in \mathbf{V}_h$ with $\|\boldsymbol{v}_h\|_1 \leq C|q_c|$ such that $\int_{\Omega_1} \nabla \cdot \boldsymbol{v}_h \, dx = q_c$.*

PROOF. Because of Assumption 10 (i), we can choose a function $\boldsymbol{v}_h^s \in \mathbf{W}_i^s$ with

$$\|\boldsymbol{v}_h^s\|_{\mathbf{H}_{00}^{1/2}(\gamma_i)} \leq C|q_c| \text{ such that } \int_{\gamma_i} \boldsymbol{v}_h^s \cdot \mathbf{n} \, d\boldsymbol{\sigma} = q_c,$$

and define a function $\boldsymbol{v}_h^m \in \mathbf{W}_i^m$ with $\|\boldsymbol{v}_h^m\|_{\mathbf{H}_{00}^{1/2}(\gamma_i)} \leq C|q_c|$ so that $\int_{\gamma_i} (\boldsymbol{v}_h^s - \boldsymbol{v}_h^m) \cdot \boldsymbol{\psi} \, d\boldsymbol{\sigma} = 0, \ \boldsymbol{\psi} \in \mathbf{M}_i$. Since $\boldsymbol{v}_h^s, \boldsymbol{v}_h^m \in \mathbf{H}_{00}^{1/2}(\gamma_i)$ both $\boldsymbol{v}_h^s$ and $\boldsymbol{v}_h^m$ can trivially be extended to functions in $\mathbf{W}_h^s$ and $\mathbf{W}_h^m$, respectively, still denoted by $\boldsymbol{v}_h^s$ and $\boldsymbol{v}_h^m$. Using the discrete harmonic extension, we obtain functions $\boldsymbol{w}_h^m \in \mathbf{X}_1$ and $\boldsymbol{w}_h^s \in \mathbf{X}_2$ so that $\boldsymbol{w}_{h|_\Gamma}^s = \boldsymbol{v}_h^s$ and $\boldsymbol{w}_{h\,|_\Gamma}^m = \boldsymbol{v}_h^m$. Defining a function $\boldsymbol{v}_h \in \mathbf{X}_h$ with $\boldsymbol{v}_{h|_{\Omega_1}} = \boldsymbol{w}_h^m$, and $\boldsymbol{v}_{h|_{\Omega_2}} = \boldsymbol{w}_h^s$, we find that $\boldsymbol{v}_h \in \mathbf{V}_h$, and from the well known property of harmonic extension we have $\|\boldsymbol{v}_h\|_1 \leq C|q_c|$. Finally, the result follows from

$$\int_{\Omega_1} \nabla \cdot \boldsymbol{v}_h \, dx = \int_\Gamma \boldsymbol{v}_h^s \cdot \mathbf{n} \, d\boldsymbol{\sigma} = \int_{\gamma_i} \boldsymbol{v}_h^s \cdot \mathbf{n} \, d\boldsymbol{\sigma} = q_c.$$

□

THEOREM 7.4. *For any $q_h \in R_h$, there exists a constant C independent of λ_1 and the meshsize such that*

$$\sup_{\boldsymbol{v}_h \in \mathbf{V}_h} \frac{\tilde{b}(\boldsymbol{v}_h, q_h)}{\|\boldsymbol{v}_h\|_1} \geq C\|q_h\|_{0,\Omega_1}.$$

PROOF. As in the continuous case, we resort to the argument due to Boland and Nicolaides [**35**] to prove the inf-sup condition. We take $q_h \in R_h$ and split $q_h = q_{0h} + q_{ch}$, where $\int_{\Omega_1} q_{0h} \, dx = 0$ and q_{ch} is the L^2-projection of q_h onto $\mathbb{R}$ such that $\int_{\Omega_1} q_h \, dx = \int_{\Omega_1} q_{ch} \, dx$. Since $q_{0h} \in R_h \cap L_0^2(\Omega_1)$, from Assumption 10 (ii), we get a $\boldsymbol{v}_{0h} \in \mathbf{X}_1 \cap \mathbf{H}_0^1(\Omega_1)$ with $\|\boldsymbol{v}_{0h}\|_{1,\Omega_1} \leq C\|q_{0h}\|_{0,\Omega_1}$ so that $\|q_{0h}\|_{0,\Omega_1}^2 = \tilde{b}(\boldsymbol{v}_{0h}, q_{0h})$. Hence

$$\|q_h\|_{0,\Omega_1}^2 = \tilde{b}(\boldsymbol{v}_{0h}, q_{0h}) + q_{ch}^2|\Omega_1|. \tag{7.3.3}$$

From Lemma 7.3, we get a $\boldsymbol{v}_{ch} \in \mathbf{V}_h$ such that $\int_{\Omega_1} \nabla \cdot \boldsymbol{v}_{ch} \, q_{ch} \, dx = q_{ch}^2|\Omega_1|$. Using this in (7.3.3), we get

$$\|q_h\|_{0,\Omega_1}^2 = \tilde{b}(\boldsymbol{v}_{0h}, q_{0h}) + \tilde{b}(\boldsymbol{v}_{ch}, q_{ch})$$

The rest of the proof follows exactly as in continuous setting. □

REMARK 7.5. *Working with bilinear or trilinear finite elements and piecewise constant pressure in the subdomain with the nearly incompressible material, it is well known that the uniform inf-sup condition does not hold, and one can observe some spurious pressure modes. Since Assumption 10 (ii) does not hold, the theoretical analysis does not cover this case. However, as we have proved in the last chapter for a problem posed in a single domain with homogeneous Dirichlet boundary condition, the spurious pressure modes do not substantially affect the displacement. Furthermore, through the numerical results we will show that the Q_1P_0 formulation and also the modified Hu-Washizu formulation can be successfully used in the subdomain with the nearly incompressible material.*

Now, we turn our attention to the ellipticity of the bilinear form $\tilde{a}(\cdot,\cdot)$ on the space $\mathbf{V}_h$. If $\partial\Omega_k \cap \partial\Omega$ has a non-zero measure for $k = 1, 2$, we can apply Korn's and Poincare's inequalities to each subdomain and obtain the desired results

$$\tilde{a}(\boldsymbol{v},\boldsymbol{v}) = \sum_{k=1}^{2} \tilde{a}_k(\boldsymbol{v},\boldsymbol{v}) \geq C \sum_{k=1}^{2} \|\boldsymbol{v}\|^2_{1,\Omega_k} = C\|\boldsymbol{v}\|^2_1, \quad \boldsymbol{v} \in \mathbf{X}_h,$$

where $\tilde{a}_k(\cdot,\cdot)$ stands for the restriction of $\tilde{a}(\cdot,\cdot)$ to the subdomain Ω_k. Thus $\tilde{a}(\cdot,\cdot)$ is elliptic on $\mathbf{X}_h \times \mathbf{X}_h$. Unfortunately, there are many interesting situations where we cannot satisfy this assumption. However, it is sufficient to have ellipticity of $\tilde{a}(\cdot,\cdot)$ in $\mathbf{V}_h \times \mathbf{V}_h$ for the problem (7.3.2) to be uniquely solvable. Since the bilinear form $\tilde{a}(\cdot,\cdot)$ does not involve λ_1 the ellipticity can been shown exactly as in [**163, 49, 87**] uniformly with respect to λ_1. It is shown in [**49, 87**] that the ellipticity constant is independent of the number and the size of different subdomains of the decomposition.

REMARK 7.6. *Using the Stokes equation in the subdomain Ω_1 instead of equation of elasticity we arrive at the Stokes flow coupled with a linear elastic body. The coupled problem can be written as: given $l \in L^2(\Omega)$ find $(\boldsymbol{u}_h, p_h) \in \mathbf{V}_h \times R_h$ such that*

$$\begin{aligned} \int_{\Omega_2} \mathcal{C}_2\boldsymbol{\varepsilon}(\boldsymbol{u}_h) : \boldsymbol{\varepsilon}(\boldsymbol{v}_h)\, dx \quad &+\mu_1 \int_{\Omega_1} \nabla\boldsymbol{u}_h : \nabla\boldsymbol{v}_h\, dx + \int_{\Omega_1} \operatorname{div}\boldsymbol{v}_h\, p_h\, dx = \quad l(\boldsymbol{v}_h), \quad \boldsymbol{v}_h \in \mathbf{V}_h \\ \int_{\Omega_1} \operatorname{div}\boldsymbol{u}_h\, q_h\, dx \quad &= \quad 0, \quad q_h \in R_h, \end{aligned}$$

where $\boldsymbol{u}_h$ restricted to the subdomain Ω_2 represents the displacement, $\boldsymbol{u}_h$ restricted to the subdomain Ω_1 represents the velocity, and μ_1 is the kinematic viscosity for the incompressible fluid. The mathematical analysis of mortar finite elements for the Stokes problem can be found in [**23, 24**].

7.3.2. A priori estimates. The immediate consequence of the above discussion is the well-posedness of the discrete problem (7.3.2). From the theory of saddle point problem, see, e.g., [**52**], we have

LEMMA 7.7. *The discrete problem* (7.3.2) *has exactly one solution $(\boldsymbol{u}_h, p_h) \in \mathbf{V}_h \times R_h$ which is uniformly stable with respect to the data $\boldsymbol{f}_i, i = 1, 2$, and there exists a constant C independent of Lamé parameter λ_1 such that*

$$\|\boldsymbol{u}_h\|_1 + \|p_h\|_{0,\Omega_1} \leq C\|\boldsymbol{f}\|_0.$$

The convergence theory is provided by an abstract result about the approximation of saddle point problems by nonconforming methods, see [**23, 72**].

LEMMA 7.8. *Assume that $(\boldsymbol{u}, p)$ and $(\boldsymbol{u}_h, p_h)$ be the solutions of problems* (7.2.6) *and* (7.3.2)*, respectively. Then, we have the following error estimate uniform with respect to λ_1:*

$$\begin{aligned} &(7.3.4) \quad \|\boldsymbol{u} - \boldsymbol{u}_h\|_1 + \|p - p_h\|_{0,\Omega_1} \\ &\leq C\left(\inf_{\boldsymbol{v}_h \in \mathbf{V}_h} \|\boldsymbol{u} - \boldsymbol{v}_h\|_1 + \inf_{q_h \in R_h} \|p - q_h\|_{0,\Omega_1} + \sup_{\boldsymbol{v}_h \in \mathbf{V}_h \setminus \{0\}} \frac{|\tilde{a}(\boldsymbol{u},\boldsymbol{v}_h) + \tilde{b}(\boldsymbol{v}_h, p) - l(\boldsymbol{v}_h)|}{\|\boldsymbol{v}_h\|_1} \right). \end{aligned}$$

We note that the first two terms in the right hand side of (7.3.4) denote the best approximation error and the last one is the consistency error.

LEMMA 7.9. *We have the following estimate for the consistency error in Lemma 7.8*

$$\sup_{\boldsymbol{v}_h\in\mathbf{V}_h\setminus\{0\}}\frac{|\tilde{a}(\boldsymbol{u},\boldsymbol{v}_h)+\tilde{b}(\boldsymbol{v}_h,p)-l(\boldsymbol{v}_h)|}{\|\boldsymbol{v}_h\|_1}=\sup_{\boldsymbol{v}_h\in\mathbf{V}_h\setminus\{0\}}\frac{|\int_\Gamma \mathcal{C}_2\boldsymbol{\varepsilon}(\boldsymbol{u}_2)\mathbf{n}\cdot[\boldsymbol{v}_h]\,d\boldsymbol{\sigma}|}{\|\boldsymbol{v}_h\|_1}.$$

PROOF.

$$\begin{aligned}\tilde{a}(\boldsymbol{u},\boldsymbol{v}_h)+\tilde{b}(\boldsymbol{v}_h,p)-l(\boldsymbol{v}_h) &= \sum_{k=1}^{2}\int_{\Omega_k}\mathcal{C}_k\boldsymbol{\varepsilon}(\boldsymbol{u}):\boldsymbol{\varepsilon}(\boldsymbol{v}_h)\,dx\\ &+ \int_{\Omega_1}(p-\lambda_1\nabla\cdot\boldsymbol{u})\nabla\cdot\boldsymbol{v}_h\,dx-l(\boldsymbol{v}_h)\\ &= \int_\Gamma \mathcal{C}_2\boldsymbol{\varepsilon}(\boldsymbol{u}_2)\mathbf{n}\cdot[\boldsymbol{v}_h]\,d\boldsymbol{\sigma},\end{aligned}$$

where in the last step we have used the second equation of (7.2.2), and $\boldsymbol{u}\in\mathbf{H}_0^1(\Omega)$. □

The a priori error estimate is obtained by combining the approximation of the saddle point problem in our nonconforming situation, see [**23, 72**], with the best approximation property of $\mathbf{V}_h$, R_h and $\mathbf{M}_h$.

THEOREM 7.10. *Assume that* $\boldsymbol{u}\in\Pi_{k=1}^2\mathbf{H}^{r_k+1}(\Omega_k)$, $p\in H^{r_1}(\Omega_1)$, *and* $\boldsymbol{\chi}:=\mathcal{C}_2\boldsymbol{\varepsilon}(\boldsymbol{u}_2)\mathbf{n}\in\Pi_{i=1}^N\mathbf{H}^{r_2-\frac{1}{2}}(\gamma_i)$ *with* $r_1\geq 0$ *and* $r_2>\frac{1}{2}$. *Moreover, assume that*

$$\inf_{p_h\in R_h}\|p-p_h\|_{0,\Omega_1}\leq Ch_1^{r_1}\|p\|_{r_1,\Omega_1},\quad p\in H^{r_1}(\Omega_1).$$

Then the following a priori error estimate holds for the discretization error

$$\|\boldsymbol{u}-\boldsymbol{u}_h\|_1+\|p-p_h\|_{0,\Omega_1}\leq C\left(\sum_{k=1}^{2}h_k^{t_k}\|\boldsymbol{u}\|_{t_k+1,\Omega_k}++h_1^{t_1}\|p\|_{t_1,\Omega_1}\right),$$

where $t_i:=min(r_i,p_i)$, $i=1,2$. *If* $0\leq r_2\leq\frac{1}{2}$, *then we have*

$$\|\boldsymbol{u}-\boldsymbol{u}_h\|_1+\|p-p_h\|_{0,\Omega_1}\leq C\left(\sum_{k=1}^{2}h_k^{t_k}\|\boldsymbol{u}\|_{t_k+1,\Omega_k}+h_1^{t_1}\|p\|_{t_1,\Omega_1}+h_2^{r_2}\sum_{i=1}^{N}\|\boldsymbol{\chi}\|_{r_2-\frac{1}{2},\gamma_i}\right),$$

where the constant C *might depend on* $\log^2 h_{mr}$ *as in Theorem 1.15.*

PROOF. The best approximation property of $\mathbf{V}_h$ has already been established in the first chapter. Hence using Lemma 7.8 it is sufficient to consider the consistency error. If $r_1>\frac{1}{2}$, the definition of space $\mathbf{V}_h$, the best approximation property of $\mathbf{M}_h$ and the trace

theorem yield for $\boldsymbol{\psi}_h \in \mathbf{M}_h$

$$\begin{aligned}\int_\Gamma \boldsymbol{\chi}\cdot[\boldsymbol{v}_h]\,d\boldsymbol{\sigma} &= \int_\Gamma (\mathcal{C}_2\boldsymbol{\varepsilon}(\boldsymbol{u}_2)\mathbf{n}-\boldsymbol{\psi}_h)\cdot[\boldsymbol{v}_h]\,d\boldsymbol{\sigma}\\ &\le \sum_{i=1}^{N}\inf_{\boldsymbol{\psi}_h\in\mathbf{M}_i}\|\mathcal{C}_2\boldsymbol{\varepsilon}(\boldsymbol{u}_2)\mathbf{n}-\boldsymbol{\psi}_h\|_{(\mathbf{H}^{1/2}(\gamma_i))'}\|[\boldsymbol{v}_h]\|_{1/2,\gamma_i}\\ &\le Ch_2^{t_2}\sum_{i=1}^{N}\|\mathcal{C}_2\boldsymbol{\varepsilon}(\boldsymbol{u}_2)\mathbf{n}\|_{t_2-1/2,\gamma_i}\|\boldsymbol{v}_h\|_1\\ &\le Ch_2^{t_2}\|\boldsymbol{u}\|_{t_2+1,\Omega_2}\|\boldsymbol{v}_h\|_1.\end{aligned}$$

We refer to Remark 1.12 for the proof of the second part. □

REMARK 7.11. *If Ω_1 is on the slave side of the interface Γ then we have to estimate the term*

$$\sum_{i=1}^{N}\inf_{\boldsymbol{\psi}_h\in\mathbf{M}_i}\|\mathcal{C}_1\boldsymbol{\varepsilon}(\boldsymbol{u}_1)\mathbf{n}-\boldsymbol{\psi}_h\|_{(\mathbf{H}^{1/2}(\gamma_i))'},$$

where now the Lagrange multiplier spaces $\mathbf{M}_i$ are defined on γ_i, $1\le i\le N$, with the mesh inherited from $\mathcal{T}_1$. In this case, assuming $r_2\ge r_1>\frac{1}{2}$, we can use the second equation of (7.2.2) *to obtain*

$$\begin{aligned}\int_\Gamma \boldsymbol{\chi}\cdot[\boldsymbol{v}_h]\,d\boldsymbol{\sigma} &\le \sum_{i=1}^{N}\inf_{\boldsymbol{\psi}_h\in\mathbf{M}_i}\|\mathcal{C}_1\boldsymbol{\varepsilon}(\boldsymbol{u}_1)\mathbf{n}-\boldsymbol{\psi}_h\|_{(\mathbf{H}^{1/2}(\gamma_i))'}\|[\boldsymbol{v}_h]\|_{1/2,\gamma_i}\\ &= \sum_{i=1}^{N}\inf_{\boldsymbol{\psi}_h\in\mathbf{M}_i}\|\mathcal{C}_2\boldsymbol{\varepsilon}(\boldsymbol{u}_2)\mathbf{n}-\boldsymbol{\psi}_h\|_{(\mathbf{H}^{1/2}(\gamma_i))'}\|[\boldsymbol{v}_h]\|_{1/2,\gamma_i}\\ &\le Ch_1^{t_1}\sum_{i=1}^{N}\|\mathcal{C}_2\boldsymbol{\varepsilon}(\boldsymbol{u}_2)\mathbf{n}\|_{t_1-1/2,\gamma_i}\|\boldsymbol{v}_h\|_1\\ &\le Ch_1^{t_1}\|\boldsymbol{u}\|_{t_1+1,\Omega_2}\|\boldsymbol{v}_h\|_1.\end{aligned}$$

7.4. Numerical results

In this section, we investigate the computational performance of our approach through some numerical examples. In particular, we compare the results from the standard approach and mortar approach for different test examples. In the following, Q_1 or Q_2 denotes that standard bilinear elements or quadratic serendipity elements are used in the whole domain Ω, whereas Q_1-Q_1P_0 or Q_1-HW denotes that Q_1P_0 or HW formulation is used in subdomains with a nearly incompressible material $\nu\to 0.5$ in combination with the standard Q_1 formulation in subdomains with smaller ν. We refer to equation (2.4.3) for the relation between Lamé parameters λ and μ, and Young's modulus E and Poisson ratio ν. In case of the HW-discretization, spaces of stress and strain are used from Case II. Similarly, Q_2-Q_2P_0 or Q_2-Q_2P_1 denotes that Q_2P_0 or Q_2P_1 formulation is used in subdomains with nearly incompressible materials, and they are combined with quadratic serendipity elements in subdomains with compressible materials. Working with bilinear and quadratic

serendipity elements linear and quadratic dual Lagrange multiplier spaces introduced in [**163**] are used to realize the weak matching condition. For the pressure space, piecewise constant pressure is used for Q_1P_0 and Q_2P_0, whereas discontinuous linear pressure is used for Q_2P_1 case. Furthermore, we do not specify the measurement units, and they should be understood with proper scaling.

Example 1: Cook's membrane problem. In this example, we consider a structure occupying a region $\Omega := \text{conv}\{(0,0),(48,44),(48,60),(0,44)\}$, where conv$\xi$ is the convex hull of the set ξ. The left boundary of Ω is fixed and an in-plane shearing load of 100N is applied along the positive y-direction on the right boundary. Here, the domain Ω is decomposed into two subdomains Ω_1 and Ω_2 with

$$\Omega_2 := \text{conv}\{(12,20.25),(36,38.75),(36,50.25),(12,38.75)\},$$

and $\Omega_1 := \Omega \backslash \bar{\Omega}_2$. The decomposition of domain Ω and the initial triangulation are given in the left picture of Figure 2.16. The material parameters are taken to be $E_1 = 250$, $E_2 = 80$, $\nu_1 = 0.4999$, and $\nu_2 = 0.35$ to get a nearly incompressible response in Ω_1. We see that uniform convergence is obtained if we work with Q_1-Q_1P_0, Q_2-Q_2P_0, Q_2-Q_2P_1 or Q_2, see Figure 7.1. In this problem, we see that Q_1-Q_1P_0 and Q_2 elements work as good as Q_2-Q_2P_0 and Q_2-Q_2P_1. To show the influence of the choice of the master and the slave side, we have given the plot of vertical tip displacement at the top right corner of the membrane in the left and right pictures of Figure 7.1 for different choices of master and slave sides. Comparing both of these pictures, we can see that there is not any essential difference between choosing Ω_1 or Ω_2 as the slave side. However, since the Lagrange multiplier space $\mathbf{M}_h$ is based on a coarser mesh if Ω_2 is chosen on the slave side, we see some influence in the first step.

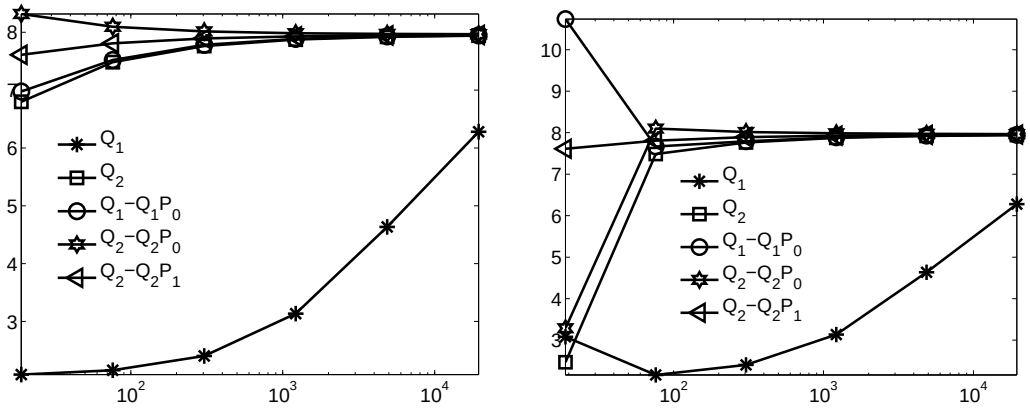

Figure 7.1: Vertical tip displacement at the top right corner versus number of elements (Ω_1 master, Ω_2 slave) (left) and (Ω_2 master, Ω_1 slave) (right), Example 1, Ω_1 nearly incompressible

In a next step, we investigate the situation with the nearly incompressible material in Ω_2 so that the material parameters are $E_1 = 80$, $E_2 = 250$, $\nu_1 = 0.35$, and $\nu_2 = 0.4999$. As before we also want to see the influence of the choice of the master and the slave side. Since lowest order elements also yield really good results, we concentrate now only on Q_1-Q_1P_0, Q_1-HW and Q_1 discretizations. The vertical tip displacement at the top right corner of the

membrane for different levels of refinement are shown in the left and the right pictures of Figure 7.2 for different choices of master and slave sides. The standard approach in both subdomains leads to locking, whereas we obtain a good convergence behavior if Q_1P_0 or the Hu-Washizu discretization is used in Ω_2. As before, we do not see any influence of the choice of the master and slave side when we refine the mesh.

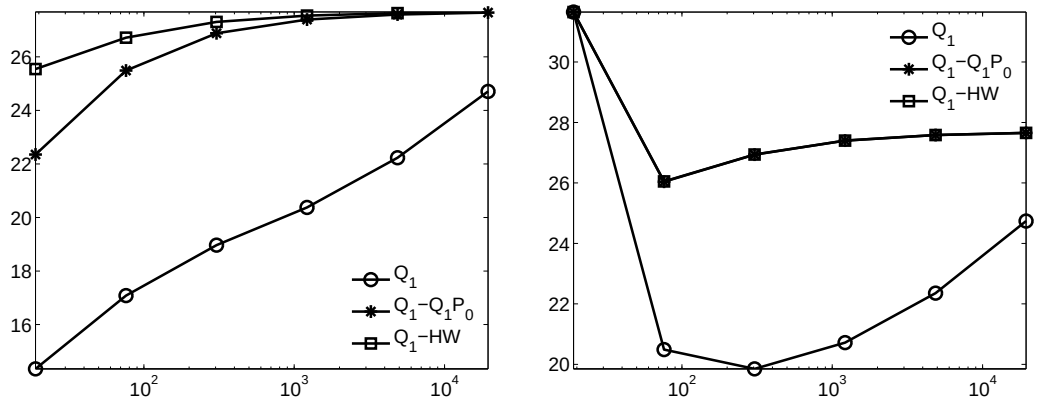

Figure 7.2: Vertical tip displacement at the top right corner versus number of elements (Ω_1 master, Ω_2 slave) (left), and (Ω_2 master, Ω_1 slave) (right), Example 1, Ω_2 nearly incompressible

Example 2: Comparison of errors in the L^2- and H^1-norms. In this example, a two-dimensional region $\Omega := (-1,1) \times (-1,1)$ is decomposed into four non-overlapping subdomains defined by $\Omega_1 := (-1,0) \times (-1,0)$, $\Omega_2 := (0,1) \times (-1,0)$, $\Omega_3 := (-1,0) \times (0,1)$ and $\Omega_4 := (0,1) \times (0,1)$. The problem for this example is taken from [**47**] slightly modified to enforce that the jump of the flux across the interface Γ is zero. Here, the exact solution $\boldsymbol{u} = (u_1, u_2)$ is

$$u_1(x,y) := \frac{\sin(2\,\pi\,y)\,(-1+\cos(2\,\pi\,x))\,(2+2\,\nu)}{E} + xy\sin(\pi\,x)\sin(\pi\,y)\,\frac{(1+\nu)\,(1-2\,\nu)}{1-\nu-2\,\nu^2+E\nu},$$

$$u_2(x,y) := \frac{\sin(2\,\pi\,x)\,(1-\cos(2\,\pi\,y))\,(2+2\,\nu)}{E} + xy\sin(\pi\,x)\sin(\pi\,y)\,\frac{(1+\nu)\,(1-2\,\nu)}{1-\nu-2\,\nu^2+E\nu},$$

where $\nu = 0.3, E = 25$ in Ω_1 and Ω_4, and $\nu = 0.4999, E = 250$ in Ω_2 and Ω_3 so that a nearly incompressible response is obtained in Ω_2 and Ω_3. In this example, the right hand side and the Dirichlet boundary conditions are computed by using the exact solution. We have given the decomposition of the domain and the initial triangulation in the left picture of Figure 7.3, and the error plot versus number of degrees of freedom for different levels of refinement for the L^2 and H^1-norms are given in the middle and the right pictures, respectively. From Figure 7.3, we can see that the optimality can be obtained by using Q_1P_0 and Q_2P_1-approaches for the nearly incompressible material, whereas the standard Q_1-approach locks. Furthermore, we can observe the sub-optimal behavior for Q_2P_0 and Q_2-discretizations.

Example 3: Three-dimensional I-beam. In this numerical test, we consider the coupling of compressible and nearly incompressible elasticity in three-dimensional elasticity. The computational domain Ω, which is an I-beam, is decomposed into three subdomains

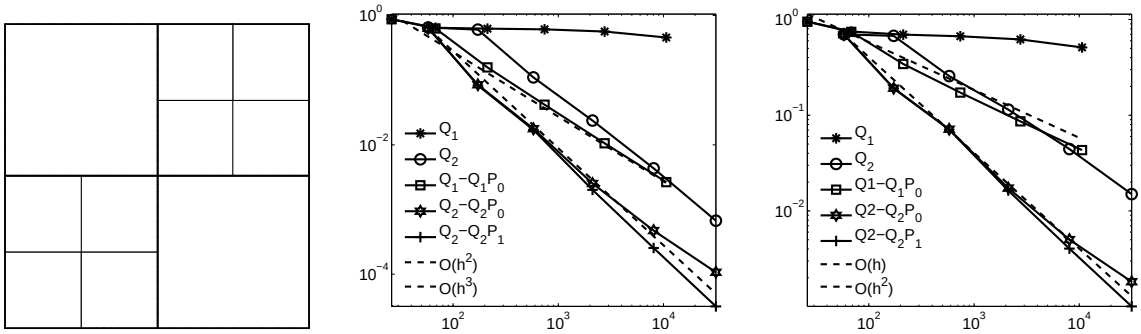

Figure 7.3: Decomposition of the domain and initial triangulation (left), error plot versus number degrees of freedom in L^2-norm (middle) and error plot versus number of degrees of freedom in H^1-norm (right), Example 2

Ω_1, Ω_2 and Ω_3 with $\Omega_1 := (0,50) \times (0,10) \times (0,2)$, $\Omega_2 := (0,50) \times (3,7) \times (2,11)$ and $\Omega_3 := (0,50) \times (0,10) \times (11,13)$. We impose zero Dirichlet boundary condition on Γ_D, where Γ_D is a part of the boundary of Ω with $x = 0$ and $x = 50$ so that the left and the right sides of each subdomain are fixed. And a constant vertical force is applied on a small part of the top boundary ($z = 13$) so that $\sigma(\mathbf{u})\mathbf{n} = \mathbf{g}_N$ on Γ_N with $\Gamma_N := \partial\Omega \backslash \Gamma_D$. The function $\mathbf{g}_N = (g_1, g_2, g_3)$ on Γ_N is given as $g_1 = g_2 = 0$, and

$$g_3 = \begin{cases} -20.35 & \text{if } 22 \le x \le 28 \text{ and } z = 13 \\ 0 & \text{otherwise} \end{cases}.$$

The material parameters are $E_1 = 250$, $\nu_1 = 0.3$, $E_2 = 300$, $\nu_2 = 0.4$, and $E_3 = 350$, $\nu_3 = 0.4999$. We have shown the setting of the problem in the left picture of Figure 7.4, and the resulting deformation of the structure is shown in the right.

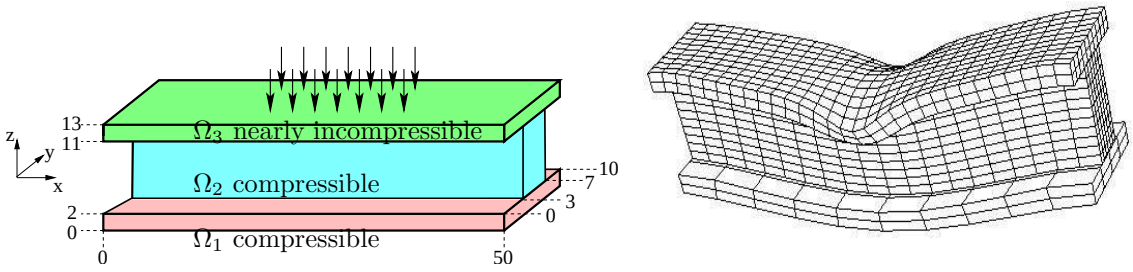

Figure 7.4: Left: I-beam decomposed into three subdomains, Right: the distorted mesh with the Hu-Washizu formulation in subdomain Ω_3

In Figure 7.5, we have shown the vertical displacement along the line $y = 0, z = 13$ versus x-coordinates. As can be seen from this figure, the standard Q_1-approach suffers from severe locking whereas the Hu-Washizu formulation in Ω (HW) and the Hu-Washizu formulation only in Ω_3 (Q_1-HW) yield fast convergence. In this figure, we have also shown the vertical displacement computed by using Q_2-Q_2P_1-approach with a one-level coarser

mesh. We can see that the numerical solution from the coupled approach with the Hu-Washizu discretization is of comparable quality even with mixed quadratic finite elements.

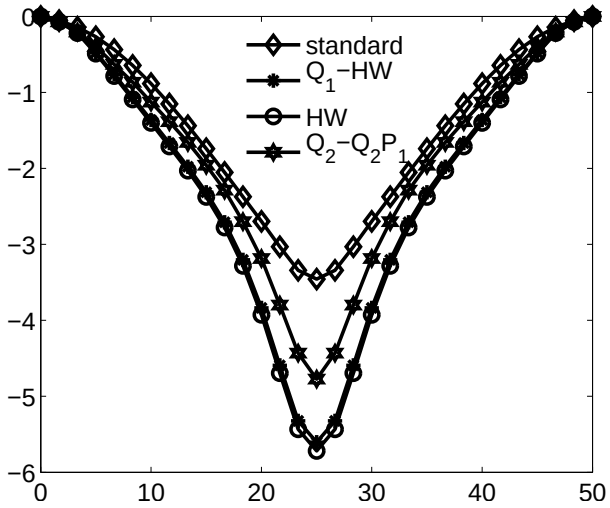

Figure 7.5: Displacement along vertical direction at the line $y = 0, z = 13$ versus x-coordinates, note: Q_2-Q_2P_1-approach is used in a one-level coarser mesh

Example 4. In this numerical test, a two-dimensional domain Ω is decomposed into three subdomains $\Omega_1 := (1.3, 2.7) \times (0, 1)$, $\Omega_2 := (0, 4) \times (1, 2)$ and $\Omega_3 := (1.3, 2.7) \times (2, 3)$, where the domains Ω_1 and Ω_3 are on the slave side of the interface. We consider a nearly incompressible soft material in Ω_2, whereas the materials in Ω_1 and Ω_3 are hard and compressible so that the material parameters are given by $E_1 = 2000, \nu_1 = 0.25$; $E_2 = 100, \nu_2 = 0.4999$; and $E_3 = 2000, \nu_3 = 0.25$. The middle subdomain Ω_2 is fixed at both left and right boundaries, whereas a traction force $60N$ per unit length is applied from the top boundary of Ω_3 and from the bottom boundary of Ω_1 to compress the subdomain Ω_2. The mixed α-formulation introduced in the last chapter for finite elasticity with neo-Hookean law is applied in the middle subdomain, whereas the standard neo-Hookean formulation is applied in the rest. We have shown the problem setting and the initial triangulation in the left picture of Figure 7.6, whereas the deformation of the domain is shown in the right. The solution is computed using Case I of the mixed formulation in Ω_2 with $\alpha = 0$. In the left and right pictures of Figure 7.7, we have plotted the horizontal and vertical displacements of the structure along the line $y = 2$ with respect to x-coordinates using different coupled approach. We can see that the standard neo-Hookean approach (SN) suffers from complete locking, whereas the mixed neo-Hookean formulation in Ω (MN); the two coupled approaches: standard neo-Hookean in Ω_1 and Ω_3 and mixed formulation in Ω_2 (SN-MN), and standard linear elasticity in Ω_1 and Ω_3 and mixed neo-Hookean in Ω_2 (SL-MN) are in good agreement with each other. In the left and right pictures of Figure 7.8, we compare the horizontal and vertical displacements along the line $y = 2$ using linear (ML) and nonlinear (MN) elasticity. In both linear and nonlinear cases, we use the mixed formulations proposed in the last chapter. In the linear case, we use Case II, whereas Case I ($\alpha = 0$) is used in the nonlinear case. In Figure 7.8, we can see that it is not reasonable

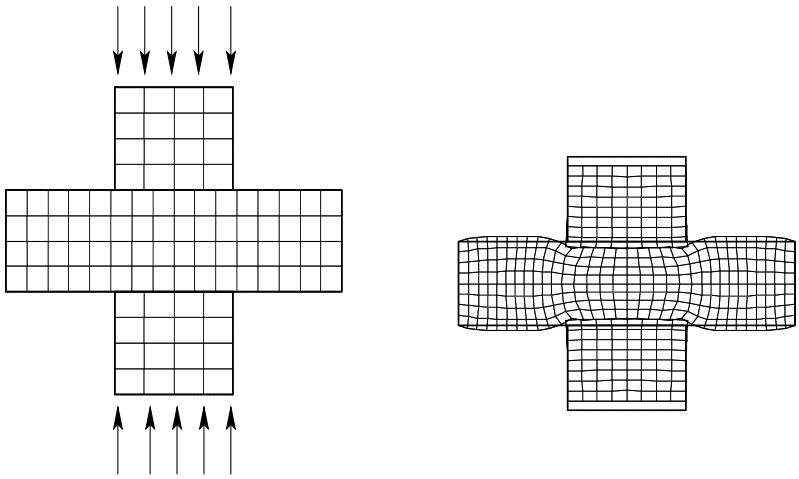

Figure 7.6: Problem setting and deformed configuration

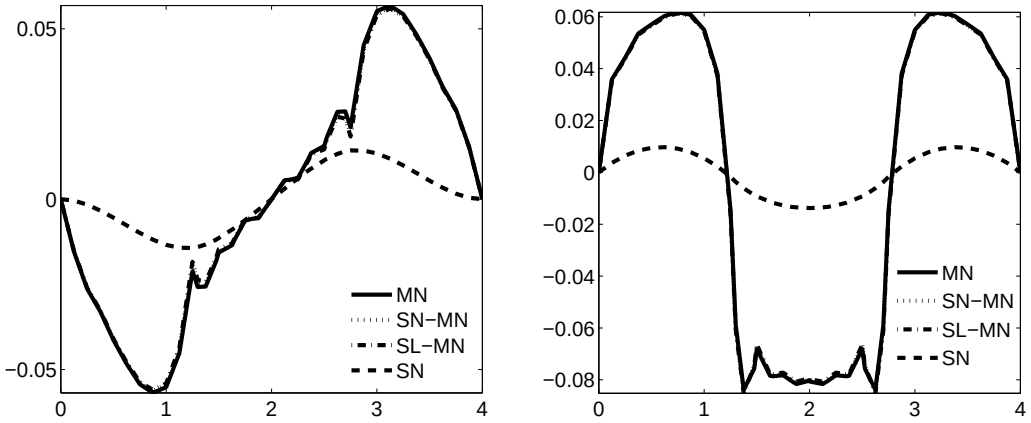

Figure 7.7: Horizontal and vertical displacement versus x-coordinates along the line $y = 2$

to use the model of linear elasticity in the whole domain Ω, whereas Figure 7.7 shows that it is reasonable to use the model of linear elasticity in Ω_1 and Ω_3.

Example 5: One cube pressed upon another. In this numerical test, the global domain Ω is composed of two cubes with dimensions $\Omega_1 = (0, 6)^3$ and $\Omega_2 = (1.3, 4.7) \times (1.3, 4.7) \times (6, 9)$. The bigger one is soft and nearly incompressible and the smaller one is hard and compressible so that the material properties are set to be $E_1 = 100, \nu_1 = 0.4999$ and $E_2 = 2000, \nu_2 = 0.3$. The lower part of the domain Ω_1 is fixed, and we apply a constant traction force $100N$ per unit area from the top of the smaller cube. We apply our mixed α-formulation ($\alpha = 0$, Case I) introduced in the last chapter with neo-Hookean law in Ω_1 whereas the standard neo-Hookean formulation is applied in the upper cube (coupled approach: SN-MN). The finite element solution is computed using several quasi-static steps with load increment. The decomposition of the domain and the triangulation is shown in the left picture of Figure 7.9, and the resulting deformation of the domain is given in the middle. In the right picture of Figure 7.9, we give the vertical displacement of the lower cube along the line $y = 3$ and $z = 3$ using different approaches. We can see

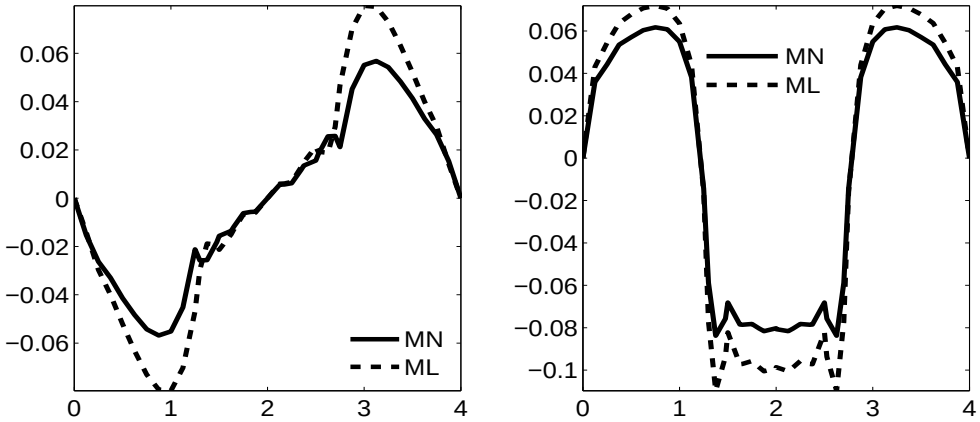

Figure 7.8: Horizontal and vertical displacements versus x-coordinates along the line $y = 2$

that the mixed approach in both subdomains (MN) and the coupled approach (SN-MN) yield good numerical results, whereas the standard approach in both subdomains shows extreme locking.

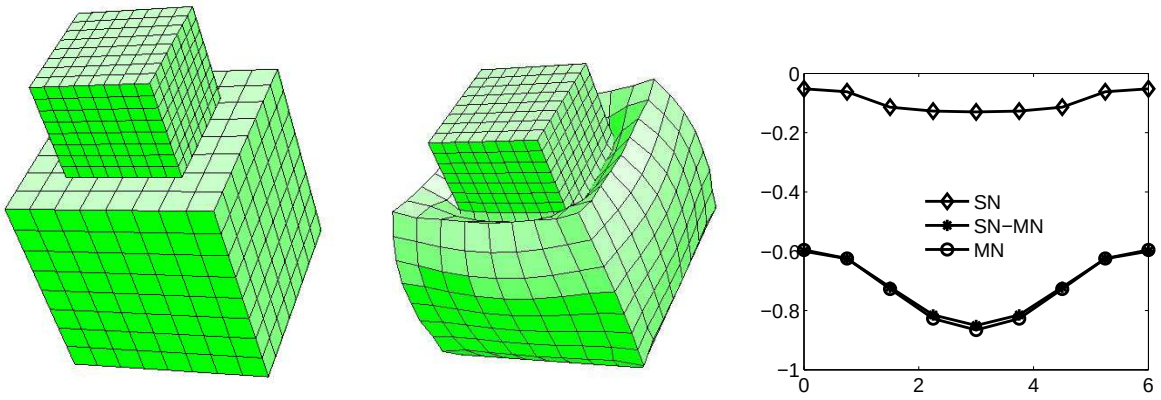

Figure 7.9: Decomposition into two subdomains and triangulation, deformation of the structure, and z-displacement versus x-coordinates along the line $y = 3$ and $z = 3$, Example 5

CHAPTER 8

Conclusion and Outlook

In this chapter, we summarize the main contribution of this thesis and give an outlook to further work.

For the theory of mortar finite elements, allowing locally refined finite element meshes and geometrically non-conforming subdivisions into subdomains as in [**99, 68**], we prove optimal a priori estimates without assuming that the dimension of the Lagrange multiplier space is equal to the dimension of the trace space of the finite element space from the slave side satisfying homogeneous boundary condition on the interface boundary. On the other hand, as in [**163, 68**], we do not require that the partitions match on the boundaries of the interfaces. Furthermore, assuming quasi-uniform meshes on each subdomain, we prove an error estimate, where the constant depending on the maximum of ratios of meshsizes at master and slave sides is replaced by the constant only depending on the logarithm of the maximum of ratios of these meshsizes.

In case of two-dimensional mortar finite elements, we have constructed higher order dual Lagrange multiplier spaces satisfying the optimality assumptions. Using an interesting relation between the biorthogonality and quadrature formulas, we prove that to obtain optimal a priori estimates it is required that the underlying finite element space should be based on Gauß-Lobatto quadrature nodes. These newly constructed dual basis functions satisfy the condition of "equal support", in the sense that the finite element basis functions and the Lagrange multiplier basis functions have the same support.

Although the construction of dual Lagrange multiplier spaces for finite element spaces of tensor product structure is straightforward, the two-dimensional construction cannot be easily extended to the three-dimensional simplicial and serendipity family of elements since these elements do not have a tensor product structure. Restricting ourselves to the quadratic case, we consider simplicial and serendipity finite elements. We show that optimal dual Lagrange multiplier spaces with "equal support" do not exist for quadratic and serendipity finite elements under the assumption that the dimension of the Lagrange multiplier space is equal to the dimension of the trace of the finite element space from the slave side with zero boundary condition on the interface boundary.

To deal with this problem, we generalize the idea of a dual Lagrange multiplier space in two ways. First, we introduce a quasi-dual Lagrange multiplier space for quadratic serendipity elements. Secondly, working with dual Lagrange multiplier spaces whose dimension is smaller than the trace of the finite element space with zero boundary condition on the interface from the slave side, we show that dual Lagrange multiplier spaces with "equal support" can be constructed for the quadratic simplicial and serendipity finite elements. For all cases, we provide numerical results.

Starting with the saddle point formulation of interface problems with the non-homogeneous jump in the flux and in the solution, we prove the existence and uniqueness of the solution of the interface problems. We show that the interface conditions do not affect the stiffness matrix and only enter into the right hand side. Numerical results are supplied to verify the theoretical results.

We have applied mortar finite elements for different coupled problems coming from physics and engineering. In particular, elasto-acoustic problems and problems coupled with different linear or nonlinear material laws are solved. Moreover, time-dependent problems with jumps in the diffusion coefficients, a coupled advective heat conduction problem and problems with sliding meshes are presented.

We have carried out a detailed analysis of a generalized Hu-Washizu formulation, of which the classical Hu-Washizu formulation is a special case. The generalization takes the form of a one-parameter family of formulations. Attention is paid to the question of well-posedness and convergence in the incompressible limit, and it is shown with a preliminary analysis that the classical Hu-Washizu formulation is not the appropriate setting in which to carry out such an analysis.

We have shown the well-posedness of the generalized formulation, subject to conditions on the spaces of stress and strain. Although the discrete inf-sup condition does not hold uniformly, the discretization error is shown to be optimal and robust, in the sense that the convergence rate does not depend on the Lamé parameter λ. This shows that the lack of stability resulting from the checkerboard mode is only confined to the stress. A λ-independent optimal error bound on the post-processed stress is derived.

We have generalized the modified Hu-Washizu formulation for geometrically nonlinear elasticity with Saint-Venant Kirchhoff law. Furthermore, a suitable three-field formulation for a general hyperelastic material law is presented. Different numerical examples are presented to illustrate the locking behavior that occurs in the incompressible limit when the conditions on the bases and on α necessary for stability are not met. The results also illustrate the good behavior that is achieved otherwise.

Finally, we consider the coupling of a compressible and a nearly incompressible material in linear elasticity. Working with a suitable discretization scheme to deal with a nearly incompressible material, we provide an error estimate uniform with respect to the Lamé parameters λ for the nearly incompressible material. A range of numerical examples of coupled problems are presented.

The mortar finite element method has already proved to be a flexible and optimal tool to couple non-conforming discretization schemes or different physical models. Working with dual Lagrange multiplier spaces, an efficient iterative solver like multigrid can easily be adapted. However, there are many open problems for the construction of these dual Lagrange multiplier spaces. Particularly in three-dimensional mortar finite elements, the construction of a dual Lagrange multiplier space is not so easy for higher order finite elements. It seems that the quasi-dual Lagrange multiplier space can be generalized to the higher order serendipity and simplicial finite elements. However, the local standard finite element basis functions should be modified as we have done in the quadratic case. Furthermore, some modification is necessary to deal with curved interfaces and arbitrary distorted quadrilateral meshes.

To treat the nearly incompressible material in linear elasticity, the Hu-Washizu formulation is shown to be a key formulation, which provides a variational background for different finite element approaches which are in use in engineering computations. The extension of the linear analysis to the general hyperelastic material law is not trivial. Finally, the coupled problem of a nearly incompressible material and a compressible material is analyzed by taking into account the fact that the finite element formulation used for the nearly incompressible material satisfies the discrete inf-sup condition. It is an open problem to analyze the coupled problem where the Hu-Washizu formulation is used for the nearly incompressible material.

Bibliography

[1] Y. Achdou and Y. Maday, *The mortar element method with overlapping subdomains*, SIAM Journal on Numerical Analysis, 40 (2002), pp. 601–628.

[2] L. Adams and Z. Li, *The immersed interface/multigrid methods for interface problems*, SIAM Journal on Scientific Computing, 24 (2002), pp. 463–479.

[3] R. Adams, *Sobolev Spaces*, Academic Press, New York, 1975.

[4] J. Alberty, C. Carstensen, S. Funken, and R. Klose, *Matlab implementation of the finite element method in elasticity*, Computing, 69 (2002), pp. 239–263.

[5] A. Alonso, A. D. Russo, C. Otero-Souto, C. Padra, and R. Rodríguez, *An adaptive finite element scheme to solve fluid-structure vibration problems on non-matching grids*, Computing and Visualization in Science, 4 (2001), pp. 67–78.

[6] U. Andelfinger and E. Ramm, *EAS-elements for two-dimensional, three-dimensional, plate and shell structures and their equivalence to HR-elements*, International Journal for Numerical Methods in Engineering, 36 (1993), pp. 1311–1337.

[7] F. Armero, *On the locking and stability of finite elements in finite deformation plane strain problems*, Computers and Structures, 75 (2000), pp. 261–290.

[8] D. Arnold, F. Brezzi, and J. Douglas, Jr., *PEERS: A new mixed finite element for plane elasticity*, Japan J. Appl. Math., 1 (1984), pp. 347–367.

[9] D. Arnold, L. Scott, and M. Vogelius, *Regular inversion of the divergence operator with dirichlet boundary conditions on a polygon*, Annali Scuola Norm. Sup. Pisa, Serie 4, 15 (1988), pp. 169–192.

[10] D. Arnold and R. Winther, *Mixed finite elements for elasticity*, Numerische Mathematik, 92 (2002), pp. 401–419.

[11] C. Atkinson and C. R. Champion, *Some boundary-value problems for the equation* $\nabla \cdot (|\nabla\phi|^N) = 0$, The Quarterly Journal of Mechanics and Applied Mathematics, 37 (1984), pp. 401–419.

[12] I. Babuška, *The finite element method for elliptic equations with discontinuous coefficients*, Computing, 5 (1970), pp. 207–213.

[13] ——, *The finite element method with Lagrangian multipliers*, Numerische Mathematik, 20 (1973), pp. 179–192.

[14] I. Babuška and M. Suri, *Locking effects in the finite element approximation of elasticity problems*, Numerische Mathematik, 62 (1992), pp. 439–463.

[15] ——, *On locking and robustness in the finite element method*, SIAM Journal on Numerical Analysis, 29 (1992), pp. 1261–1293.

[16] J. Ball, *Convexity conditions and existence theorems in nonlinear elasticity*, Archive for Rational Mechanics and Analysis, 63 (1977), pp. 337–403.

[17] P. Bastian, K. Birken, K. Johannsen, S. Lang, N. Neuss, H. Rentz–Reichert, and C. Wieners, *UG – a flexible software toolbox for solving partial differential equations*, Computing and Visualization in Science, 1 (1997), pp. 27–40.

[18] R. Becker, P. Hansbo, and R. Stenberg, *A finite element method for domain decomposition with non-matching grids*, Mathematical Modelling and Numerical Analysis, 37 (2003), pp. 209–225.

[19] F. Belgacem, P. Hild, and P. Laborde, *The mortar finite element method for contact problems*, Mathematical and Computer Modelling, 28 (1998), pp. 263–271.

[20] T. Belytschko and W. Bachrach, *Efficient implementation of quadrilaterals with high coarse-mesh accuracy*, Computer Methods in Applied Mechanics and Engineering, 54 (1986), pp. 279–301.
[21] T. Belytschko, W. Liu, and B. Moran, *Nonlinear finite elements for continua and structures*, John Wiley and Sons, Ney York, 2000.
[22] F. Ben Belgacem, *The mortar finite element method with Lagrange multipliers*, Numerische Mathematik, 84 (1999), pp. 173–197.
[23] ——, *The mixed mortar finite element method for the incompressible Stokes problem: Convergence analysis*, SIAM Journal on Numerical Analysis, 37 (2000), pp. 1085–1100.
[24] ——, *A stabilized domain decomposition method with nonmatching grids for the Stokes problem in three dimensions*, SIAM Journal on Numerical Analysis, 42 (2004), pp. 667–685.
[25] F. Ben Belgacem, P. Hild, and P. Laborde, *Extension of the mortar finite element method to a variational inequality modeling unilateral contact*, Mathematical Models and Methods in Applied Sciences, 9 (1999), pp. 287–303.
[26] F. Ben Belgacem and Y. Maday, *The mortar element method for three dimensional finite elements*, Mathematical Modelling and Numerical Analysis, 31 (1997), pp. 289–302.
[27] F. Ben Belgacem, P. Seshaiyer, and M. Suri, *Optimal convergence rates of h-p mortar finite element methods for second-order elliptic problems*, Mathematical Modelling and Numerical Analysis, 34 (2000), pp. 591–606.
[28] A. Bermúdez, R. Duran, M. Muschietti, R. Rodríguez, and J. Solomin, *Finite element vibration analysis of fluid-solid systems without spurious modes*, SIAM Journal on Numerical Analysis, 32 (1995), pp. 1280–1295.
[29] A. Bermúdez and R. Rodríguez, *Finite element computation of the vibration modes of a a fluid-solid system*, Computer Methods in Applied Mechanics and Engineering, 119 (1994), pp. 355–370.
[30] C. Bernardi, M. Dauge, and Y. Maday, *Compatibilité de traces aux arêtes et coins d'un polyèdre. (compatibility of traces on the edges and corners of a polyhedron)*, C. R. Acad. Sci., Paris, Sér. I, Math., 331 (2000), pp. 689–684.
[31] ——, *Polynomials in the Sobolev World*, tech. rep., Preprint R03038, the Laboratoire Jacques-Louis Lions, 2003.
[32] C. Bernardi, N. Debit, and Y. Maday, *Coupling finite element and spectral methods: First results*, Mathematics of Computation, 54 (1990), pp. 21–39.
[33] C. Bernardi, Y. Maday, and A. Patera, *Domain decomposition by the mortar element method*, in Asymptotic and numerical methods for partial differential equations with critical parameters, H. K. et al., ed., Reidel, Dordrecht, 1993, pp. 269–286.
[34] ——, *A new nonconforming approach to domain decomposition: the mortar element method*, in Nonlinear partial differential equations and their applications, H. B. et al., ed., Paris, 1994, pp. 13–51.
[35] J. Boland and R. Nicolaides, *Stability of finite elements under divergence constraints*, SIAM Journal on Numerical Analysis, 20 (1983), pp. 723–731.
[36] L. Bos, *On certain configurations of points in $\mathbb{R}^n$ which are unisolvent for polynomial interpolation*, Journal of Approximation Theory, 64 (1991), pp. 271–280.
[37] L. Bos, M. Taylor, and B. Wingate, *Tensor product Gauss-lobatto points are Fekete points for the cube*, Mathematics of Computation, 70 (2000), pp. 1543–1547.
[38] D. Braess, *Stability of saddle point problems with penalty*, Mathematical Modelling and Numerical Analysis, 30 (1996), pp. 731–742.
[39] ——, *Enhanced assumed strain elements and locking in membrane problems*, Computer Methods in Applied Mechanics and Engineering, 165 (1998), pp. 155–174.
[40] ——, *Finite Elements. Theory, fast solver, and applications in solid mechanics*, Cambridge University Press, Second Edition, 2001.
[41] D. Braess, C. Carstensen, and B. Reddy, *Uniform convergence and a posteriori error estimators for the enhanced strain finite element method*, Numerische Mathematik, 96 (2004), pp. 461–479.
[42] D. Braess and W. Dahmen, *Stability estimates of the mortar finite element method for 3–dimensional problems*, East–West Journal of Numerical Mathematics, 6 (1998), pp. 249–264.

[43] D. Braess and W. Dahmen, *The mortar element method revisited– what are the right norms?*, in Thirteenth International Conference on Domain Decomposition Methods, N. Debit, M. Garbey, R. Hoppe, J. Pèriaux, D. Keyes, and Y. Kuznetsov, eds., 2001, pp. 27–40.
[44] D. Braess, W. Dahmen, and C. Wieners, *A multigrid algorithm for the mortar finite element method*, SIAM Journal on Numerical Analysis, 37 (1999), pp. 48–69.
[45] D. Braess and P.-B. Ming, *A finite element method for nearly incompressible elasticity problems*, Mathematics of Computation, 74 (2005), pp. 25–52.
[46] J. Bramble and J. King, *A finite element method for interface problems in domains with smooth boundaries and interfaces*, Advances in Computational Mathematics, 6 (1996), pp. 109–138.
[47] S. Brenner, *A nonconforming mixed multigrid method for the pure displacement problem in planar linear elasticity*, SIAM Journal on Numerical Analysis, 30 (1993), pp. 116–135.
[48] ——, *A nonconforming mixed multigrid method for the pure traction problem in planar linear elasticity*, Mathematics of Computation, 63 (1994), pp. 435–460.
[49] ——, *Korn's inequalities for piecewise H^1 vector fields*, Mathematics of Computation, 73 (2004), pp. 1067–1087.
[50] S. Brenner and L. Scott, *The Mathematical Theory of Finite Element Methods*, Springer–Verlag, New York, 1994.
[51] S. Brenner and L. Sung, *Linear finite element methods for planar linear elasticity*, Mathematics of Computation, 59 (1992), pp. 321–338.
[52] F. Brezzi and M. Fortin, *Mixed and hybrid finite element methods*, Springer–Verlag, New York, 1991.
[53] ——, *A minimal stabilization procedure for mixed finite element methods*, Numerische Mathematik, 89 (2001), pp. 457–491.
[54] F. Brezzi, L. Franca, D. Marini, and A. Russo, *Stabilization techniques for domain decomposition methods with non–matching grids*, in Proceedings of the 9th International Conference on Domain Decomposition, P. Bjørstad, M. Espedal, and D. Keyes, eds., Bergen, 1998, Domain Decomposition Press, pp. 1–11.
[55] F. Brezzi and D. Marini, *Error estimates for the three-field formulation with bubble stabilization*, Mathematics of Computation, 70 (2001), pp. 911–934.
[56] U. Brink and E. Stein, *On some mixed finite element methods for incompressible and nearly incompressible finite elasticity*, Computational Mechanics, 19 (1996), pp. 105–119.
[57] L. Brutman, *Lebesgue functions for polynomial interpolation—a survey*, Ann. Numer. Math., 4 (1997), pp. 111–127.
[58] A. Buffa, *Error estimate for a stabilised domain decomposition method with nonmatching grids*, Numerische Mathematik, 90 (2002), pp. 617–640.
[59] X.-C. Cai, M. Dryja, and M. Sarkis, *Overlapping nonmatching grid mortar element methods for elliptic problems*, SIAM Journal on Numerical Analysis, 36 (1998), pp. 581–606.
[60] Y. Cao and M. Gunzburger, *Least-squares finite element approximations to solutions of interface problems*, SIAM Journal on Numerical Analysis, 35 (1998), pp. 393–405.
[61] K. Chavan, B. Lamichhane, and B. Wohlmuth, *Locking-free finite element methods for linear and nonlinear elasticity in 2D and 3D*, Tech. Rep. 13, Universität Stuttgart, SFB 404, 2005.
[62] Z. Chen and J. Zou, *Finite element methods and their convergence for elliptic and parabolic interface problems*, Numerische Mathematik, 79 (1998), pp. 175–202.
[63] P. Ciarlet, *The finite element method for elliptic problems*, North Holland, Amsterdam, 1978.
[64] P. Ciarlet, *Mathematical Elasticity Volume I: Three-Dimensional Elasticity*, North-Holland, Amsterdam, 1988.
[65] P. Clément, *Approximation by finite element functions using local regularization*, RAIRO Anal. Numér., 9 (1975), pp. 77–84.
[66] G. Cohen, P. Joly, J. Roberts, and N. Tordjman, *Higher order triangular finite elements with mass lumping for the wave equation*, SIAM Journal on Numerical Analysis, 38 (2001), pp. 2047–2078.
[67] M. Costabel, *Boundary integral equations on lipschitz domains: Elementary results*, SIAM Journal on Mathematical Analysis, 19 (1988), pp. 613–626.

[68] W. Dahmen, B. Faermann, I. Graham, W. Hackbusch, and S. Sauter, *Inverse inequalities on non-quasiuniform meshes and application to the mortar element method*, Mathematics of Computation, 73 (2003), pp. 1107–1138.
[69] W. Dahmen and R. Stevenson, *Element-by-element construction of wavelets satisfying stability and moment conditions*, SIAM Journal on Numerical Analysis, 37 (1999), pp. 319–352.
[70] P. Davis and R. Rabinowitz, *Methods for Numerical Integration*, Academic Press, Orlando, 1985.
[71] E. de Souza, N. Peric, M. Dutko, and D. Owen, *Design of simple low order finite elements for large strain analysis of nearly incompressible solids*, International Journal of Solids and Structures, 33 (1996), pp. 3277–3296.
[72] N. Debit and Y. Maday, *The coupling of spectral and finite element method for the approximation of the Stokes problem*, in Computational Mathematics and Applications, Pavia, 1989, 8th France-USSR-Italy Joint Symposium Proceedings, pp. 139–163.
[73] J. Djoko, B. Lamichhane, B. Reddy, and B. Wohlmuth, *Conditions for equivalence between the Hu-Washizu and related formulations, and computational behavior in the incompressible limit*, Computer Methods in Applied Mechanics and Engineering, (2005). Published online.
[74] R. Falk, *Nonconforming finite element methods for the equations of linear elasticity*, Mathematics of Computation, 57 (1991), pp. 529–550.
[75] B. Flemisch, J. Melenk, and B. Wohlmuth, *Mortar methods with curved interfaces*, Applied Numerical Mathematics, 54 (2005), pp. 339–361.
[76] B. Flemisch and B. Wohlmuth, *A domain decomposition method on nested domains and non-matching grids*, Numerical Methods for Partial Differential Equations, 20 (2004), pp. 374–387.
[77] ——, *Nonconforming methods for nonlinear elasticity problems*, Tech. Rep. 03, Universität Stuttgart, SFB 404, 2005.
[78] ——, *Stable Lagrange multipliers for quadrilateral meshes of curved interfaces in 3D*, Tech. Rep. IANS 2005/005, University of Stuttgart, 2005.
[79] G. Galdi, *An Introduction to the Mathematical Theory of the Navier-Stokes Equations, Volume I*, vol. 38 of Springer Tracts in Natural Philosophy, Springer, first revised ed., 1997.
[80] V. Girault and P.-A. Raviart, *Finite Element Methods for Navier-Stokes Equations*, Springer-Verlag, Berlin, 1986.
[81] S. Glaser and F. Armero, *On the formulation of enhanced strain finite elements in finite deformation*, Engineering Compuations, 14 (1997), pp. 759–791.
[82] J. Gopalakrishnan, *Mortar estimates independent of number of subdomains*, East–West Journal of Numerical Mathematics, 8 (2000), pp. 111–125.
[83] P. Grisvard, *Elliptic problems in nonsmooth domains*, vol. 24 of Monographs and Studies in Mathematics, Pitman (Advanced Publishing Program), Boston, MA, 1985.
[84] ——, *Singularities in boundary value problems*, vol. 22 of Research Notes in Applied Mathematics, Springer-Verlag, Masson, 1992.
[85] A. Hansbo and P. Hansbo, *An unfitted finite element method, based on Nitsche's method, for elliptic interface problems*, Computer Methods in Applied Mechanics and Engineering, 191 (2002), pp. 5537–5552.
[86] P. Hansbo and J. Hermansson, *Nitsche's method for coupling non-matching meshes in fluid-structure vibration problems*, Computational Mechanics, 32 (2003), pp. 134–139.
[87] P. Hauret and P. L. Tallec, *Stabilized discontinuous mortar formulation for elastostatics and elastodynamics problems - Part I: formulation and analysis*, tech. rep., CMAP Internal Report 553, Ecole Polytechnique, France, 2004.
[88] ——, *A stabilized discontinuous mortar formulation for elastostatics and elastodynamics problems - Part II: discontinuous Lagrange multipliers*, tech. rep., CMAP Internal Report 554, Ecole Polytechnique, France, 2004.
[89] B. Heinrich and S. Nicaise, *Nitsche mortar finite element method for transmission problems with singularities*, IMA Journal of Numerical Analysis, 23 (2003), pp. 331–358.
[90] L. Herrmann, *Elasticity equations for incompressible and nearly incompressible materials by a variational theorem*, AIAA Journal, 3 (1965), pp. 1896–1900.

[91] J. Hesthaven, *From electrostatics to almost optimal nodal sets for polynomial interpolation in a simplex*, SIAM Journal on Numerical Analysis, 35 (1998), pp. 655–676.
[92] P. Hild and P. Laborde, *Quadratic finite element methods for unilateral contact problems*, Applied Numerical Mathematics, 41 (2002), pp. 401–421.
[93] H. Hu, *On some variational principles in the theory of elasticity and the theory of plasticity*, Scientia Sinica, 4 (1955), pp. 33–54.
[94] J. Huang and J. Zou, *Some new a priori estimates for second-order elliptic and parabolic interface problems*, J. Differ. Equations, 184 (2002), pp. 570–586.
[95] S. Hüeber and B. Wohlmuth, *An optimal a priori error estimate for non-linear multibody contact problems*, SIAM Journal on Numerical Analysis, 43 (2005), pp. 157–173.
[96] T. Hughes, *The finite element method: Linear, static and dynamic finite element analysis*, Prentice-Hall, 1987.
[97] E. Kasper and R. Taylor, *A mixed-enhanced strain method. Part I: geometrically linear problems*, Computers and Structures, 75 (2000), pp. 237–250.
[98] ——, *A mixed-enhanced strain method. Part II: geometrically nonlinear problems*, Computers and Structures, 75 (2000), pp. 251–260.
[99] C. Kim, R. Lazarov, J. Pasciak, and P. Vassilevski, *Multiplier spaces for the mortar finite element method in three dimensions*, SIAM Journal on Numerical Analysis, 39 (2001), pp. 519–538.
[100] J. Korelc and P. Wriggers., *An efficient 3D enhanced strain element with Taylor expansion of the shape functions*, Computational Mechanics, 19 (1996), pp. 30–40.
[101] M. Küssner and B. Reddy, *The equivalent parallelogram and parallelepiped, and their application to stabilized finite elements in two and three dimensions*, Computer Methods in Applied Mechanics and Engineering, 190 (2001), pp. 1967–1983.
[102] B. Lamichhane, B. Reddy, and B. Wohlmuth, *Convergence in the incompressible limit of finite element approximations based on the hu-washizu formulation*, Tech. Rep. 05, University of Stuttgart, SFB 404, 2004.
[103] B. Lamichhane, R. Stevenson, and B. Wohlmuth, *Higher order mortar finite element methods in 3D with dual Lagrange multiplier bases*, Numerische Mathematik, 102 (2005), pp. 93–121.
[104] B. Lamichhane and B. Wohlmuth, *Higher order dual Lagrange multiplier spaces for mortar finite element discretizations*, CALCOLO, 39 (2002), pp. 219–237.
[105] ——, *Mortar finite elements for interface problems*, Computing, 72 (2004), pp. 333–348.
[106] ——, *Mortar finite elements with dual Lagrange multipliers: Some applications*, in Fifteenth International Conference on Domain Decomposition Methods, R. Kornhuber, R. Hoppe, J. Pèriaux, O. Pironneau, O. Widlund, and J. Xu, eds., 2004, pp. 319–326.
[107] ——, *A quasi-dual Lagrange multiplier space for serendipity mortar finite elements in 3D*, Mathematical Modelling and Numerical Analysis, 38 (2004), pp. 73–92.
[108] ——, *Biorthogonal bases with local support and approximation properties*, Tech. Rep. 02, University of Stuttgart, SFB 404, 2005. To appear in Mathematics of Computation.
[109] T. Laursen, *Computational Contact and Impact Mechanics*, Springer, 2002.
[110] C.-O. Lee, J. Lee, and D. Sheen, *A locking-free nonconforming finite element method for planar linear elasticity*, Advances in Computational Mathematics, 19 (2003), pp. 277–291.
[111] R. LeVeque and Z. Li, *The immersed interface method for elliptic equations with discontinuous coefficients and singular sources*, SIAM Journal on Numerical Analysis, 31 (1994), pp. 1019–1044.
[112] Z. Li, *Existence of minimizers and microstructure in nonlinear elasticity*, Nonlinear Analysis, Theory Methods and Applications, 27 (1996), pp. 297–308.
[113] ——, *A fast iterative algorithm for elliptic interface problems*, SIAM Journal on Numerical Analysis, 35 (1998), pp. 230–254.
[114] J.-L. Lions and E. Magenes, *Non-homogeneous boundary value problems and applications. Vol. I*, Springer-Verlag, New York, 1972. Translated from the French by P. Kenneth, Die Grundlehren der mathematischen Wissenschaften, Band 181.
[115] W. Liu, *Degenerate quasilinear elliptic equations arising from bimaterial problems in elastic-plastic mechanics*, Nonlinear Analysis, 35 (1999), pp. 517–529.

[116] W. Liu and J. Barret, *A remark on the regularity of the solutions of the p-Laplacian and its application*, Journal of Mathematical Analysis and Applications, 178 (1993), pp. 470–488.
[117] W. Liu and N. Yan, *Quasi-norm local error estimators for p-Laplacian*, SIAM Journal on Numerical Analysis, 39 (2001), pp. 100–127.
[118] L. Marcinkowski, *A mortar finite element method for fourth order problems in two dimensions with Lagrange multipliers*, SIAM Journal on Numerical Analysis, 42 (2005), pp. 1998–2019.
[119] T. McDevitt and T. Laursen, *A mortar-finite element formulation for frictional contact problems*, International Journal for Numerical Methods in Engineering, 48 (2000), pp. 1525–1547.
[120] D. Mijuca, *On hexahedral finite element HC8/27 in elasticity*, Computational Mechanics, 33 (2004), pp. 466–480.
[121] J. Nagtegaal, D. Parks, and J. Rice, *On numerically accurate finite element solutions in the fully plastic range*, Computer Methods in Applied Mechanics and Engineering, 4 (1974), pp. 153–177.
[122] Z. Néder, K. Váradi, L. Mán, and K. Friedrich, *Numerical and finite element contact temperature analysis of steel-bronze real surfaces in dry sliding contact*, Tribology Transactions, 42 (1999), pp. 453–462.
[123] R. Ogden, *Non-Linear Elastic Deformations*, Dover Publications, Inc., Mineola, New York, 1997.
[124] P. Oswald and B. Wohlmuth, *On polynomial reproduction of dual FE bases*, in Thirteenth International Conference on Domain Decomposition Methods, N. Debit, M. Garbey, R. Hoppe, J. Pèriaux, D. Keyes, and Y. Kuznetsov, eds., 2001, pp. 85–96.
[125] R. Pasquetti and F. Rapetti, *Spectral element methods on triangles and quadrilaterals: comparisons and applications*, Journal of Computational Physics, 198 (2004), pp. 349–362.
[126] L. Pavarino and A. Toselli, *Recent Developments in Domain Decomposition Methods*, Springer, 2002.
[127] B. Pere and I. Paćzelt, *A mapping technique for a heat conduction problem on moving mesh using the hp-version of the finite element method*, Journal of Computational and Applied Mechanics, 3 (2002), pp. 169–191.
[128] T. Pian and K. Sumihara, *Rational approach for assumed stress finite elements*, International Journal for Numerical Methods in Engineering, 20 (1984), pp. 1685–1695.
[129] R. Piltner and R. Taylor, *A systematic construction of b-bar functions for linear and nonlinear mixed-enhanced finite elements for plane elasticity problems*, International Journal for Numerical Methods in Engineering, 44 (1999), pp. 615–639.
[130] A. Quarteroni and A. Valli, *Numerical approximation of partial differential equations*, Springer–Verlag, Berlin, 1994.
[131] ———, *Domain Decomposition Methods for Partial Differential Equations*, Numerical Mathematics and Scientific Computation, Oxford University Press, 1999.
[132] W. Rachowicz, D. Pardo, and L. Demkowicz, *Fully automatic hp-adaptivity in three dimensions*, Tech. Rep. ICES 04-29, 2004, Institute for Computational and Engineering Sciences, The University of Texas at Austin, 2004. To appear in Computer Methods in Applied Mechanics and Engineering.
[133] B. Reddy and J. Simo, *Stability and convergence of a class of enhanced strain methods*, SIAM Journal on Numerical Analysis, 32 (1995), pp. 1705–1728.
[134] S. Reese, P. Wriggers, and B. Reddy, *A new locking-free brick element technique for large deformation problems in elasticity*, Computers and Structures, 75 (2000), pp. 291–304.
[135] E. Reissner and S. Atluri, *On the formulation of variational theorems involving volume constraints*, Computational Mechanics, 5 (1989), pp. 337–344.
[136] M. Renardy and R. Rogers, *An Introduction to Partial Differential Equations*, Springer-Verlag, 2004.
[137] G. Romano, F. M. de Sciarra, and M. Diaco, *Well-posedness and numerical performances of the strain gap method*, International Journal for Numerical Methods in Engineering, 51 (2001), pp. 103–126.

[138] L. Scott and M. Vogelius, *Norm estimates for a maximal right inverse of the divergence operator in spaces of piecewise polynomials*, Mathematical Modelling and Numerical Analysis, 19 (1985), pp. 111–143.
[139] L. Scott and S. Zhang, *Finite element interpolation of nonsmooth functions satisfying boundary conditions*, Mathematics of Computation, 54 (1990), pp. 483–493.
[140] P. Seshaiyer and M. Suri, *Uniform hp convergence results for the mortar finite element method*, Mathematics of Computation, 69 (2000), pp. 521–546.
[141] J. Simo and F. Armero, *Geometrically nonlinear enhanced strain mixed methods and the method of incompatible modes*, International Journal for Numerical Methods in Engineering, 33 (1992), pp. 1413–1449.
[142] J. Simo, F. Armero, and R. Taylor, *Improved versions of assumed enhanced tri-linear elements for 3D finite deformation problems*, Computer Methods in Applied Mechanics and Engineering, 110 (1993), pp. 359–386.
[143] J. Simo and M. Rifai, *A class of assumed strain method and the methods of incompatible modes*, International Journal for Numerical Methods in Engineering, 29 (1990), pp. 1595–1638.
[144] J. Simo, R. Taylor, and K. Pister, *Variational and projection methods for the volume constraint in finite deformation elasto-plasticity*, Computer Methods in Applied Mechanics and Engineering, 51 (1985), pp. 177–208.
[145] B. Smith, P. Bjørstad, and W. Gropp, *Domain Decomposition: Parallel Multilevel Methods for Elliptic Partial Differential Equations*, Cambridge University Press, 1996.
[146] E. Stein and M. Rüter, *Finite element methods for elasticity with error-controlled discretization and model adaptivity*, in Encyclopedia of Computational Mechanics, E. Stein, R. de Borst, and T. Hughes, eds., Wiley, 2004, pp. 5–58.
[147] R. Stevenson, *Locally supported, piecewise polynomial biorthogonal wavelets on non-uniform meshes*, Constructive Approximation, 19 (2003), pp. 477–508.
[148] H. Stolarski and T. Belytschko, *Limitation principles for mixed finite elements based on the Hu-Washizu variational formulation*, Computer Methods in Applied Mechanics and Engineering, 60 (1987), pp. 195–216.
[149] M. Taylor, B. Wingate, and R. Vincent, *An algorithm for computing Fekete points in the triangle*, SIAM Journal on Numerical Analysis, 38 (2000), pp. 1707–1720.
[150] S. Timoshenko and J. Goodier, *Theory of Elasticity*, McGraw-Hill, New York, 3rd ed., 1970.
[151] A. Toselli and O. Widlund, *Domain Decomposition Methods - Algorithms and Theory*, Springer, 2005.
[152] H. Triebel, *Interpolation theory, function spaces, differential operators*, vol. 18 of North-Holland Mathematical Library, North-Holland Publishing Co., Amsterdam, 1978.
[153] P. van den Bogert, R. de Borst, G. Luiten, and J. Zeilmaker, *Robust finite elements for 3D analysis of rubber-like materials*, Engineering Computations, 8 (1991), pp. 3–17.
[154] M. Vogelius, *An analysis of the p-version of the finite element method for nearly incompressible materials. Uniformly valid, optimal error estimates*, Numerische Mathematik, 41 (1983), pp. 39–53.
[155] T. Warburton, L. Pavarino, and J. Hesthaven, *A pseudo-spectral scheme for the incompressible Navier-Stokes equations using unstructured nodal elements*, Journal of Computational Physics, 164 (2000), pp. 1–21.
[156] K. Washizu, *Variational methods in elasticity and plasticity*, Pergamon Press, Oxford, 3rd ed., 1982.
[157] A. Wiegmann and K. Bube, *The explicit-jump immersed interface method: Finite difference methods for pdes with piecewise smooth solutions*, SIAM Journal on Numerical Analysis, 37 (2000), pp. 827–862.
[158] C. Wieners, *Robust multigrid methods for nearly incompressible linear elasticity*, Computing, 64 (2000), pp. 289–306.
[159] C. Wieners and B. Wohlmuth, *The coupling of mixed and conforming finite element discretizations*, in Proceedings of the 10th International Conference on Domain Decomposition, J. Mandel, C. Farhat, and X. Cai, eds., AMS, Contemporary Mathematics series, 1998, pp. 546–553.

[160] C. Wieners and B. Wohlmuth, *Duality estimates and multigrid analysis for saddle point problems arising from mortar discretizations*, SIAM Journal on Scientific Computing, 24 (2003), pp. 2163–2184.
[161] B. Wohlmuth, *A mortar finite element method using dual spaces for the Lagrange multiplier*, SIAM Journal on Numerical Analysis, 38 (2000), pp. 989–1012.
[162] ——, *Multigrid methods for saddlepoint problems arising from mortar finite element discretizations*, Electronic Transactions on Numerical Analysis, 11 (2000), pp. 43–54.
[163] ——, *Discretization Methods and Iterative Solvers Based on Domain Decomposition*, vol. 17 of LNCS, Springer Heidelberg, 2001.
[164] ——, *A comparison of dual Lagrange multiplier spaces for mortar finite element discretizations*, Mathematical Modelling and Numerical Analysis, 36 (2002), pp. 995–1012.
[165] ——, *A V-cycle multigrid approach for mortar finite elements*, SIAM Journal on Numerical Analysis, 42 (2005), pp. 2476–2495.
[166] B. Wohlmuth and R. Krause, *Multigrid methods based on the unconstrained product space arising from mortar finite element discretizations*, SIAM Journal on Numerical Analysis, 39 (2001), pp. 192–213.
[167] B. Wohlmuth and R. Krause, *Monotone multigrid methods on nonmatching grids for nonlinear multibody contact problems*, SIAM Journal on Scientific Computing, 25 (2003), pp. 324–347.
[168] P. Wriggers, *Nichtlineare Finite-Element-Methoden*, Springer, 2001.
[169] ——, *Computational Contact Mechanics*, Wiley, 2002.
[170] P. Wriggers and S. Reese, *A note on enhanced strain methods for large deformations*, Computer Methods in Applied Mechanics and Engineering, 135 (1996), pp. 201–209.
[171] J. Xu and J. Zou, *Some non-overlapping domain decomposition methods*, SIAM Review, 40 (1998), pp. 857–914.
[172] T.-X. Zhou and Y.-F. Nie, *Combined hybrid approach to finite element schemes of high performance*, International Journal for Numerical Methods in Engineering, 51 (2001), pp. 181–202.